Aalto University publication series
Doctoral Theses 60/2025

Optimization and time-series models for large-scale integration of variable renewable energy sources

Tuomas Rintamäki

A doctoral thesis completed for the degree of Doctor of Science (Technology) to be defended, with the permission of the Aalto University School of Science, at a public examination held at the lecture hall H304 (Otakaari 1, Espoo, Finland) of the school on 25 April 2025 at 12 noon.

Aalto University
School of Science
Department of Mathematics and Systems Analysis

Supervising professor
Professor Ahti Salo, Aalto University, Finland

Thesis advisors
Professor Ahti Salo, Aalto University, Finland
Professor Afzal Siddiqui, Stockholm University, Sweden; Aalto University, Finland
Professor Fabricio Oliveira, Aalto University, Finland

Preliminary examiners
Professor Pierre-Olivier Pineau, HEC Montréal, Canada
Professor Ramteen Sioshansi, Carnegie Mellon University, USA

Opponent
Professor Ramteen Sioshansi, Carnegie Mellon University, USA

Aalto University publication series
Doctoral Theses 60/2025

ISBN 978-952-64-2457-6 (soft cover)
ISBN 978-952-64-2458-3 (PDF)
ISSN 1799-4934 (printed)
ISSN 1799-4942 (PDF)

https://urn.fi/URN:ISBN:978-952-64-2458-3
Unigrafia Oy
Helsinki 2025

Aalto University

ABSTRACT

Author Tuomas Rintamäki

Name of the doctoral thesis Optimization and time-series models for large-scale integration of variable renewable energy sources

Article-based thesis

Number of pages 111

Keywords optimization, time-series models, game theory, renewable energy, power systems

Traditionally, power systems have consisted of highly predictable loads and controllable generation sources. Global goals to reduce emissions have motivated the large-scale introduction of variable renewable energy sources (VRES) in these systems. VRES such as wind and solar power are less predictable, controllable, and have zero marginal costs. Consequently, the large-scale deployment of VRES affects power system adequacy and flexibility requirements as well as the pricing of electricity in day-ahead and intraday markets.

This Dissertation develops optimization and time-series models to answer research questions related to the large-scale integration of VRES in power markets. We build on real power system data to implement autoregressive time-series models with exogenous variables to estimate the impact of wind and solar power on power prices in the Nordic and Northwestern European regions. Moreover, we develop three mathematical optimization models: (i) a bi-level model to optimize capacity payments to flexible conventional generation to reduce expected balancing costs due to the variability of VRES; (ii) a bi-level model to take the perspective of a flexible generator jointly optimizing day-ahead and intraday offerings in the presence of VRES; (iii) a tri-level stochastic adaptive robust optimization model for long-term generation and transmission expansion to meet emission-reduction targets while considering uncertain demand and VRES. For each optimization model (i)-(iii), we develop improved solution methods that make case studies involving detailed power system data computationally feasible.

The main contributions of this Dissertation are as follows. First, the time-series and optimization models expand on the state-of-the-art by accounting for new features, such as intraday market dispatch, additional time scales, or operational details. Second, we develop linearization, reformulation, and decomposition methods to solve the optimization problems efficiently and accurately. Third, applying our time-series and optimization models to real power data from the Nordic and Northwestern European countries, we address research questions on the impact of large-scale integration of VRES on power system adequacy, flexibility requirements, and power market prices. Our insights include e.g. a long-term transmission and generation expansion plan to meet emission-reduction goals as well as estimates about the impact of wind and solar power on day-ahead prices. Such insights can support the design of more effective policies for VRES integration and serve to inform producers and consumers alike on the impact of VRES. The results of the Dissertation have been exploited by other researchers in estimating the impact of VRES in other regions, for example.

Aalto-yliopisto

TIIVISTELMÄ

Tekijä Tuomas Rintamäki

Väitöskirjan nimi Optimointi- ja aikasarjamalleja vaihtelevien uusiutuvien energialähteiden laaja-alaiseen integroimiseen

Artikkeliväitöskirja

Sivumäärä 111

Avainsanat optimointi, aikasarjamalli, peliteoria, uusiutuva energia, sähköjärjestelmä

Aiemmin sähköjärjestelmät ovat koostuneet hyvin ennakoitavasta kulutuksesta sekä säädettävästä tuotannosta. Globaalit päästövähennystavoitteet ovat johtaneet vaihtelevien uusiutuvien energiamuotojen laaja-alaiseen käyttöönottoon näissä järjestelmissä. Vaihtelevat uusiutuvat energiamuodot kuten tuuli- ja aurinkovoima ovat heikommin ennakoitavia ja säädettäviä eikä niillä ole marginaalituotantokustannuksia. Tästä johtuen näiden laaja-alainen käyttöönotto vaikuttaa sähköjärjestelmien riittävyys- ja joustavuusvaatimuksiin sekä sähkön hinnoitteluun seuraavan päivän ja päivänsisäisissä markkinoissa.

Väitöskirjassa kehitetään uusia optimointi- ja aikasarjamalleja vastaamaan tutkimuskysymyksiin, jotka liittyvät vaihtelevan uusiutuvan energiamuotojen laaja-alaiseen integroimiseen sähköjärjestelmiin. Siksi työssä estimoidaan tuuli- ja aurinkovoiman vaikutuksen sähkönhintoihin pohjoismaalaisissa ja länsieurooppalaisissa sähköjärjestelmissä kehittämällä autoregressiivisen aikasarjamallin ulkopuolisilla muuttujilla. Lisäksi työssä kehitetään seuraavat kolme optimointimallia: (i) kaksitasoinen optimointimalli, joka määrittää kapasiteettimaksut joustaville tuotantomuodoille, jotta sähköjärjestelmän joustavuus ja odotetut kustannukset ovat optimaaliset, (ii) kaksitasoinen optimointimalli, joka optimoi joustavan tuottajan tarjoukset seuraavan päivän ja päivänsisäiselle markkinalle huomoiden uusiutuvan energian vaihtelevuuden, (iii) kolmitasoinen stokastinen ja robusti optimointimalli, joka optimoi pitkänajan tuotanto- ja siirtolinjainvestoinnit päästötavoitteiden saavuttamiseksi huomioiden uusiutuvan energian ja kulutuksen epävarmuuden. Kullekin optimointimallille (i)-(iii) kehitetään tehokkaita ratkaisumenetelmiä numeerisia tapaustutkimuksia varten, joissa käytetään yksityiskohtaista sähköjärjestelmädataa.

Väitöskirjassa on kolme pääkontribuutiota. Ensinnäkin aikasarja- ja optimointimallit yleistävät aiempia malleja ottamalla huomioon uusia ominaisuuksia, kuten päivänsisäisen markkinan, aikaulottuvuuden tai uusia tuotannollisia yksityiskohtia. Toiseksi siinä esitetään uusia linearisointi-, reformulointi- ja hajotelmatekniikoita, joiden avulla optimointimallit saadaan ratkaistua nopeasti ja tarkasti. Kolmanneksi se vastaa tutkimuskysymyksiin laajamittaisen uusiutuvan energian integroimiseen sekä sen vaikutuksiin sähkönhintoihin hyödyntämällä pohjoismaalaista ja länsieurooppalaista markkinadataa. Väitöskirjassa tuotetaan tutkimustietoa esimerkiksi päästöjä vähentävästä pitkän aikavälin siirto- ja tuotantokapasiteetin laajentumisesta ja tuuli- ja aurinkovoiman vaikutuksista sähkönhintoihin. Tämä tieto on hyödyttää sekä tuottajia että kuluttajia ja se auttaa suunnittelemaan mekanismeja, joilla uusiutuvan energian lähteitä voidaan integroida helpommin. Väitöskirjan menetelmiä on hyödynnetty muissa tutkimuksissa esimerkiksi arvioitaessa vaihtelevan uusiutuvan energia vaikutuksia muissa maissa.

Preface

I want to thank Professors Afzal Siddiqui, Ahti Salo, and Fabricio Oliveira for their guidance. I am grateful to Aalto University and the STEEM project of the Aalto Energy Efficiency for enabling my studies. I'd like to thank my wife, family, and friends for their support.

January 19, 2025,

Contents

List of Publications

This thesis consists of an overview and of the following publications which are referred to in the text by their Roman numerals.

I T. Rintamäki, A. S. Siddiqui, and A. Salo. Does renewable energy generation decrease the volatility of electricity prices? An analysis of Denmark and Germany. *Energy Economics*, 62, 270-282, 2017.

II T. Rintamäki, A. S. Siddiqui, and A. Salo. How much is enough? Optimal support payments in a renewable-rich power system. *Energy*, 117(1), 300-313, 2016.

III T. Rintamäki, A. S. Siddiqui, and A. Salo. Strategic offering of a flexible producer in day-ahead and intraday power markets. *European Journal of Operational Research*, 284(3), 1136-1153, 2020.

IV T. Rintamäki, F. Oliveira, A. S. Siddiqui, and A. Salo. Achieving emission-reduction goals: Multi-period power-system expansion under short-term operational uncertainty. *IEEE Transactions on Power Systems*, 39(1), 119-131, 2024.

Author's Contribution

Publication I: "Does renewable energy generation decrease the volatility of electricity prices? An analysis of Denmark and Germany"

Rintamäki is the primary author. Siddiqui and Salo proposed the topic and research questions with contributions from Rintamäki. Rintamäki independently collected data, formulated the mathematical model, implemented the model in R, and computed the results guided by feedback from Siddiqui and Salo. Rintamäki wrote the paper guided by comments from Siddiqui and Salo.

Publication II: "How much is enough? Optimal support payments in a renewable-rich power system"

Rintamäki is the primary author. Rintamäki proposed the topic and Rintamäki, Siddiqui, and Salo defined the research questions. Rintamäki independently collected data, formulated the mathematical model, implemented the model in GAMS, and computed the results guided by feedback from Siddiqui and Salo. Rintamäki wrote the paper guided by comments from Siddiqui and Salo.

Publication III: "Strategic offering of a flexible producer in day-ahead and intraday power markets"

Rintamäki is the primary author. Rintamäki proposed the topic and Rintamäki, Siddiqui, and Salo defined the research questions. Rintamäki independently collected data, formulated the mathematical model, implemented the model in Python, and computed the results guided by feedback from Siddiqui and Salo. Rintamäki wrote the paper guided by comments from Siddiqui and Salo.

Publication IV: "Achieving emission-reduction goals: Multi-period power-system expansion under short-term operational uncertainty"

Rintamäki is the primary author. Rintamäki proposed the topic and Rintamäki, Oliveira, Siddiqui, and Salo defined the research questions. Rintamäki independently collected data, formulated the mathematical model, implemented the model in Python, and computed the results guided by feedback from Oliveira and Siddiqui. Oliveira contributed significantly to model formulation and computational solution approach. Rintamäki wrote the paper guided by comments from Siddiqui, Oliveira and Salo.

Abbreviations

ARO	Adaptive Robust Optimization
EPEC	Equilibrium Problem with Equilibrium Constraints
GARCH	Generalized Autoregressive Conditional Heteroskedasticity model
KKT	Karush-Kuhn-Tucker conditions
LP	Linear Programming
MILP	Mixed-Integer Linear Program
MIQP	Mixed-Integer Quadratic Program
RO	Robust Optimization
SARMAX	Seasonal Autoregressive Moving Average Model with Exogenous Variables
SARO	Stochastic Adaptive Robust Optimization
SP	Stochastic Programming
VRES	Variable Renewable Energy Sources

1. Introduction

1.1 Background

Power systems are characterized by the unique constraint that electricity supply must always meet demand to maintain a stable frequency in the electricity transmission grid. Electricity demand can be forecasted multiple days ahead with high accuracy thanks to factors such as known industrial processes, predictable patterns in residential consumption, and high correlation with temperature and other weather conditions [1]. Traditionally, electricity is generated using predictable and controllable sources such as coal- and gas-fired plants, hydropower, and nuclear. Power exchanges such as Nord Pool Spot in the Nordic countries provide a day-ahead market for producers and consumers to sell and buy electricity for each hour in the following day. Market participants can make changes to the day-ahead sales and purchases in intraday and balancing markets [2].

In recent years, global treaties such as the Paris agreement [3] have been introduced to reduce the risks of climate change by seeking to limit the increase in the global average temperature by reducing greenhouse gas (GHG) emissions [4]. Electricity and heat generation is among the top sources of emissions globally [5]. This has led to national policies for subsidizing investments in low-emission renewable electricity sources (RES) as well as technological advancements decreasing the levelized cost of electricity for these sources. Consequently, large amounts of RES are introduced in Europe, the US, Japan, and other regions [6, 7, 8]. In Europe, for example, the share of energy from renewable sources has grown from 16.66% in 2013 to 23.04% in 2022 [9].

Much of the new capacity is variable RES (VRES) such as wind and solar power that has zero marginal costs, is not controllable, and whose output can be predicted less accurately than that of fossil-fuel or hydro plants, for example. Integrating substantial, zero marginal cost VRES capacities into existing power systems can make conventional controllable generation capacity unprofitable in the day-ahead market [10]. Meanwhile, large-scale variability can cause challenges in managing the supply-demand balance and increase costs in the intraday markets [11]. Consequently, policies such as capacity mechanisms may be required to ensure controllable generation capacity in the system to guarantee resource adequacy [12].

Besides policy changes, power system changes may be required to make large-scale integration of VRES feasible. These changes can include additional investments in transmission and generation capacity, demand-side response, and deployment of electricity storage [13, 14, 15, 16], for example. Moreover, alternative market-clearing mechanisms may be better equipped to handle the variability of RES [17].

Power systems lend themselves well to mathematical modeling. Many power system organizations in the world have made detailed time-series data on their operations, generation, and consumption publicly available, thereby facilitating the use of empirical methods such as time-series modeling [18, 19]. Commonly used empirical methods include linear regression, clustering, dimensionality reduction, autoregressive models, and neural networks [20].

Also, in many power systems the market-clearing and dispatch problem is solved using an algorithm to maximize some economic utility function considering the constraints on the supply-demand equilibrium, transmission grid, and more. Such a setup can be formulated using an optimization framework [21]. An extension of this is the so-called bi-level optimization model, which makes it possible to capture the interaction of multiple agents such as a generation company making strategic generation and investment decisions as a leader and the rest of the power system as a follower, i.e., a Stackelberg game [22]. Another extension is robust and stochastic optimization where some variables or parameters of the optimization model such as the VRES generation are not deterministic but uncertain [23]. Indeed, electricity companies need optimization models to support decisions related to long-term resource planning, short-term dispatching, and real-time operations [24].

For large-scale power systems with high time frequency and plenty of operational details, time-series and optimization models can become computationally prohibitive. To this end, many references develop reformulation, decomposition, approximation, and other customized algorithmic techniques to render these models computationally feasible [22, 25, 26].

1.2 Dissertation objectives and contributions

In this dissertation, we develop novel time-series and optimization models to answer research questions related to the large-scale integration of VRES in power markets. We focus on the Nordic and Western European region in our case studies because data are readily available. Also, we seek to develop reformulation, linearization, and decomposition techniques to solve these problems computationally more efficiently. In particular, our main research questions are

RQ1) How does large-scale VRES affect power pricing?

RQ2) How can large-scale VRES be integrated in power systems?

More specifically, Paper I implements an autoregressive time-series model with exogenous variables to estimate the impact of large-scale VRES generation on electricity prices and their volatility using data from the Nordic region. Therefore, Paper I addresses the research question RQ1. Paper II develops a bi-level optimization model with a novel constraint-based reformulation of the dispatch problem to study optimal support payments to incentivize flexible generation remain available to balance VRES. Paper II addresses the research question RQ2 by exploring how such payments can help improve power system adequacy in the presence of large VRES variability. Paper III takes the perspective of a strategic producer with flexible generation using a novel bi-level optimization model capturing both day-ahead and intraday markets. Paper III studies how such a producer can affect market prices given VRES variability (RQ1). Paper III extends an existing linearization scheme to render the problem computationally feasible. Finally, Paper IV develops a tri-level robust optimization model for long-term generation and capacity expansion to meet emission-reduction targets while facing short-term uncertain demand and VRES (RQ2). Paper IV uses Benders decomposition and problem reformulation to speed up solution times for large-scale problem instances. Table 1.1 summarizes the methods and research questions in the papers.

	Time series	Optimization	RQ1	RQ2
Paper I	X		X	
Paper II		X		X
Paper III		X	X	
Paper IV		X		X

Table 1.1. Methods and research questions of the papers in this dissertation

The main contributions of this dissertation are:

1. The development of novel time-series and optimization models;
2. Computationally efficient solution methods for these optimization models;
3. The application of these models to real power systems using data to generate insights into the large-scale integration of VRES to provide guidance to policymakers and practitioners.

More specifically, Paper I focuses on the contributions 1 and 3 by developing a novel time-series model and estimating the impact of VRES on power prices (RQ1). Meanwhile, Papers II-IV focus on the contributions 1-3 as they develop a novel optimization model, an efficient solution method for the model, and by building case studies using market data to address RQ1 or RQ2.

2. Methodological background

2.1 Time-series modeling

Power systems generate time-series data on operations and markets, including generation, transmission flows, load, outages, prices, volumes, and so on. These data contain patterns based on the time of the day and consumer behavior, for example, and can be readily analyzed with time-series models. Figure 2.1 shows that average day-ahead electricity prices in Finland in 2015 were higher during weekdays than during the weekend and that the prices are higher during working hours than during the night.

A common time-series model employed in the literature is the seasonal autoregressive moving average model with exogenous variables (SARMAX$(p,q)(P,Q)[s]$) [27]:

$$y_t = \alpha_0 + \sum_{i=1}^{p} \alpha_i y_{t-i} + \sum_{i=1}^{q} \beta_i \epsilon_{t-i} + \sum_{i=1}^{P} \alpha_{i\cdot s} y_{t-i\cdot s} + \sum_{i=1}^{Q} \beta_{i\cdot s} \epsilon_{t-i\cdot s} + \epsilon_t + \gamma^\top x_t, \quad (2.1)$$

where the dependent variable $y_t \in \mathbb{R}$ at time point t is explained using (i) p lagged values y_{t-i}, (ii) q Gaussian white noise error terms $\epsilon_{t-i} \in \mathbb{R}$, (iii) P seasonal lagged values $y_{t-i\cdot s}$ with periodicity of s, (iv) Q seasonal Gaussian white noise error terms $\epsilon_{t-i\cdot s}$ with periodicity of s, and (v) a vector of exogenous variables $x_t \in \mathbb{R}^m$ with the coefficients α_i, β_i, $\alpha_{i\cdot s}$, $\beta_{i\cdot s} \in \mathbb{R}$, and $\gamma \in \mathbb{R}^m$, respectively.

The SARMAX model assumes that the time series y_t is stationary so that the distribution of y_t does not depend on t [27]. More specifically,

$$\begin{aligned} &P(y_{t_1} \leq v_1, \ldots, y_{t_k} \leq v_k) \quad (2.2)\\ &= P(y_{t_1+h} \leq v_1, \ldots, y_{t_k+h} \leq v_k) \quad \forall t_1, \ldots, t_k, \forall h, \forall v_1, \ldots, v_k. \end{aligned}$$

The lags p, q, P, Q, and s can be identified with the help of autocorrelation function (ACF) and partial autocorrelation function (PACF) plots [27].

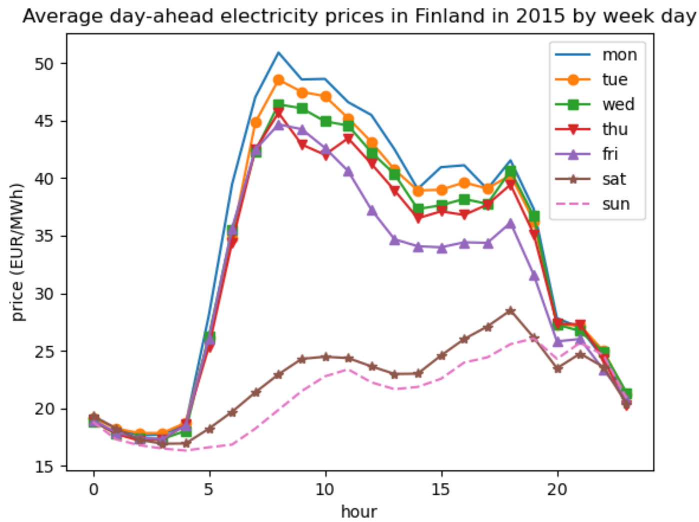

Figure 2.1. Average day-ahead electricity prices in Finland in 2015 by week day. Data source: Nord Pool

After choosing the lags p, q, P, Q, and s, the SARMAX model can be fitted using least squares. Implementations are available in software such as R [28]. The errors of the fitted time series $\hat{y}_t$ for n observations can be measured using the sum of squared errors (SSE):

$$\text{SSE} = \sum_{t=1}^{n} (y_t - \hat{y}_t)^2. \tag{2.3}$$

The goodness of fit for a specific choice of the lags considering the total number of coefficients k can be computed using for example the Akaike Information Criterion (AIC) [27]:

$$\text{AIC} = \log \frac{\text{SSE}}{n} + \frac{n + 2k}{n}. \tag{2.4}$$

In power markets, the dependent variable y_t can be the power price in hour t, for example, and the exogenous variables x_t can be the average wind power output during hour t. The selected lags and estimated values of the coefficients such as α and γ make it possible to interpret the driving factors for the time series. Also, the model can be used to predict future time steps t based on the realized or predicted values for the dependent and exogenous variables.

Besides the SARMAX family, common approaches to time-series analysis include generalized autoregressive conditional heteroskedasticity (GARCH) and deep neural networks (DNN) models [19, 29]. While the SARMAX model assumes homoskedasticity, i.e., the model error terms

ϵ_t are sampled from a Gaussian distribution with a constant variance, the GARCH model allows for heteroskedasticity. Thus, the variance can depend on time, which can help model time-series volatility, for example. Meanwhile, DNNs such as multi-layer perceptrons, convolutional neural networks, long short-term memory (LSTM), and other architectures can be used to fit arbitrarily complex differentiable non-linear functions to the time-series data using stochastic gradient descent [30].

2.2 Mathematical programming

In mathematical programming models, an objective function is minimized with respect to decision variables subject to a set of constraints. A general form of such an optimization model is [31]

$$\underset{x}{\text{minimize}} \quad f(x) \tag{2.5}$$

subject to

$$g_i(x) \leq 0, \quad i = 1, \ldots, m, \tag{2.6}$$

where $x = (x_1, \ldots, x_n) \in \mathbb{R}^n$ is a vector of decision variables, $f(x) : \mathbb{R}^n \to \mathbb{R}$ an objective function, and $g_i(x) : \mathbb{R}^n \to \mathbb{R}$ are the constraint functions. A vector x^* is optimal and, thus, a solution to Eqs. (2.5)-(2.6) if it gives the smallest value to the objective function while satisfying the constraints.

When the functions f and g_i are affine, i.e. of the form $c^T x + b$, where $c \in \mathbb{R}^n$ and $b \in \mathbb{R}$, then the problem in Eqs. (2.5)-(2.6) becomes a linear program (LP), which can be solved to optimality using the simplex algorithm, for example [31]. Another important case is when the functions f and g are convex. That is, if for all x, y in the domain of function f (denoted by $x, y \in dom f$) and $0 \leq \theta \leq 1$

$$f(\theta x + (1-\theta)y) \leq \theta f(x) + (1-\theta) f(y), \tag{2.7}$$

then the problem is a convex optimization problem, which can be solved to optimality using interior-point methods such as the barrier method [31]. If the functions f and g are affine and one or more of the components of the decision variable vector x are constrained to integers, then the problem becomes a mixed-integer linear program (MILP), which can be solved using the branch-and-bound algorithm, for example [32]. Typically, the optimization problem is represented and solved using software such as Gurobi [32]

Many interactions in power markets can be modeled using optimization models. For example, Nord Pool Spot runs an algorithm that maximizes social welfare objective function with respect to supply and demand variables given constraints such as limited transmission capacity between areas [33]. In other words, the electricity market-clearing problem can be represented using the above optimization problem.

A variant of the above optimization model is so-called bi-level optimization, where one of the constraints involves another optimization problem [34]. Bi-level problems are commonly used to model the impact of upper-level decision variables such as generation and transmission investment in a lower-level problem such as the market clearing [35]. In such cases, the problem is often an instance of a Mathematical Program with Equilibrium Constraints (MPEC). More specifically, as in [34], we have

$$\underset{x,y}{\text{minimize}} \quad F(x,y) \tag{2.8}$$

subject to

$$G_k(x,y) \leq 0, \quad k = 1,\ldots,K \tag{2.9}$$

$$y \in \arg\min_{y}\{f(x,y) : g_j(x,y) \leq 0, j = 1,\ldots,J\}, \tag{2.10}$$

where $x \in \mathbb{R}^n$ and $y \in \mathbb{R}^m$ are upper- and lower-level decision variables, respectively, $F(x,y) : \mathbb{R}^n \times \mathbb{R}^m \to \mathbb{R}$ and $f(x,y) : \mathbb{R}^n \times \mathbb{R}^m \to \mathbb{R}$ are the upper- and lower-level objective functions, and $G_k(x,y) : \mathbb{R}^n \times \mathbb{R}^m \to \mathbb{R}$, and $g_j(x,y) : \mathbb{R}^n \times \mathbb{R}^m \to \mathbb{R}$ are the upper- and lower-level constraint functions, respectively.

When the lower-level problem in Eq. (2.10) is convex (given a fixed x), the bi-level problem can reduced to a single-level optimization problem by replacing the lower-level problem with its Karush-Kuhn-Tucker (KKT) conditions [34]. The so-called Lagrangian of Eq. (2.10) is

$$\mathcal{L}(x,y,\mu) = f(x,y) + \sum_{j=1}^{J} \mu_j g_j(x,y), \tag{2.11}$$

where μ_j are Lagrange multipliers. As in [34], the KKT conditions are

$$\nabla_y L(x,y,\mu) = 0 \tag{2.12}$$

$$g_j(x,y) \leq 0,\ j = 1,\ldots,J \tag{2.13}$$

$$\mu_j g_j(x,y) = 0,\ j = 1,\ldots,J \tag{2.14}$$

$$\mu_j \geq 0,\ j = 1,\ldots,J. \tag{2.15}$$

Consequently, the bi-level problem in Eqs. (2.8) - (2.10) becomes [34]

$$\underset{x,y,\mu}{\text{minimize}} \quad F(x,y) \tag{2.16}$$

subject to

$$G_k(x, y) \leq 0, \quad k = 1, \ldots, K \tag{2.17}$$

$$\text{Eqs. (2.12) - (2.15).} \tag{2.18}$$

Depending on the functions F and G and decision variables x, the problem in Eqs. (2.16) - (2.18) can be reformulated as an MILP, for example, and, therefore, be readily solvable. Often, the bilinear terms in Eq. (2.14) can be linearized by using techniques such as disjunctive constraints [22] or binary expansion [36]. Also, the KKT conditions in Eq. (2.18) can represent multiple follower players and the solution to the KKT conditions is a Nash equilibrium among those players [21].

In the generic optimization problem in Eqs. (2.5) - (2.6), the functions f and g are deterministic and known exactly. Yet, in many applications such as the electricity market, this is typically not the case as many parameters like the VRES output are random variables. Stochastic programming (SP) is a framework in which some parameters of the optimization problem are uncertain [35]. For example, consider the two-stage linear SP problem [37], where $x \in \mathbb{R}^n$ are first-stage decision variables, $c \in \mathbb{R}^n$, $A \in \mathbb{R}^{n\times n}$, $b \in \mathbb{R}^n$, and $W \in \mathbb{R}^{n\times m}$ are known parameters, $y \in \mathbb{R}^m$ are second-stage decision variables, and ξ is the collection of random variables $q(\omega) \in \mathbb{R}^m$, $T(\omega) \in \mathbb{R}^{n\times n}$, and $h(\omega) \in \mathbb{R}^n$ dependent on a random event ω:

$$\underset{x,y}{\text{minimize}} \quad c^\top x + \mathbb{E}_\xi[q(\omega)^\top y] \tag{2.19}$$

subject to

$$Ax = b \tag{2.20}$$

$$T(\omega)x + Wy = h(\omega). \tag{2.21}$$

Here, the first-stage decisions x are made before the realization of the random variables ξ. In the second stage, the random variable ξ becomes known and the second-stage decisions y are taken [37].

SP assumes that the probability distribution of random variables ξ is known. However, for many probability distributions, the above problem can be difficult to solve in a closed form. Therefore, it is often assumed that the probability distribution can be approximated by taking a finite number (S) of realizations $\xi_1, \ldots, \xi_S$ of the random variable ξ called scenarios with their associated probabilities $p_1, \ldots, p_S$. This gives the deterministic equivalent [37]:

$$\underset{x,y_s}{\text{minimize}} \quad c^\top x + \sum_{s=1}^{S} p_s q_s^\top y_s \tag{2.22}$$

subject to

$$Ax = b \tag{2.23}$$

$$T_s x + W y_s = h_s \quad \forall s = 1, \dots, S. \tag{2.24}$$

The deterministic equivalent is an LP that can be solved. However, the number of constraints (2.24) and variables y_s grows linearly with the number of scenarios S, which can cause solution times to soar when S is large.

Another framework for modeling uncertainty is robust optimization (RO), where instead of using a random variable ξ, it is assumed that the uncertain parameters can take any value in an uncertainty set $\mathcal{U}$ [38]. Consequently, the decision variables of the problem are optimized considering the worst-case realization of the uncertain parameters. This can be an appropriate approach in application areas such as power system reliability [39]. More specifically, following [38], given uncertain matrix $A \in \mathbb{R}^{n\times n} \in \mathcal{U}$ with its row vectors $a_i^\top \in \mathbb{R}^n \in \mathcal{U}_i \, \forall i = 1, \dots, n$ and known vector $c \in \mathbb{R}^n$ and scalars $b_i \, \forall i = 1, \dots, n$, a robust linear optimization problem is given by

$$\underset{x}{\text{minimize}} \quad c^\top x \tag{2.25}$$

subject to

$$a_i^\top x \leq b_i \quad \forall i = 1, \dots, n. \tag{2.26}$$

The robust LP can be solved for certain uncertainty sets $\mathcal{U}$. For example, if the uncertainty set is polyhedral, i.e., $\mathcal{U}_i = \{D_i a_i \leq d_i\} \, \forall i = 1, \dots, n$ for known $D_i \in \mathbb{R}^{m_i \times n}$ and $d_i \in \mathbb{R}^{m_i}$, then following [38] we obtain the following problem:

$$\underset{x}{\text{minimize}} \quad c^\top x \tag{2.27}$$

subject to

$$\max_{\{D_i a_i \leq d_i\}} a_i^\top x \leq b_i \quad \forall i = 1, \dots, n. \tag{2.28}$$

The subproblem in Eq. (2.28) can be solved using duality [38]. Given the Lagrange multipliers $\mu_i \geq 0$, the Lagrangian of the subproblem is $\mathcal{L}(a_i, \mu_i) = -a_i^\top x + \mu_i^\top (D_i a_i - d_i) = -\mu_i^\top d_i + (\mu_i^\top D_i - x^\top) a_i$. The dual problem is

$$\underset{\mu_i}{\text{minimize}} \quad \mu_i^\top d_i \tag{2.29}$$

subject to

$$D_i^\top \mu_i = x \quad \forall i = 1, \dots, n \tag{2.30}$$

$$\mu_i \geq 0 \quad \forall i = 1, \dots, n. \tag{2.31}$$

Consequently, for this choice of the uncertainty set, the robust LP can be written as an LP [38]:

$$\underset{x,\mu_i}{\text{minimize}} \quad c^\top x \tag{2.32}$$

subject to

$$\mu_i^\top d_i \leq b_i \quad \forall i = 1, \ldots, n \tag{2.33}$$

$$D_i^\top \mu_i = x \quad \forall i = 1, \ldots, n \tag{2.34}$$

$$\mu_i \geq 0 \quad \forall i = 1, \ldots, n. \tag{2.35}$$

If the RO problem has two stages as SP, then it is called adaptive robust optimization (ARO) [40]. We follow [40] by defining first- and second-stage decision variables $x \in \mathbb{R}^n$ and $y \in \mathbb{R}^m$, respectively, and known parameters $c \in \mathbb{R}^n$, $b \in \mathbb{R}^m$, $F, A \in \mathbb{R}^{n\times n}$, $B \in \mathbb{R}^{n\times m}$, $H \in \mathbb{R}^{m\times m}$, and $f, g \in \mathbb{R}^n$ as well as an uncertain variable $a \in \mathcal{U}$, and uncertain parameter $h(a) \in \mathbb{R}^m$, to obtain an ARO problem:

$$\underset{x,y}{\text{minimize}} \left(c^\top x + \underset{a\in\mathcal{U}}{\text{maximize}}\, b^\top y(a) \right) \tag{2.36}$$

subject to

$$Fx \leq f \tag{2.37}$$

$$Ax + By(a) \leq g \tag{2.38}$$

$$Hy(a) \leq h(a). \tag{2.39}$$

Here, similar to the two-stage SP, the first-stage decisions x are made before the realization of the second-stage uncertain variables a is known. In the second stage, the second-stage decisions y are made in a response to the worst-case realization of a (as denoted by $y(a)$). Following [40], we set $\Omega(x, a) = \{y : Hy \leq h(a); Ax + By \leq g\}$ so the problem can be reformulated as

$$\underset{x}{\text{minimize}} \left(c^\top x + \underset{a\in\mathcal{U}}{\text{maximize}}\, \underset{y\in\Omega(x,a)}{\text{minimize}}\, b^\top y \right) \tag{2.40}$$

subject to

$$Fx \leq f. \tag{2.41}$$

The problem in Eqs. (2.40)-(2.41) is tri-level in the sense that (i) first, the outer minimization selects x, then (ii) the inner maximization selects worst-case a, and finally (iii) the innermost minimization selects y in response to x and a. A typical procedure to solve this problem is to write the dual of the third-level problem in Eq. (2.40) and then employ a two-level algorithm that alternates between solving the outer minimization and inner maximization problem [40].

If one of the known parameters in the ARO problem in Eqs. (2.36)-(2.39) is uncertain so that it depends on a random event ω, e.g. $A(\omega)$, then we have a framework combining both SP and RO in two or more stages that is called stochastic adaptive robust optimization (SARO) [23]. In this framework, we can choose to use SP for certain parameters and RO for some other parameters, depending on what is the most appropriate way to model those parameters [23].

2.3 Clustering methods

It is desirable to use data from power markets to build representative case studies to address research questions. At times, it is not viable to use raw market data as an input to models if the high dimensionality or frequency of the data leads to excessive computational times, for example. This can be the case in SP, for example, if the number of scenarios S is too large. In such cases, methods such as k-means clustering can be effective at reducing the number of scenarios while modeling the probability distribution of the uncertain parameters sufficiently accurately [41]. The k-means clustering algorithm is given by Algorithm 1 [42].

Algorithm 1: k-means clustering. n vectors are reduced to k clusters.

Input: Input data $x_i \in \mathbb{R}^m \quad \forall i = 1, \ldots, n$, the desired number of clusters k

Output: k clusters $\mu_1 \ldots \mu_k \in \mathbb{R}^m$

1 Randomly select a subset of k vectors $\mu_1, \ldots, \mu_k$ from x_i ;

2 **while** μ_k *have not converged* **do**

3 $\quad c_i = \underset{j}{\operatorname{argmin}} \|x_i - \mu_j\|_2, \quad \forall i = 1, \ldots, n$;

4 $\quad \mu_j = \frac{\sum_{i=1}^{n} 1_{c_i=j} x_i}{\sum_{i=1}^{n} 1_{c_i=j}}, \quad \forall j = 1, \ldots, k$

Another approach to clustering is hierarchical clustering, which does not require setting the number of clusters k in advance. Agglomerative hierarchical clustering assigns each data point in a separate cluster and iteratively combines clusters using a distance metric. By contrast, divisive hierarchical clustering assigns all data points in the same cluster and iteratively splits the data points into smaller clusters. In power markets, hierarchical clustering can useful to find e.g. find representative days of a long time series [43].

3. Contributions of the papers

3.1 Paper I

Paper I studies the impact of VRES such as wind and solar power on power prices and their volatility to address our research question RQ1. We build a SARMAX$(p,q)(P,Q)[s]$ model and estimate its coefficients using power market data from Denmark and Germany. We compare multiple configurations of the parameters $p, q, P, Q,$ and s as guided by ACF and PACF plots and select the configuration with the best fit as measured by the AIC score.

The paper presents novel results on the price impact of VRES and corroborates the findings of earlier papers [19, 44, 45]. In particular, we find that, in Denmark, wind power decreases daily price volatility by flattening the hourly price profile (RQ1). This is because wind power generation in Denmark is, on average, higher during peak hours, which reduces the need for expensive peak generators. However, in Germany, wind power increases daily price volatility. This is caused by an increasing difference in the peak and off-peak prices as the German power system has limited flexibility during off-peak hours when the wind power generation in Germany is, on average, higher. By contrast, Denmark has access to flexible hydro power generation through its transmission lines to Norway and Sweden.

Also, we find that solar power decreases daily price volatility in Germany. This is because the generation of solar power is highest during peak hours, which helps reduce the need for expensive peak generators. Moreover, we find that VRES increases the volatility of weekly prices due to the intermittency of solar and wind power over multiple days.

The paper helps policymakers, producers, and consumers to understand how VRES affects short-term power prices and their volatility. Also, its estimates can be used to forecast power prices changes as VRES penetration increases over time.

3.2 Paper II

Paper II studies how intraday balancing volumes and costs are affected by support payments to generators with high marginal costs but flexible capacity in a renewable-rich power system. In particular, we seek to study if such payments can improve power system adequacy in scenarios with high VRES variability (RQ2). Earlier studies have estimated that transmission congestion costs and power system flexibility requirements increase with higher VRES penetration [46, 47]. To this end, we develop a bi-level programming model to minimize the total cost of support payments and generation in the day-ahead and intraday balancing markets. The upper level of the model represents the selection of the support payments and clearing of the day-ahead market while the lower level clears the balancing market.

We reformulate the day-ahead market-clearing problem using a novel set of constraints in order to avoid complicating nonlinear terms that would otherwise arise if the day-ahead and balancing markets would both be represented as lower-level problems with dependencies between each other. This reformulation makes it possible to solve large-scale problem instances with many time steps and scenarios.

We use a detailed representation of the German power system as a case study and find that support payments to flexible generators can reduce the total cost of the system. We run out-of-sample simulations with high demand and VRES variability and show that support payments can improve power system adequacy (RQ2). Our results corroborate the empirical results of [48] that suggest that capacity payments to flexible producers can help them bid lower in the day-ahead market and hence remain available for dispatch. Therefore, the insights from the paper can be used to design policies such as capacity mechanism to integrate growing VRES while ensuring resource adequacy. However, policymakers need to adjust support payments carefully because excessive support payments can lead to higher costs for consumers.

Finally, with our reformulation approach, the modeler can choose an objective function other than social welfare maximization while ensuring the correct merit curve in day-ahead market clearing. Consequently, the reformulation can be used to determine the optimal level of other variables such as emission prices in order to induce target emission-reduction levels that consider both day-ahead and intraday markets.

3.3 Paper III

Paper III develops a novel bi-level model to study strategies that flexible producer has in submitting offers in day-ahead and intraday markets. The upper level of the model represents the profit-maximization problem of the flexible producer, and the lower-level problems represent the day-ahead and intraday market-clearing problems. The model and a stylized 3-node network are analyzed to explore a range of offering strategies that allow a flexible producer to increase its profits. For example, the producer can offer a lower volume in the day-ahead market if it anticipates a deficit in the intraday market. Such a deficit can be caused by lower-than-expected VRES output, limited ramping capabilities of other producers or a congestion in the transmission network, for example. Likewise, the producer can offer excessive volumes in the day-ahead market if it anticipates a surplus in the intraday market. A surplus can occur if the generation of wind or solar power is higher than expected, for example. We use a Nordic power system in a case study to show that such offering strategies can affect market prices in real power exchanges (RQ1). Also, the offering strategies can lead to higher total costs compared to perfect competition. Our results corroborate those of [49].

We expand an existing linearization technique [36] to support negative variable values to render the model computationally feasible. Also, we show that an alternative market dispatch mechanism that considers VRES variability [17] can reduce the costs of strategic offering.

The findings give policymakers insights into strategic offering in power markets and how the variability of VRES may enable such strategies. This can help policymakers to develop measures to mitigate the negative impacts of strategic offering on market prices.

3.4 Paper IV

Paper IV proposes a SARO model for long-term (multi-year) power system expansion with emission targets under short-term (hourly) operational uncertainty. The SARO model is a tri-level model where the first level invests in long-term generation and transmission capacity expansion while considering the second and third levels, where the second level chooses worst-case long-term demand levels and the third level represents the short-term market clearing with stochastic demand, generation and transmission capacity as well as a constraint on maximum emission levels. In other words, the model seeks to find the least-cost generation and transmission expansion plan while reaching emission targets and keeping the power system operational in the presence of uncertain VRES and worst-case demand (RQ2). This paper expands on earlier work such as [23] by adding multiple time-scales and explicitly considering VRES investments to meet emission goals.

To make the model computationally feasible, we apply a column-and-constraint algorithm that alternates between solving a master problem and subproblem. Compared to earlier work [23, 50], we accelerate the master problem by applying Benders decomposition and identifying the subproblem as a mixed-integer quadratic problem (MIQP), which can be solved faster than earlier approaches that linearize the subproblem and solve it as an MILP.

We apply the model to a realistic case study for the Nordic and Baltic region with a multi-year and multi-hour time windows and an objective to reduce emissions. The optimal plan is found to include a significant investment in wind power and transmission capacity. The model can be used by policymakers to create long-term plans to meet emission goals.

4. Discussion

Predicting short-term power prices is important for consumers and producers for optimizing their respective objectives. Paper I studies the impact of VRES on short-term power prices. Several researchers, e.g. [51, 52], have recently expanded on the analysis of Paper I in the same geographical region while others have used similar methodologies to study the impact of VRES in other geographies [53, 54]. Future research could use enhanced methods such as separate training and validation datasets for model selection and higher capacity models such as GARCH and DNNs to arrive at more accurate estimates of the impact of VRES [55].

With increasing wind and solar power penetration, the accuracy of weather forecasts is becoming increasingly important. More accurate wind and solar power forecasts can improve price forecasts and subsequent planning decisions. For example, [56] improve wind power prediction accuracy for specific locations by post-processing predictions generated from standard weather models. Also, [57] propose the organization of multiple intraday auctions to give market participants access to more accurate VRES output predictions.

The variability of VRES can lead to higher balancing costs and flexibility requirements in the power system. The empirical results of [48] suggest that capacity payments can help flexible producers to submit lower bids in the day-ahead market and, thus, remain available for dispatch. This is aligned with the results of Paper II, which finds that support payments to flexible producers can reduce balancing costs and improve power system adequacy. However, [58] find that market players can engage in strategies such as virtual bidding and self-scheduling to reduce the balancing costs caused by VRES, which in turn reduces the need for alternative market designs. Indeed, new mechanisms such as capacity payments need to be evaluated carefully as they can be gamed or have adverse impacts on existing or future desirable investments.

Higher variability of short-term power prices can create new opportunities for flexible producers and consumers. In our Paper III, we find that a strategic flexible producer can benefit from VRES variability by coordinating its offering to day-ahead and balancing markets. However, such behavior can increase costs for consumers. While price-taking storage systems [59] and demand-side response [15] become particularly viable due to arbitrage of short-term power price variability, they also have a flattening impact on power prices.

In some geographies, it may be possible to balance VRES variability by carefully planning the expansion of generation and transmission capacity. For example, [60] reduce the variation in total VRES output by building wind and solar power in locations that consider the spatio-temporal correlation in their output. Likewise, in some locations, it can be possible to build transmission lines to connect high demand and wind power output locations [61]. Our Paper IV implicitly considers such effects in long-term planning by using representative days to capture load and VRES output.

The optimization models in Papers II-IV are parameterized such that they can be readily expanded. One avenue is to apply these models to further regions to study whether similar insights can be gained outside the Nordic countries and Western Europe. Another avenue is to add decision variables and constraints to build more realistic models with storage and demand-side response, additional sources of uncertainty such as transmission and generation outages, and more detailed representations of the transmission network and generation assets including their ramping and start-up times and costs.

A more fundamental change to our models would be to model multiple market participants in more detail. Specifically, the bi-level optimization framework in Papers II and III considers two agents, a leader and a follower. The tri-level model in Paper IV introduces the selection of the worst-case demand as a third agent. A more generic approach is the so-called Equilibrium Problems with Equilibrium Constraints (EPEC) model that represents multiple agents [21]. Such models more accurately represent power markets in which there are multiple independent producers and consumers who seek to maximize their respective objective functions, thereby leading to more accurate insights. In particular, in Paper IV, we consider a central planner creating an optimal plan for generation and transmission expansion, which may differ from the expansion plans made by multiple independent market participants. However, EPEC problems are computationally challenging to solve and solution algorithms may fail to find a Nash equilibrium among all the agents [21].

The models used in Papers I-IV are limited in the number of operational details and the size of the problem instances partly because of limited computational capacity. While we developed more efficient solution methods to make the problem instances tractable, it is expected that increasing computational capacity will make it possible to solve larger model instances. Also, advances in solution techniques such as approximation methods [25] will be useful to researchers and practitioners in this regard.

The results of Papers I-IV are generally well-founded as we have used out-of-sample simulations to show that our insights hold outside specific scenarios. Therefore, these papers provide a good starting point for many of the aforementioned modeling improvements and future research directions that can be expected to provide even more informative results to support the integration of VRES to power systems.

References

[1] N. Charlton and C. Singleton. A refined parametric model for short term load forecasting. *International Journal of Forecasting*, 30(2):364–368, 2014.

[2] Nord Pool. Intraday market, 2024. https://www.nordpoolgroup.com/en/the-power-market/Intraday-market/.

[3] United Nations. Paris agreement, 2015. https://unfccc.int/sites/default/files/english_paris_agreement.pdf.

[4] United Nations. 1.5°C: what it means and why it matters, 2024. https://www.un.org/en/climatechange/science/climate-issues/degrees-matter.

[5] United States Environmental Protection Agency. Global greenhouse gas overview, 2024. https://www.epa.gov/ghgemissions/global-greenhouse-gas-overview.

[6] K. Hansen, B.V. Mathiesen, and I. R. Skov. Full energy system transition towards 100% renewable energy in Germany in 2050. *Renewable and Sustainable Energy Reviews*, 102:1–13, 2019.

[7] P. Colbertaldo, S. B. Agustin, S. Campanari, and J. Brouwer. Impact of hydrogen energy storage on California electric power system: Towards 100% renewable electricity. *International Journal of Hydrogen Energy*, 44(19):9558–9576, 2019.

[8] M. Esteban, J. Portugal-Pereira, B. C. Mclellan, J. Bricker, H. Farzaneh, N. Djalilova, K. N. Ishihara, H. Takagi, and V. Roeber. 100% renewable energy system in Japan: Smoothening and ancillary services. *Applied Energy*, 224:698–707, 2018.

[9] European Commission. EU climate action, 2019. https://ec.europa.eu/clima/citizens/eu_en.

[10] J. Winkler, A. Gaio, B. Pfluger, and M. Ragwitz. Impact of renewables on electricity markets – do support schemes matter? *Energy Policy*, 93:157–167, 2016.

[11] K. Van den Bergh, D. Couckuyt, E. Delarue, and W. D'haeseleer. Redispatching in an interconnected electricity system with high renewables penetration. *Electric Power Systems Research*, 127:64–72, 2015.

[12] M. Kozlova, K. Huhta, and A. Lohrmann. The interface between support schemes for renewable energy and security of supply: Reviewing capacity mechanisms and support schemes for renewable energy in Europe. *Energy Policy*, 181:113707, 2023.

[13] X. Chen, J. Lv, M. B. McElroy, X. Han, C. P. Nielsen, and J. Wen. Power system capacity expansion under higher penetration of renewables considering flexibility constraints and low carbon policies. *IEEE Transactions on Power Systems*, 33(6):6240–6253, 2018.

[14] S. Yin and J. Wang. Generation and transmission expansion planning towards a 100% renewable future. *IEEE Transactions on Power Systems*, 37(4):3274–3285, 2022.

[15] M. McPherson and B. Stoll. Demand response for variable renewable energy integration: A proposed approach and its impacts. *Energy*, 197:117205, 2020.

[16] M. Auguadra, D. Ribó-Pérez, and T. Gómez-Navarro. Planning the deployment of energy storage systems to integrate high shares of renewables: The Spain case study. *Energy*, 264:126275, 2023.

[17] J. M. Morales, M. Zugno, S. Pineda, and P. Pinson. Electricity market clearing with improved scheduling of stochastic production. *European Journal of Operational Research*, 235(3):765–774, 2014.

[18] J. Mauritzen. Dead battery? Wind power, the spot market, and hydropower interaction in the Nordic electricity market. *The Energy Journal*, 34(1):103–123, 2013.

[19] J. C. Ketterer. The impact of wind power generation on the electricity price in Germany. *Energy Economics*, 44:270–280, 2014.

[20] J. Lago, G. Marcjasz, B. De Schutter, and R. Weron. Forecasting day-ahead electricity prices: A review of state-of-the-art algorithms, best practices and an open-access benchmark. *Applied Energy*, 293:116983, 2021.

[21] S. A. Gabriel, A. J. Conejo, J. D. Fuller, B. F. Hobbs, and C. Ruiz. *Complementarity Modeling in Energy Markets*. Springer, 2012.

[22] S. A. Gabriel and F. U. Leuthold. Solving discretely-constrained MPEC problems with applications in electric power markets. *Energy Economics*, 32(1):3–14, 2010.

[23] L. Baringo and A. Baringo. A stochastic adaptive robust optimization approach for the generation and transmission expansion planning. *IEEE Transaction on Power Systems*, 33(1):792–802, 2018.

[24] B. F. Hobbs. Optimization methods for electric utility resource planning. *European Journal of Operational Research*, 83(1):1–20, 1995.

[25] R. Mínguez, R. García-Bertrand, J. M. Arroyo, and N. Alguacil. On the solution of large-scale robust transmission network expansion planning under uncertain demand and generation capacity. *IEEE Transactions on Power Systems*, 33(2):1242–1251, 2018.

[26] J. Li, Z. Li, F. Liu, H. Ye, X. Zhang, S. Mei, and N. Chang. Robust coordinated transmission and generation expansion planning considering ramping requirements and construction periods. *IEEE Transactions on Power Systems*, 33(1):268–280, 2018.

[27] R. H. Shumway and D. S. Stoffer. *Time Series Analysis and Its Applications: With R Examples*. Springer, 2011.

[28] R Core Team. ARIMA modelling of time series, 2024. https://stat.ethz.ch/R-manual/R-devel/library/stats/html/arima.html.

[29] M. Lehna, F. Scheller, and H. Herwartz. Forecasting day-ahead electricity prices: A comparison of time series and neural network models taking external regressors into account. *Energy Economics*, 106:105742, 2022.

[30] I. Goodfellow, Y. Bengio, and A. Courville. *Deep Learning*. MIT Press, 2016. http://www.deeplearningbook.org.

[31] S. Boyd and L. Vandenberghe. *Convex Optimization*. Cambridge University Press, 2009.

[32] Gurobi Optimization, LLC. Mixed-Integer Programming (MIP) – A Primer on the Basics, 2024. https://www.gurobi.com/resources/mixed-integer-programming-mip-a-primer-on-the-basics/.

[33] Nord Pool. Price calculation, 2023. https://www.nordpoolgroup.com/en/trading/Day-ahead-trading/Price-calculation/.

[34] A. Sinha, P. Malo, and K. Deb. A review on bilevel optimization: From classical to evolutionary approaches and applications. *IEEE Transactions on Evolutionary Computation*, 22(2):276–295, 2018.

[35] L. Baringo and A. J. Conejo. Transmission and wind power investment. *IEEE Transactions on Power Systems*, 27(2):885–893, 2012.

[36] L.A. Barroso, R.D. Carneiro, S. Granville, M. V. Pereira, and M. H. C. Fampa. Nash equilibrium in strategic bidding: a binary expansion approach. *IEEE Transactions on Power Systems*, 21(2):629–638, 2006.

[37] J. R. Birge and F. Louveaux. *Introduction to Stochastic Programming*. Springer, 2011.

[38] D. Bertsimas, D. B. Brown, and C. Caramanis. Theory and applications of robust optimization. *SIAM Review*, 53(3):464–501, 2011.

[39] A. Moreira, D. Pozo, A. Street, and E. Sauma. Reliable renewable generation and transmission expansion planning: Co-optimizing system's resources for meeting renewable targets. *IEEE Transactions on Power Systems*, 32(4):3246–3257, 2017.

[40] D. Bertsimas, E. Litvinov, X. A. Sun, J. Zhao, and T. Zheng. Adaptive robust optimization for the security constrained unit commitment problem. *IEEE Transactions on Power Systems*, 28(1):52–63, 2013.

[41] L. Baringo and A. J. Conejo. Correlated wind-power production and electric load scenarios for investment decisions. *Applied Energy*, 101:475–482, 2013.

[42] Chris Piech. K means, 2013. https://stanford.edu/~cpiech/cs221/handouts/kmeans.html.

[43] P. Nahmmacher, E. Schmid, L. Hirth, and B. Knopf. Carpe diem: A novel approach to select representative days for long-term power system modeling. *Energy*, 112:430–442, 2016.

[44] J. Mauritzen. What happens when it's windy in Denmark? An empirical analysis of wind power on price volatility in the Nordic electricity market. *Discussion Papers 2010/18, Department of Business and Management Science, Norwegian School of Economics.*, 2010.

[45] T. Jónsson, P. Pinson, and H. Madsen. On the market impact of wind energy forecasts. *Energy Economics*, 32(2):313–320, 2010.

[46] F. Kunz. Improving congestion management: How to facilitate the integration of renewable generation in Germany. *The Energy Journal*, 34(4):55–78, 2013.

[47] M. Huber, D. Dimkova, and T. Hamacher. Integration of wind and solar power in Europe: Assessment of flexibility requirements. *Energy*, 69:236–246, 2014.

[48] A. Cardoso Marques, J. Alberto Fuinhas, and D. Pereira Macedo. The impact of feed-in and capacity policies on electricity generation from renewable energy sources in Spain. *Utilities Policy*, 56:159–168, 2019.

[49] T. Dai and W. Qiao. Optimal bidding strategy of a strategic wind power producer in the short-term market. *IEEE Transactions on Sustainable Energy*, 6(3):707–719, 2015.

[50] R. Mínguez and R. García-Bertrand. Robust transmission network expansion planning in energy systems: Improving computational performance. *European Journal of Operational Research*, 248(1):21–32, 2016.

[51] K. Maciejowska. Assessing the impact of renewable energy sources on the electricity price level and variability – a quantile regression approach. *Energy Economics*, 85:104532, 2020.

[52] E. Hosius, J. V. Seebaß, B. Wacker, and J. C. Schlüter. The impact of offshore wind energy on Northern European wholesale electricity prices. *Applied Energy*, 341:120910, 2023.

[53] D. Pereira Macedo, A. Cardoso Marques, and O. Damette. The impact of the integration of renewable energy sources in the electricity price formation: is the merit-order effect occurring in Portugal? *Utilities Policy*, 66:101080, 2020.

[54] A. Rai and O. Nunn. On the impact of increasing penetration of variable renewables on electricity spot price extremes in Australia. *Economic Analysis and Policy*, 67:67–86, 2020.

[55] B. Ehsani, P.-O. Pineau, and L. Charlin. Price forecasting in the Ontario electricity market via TriConvGRU hybrid model: Univariate vs. multivariate frameworks. *Applied Energy*, 359:122649, 2024.

[56] C. Gilbert, J. W. Messner, P. Pinson, P.-J. Trombe, R. Verzijlbergh, P. van Dorp, and H. Jonker. Statistical post-processing of turbulence-resolving weather forecasts for offshore wind power forecasting. *Wind Energy*, 23(4):884–897, 2020.

[57] C. Hohl, C. Lo Prete, A. Radhakrishnan, and M. Webster. Intraday markets, wind integration and uplift payments in a regional U.S. power system. *Energy Policy*, 175:113503, 2023.

[58] J. Kazempour and B. F. Hobbs. Value of flexible resources, virtual bidding, and self-scheduling in two-settlement electricity markets with wind generation—part II: ISO models and application. *IEEE Transactions on Power Systems*, 33(1):760–770, 2018.

[59] R. Sioshansi, P. Denholm, T. Jenkin, and J. Weiss. Estimating the value of electricity storage in PJM: Arbitrage and some welfare effects. *Energy Economics*, 31(2):269–277, 2009.

[60] S. Jerez, R.M. Trigo, A. Sarsa, R. Lorente-Plazas, D. Pozo-Vázquez, and J.P. Montávez. Spatio-temporal complementarity between solar and wind power in the Iberian peninsula. *Energy Procedia*, 40:48–57, 2013.

[61] H. Weigt, T. Jeske, F. Leuthold, and C. von Hirschhausen. “Take the long way down”: Integration of large-scale North Sea wind using HVDC transmission. *Energy Policy*, 38(7), 2010.

Publication I

T. Rintamäki, A. S. Siddiqui, and A. Salo. Does renewable energy generation decrease the volatility of electricity prices? An analysis of Denmark and Germany. *Energy Economics*, 62, 270-282, 2017.

Energy Economics 62 (2017) 270–282

Contents lists available at ScienceDirect

Energy Economics

journal homepage: www.elsevier.com/locate/eneco

Does renewable energy generation decrease the volatility of electricity prices? An analysis of Denmark and Germany

Tuomas Rintamäki[a], Afzal S. Siddiqui[b,c,*], Ahti Salo[a]

[a]Systems Analysis Laboratory, Department of Mathematics and Systems Analysis, School of Science, Aalto University, Finland
[b]Department of Statistical Science, University College London, UK
[c]Department of Computer and Systems Sciences, Stockholm University, Sweden

ARTICLE INFO

Article history:
Received 20 April 2016
Received in revised form 6 December 2016
Accepted 30 December 2016
Available online 11 January 2017

JEL classification:
C22
Q41
Q42

Keywords:
Electricity price volatility
Time-series model
Wind power
Solar power
Nord Pool
EEX

ABSTRACT

Although variable renewable energy (VRE) technologies with zero marginal costs decrease electricity prices, the literature is inconclusive about how the resulting shift in the supply curves impacts price volatility. Because the flexibility to respond to high peak and low off-peak prices is crucial for demand-response applications and may compensate for the losses of conventional generators caused by lower average prices, there is a need to understand how the penetration of VRE affects volatility. In this paper, we build distributed lag models with Danish and German data to estimate the impact of VRE generation on electricity price volatility. We find that in Denmark wind power decreases the daily volatility of prices by flattening the hourly price profile, but in Germany it increases the volatility because it has a stronger impact on off-peak prices. Our analysis suggests that access to flexible generation capacity and wind power generation patterns contribute to these differing impacts. Meanwhile, solar power decreases price volatility in Germany. By contrast, the weekly volatility of prices increases in both areas due to the intermittency of VRE. Thus, policy measures for facilitating the integration of VRE should be tailored to such region-specific patterns.

1. Introduction

The adoption of variable renewable energy (VRE) technologies is having profound consequences for the electric power industry. For example, buttressed by subsidies and priority grid access, solar and wind power generation in Germany comprised 25% of national electricity output in 2013 and facilitated a 30% reduction in CO_2 emissions relative to 1990 levels (von Hirschhausen, 2014). Likewise, neighbouring Denmark has adopted VRE-friendly policies enabling it to meet nearly 40% of its electricity needs through wind (Energinet.dk, 2015). However, similar shares of VRE generation in different electricity markets have resulted in contrasting effects on daily price volatility, which will affect the profitability of conventional power plants. Indeed, via a supply-function equilibrium model, Green and Vasilakos (2010) demonstrate that the incorporation of intermittent renewable resources can increase price volatility in the British electricity industry. Such a change in market will likely lead to an optimal generation mix using more gas-fired plants in the long run (Green and Vasilakos, 2011). Hence, understanding how VRE generation affects price volatility and uncovering the drivers of these effects is important for both power companies and regulators dealing with a transition to a more sustainable energy system.

While fundamental models are often used to examine policy implications, e.g., in terms of transmission expansion to accommodate increased VRE capacity (Egerer et al., 2013), such models need to be sufficiently detailed to capture the subtle changes that we seek to detect here. In particular, building and calibrating large-scale fundamental models with interconnected regions is often confounded by the complexities of deregulated electricity industries and the associated data requirements at the plant level, for example. By contrast, since the electricity industry is one of the few infrastructure industries with liquid markets and publicly available data on prices as well as cross-border transmission flows, we exploit this feature in taking an empirical approach to understand the effects of VRE generation on price volatility in Danish and German electricity markets.

Our methodology is largely based on Mauritzen (2010) who represents the volatility of prices via a seasonal autoregressive

* Corresponding author.
E-mail addresses: tuomas.rintamaki@aalto.fi (T. Rintamäki), afzal.siddiqui@ucl.ac.uk (A.S. Siddiqui), ahti.salo@aalto.fi (A. Salo).

http://dx.doi.org/10.1016/j.eneco.2016.12.019
0140-9883/

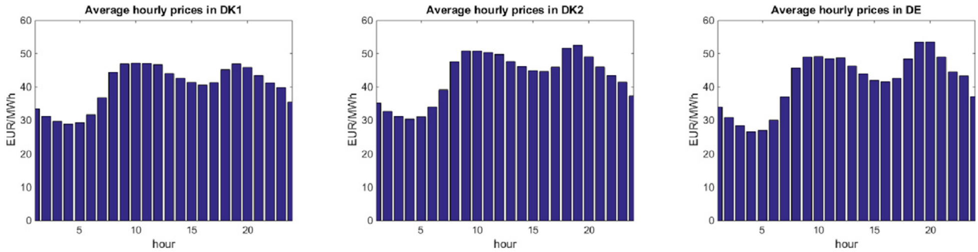

(a) DK1. (b) DK2. (c) DE.

Fig. 1. Average hourly electricity prices for DK1, DK2, and DE from 2010 to 2014.

moving average (SARMA) model in which wind power production is an exogenous variable. This methodology yields results that are straightforward to interpret and makes it possible to develop forecasts for electricity price volatility based on the data from previous days and information on regular consumption patterns. His conclusion is that Danish wind power decreases the daily volatility of the area prices in Denmark. On the contrary, Ketterer (2014) uses a generalised autoregressive conditional heteroscedasticity (GARCH) model and finds that German wind power increases the daily volatility of German electricity prices. Explaining these results using data from the two markets and distilling their implications for electricity markets in general is the objective of this paper.

We proceed by first confirming the differing impacts of wind power on price volatility in these two markets and then explaining them by dividing the dataset into peak and off-peak hours with separate regressions for each subset of hours. This allows us to analyse changes in volatility by relating them to supply-curve elasticities and to the patterns of wind and solar power production as well as cross-border exchanges. Partitioning the dataset reveals that wind power output decreases daily price volatility in Denmark because wind speeds are roughly evenly distributed throughout the day. Relative to its average electricity demand, Denmark has high transmission capacity to the Nordic countries with large hydropower reservoirs, which may also explain Denmark's reduction in daily price volatility as both peak and off-peak hour prices are estimated to decrease nearly equally due to wind power generation. In Germany, however, there is an increase in price volatility because of greater wind power output during off-peak hours. Moreover, Germany's cross-border transmission lines are smaller relative to its average electricity demand, and it has limited access to flexible hydro generation. As a consequence, prices diverge as the price-decreasing impact of wind power is amplified during off-peak hours. Over a weekly time horizon, the level and the standard deviation of total VRE generation are found to increase the weekly volatility of electricity prices in both countries.

For producers and consumers alike, our empirical analysis not only corroborates earlier findings but also explains them by proposing plausible drivers. The implication of our results is that the allocation of generation and demand is becoming more important as average power prices decrease, but the achievable profit on different days varies significantly. To prevent intermittent renewable generation from threatening the stability of the power system, investments in flexible generation, extensions to the transmission network, integration of adjacent markets, and demand response will be required in the future. Moreover, additional trading opportunities by both producers and large consumers in intraday and balancing markets may be desirable (Mauritzen, 2015).

This paper is organised as follows. In Section 2, we review the literature on the impacts of VRE on Danish and German electricity markets, in particular. In Section 3, we present our model and analyse the time-series data. Section 4 presents the results for the effects of VRE generation on daily and weekly volatility. Finally, in Section 5, we provide conclusions and discuss directions for future research. Details on model selection and robustness checks are provided in the Appendix.

2. Literature review

The adoption of wind and solar generation technologies worldwide has necessitated a need to assess both the availability of resources (Yip et al., 2016) and their impact on electricity markets (González-Aparicio and Zucker, 2015). Many studies have investigated the effect of wind power production on price levels and

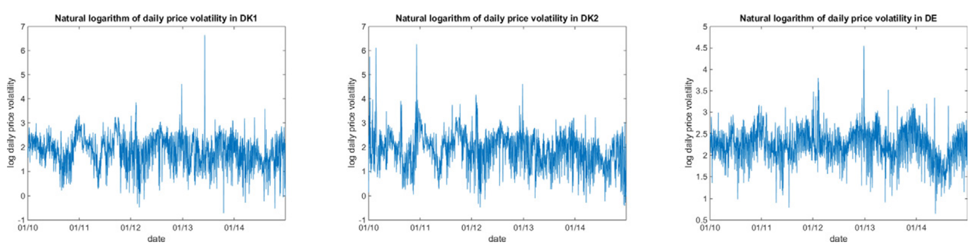

(a) DK1. (b) DK2. (c) DE.

Fig. 2. The natural logarithm of daily price volatility of DK1, DK2, and DE prices from 2010 to 2014.

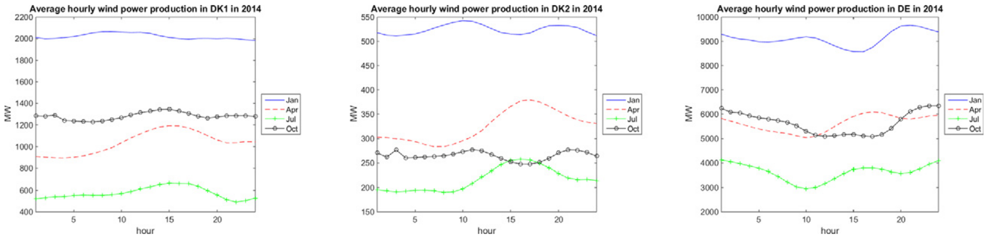

(a) DK1. (b) DK2. (c) DE.

Fig. 3. Average hourly wind power in DK1, DK2, and DE in selected months in 2014.

reached the common conclusion that wind power decreases prices. For example, Jónsson et al. (2010) employ the same hourly Danish wind power forecast data that are used by market players to place their bids. They build a non-parametric regression model to study price levels as well as the distribution of the prices at different wind power levels. Their conclusion is that higher wind power penetration in the day-ahead market decreases Danish prices and volatility substantially.

In Germany, price volatility has been studied by incorporating various market-related measures as exogenous variables (Kalantzis and Milonas, 2013; Frömmel et al., 2014). Only recently have there been studies on the direct effects of growing capacity of wind and solar power on electricity prices. Ketterer (2014) finds that higher wind power production leads to higher daily volatility. Moreover, she notes that regardless of the regulatory change in 2010, which forced the German transmission system operators to publish day-ahead forecasts for VRE generation in their area, the volatility-increasing effect has prevailed. Because the price-decreasing impact of solar power is stable during peak hours (Paraschiv et al., 2014), it is likely that solar power decreases price volatility.

Besides patterns of solar and wind power production, transmission flows also affect the volatility of electricity prices as suggested by the complementarity model by Morales et al. (2011), who use wind power scenarios as inputs. By adopting the same time-series framework as in Mauritzen (2010) and Mauritzen (2013) investigates how wind power affects the cross-border transmission of electricity between Denmark and Norway. His conclusion is that when more (less) wind power is produced in Denmark, exports to (imports from) Norway are higher while Norwegian hydropower plants produce less (more). Zugno et al. (2013) find a similar pattern between Germany and hydro-dominant Austria and Switzerland, but these transmission lines are closer to congestion. Moreover, the flow to the Nordic countries from Germany is low, and the flow to its neighbouring countries with inflexible generation such as France does not respond much to changes in wind power.

Building on assumptions about extended cross-border transmission and VRE capacity in 2030, Jaehnert et al. (2013) find that price spikes and dips become more frequent in the European power market. Due to the large price difference between the Nordic and German markets, also additional investments in transmission capacity become optimal. In similar scenarios, Farahmand et al. (2012) find that the integration of Nordic and German balancing markets via simultaneous dispatching can reduce balancing costs considerably because VRE generation forecast errors with opposite signs can be netted.

In addition to explaining the results of Ketterer (2014) and Mauritzen (2010), our approach of dividing the data into off-peak and peak hours contributes to the literature on estimating the impact of renewable generation on electricity price levels (see Würzburg et al., 2013; Mulder and Scholtens, 2013; Paraschiv et al., 2014; Gelabert et al., 2011, for example) by providing insights on how the price-decreasing impact is distributed during the day. To this end, Barthelmie et al. (1996) and Holttinen (2005) suggest that Danish wind power peaks in the afternoon and the effect is more pronounced in summers. On the other hand, He et al. (2012) and Huber et al. (2014) show that German wind power tends to peak at night and also in summer afternoons.

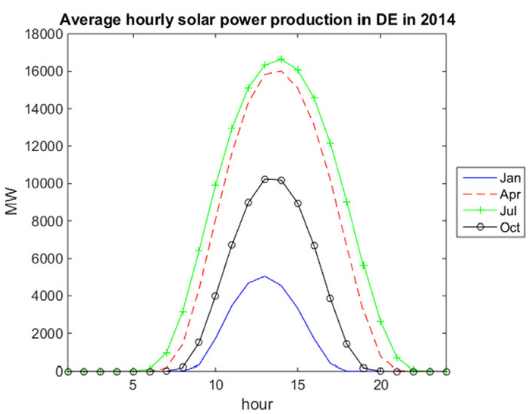

Fig. 4. Average hourly solar power in DE in selected months in 2014.

3. Methodology and data

3.1. Model

To estimate the effect of exogenous variables such as wind and solar power on a dependent variable of interest such as electricity price volatility, we use the seasonally adjusted autoregressive moving average (SARMA(p,q)(P,Q)[s]) model (Shumway and Stoffer, 2011):

$$v_t = \alpha_0 + \sum_{i=1}^{p} \alpha_i v_{t-i} + \sum_{i=1}^{q} \beta_i \epsilon_{t-i} + \sum_{i=1}^{P} \alpha_{i \bullet s} v_{t-i \bullet s} + \sum_{i=1}^{Q} \beta_{i \bullet s} \epsilon_{t-i \bullet s} + \epsilon_t + \gamma^{\top} x_t, \quad (1)$$

where v_t is the dependent variable during time period t and x_t a vector of exogenous variables. There are p autoregressive (AR) terms v_{t-i}, q moving average (MA) terms ϵ_{t-i}, P seasonal autoregressive

Table 1
Exogenous variables in our models. We take the natural logarithm of all variables except $exim_d^{op1}$, $exim_d^{op2}$, $exim_d^{p}$, and $exim_w$.

Variable	Explanation
v_d	Standard deviation of hourly prices on day d (€/MWh)
p_d^{op1}	Average off-peak 1 prices on day d (€/MWh)
p_d^{op2}	Average off-peak 2 prices on day d (€/MWh)
p_d^{p}	Average peak prices on day d (€/MWh)
$wind_d$	Average wind power on day d (MW)
$wind_d^{op1}$	Average off-peak 1 wind power on day d (MW)
$wind_d^{op2}$	Average off-peak 2 wind power on day d (MW)
$wind_d^{p}$	Average peak wind power on day d (MW)
$wind\_pen_d$	Average wind power penetration on day d
$wind\_pen_d^{op1}$	Average off-peak 1 wind power penetration on day d
$wind\_pen_d^{op2}$	Average off-peak 2 wind power penetration on day d
$wind\_pen_d^{p}$	Average peak wind power penetration on day d
$solar_d$	Average solar power on day d (MW)
$solar_d^{p}$	Average peak solar power on day d (MW)
$solar\_pen_d$	Average solar power penetration on day d
$solar\_pen_d^{p}$	Average peak solar power penetration on day d
vre_d	Average wind and solar power on day d (MW)
vre_d^{p}	Average peak wind and solar power on day d (MW)
vre_pen_d	Average wind and solar power penetration on day d
$vre\_pen_d^{p}$	Average peak wind and solar power penetration on day d
$exim_d^{op1}$	Average off-peak 1 export/import on day d (GW)
$exim_d^{op2}$	Average off-peak 2 export/import on day d (GW)
$exim_d^{p}$	Average peak export/import on day d (GW)
gas_d	Average spot gas price on day d (€/MWh)
v_w	Standard deviation of daily average prices during week w (€/MWh)
$wind_w$	Average wind power during week w (MW)
$wind_w^{std}$	Standard deviation of average daily wind power outputs during week w (MW)
$wind\_pen_w$	Average wind power penetration during week w
$solar_w$	Average solar power during week w (MW)
$solar\_pen_w$	Average solar power penetration during week w
vre_w	Average wind and solar power during week w (MW)
vre_w^{std}	Standard deviation of average daily wind and solar power outputs during week w (MW)
vre_pen_w	Average wind and solar power penetration during week w
$exim_w$	Average export/import during week w (GW)
gas_w	Average gas price during week w (€/MWh)

(SAR) terms $v_{t-i \cdot s}$ with periodicity of s, and Q seasonal moving average (SMA) terms $\epsilon_{t-i \cdot s}$ with periodicity of s with the coefficients α_i, β_i, $\alpha_{i \cdot s}$, and $\beta_{i \cdot s}$, respectively. In other words, the terms v_{t-i} are lagged values of v_t and ϵ_{t-i} Gaussian white noise error terms. The impact of the exogenous variables on price volatility is estimated by the parameter vector γ using R (R Core Team, 2015).

3.2. Summary statistics

Our data for the two Danish areas (Western Denmark, DK1 and Eastern Denmark, DK2) consist of hourly area prices (in €/MWh), forecasted hourly wind power production (in MW), forecasted hourly demand (in MW), and hourly cross-border flows between

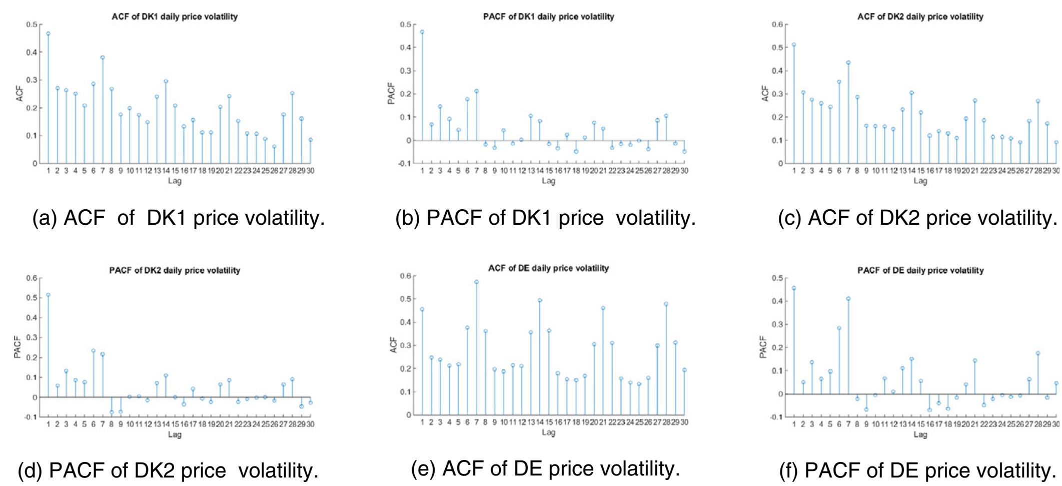

(a) ACF of DK1 price volatility. (b) PACF of DK1 price volatility. (c) ACF of DK2 price volatility.

(d) PACF of DK2 price volatility. (e) ACF of DE price volatility. (f) PACF of DE price volatility.

Fig. 5. ACF and PACF plots of DK1, DK2, and DE daily price volatility.

Table 2
The effect of different explanatory variables on DK1 daily price volatility. All coefficients are statistically significant at the 1% level unless otherwise noted.

Variable	Model					
	Model 1	Model 2	Model 3	Model 4	Model 5	Model 6
$wind_d$	−0.0892		−0.0731	−0.0906		−0.0889
	(0.0158)		(0.0193)	(0.0194)		(0.0158)
$wind\_pen_d$		−0.0867			−0.0879	
		(0.0160)			(0.0198)	
$exim_d^{op1}$			0.0641[b]	0.1004	0.1017	
			(0.0328)	(0.0331)	(0.0334)	
$exim_d^{p}$			0.0783[a]	−0.0806	−0.0850	
			(0.0374)	(0.0308)	(0.0307)	
$exim_d^{op2}$			−0.2241			
			(0.0305)			
Δgas_d						0.3324[c]
						(0.4080)
α_0	2.3918	1.7080	2.2531	2.3566	1.6605	2.3649
α_1	1.2236	1.2210	1.2546	1.2450	1.2437	1.2210
α_2	−0.2526	−0.2504	−0.2787	−0.2728	−0.2718	−0.2510
α_7	1.0711	1.0706	1.0811	1.0751	1.0747	1.0699
α_{14}	−0.0726	−0.0721	−0.08232	−0.0769	−0.0766	−0.0731
β_1	−0.8635	−0.8632	−0.8698	−0.8669	−0.8666	−0.8625
β_7	−0.9804	−0.9804	−0.9825	−0.9792	−0.9791	−0.9803
AIC	2878.82	2881.50	2820.47	2871.62	2873.72	2879.57
L-B	30	30	28	30	30	30

[a] Significant at 5% level.
[b] Significant at 10% level.
[c] Not significant.

zones DK1-NO2, DK1-SE3, and DK2-SE4 (in MW) in the day-ahead spot market (data source: Nord Pool Spot, 2016). We ignore Danish solar power because of its negligible capacity (Energinet.dk, 2014). For Germany (DE), we use hourly German prices (in €/MWh, Epex Spot, 2016), forecasted hourly wind and solar power production (in MW, EEX Transparency, 2016), forecasted hourly demand (in MW, ENTSO-E Transparency, 2016b), and hourly cross-border flows between Germany and France (in MW, ENTSO-E Transparency, 2016a). We account for fuel prices by including the daily natural gas spot price (in €/MWh, at the NetConnect Germany hub, Bloomberg, 2016). The dataset spans 1 January 2010 to 31 December 2014 and 1 January 2012 to 31 December 2014 for Denmark and Germany, respectively. The dataset for Germany is restricted by public data on cross-border flows.

Because prices are calculated by the exchanges, there are no measurement uncertainties or gaps. We employ VRE and demand forecasts for modelling instead of realised values because only forecasts are available for market participants when determining their bids to the day-ahead market. Thus, prices and volatility are affected by bidding decisions, which might have been different under perfect knowledge of forecast errors. For Germany, there are a few missing days in the ENTSO-E demand forecast time series; for these, we use realised values. Following the convention of the exchanges, we also divide the dataset into three blocks called off-peak 1 hours (from 12

Table 3
The effect of different explanatory variables on DK2 daily price volatility. All coefficients are statistically significant at the 1% level unless otherwise noted.

Variable	Model					
	Model 1	Model 2	Model 3	Model 4	Model 5	Model 6
$wind_d$	−0.0696		−0.0517	−0.0604		−0.0686
	(0.0147)		(0.0164)	(0.0165)		(0.0146)
$wind\_pen_d$		−0.0654			−0.0544	
		(0.0149)			(0.0167)	
$exim_d^{op1}$			−0.0171[a]	−0.0070[a]	−0.0119[a]	
			(0.0418)	(0.0430)	(0.0433)	
$exim_d^{p}$			0.1462	−0.0474[a]	−0.0516[a]	
			(0.0481)	(0.0416)	(0.0416)	
$exim_d^{op2}$			−0.3060			
			(0.0395)			
Δgas_d						−0.3214[a]
						(0.4306)
α_0	2.2065	1.7110	2.0966	2.1547	1.7289	2.2035
α_1	1.2329	1.2302	1.2677	1.2313	1.2289	1.2305
α_2	−0.2685	−0.2660	−0.2960	−0.2679	−0.2658	−0.2673
α_7	1.1054	1.1066	1.1078	1.1045	1.1060	1.1046
α_{14}	−0.1058	−0.1069	−0.1081	−0.1050	−0.1063	−0.1050
β_1	−0.8378	−0.8371	−0.8504	−0.8332	−0.8329	−0.8368
β_7	−0.9886	−0.9904	−0.9912	−0.9875	−0.9894	−0.9875
AIC	3159.90	3163.27	3106.16	3162.16	3164.78	3134.09
L-B	30	30	30	30	30	9

[a] Not significant.

Table 4
The effect of different explanatory variables on DE price volatility. All coefficients are statistically significant at the 1% level unless otherwise noted.

	Model								
Variable	Model 1	Model 2	Model 3	Model 4	Model 5	Model 6	Model 7	Model 8	Model 9
$wind_d$	0.0328[a]		0.0296[a]					0.0367[a]	0.0320[a]
	(0.0146)		(0.0147)					(0.0147)	(0.0148)
$\Delta solar_d$		−0.0379[a]	−0.0350[b]					−0.0205[c]	−0.0339[b]
		(0.0191)	(0.0191)					(0.0191)	(0.0191)
vre_d				0.0187[c]					
				(0.0227)					
$wind\_pen_d$					0.0350[a]				
					(0.0147)				
$\Delta solar\_pen_d$						−0.0466[a]			
						(0.0187)			
vre_pen_d							0.0203[c]		
							(0.0220)		
$exim_d^{op1}$								0.0853	
								(0.0117)	
$exim_d^{p}$								−0.0781	
								(0.0137)	
$exim_d^{op2}$								0.0211[c]	
								(0.0134)	
Δgas_d									−0.3840[c]
									(0.3308)
α_0	1.9167	2.2698	2.0009	2.0691	2.3221	2.2432	2.2764	1.9351	1.9710
α_1	1.1513	1.1657	1.1613	1.1459	1.1525	1.1675	1.1532	1.1508	1.1615
α_2	−0.1622	−0.1752	−0.1711	−0.1576	−0.1633	−0.1773	−0.1637	−0.1623	−0.1716
α_7	1.1764	1.1724	1.1749	1.1717	1.1770	1.1722	1.1737	1.1686	1.1788
α_{14}	−0.1766	−0.1725	−0.1752	−0.1719	−0.1772	−0.1724	−0.1739	−0.1688	−0.1789
β_1	−0.9165	−0.9168	−0.9190	−0.9108	−0.9167	−0.9163	−0.9140	−0.9276	−0.9189
β_7	−0.9896[c]	−0.9911	−0.9870	−0.9885	−0.9890	−0.9910	−0.9898	−0.9888	−0.9914
AIC	487.73	488.60	486.92	492.33	487.13	486.39	491.88	434.13	486.92
L-B	30	30	30	30	30	30	30	30	30

[a] Significant at 5% level.
[b] Significant at 10% level.
[c] Not significant.

AM to 9 AM), peak hours (9 AM to 9 PM), and off-peak 2 hours (9 PM to 12 AM).

Our measure of price volatility for day d in Eq. (1) is the logarithm of the standard deviation calculated from hourly prices p_h and the average daily price $p_d = \frac{1}{24}\sum_{h=1}^{24} p_h$, i.e.,

$$v_d = \ln\left(\sqrt{\frac{1}{24}\sum_{h=1}^{24}(p_h - p_d)^2}\right). \tag{2}$$

As an example of longer time windows, we consider weekly price volatility, which is computed from daily average prices p_d and weekly average prices $p_w = \frac{1}{7}\sum_{d=1}^{7} p_d$.

$$v_w = \ln\left(\sqrt{\frac{1}{7}\sum_{d=1}^{7}(p_d - p_w)^2}\right) \tag{3}$$

We take the natural logarithm to make the time series stationary and to improve the model fit. Also, all exogenous variables x_t in Eq. (1) except for cross-border flows are transformed into natural logarithm form, and, thus, their coefficients γ can be interpreted as elasticities. This assumption of constant elasticity between the exogenous variables and price volatility is more reasonable than assuming that changes in demand, for example, lead to equal changes in price volatility at different demand levels. Because cross-border flows take positive and negative values depending on the direction of the flow, we scale the figures by 1000 MW to obtain values close to those of the logarithmic variables.

Fig. 1a, b, and c show the average hourly price profile for DK1, DK2, and DE, respectively, resulting from demand patterns. During morning and evening high-load hours, the price is usually driven by thermal plants with higher marginal costs of production. In low-load times, such as night time, prices are set by thermal plants lower in the merit order. On the other hand, Fig. 2a, b, and c show how the daily volatility of DK1, DK2, and DE prices has developed from 2010 to 2014, respectively. There is no clear increasing or decreasing trend in the price volatility of the areas, but the average volatility of Danish prices is lower than that of Germany.

Fig. 3a and b confirm that Danish wind power peaks in the afternoon. In turn, Fig. 3c shows that the production of German wind power is highest at night. The solar power profile in Germany is similar in each month with production only from 6 AM to 8 PM (Fig. 4). We define the wind and solar power penetration during period t as the share of average wind or solar power generation ($wind_t$, $solar_t$) of the average demand ($load_t$) during that period t.

$$wind\_pen_t = \frac{wind_t}{load_t} \quad \text{and} \quad solar\_pen_t = \frac{solar_t}{load_t} \tag{4}$$

3.3. Stability checks

We confirm the stationarity of the time series by applying the augmented Dickey–Fuller (ADF) test. Table 11 in the Appendix shows that all daily time series pass the test at the 10% level until lag 15 except for German solar power, solar power penetration, and gas price, which are differenced to make them stationary. For weekly data, since the gas price, Danish exports, German wind and solar power, and their penetration fail the test already at low lags, we difference these time series. Table 12 in the Appendix shows that all time series pass the test after differencing except for weekly average

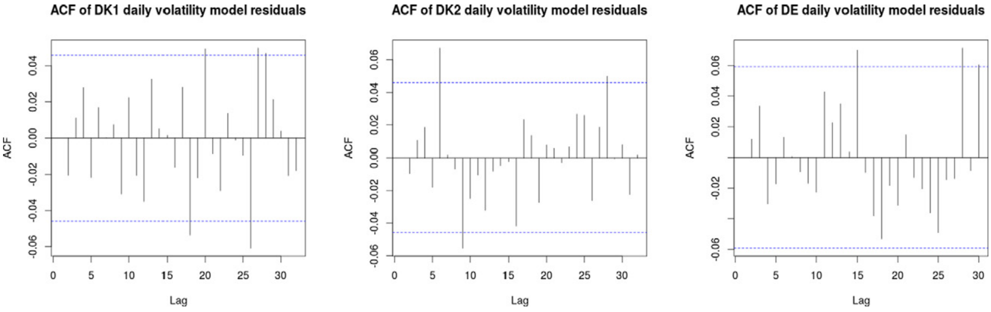

(a) DK1. (b) DK2. (c) DE.

Fig. 6. ACF plot of the residuals of the daily price volatility model 1 for DK1, DK2 and DE.

solar power generation and penetration, which reduces the robustness of the results on their impact. In the regressions, we will use the differenced variables prefixed with Δ whenever necessary. For the notation, please refer to Table 1.

Autocorrelation (ACF) and partial autocorrelation functions (PACFs) of the dependent variable in Eq. (1) can be used to specify the order (p,q)(P,Q)[s] of the model. The ACF and PACF of daily price volatility time series from DK1 and DK2 in Fig. 5a, b, c, and d, respectively, and from DE in Fig. 5e and f have high peaks at the first lag and then near multiples of seven indicating a weekly pattern in price volatility (Shumway and Stoffer, 2011). All autocorrelation functions have a downward trend as older data are less relevant.

For both Denmark and Germany, we select the model (1) by stepwise addition of independent variables starting from a SARMA(1,0)(1,0)[7] model, as indicated by the ACF and PACF plots. In the selection process, we omit all exogenous variables x_t and require all coefficients α and β to be statistically significant at the 5% level. If a variable in a particular model (p,q)(P,Q) becomes statistically insignificant, then we do not add new variables because they are likely to be insignificant, too. Also, if the addition of a new variable does not improve the Akaike Information Criterion (AIC) compared to the previous model, then we stop. To compare the candidates obtained in this process, we assess the AIC score, perform the Ljung-Box (L-B) test for residual autocorrelation, and examine the Q-Q, ACF, and PACF plots of the residuals of the models. Because of the large number of observations, we can expect to obtain unbiased estimators and residuals with little serial correlation. The model selection results are reported in Tables 13–15 of the Appendix, where we have omitted models that fail improve the AIC score or have insignificant variables.

We note that the optimal fit would be obtained if model (1) were to be specified separately for each subset of exogenous variables x_t. However, very different specifications could make it difficult to compare the effect of the exogenous variables. Therefore, we present results for alternative model specifications in Tables 16–18 of the Appendix to see the sensitivity of the results obtained using the above process.

4. Results

4.1. Daily volatility

We run separate regressions for both Danish areas, DK1 and DK2, and Germany, DE, to estimate the impact of different explanatory variables on the corresponding area price volatility. For all areas, we obtain the following SARMA(2,1)(2,1)[7] model (see Table 13 in the Appendix for model search iterations):

$$v_d = \alpha_0 + \alpha_1 v_{d-1} + \alpha_2 v_{d-2} + \alpha_7 v_{d-7} + \alpha_{14} v_{d-14} + \epsilon_d + \beta_1 \epsilon_{d-1} + \beta_7 \epsilon_{d-7}. \tag{5}$$

The AR(1) and AR(2) terms account for short-term price volatility development, and the SAR(1) and SAR(2) terms deal with the weekly seasonality in the data. Adding MA(1) and SMA(1) terms provides stochastic parts to the development of the price volatility and improves the fit of the model. Various exogenous variables with the associated parameters, i.e., the term $\gamma^\top x_t$ in Eq. (1), are added to the right-hand side of this model. For example, model 1 for DK1 in Table 2 is

$$\begin{aligned} v_d = {} & \alpha_0 + \alpha_1 v_{d-1} + \alpha_2 v_{d-2} + \alpha_7 v_{d-7} + \alpha_{14} v_{d-14} + \epsilon_d \\ & + \beta_1 \epsilon_{d-1} + \beta_7 \epsilon_{d-7} + \gamma\ wind_d. \end{aligned} \tag{6}$$

In Tables 2 and 3, the main finding is that the coefficient for wind power, $wind_d$, in DK1 at −0.0892 and in DK2 at −0.0696 in model 1 is statistically significantly different from zero at the 1% level according to a *Z*-test. For both areas, the interpretation is that increasing the amount of daily wind power production by 1% decreases the daily volatility of prices by 0.06–0.09%.[1] The effect is slightly stronger in DK1 than DK2, most likely due to the combination of higher wind power capacity and lower demand in DK1. Moreover, model 2 in Tables 2 and 3 indicates that the higher the wind power penetration, $wind\_pen_d$, is, the lower the price volatility.

Mauritzen (2010) runs similar regressions with a SARMA(2,2)(1,2)[7] model. Our result for DK1 is in line with Mauritzen, but his estimate for the coefficient for DK2 is not statistically significant. The most probable explanation for the difference is that his data span 2002 to 2007, whereas our more recent dataset includes higher wind power capacity in DK2, and, thus, its market impact is likely to be stronger.

In models 3 and 4, we control for exports to and imports from hydro-dominant Sweden and Norway in morning off-peak, peak, and evening off-peak hours ($exim_d^{op1}$, $exim_d^{p}$, and $exim_d^{op2}$, respectively)

[1] Consider a model $\ln y = \alpha + \beta^\top z + \gamma \ln x$. Fixing z, with two different values, x_2 and x_1, we have $\ln y_2 - \ln y_1 = \gamma(\ln x_2 - \ln x_1) \iff \ln \frac{y_2}{y_1} = \gamma \ln \frac{x_2}{x_1} \iff \frac{y_2 - y_1}{y_1} = \left(\frac{x_2}{x_1}\right)^\gamma - 1$. Numerically, the approximation $\frac{y_2-y_1}{y_1} \approx \gamma\left(\frac{x_2-x_1}{x_1}\right)$ deviates from the true value of $\frac{y_2-y_1}{y_1}$ by less than 0.004 percentage points when $\frac{x_2-x_1}{x_1} = 0.01$ and $|\gamma| \leq 0.5$.

Table 5
The effect of different explanatory variables on DK1 price level in each block. All coefficients are statistically significant at the 1% level.

	Block					
Variable	Off-peak 1	Off-peak 1	Peak	Peak	Off-peak 2	Off-peak 2
$wind_d$	−0.1090		−0.0726		−0.0647	
	(0.0092)		(0.0052)		(0.0051)	
$wind\_pen_d$		−0.1153		−0.0791		−0.0667
		(0.0092)		(0.0052)		(0.0051)
$exim_d$	−0.1454	−0.1373	−0.1073	−0.0996	−0.0865	−0.0854
	(0.0183)	(0.0182)	(0.0091)	(0.0091)	(0.0088)	(0.0087)
α_0	4.1465	3.3179	4.1694	3.5878	4.0406	3.5412
α_1	1.1511	1.1505	1.1730	1.1687	1.0622	1.0626
α_2	−0.1922	−0.1904	−0.2240	−0.2195	−0.0933	−0.0922
α_7	0.9475	0.9456	0.9535	0.9533	0.9704	0.9683
β_1	−0.7910	−0.7951	−0.7615	−0.7632	−0.7222	−0.7254
β_7	−0.8791	−0.8835	−0.7990	−0.8082	−0.9359	−0.9391
AIC	792.47	776.51	−1197.78	−1229.52	−1331.94	−1343.87
L-B	30	30	4	4	4	4

and find nearly unchanged coefficients for wind power in both areas. The same is true for wind power penetration in model 5. Because the spot market transmission flows are likely to be endogenous with the price volatility, we cannot draw causal conclusions about their impact (Mauritzen, 2013). However, model 4 for DK1 suggests that exports during morning off-peak hours are positively correlated with daily price volatility, but, during peak hours, the correlation is negative. This is explained by the fact that greater difference between the peak and off-peak hours implies high exports (imports) in the off-peak (peak) hours. By contrast, for DK2, the impact of cross-border exchange is inconclusive in model 4, which can be attributed to the fact that DK2 is connected only to the SE4 bidding area with practically no hydro reservoirs, whereas DK1 is connected to large reservoirs in bidding areas NO2 and SE3 (Nord Pool Spot, 2014). These results are in line with Green and Vasilakos (2012), who find that Denmark exports excess wind power to Norway and Sweden in off-peak hours, in particular, and that the volume of this exchange is higher for DK1 than DK2.

With model 6, we test for the impact of the first difference of natural gas prices, Δgas_d, and find no statistically significant effect on DK1 and DK2 daily price volatility. We note that the daily changes in natural gas spot prices are small, and, thus, they are unlikely to affect short-term bidding behaviour significantly. Moreover, some producers may have longer-term gas contracts instead of relying on spot gas.

Increasing the daily German wind power, $wind_d$, by 1% increases the daily volatility of German prices by 0.03% as indicated by model 1 in Table 4. The result is in line with Ketterer (2014) whose estimate from a rolling regression ranges from 0% to approximately 0.05%. However, when the first difference in daily solar power production, $\Delta solar_d$, increases by 1%, the daily volatility of German prices decreases by 0.04% in model 2. This indicates that also a higher absolute level of solar power leads to lower daily price volatility. Model 3 confirms the signs of the coefficients in the presence of both wind and solar power. Yet, when we combine wind and solar power in variable vre_d in model 4, the coefficient becomes statistically insignificant, which is likely to be caused by the opposing effects of wind and solar power. We arrive at the same conclusions by using the penetration of wind, solar, or the combined generation, i.e., $wind\_pen_d$, $solar\_pen_d$, and vre_pen_d, respectively, as an exogenous variable in models 5–7.

Controlling for the cross-border flow between Germany and France in model 8 keeps the coefficients for $wind_d$ and $\Delta solar_d$ close to the earlier estimates. Positive and negative coefficients for the morning off-peak and peak hour transmission flow ($exim_d^{op1}$ and $exim_d^{p}$), respectively, suggest higher price volatility when exports change to imports during the day. Finally, model 9 shows, in agreement with the result for Denmark, that the first difference of gas prices, Δgas_d, does not have an impact on the daily volatility of German prices.

For all areas, the AIC scores in Table 13 in the Appendix improve after adding the exogenous variables to Eq. (5). In Tables 2–4, we report the lag at which the Ljung-Box test fails at a 1% significance level. The models for DK2 have some autocorrelation at lag 9, but the models for DK1 and DE perform well with all lags. However, Fig. 6a–c show that the ACF plot of the residuals of model 1 for DK1 and DK2 and model 4 for Germany stay within the 95% confidence interval with very few exceptions. As a cross-check, we estimate alternative

Table 6
The effect of different explanatory variables on DK2 price level in each block. All coefficients are statistically significant at the 1% level.

	Block					
Variable	Off-peak 1	Off-peak 1	Peak	Peak	Off-peak 2	Off-peak 2
$wind_d$	−0.0796		−0.0570		−0.0543	
	(0.0068)		(0.0042)		(0.0045)	
$wind\_pen_d$		−0.0813		−0.0596		−0.0557
		(0.0068)		(0.0042)		(0.0045)
$exim_d$	−0.0910	−0.0890	−0.0658	−0.0615	−0.0471	−0.0451
	(0.0205)	(0.0205)	(0.0122)	(0.0122)	(0.0122)	(0.0122)
α_0	3.8882	3.3140	4.0757	3.6436	3.9298	3.5348
α_1	1.1808	1.1804	1.2429	1.2405	1.0707	1.0698
α_2	−0.2303	−0.2301	−0.2909	−0.2889	−0.1073	−0.1070
α_7	0.9019	0.8978	0.9608	0.9605	0.9627	0.9641
β_1	−0.7384	−0.7401	−0.7500	−0.7506	−0.7208	−0.7217
β_7	−0.7794	−0.7766	−0.7912	−0.7949	−0.9186	−0.9220
AIC	623.24	617.20	−1033.78	−1049.23	−842.63	−850.23
L-B	30	30	4	6	5	5

Table 7
The effect of different explanatory variables on DE price level in each block. All coefficients are statistically significant at the 1% the level unless otherwise noted.

	Block									
Variable	Off-peak 1	Off-peak 1	Peak	Peak	Peak	Peak	Peak	Peak	Off-peak 2	Off-peak 2
$wind_d$	−0.3073 (0.0156)		−0.1530 (0.0090)						−0.1874 (0.0079)	
$wind\_pen_d$		−0.3243 (0.0151)		−0.1667 (0.0087)						−0.1915 (0.0078)
$\Delta solar_d$					−0.0528 (0.0142)					
$\Delta solar\_pen_d$						−0.0807 (0.0138)				
vre_d							−0.3602 (0.0158)			
vre_pen_d								−0.3984 (0.0145)		
$exim_d$	0.0436 (0.0107)	0.0440 (0.0101)	0.0187 (0.0072)	0.0193 (0.0070)	0.0096[c] (0.0082)	0.0107[c] (0.0081)	0.0284 (0.0066)	0.0286 (0.0061)	0.0444 (0.0059)	0.0422 (0.0058)
α_0	5.8789	2.5388	4.9809	3.2649	3.7043	3.7006	7.0370	3.0252	5.1723	3.1432
α_1	−0.5556	−0.5669	0.9730	0.9757	0.9555	0.9735	0.8819	0.8652	0.5906	0.6052
α_2	0.2948	0.2815	−0.1192[a]	−0.1206[a]	−0.1394[b]	−0.1497[a]	−0.0801[c]	−0.0717[c]	0.0991[c]	0.0924[c]
α_7	0.9167	0.9184	0.9338	0.9327	0.9280	0.9283	0.9322	0.9272	0.9614	0.9586
β_1	0.9225	0.9229	−0.6736	−0.6763	−0.6016	−0.6135	−0.6452	−0.6335	−0.3428[a]	−0.3561[a]
β_7	−0.7339	−0.7575	−0.5912	−0.6016	−0.6093	−0.6152	−0.5658	−0.5863	−0.8166	−0.8258
AIC	601.62	550.09	−223.51	−282.05	−2.58	−22.43	−379.56	−534.03	−829.03	−856.04
L-B	4	4	30	30	30	30	14	14	30	30

[a] Significant at 5% level.
[b] Significant at 10% level.
[c] Not significant.

models (see Table 16 in the Appendix) and find that the estimated parameters for wind and solar power are robust with respect to the specification.

4.2. Analysis of intraday effects

Next, we investigate further why wind power decreases the daily volatility in Denmark but increases it in Germany. Given the hourly price profiles in Fig. 1a, b, and c, the volatility-increasing impact of wind power can be explained if prices in off-peak 1 and 2 decrease more than during peak hours, leading to divergent prices. On the other hand, the volatility will decrease if peak prices decrease more than off-peak prices so that the hourly price profile becomes flatter.

To test these possibilities, we perform similar regressions as in the previous section for each block, except that the logarithm of the standard deviation of hourly prices, v_d, is replaced by the logarithm of the average price of each block (p_d^{op1}, p_d^p, and p_d^{op2}). Model iteration steps in Table 14 in the Appendix show that the best models for DK1, DK2 and DE are SARMA(2,1)(2,1)[7], SARMA(1,2)(1,2)[7], and SARMA(1,1)(1,2)[7], respectively, using data for peak hours.

However, the addition of exogenous variables to these model causes many variables become statistically insignificant (see Table 17 in the Appendix). Therefore, we step down to a simpler SARMA(2,1)(1,1)[7] model, which for DK1, DK2, and DE differs only by 2.13, 21.64, and 5.25 from the best models in terms of AIC score, respectively. Moreover, the results for different areas can be more readily compared by using a common model. Nevertheless, we consider the best area models in Table 17 of the Appendix. The final SARMA(2,1)(1,1)[7] model is as follows:

$$p_d^b = \alpha_0 + \alpha_1 p_{d-1}^b + \alpha_2 p_{d-2}^b + \alpha_7 p_{d-7}^b + \epsilon_d + \beta_1 \epsilon_{d-1} + \beta_7 \epsilon_{d-7}, \quad (7)$$

where b is the block $\in\{op1, op2, p\}$. Similar to the model in Eq. (6), the exogenous variables are added to the right-hand side of Eq. (7). We note that the instances with a negative average price for a block are removed from our dataset. For DK1, DK2, and DE, there are 13, 10, and 15 such off-peak blocks, respectively. Since the total number of observations is 1813, 1816, and 1081, respectively, we expect that the impact of removing these observations on the coefficients for off-peak blocks is slightly positive at most.

Tables 5 and 6 have the results of the regressions for DK1 and DK2, respectively. The coefficient for average wind power during peak hours, $wind_d^p$, for example, is at the intersection of row $wind_d$ and the column "Peak". Thus, the coefficients for peak-hour wind power, $wind_d^p$, are −0.0726 and −0.0570, respectively, which differ by only 0.01–0.04 units from those for morning and evening off-peak hours, $wind_d^{op1}$ and $wind_d^{op2}$, respectively. Hence, increasing wind power in the peak hours, for example, by 1% causes a 0.07% and 0.06% decline in the average peak price in DK1 and DK2, respectively. Our approximate estimate of the average price-decreasing impact of doubling wind power penetration, $wind\_pen_d$, at 6% is comparable to Jónsson et al. (2010) who estimate that increasing wind power penetration from 20% up to 40% decreases DK1 prices approximately 10%.[2]

Fig. 3a shows that in Denmark there is a peak in wind output during peak hours, which amplifies the total impact of wind power on peak hours relative to off-peak hours. Combined with the small difference between peak and off-peak hour coefficients, this supports the hypothesis that wind power contributes to the flattening of the intraday price profile by decreasing peak prices more than off-peak prices in absolute terms.

Moreover, exchange with the hydro-dominant Nordic countries may contribute to similar flattening of the intraday price curve as the coefficients for peak hour cross-border flows $exim_d^p$ are negative at −0.10 and they differ only slightly from those for morning and evening off-peak hours, $exim_d^{op1}$ and $exim_d^{op2}$, respectively. As the capacities of the associated transmission lines exceed the average DK1 and DK2 wind power forecast in our dataset substantially, the impact of cross-border exchange on DK1 and DK2 electricity prices is significant.

Because the estimated coefficients for the impact of wind power and export in different blocks have higher absolute values for DK1 than DK2, daily DK1 prices are more likely to drop more than daily

[2] Although our estimate is computed using the exact formula $\frac{y_2 - y_1}{y_1} = \left(\frac{x_2}{x_1}\right)^{\gamma} - 1$, the estimate is approximate as the true coefficient, γ, is likely to be different at different wind power penetration levels.

Table 8
The effect of different explanatory variables on DK1 weekly price volatility. All coefficients are statistically significant at the 1% level unless otherwise noted.

Variable	Model					
	Model 1	Model 2	Model 3	Model 4	Model 5	Model 6
$wind_w$	0.1820[a] (0.0711)		0.1636[a] (0.0790)			
$wind\_pen_w$		0.2098 (0.0723)		0.1969[a] (0.0803)		
$\Delta exim_w$			0.0410[b] (0.0761)	0.0288[b] (0.0759)		
$wind_w^{std}$					0.3653 (0.0731)	
Δgas_w						0.4286[b] (0.5424)
α_0	0.4021[b]	1.8344	0.5223[b]	1.8186	−0.5931[b]	1.6036
α_1	0.3073	0.3059	0.3043	0.3032	0.3030	0.3298
β_4	0.1990	0.1989	0.2027	0.2018	0.1877	0.2100
AIC	427.39	425.81	428.26	426.55	409.97	434.39
L-B	30	30	30	30	30	30

[a] Significant at 5% level.
[b] Not significant.

DK2 prices for a comparable increase in wind power or exports. In agreement with the results in Section 4.1, daily DK1 price volatility is likely to drop more than daily DK2 price volatility due to lower absolute level of prices.

For Germany, Table 7 shows that the coefficients for wind power are −0.1530, −0.3073, and −0.1874 for peak ($wind_d^p$), morning off-peak ($wind_d^{op1}$), and evening off-peak hours ($wind_d^{op2}$), respectively. Similar coefficients are confirmed by wind power penetration, $wind\_pen_d$, too. The fact that the coefficients for morning and evening off-peak hours in Germany are more negative than the coefficient for peak hours indicates that the supply curves for off-peak hours are more sensitive than the supply curves for peak hours. Indeed, Paraschiv et al. (2014) find that the impact of wind power on German prices has been up to 3.5 times higher in the morning off-peak than in the peak hours, but the difference has decreased over time. Thus, if there is an increase in wind power production during off-peak hours, then prices will fall more than in peak hours for a comparative increase in wind output. This is true especially in morning off-peak hours where the impact is twofold.

In addition, the fact that German wind power peaks during off-peak hours (Fig. 3c) suggests that German off-peak prices can decrease more compared to peak prices in absolute terms, thereby resulting in higher daily price volatility in keeping with the findings of Section 4.1. In practice, this means that morning off-peak prices, in particular, can crash due to the combination of wind power production and low demand. By contrast, peak-hour prices with high demand decrease only slightly.

Increasing the first difference of average German solar power production, $\Delta solar_d$, by 1% decreases peak prices by 0.05% as indicated by Table 7. Furthermore, when we add peak-hour wind and solar power, the parameter estimates for the average combined generation, vre_d, and its penetration, vre_pen_d, are approximately twice as large as the coefficients for wind power, which suggests an equal contribution from solar power. The inconclusive impact of combined VRE generation on German daily price volatility in Section 4.1 can be explained by the fact that the coefficient for wind power in morning off-peak hours at −0.3073 and the coefficient for combined generation in peak hours at −0.3602 are rather close to each other, thereby indicating that these blocks decrease by nearly the same amount. However, because the coefficient for wind power in the evening off-peak hours is less negative at −0.1874, the overall impact of VRE generation on daily price volatility in Germany is likely to be slightly positive on average because evening off-peak hours diverge, which is also supported by the average hourly prices in Fig. 1c.

All the coefficients for cross-border flows between Germany and France, $exim_d$, are positive. Germany is a net exporter over these transmission lines meaning that the higher the export from Germany to France, the higher the German prices. Similar to wind power, the higher coefficients for off-peak hours, $exim_d^{op1}$ and $exim_d^{op2}$, than for peak hours, $exim_d^p$, imply a higher price sensitivity during the off-peak hours. However, the magnitudes of the coefficients for $exim_d$ are relatively small, which indicates that the cross-border exchange with France has a limited correlation with the German price level. Indeed, the possibilities to balance excess VRE generation are limited as the capacity of these transmission lines is only 30% of average VRE forecast in our dataset and the flows to hydro-dominant Austria and Switzerland approach congestion as the VRE penetration grows (Zugno et al., 2013).

The AIC scores of the models for Denmark and Germany improve significantly when external variables are added to the model in Eq. (7). Ljung-Box tests for some models fail already at low lags, which indicate that there is some serial correlation in our models. We estimated models with additional AR and MA terms, which pass the Ljung-Box test up to lag 30, and find that the estimated parameters for DK1, DK2, and DE external variables in Tables 5–7 are robust. Also, Table 17 in the Appendix shows that the results hold with the best area models, too, although they improve the AIC scores only for Germany.

4.3. Weekly volatility

We now extend the analysis to a weekly horizon by specifying a model that includes the weekly price volatility in Eq. (3) and the weekly average wind, solar, and combined production. The general model is

$$v_w = \alpha_0 + \sum_{i=1}^{p} \alpha_i v_{w-i} + \sum_{i=1}^{q} \beta_i \epsilon_{w-i} + \sum_{i=1}^{P} \alpha_{i \cdot s} v_{w-i \cdot s} + \sum_{i=1}^{Q} \beta_{i \cdot s} \epsilon_{w-i \cdot s} + \epsilon_w + \gamma^\top x_w, \tag{8}$$

Unlike the daily models, weekly volatility is affected by several factors such as power plant and transmission line availability and changes in bidding behaviour, which may not have any seasonality. Therefore, we start with the simplest models such as AR(1) and MA(1) but try also a four-week, i.e., monthly, seasonality (Weron, 2014). Table 15 in the Appendix reports the model iterations. For

Table 9
The effect of different explanatory variables on DK2 weekly price volatility. All coefficients are statistically significant at the 1% level unless otherwise noted.

Variable	Model					
	Model 1	Model 2	Model 3	Model 4	Model 5	Model 6
$wind_w$	0.0621[b] (0.0720)		0.0045[b] (0.0746)			
$wind\_pen_w$		0.0465[b] (0.0729)		−0.0100[b] (0.0752)		
$\Delta exim_w$			0.2457[a] (0.1125)	0.2533[a] (0.1122)		
$wind_w^{std}$					0.1842[a] (0.0749)	
Δgas_w						0.2222[b] (0.6070)
α_0	1.3173	1.7411	1.6084	1.6122	0.7595[a]	1.6318
α_1	0.3445	0.3465	0.3246	0.3247	0.3459	0.3238
β_4	0.1710[a]	0.1744[a]	0.1642[a]	0.1664[a]	0.1500[a]	0.1555[a]
AIC	498.58	498.92	479.82	479.81	493.48	485.21
L-B	30	30	30	30	30	30

[a] Significant at 5% level.
[b] Not significant.

the Danish areas, models with the monthly seasonality show the best performance, but they are found to be statistically insignificant for Germany. AR(1), which is the best model for Germany, fails the Ljung-Box test with Danish data already at low lags. Therefore, we run SARMA(1,0)(0,1)[4] for Danish and AR(1) for German data:

$$v_w = \alpha_0 + \alpha_1 v_{w-1} + \beta_4 \epsilon_{w-4} + \epsilon_w \tag{9}$$

$$v_w = \alpha_0 + \alpha_1 v_{w-1} + \epsilon_w. \tag{10}$$

In Eqs. (9) and (10), the AR(1) term approximates the current volatility with the previous one. In addition, an SMA(1) term in the Danish model (9) deals with monthly seasonality.

We find that increasing the weekly average wind power, $wind_w$, by 1% increases the weekly volatility of DK1 prices by 0.18% as indicated by model 1 in Table 8. For DK2, the effect is inconclusive in model 1 in Table 9, which may be attributed to lower wind power capacity. These results apply for weekly wind power penetration, $wind\_pen_w$, in model 2. Furthermore, controlling for the first difference of weekly average exports, $\Delta exim_w$, in models 3 and 4 does not change the conclusions for wind power and its penetration. However, the standard deviation of daily average wind power outputs, i.e., the intermittency of daily wind power increases the weekly price volatility by 0.37% and 0.18% both in DK1 and DK2 in model 5, respectively. Similar to the daily volatility results, model 6 shows that the change in weekly average natural gas price, Δgas_w, does not have an impact on the weekly price volatility. Table 18 in the Appendix confirms the conclusions using an alternative ARMA(1,1) model.

In Germany, increasing the first difference of weekly average wind power by 1% increases weekly price volatility by 0.11% as suggested by the coefficient for $\Delta wind_w$ in Table 10. This is supported by the comparative effect of the first difference of weekly average wind power penetration, $\Delta wind\_pen_w$, in model 2. The positive

Table 10
The effect of different explanatory variables on German weekly price volatility. All coefficients are statistically significant at the 1% level unless otherwise noted.

Variable	Model									
	Model 1	Model 2	Model 3	Model 4	Model 5	Model 6	Model 7	Model 8	Model 9	Model 10
$\Delta wind_w$	0.1051[b] (0.0591)							0.1095[b] (0.0597)		
$\Delta wind\_pen_w$		0.1407[a] (0.0593)								
$\Delta solar_w$			−0.1707[c] (0.1130)						−0.1793[c] (0.1137)	
$\Delta solar\_pen_w$				−0.1432[c] (0.1122)						
vre_w					0.1322[c] (0.1174)					
vre_pen_w						0.1513[c] (0.1096)				
Δvre_w^{std}							0.1083[a] (0.0551)			
$exim_w$								0.0282[c] (0.0368)	0.0289[c] (0.0383)	
Δgas_w										−2.0427[a] (0.8334)
α_0	1.9668	1.9669	1.9676	1.9676	0.7636[c]	2.2393	1.9663	1.9406	1.9408	1.9669
α_1	0.1676[a]	0.1610[b]	0.2058	0.2070	0.1726[a]	0.1759[a]	0.1699[a]	0.1559[b]	0.1963[a]	0.2019[a]
AIC	170.97	168.44	171.96	172.6	173.68	173.05	170.28	172.39	173.39	168.32
L-B	30	30	30	30	30	30	30	30	30	30

[a] Significant at 5% level.
[b] Significant at 10% level.
[c] Not significant.

coefficients for the first differences indicate that higher weekly average wind power is associated with higher weekly price volatility in Germany. However, models 3 and 4 are inconclusive regarding the impact of the first difference in weekly average solar power, $\Delta solar_w$, and its penetration, $\Delta solar\_pen_w$, because the coefficients are statistically insignificant. As in the daily volatility model, the effect is likely negative because the coefficient estimates are negative. Consequently, the impact of weekly average VRE generation, vre_w, and its penetration, vre_pen_w, is inconclusive in models 5 and 6, respectively. Nevertheless, increasing the change in the standard deviation of VRE generation, Δvre_w^{std}, by 1% increases weekly price volatility by 0.11% in model 7. In models 8 and 9, the inclusion of weekly average exports, $exim_w$, does not change the earlier conclusions on the impact of weekly wind and solar power. Counterintuitively, we find a negative impact of the first difference of weekly average gas price, Δgas_w, on the weekly volatility of prices, but the very high coefficient, −2.0427, makes the result unreliable.

The results for Danish and German VRE generation intermittency, $wind_w^{std}$ and Δvre_w^{std}, respectively, can be explained by day-to-day horizontal parallel shifts of the supply curve. When the installed VRE capacity increases, the available supply increases and the parallel shifts are larger, which contributes to the growing weekly volatility. In both countries, the impact can be amplified by highly clustered wind power farms (Elberg and Hagspiel, 2015). However, the average weekly solar power is not found to contribute to the weekly price volatility, which can be explained by the peak-price-decreasing impact of solar power in Germany.

5. Conclusions

Our analyses suggest that wind and solar power production have statistically and economically significant effects on day-ahead price volatility in Denmark and Germany. In the short run, Danish daily price volatility is lower when there is more wind power production. By contrast, wind power increases the daily price volatility in Germany. However, our results are aligned with those of Jónsson et al. (2010), Mauritzen (2010), and Ketterer (2014). In Denmark, the price-decreasing impact of wind power is distributed evenly during different times of day, and there is a peak in average wind power production during peak hours. In Germany, off-peak hours are most sensitive to downward pressure in prices, and wind power is, on average, highest during these hours. Also, we find evidence that the contrasting impact of wind power on price volatility is partly due to the fact that Denmark has access to large hydropower reservoirs in the Nordic countries, whereas Germany's cross-border transmission lines are small relative to the size of its power system and it has limited access to flexible generation capacity. On the other hand, solar power is produced only during peak hours, which decreases daily volatility by decreasing high peak hour prices in Germany. Because wind and solar power have opposite effects on daily price volatility, results on their combined impact are inconclusive.

Our weekly results suggest that the standard deviation of daily average VRE generation increases the weekly volatility of Danish and German prices. These impacts can be attributed to the high day-to-day variability of wind and solar power production. Moreover, the higher the average weekly wind power, the higher the weekly price volatility.

In periods with high price volatility, producers and consumers need to optimise their generation and demand allocation to maximise their profits and to minimise their costs, respectively. From the power system point of view, the adoption of more VRE requires mechanisms to cope with intermittent supply and to decrease balancing costs (Kunz, 2013). The results for Denmark suggest that access to flexible capacity via adequate transmission capacity can reduce short-term volatility. In addition, measures such as i) capacity payments that incentivise flexible plants (Hach and Spinler, 2016), ii) dispersing wind and solar power farms (Elberg and Hagspiel, 2015), and iii) integration of adjacent markets (Farahmand et al., 2012) can be utilised. On the consumer side, enhanced understanding of the causes of volatility can be used to design tariffs that incentivise demand response (Dupont et al., 2014), which is likely to mitigate the costs of balancing caused by the intermittency of VRE.

The limitations of our distributed lag models need to be recognised. First, they estimate a single coefficient to represent the impact of VRE generation on price volatility even if the impact is more dynamic and dependent on the market situation. We have studied only the whole dataset, while the impacts may change over time. Second, the high frequency of trading in electricity markets means that time-series models may not capture processes driving price formation very accurately, which causes errors in the estimated coefficients for VRE. Nevertheless, our checks corroborate the robustness of our findings based on standard time-series methods.

A subject for further research could be to use different modelling techniques. Similar to Ketterer (2014), the impact of wind power on Danish price volatility could be established using a GARCH model. On the other hand, German price volatility could be explored as a function of time and VRE penetration using the non-parametric regression model of Jónsson et al. (2010). Also, the link between VRE generation levels and supply curve elasticities can be established more formally using real supply and demand curve data (see Dillig et al., 2016) or agent-based or complementarity models. Another avenue for future research is to estimate the impact of VRE generation on price volatility in other renewable-rich locations such as Spain, Ireland, and California. Moreover, as the absolute value of the VRE forecast errors is likely to increase when the VRE capacity increases, trading volumes and prices on various intraday markets are subject to change.

Acknowledgements

This research has been supported by funding from the STEEM project of the Aalto Energy Efficiency programme.

Feedback from the editor and two anonymous referees has greatly improved the paper. Any remaining errors are the authors' own.

Appendix A. Supplementary data

Supplementary data to this article can be found online at http://dx.doi.org/10.1016/j.eneco.2016.12.019.

References

Barthelmie, R., Courtney, M., Hjstrup, J., Larsen, S., 1996. Meteorological aspects of offshore wind energy: observations from the Vindeby wind farm. J. Wind Eng. Ind. Aerodyn. 62 (2-3), 191–211.

Bloomberg, L.P., 2016. Netconnect Germany Spot Gas Prices. Retrieved from Bloomberg database, ticker EEXGNCGR.

Dillig, M., Jung, M., Karl, J., 2016. The impact of renewables on electricity prices in Germany — an estimation based on historic spot prices in the years 2011–2013. Renew. Sustain. Energy Rev. 57, 7–15.

Dupont, B., Jonghe, C.D., Olmos, L., Belmans, R., 2014. Demand response with locational dynamic pricing to support the integration of renewables. Energy Policy 67, 344–354.

Transparency, E.E.X., 2016. Ex-Ante Solar & Wind Power Production. https://www.eex-transparency.com/homepage/power/germany/production/usage/solar-wind-power-production.

Egerer, J., Kunz, F., von Hirschhausen, C., 2013. Development scenarios for the North and Baltic Seas grid — a welfare economic analysis. Util. Policy 27, 123–134.

Elberg, C., Hagspiel, S., 2015. Spatial dependencies of wind power and interrelations with spot price dynamics. Eur. J. Oper. Res. 241 (1), 260–272.

Energinet.dk, 2014. Solar Power. http://www.energinet.dk/EN/KLIMA-OG-MILJOE/Miljoerapportering/VE-produktion/Sider/Sol.aspx.

Energinet.dk, 2015. Wind Turbines Reached Record Level in 2014. . http://energinet.dk/EN/El/Nyheder/Sider/Vindmoeller-slog-rekord-i-2014.aspx.

Transparency, ENTSO-E, 2016a. Scheduled Commercial Exchanges. https://transparency.entsoe.eu/transmission-domain/r2/scheduledCommercialExchangesDayAhead/show.

Transparency, ENTSO-E, 2016b. Total Load — Day Ahead/Actual. https://transparency.entsoe.eu/load-domain/r2/totalLoadR2/show

Spot, Epex, 2016. Epex Spot Auction. https://www.epexspot.com/en/market-data/dayaheadauction.

Farahmand, H., Aigner, T., Doorman, G., Korpas, M., Huertas-Hernando, D., 2012. Balancing market integration in the Northern European continent: a 2030 case study. IEEE Trans. Sustainable Energy 3 (4), 918–930.

Frömmel, M., Han, X., Kratochvil, S., 2014. Modeling the daily electricity price volatility with realized measures. Energy Econ. 44, 492–502.

Gelabert, L., Labandeira, X., Linares, P., 2011. An ex-post analysis of the effect of renewables and cogeneration on Spanish electricity prices. Energy Econ. 33 (S1), S59–S65.

González-Aparicio, I., Zucker, A., 2015. Impact of wind power uncertainty forecasting on the market integration of wind energy in Spain. Appl. Energy 159, 334–349.

Green, R., Vasilakos, N., 2010. Market behaviour with large amounts of intermittent generation. Energy Policy 38 (7), 3211–3220.

Green, R., Vasilakos, N., 2011. The Long-term Impact of Wind Power on Electricity Prices and Generating Power. ESRC Centre for Competition Policy Working Paper Series Available at SSRN. http://papers.ssrn.com/sol3/papers.cfm?abstract_id=1851311.

Green, R., Vasilakos, N., 2012. Storing wind for a rainy day: what kind of electricity does Denmark export? Energy J. 33 (3), 1–22.

Hach, D., Spinler, S., 2016. Capacity payment impact on gas-fired generation investments under rising renewable feed-in — a real options analysis. Energy Econ. 53, 270–280.

He, Y., Hildmann, M., Andersson, G., 2012. Modeling the wind power in-feed in Germany by data decomposition and time series analysis. Power and Energy Society General Meeting, 2012 IEEEpp. 1–8

Holttinen, H., 2005. Hourly wind power variations in the Nordic countries. Wind Energy 8 (2), 173–195.

Huber, M., Dimkova, D., Hamacher, T., 2014. Integration of wind and solar power in Europe: assessment of flexibility requirements. Energy 69, 236–246.

Jaehnert, S., Wolfgang, O., Farahmand, H., Völler, S., Huertas-Hernando, D., 2013. Transmission expansion planning in Northern Europe in 2030 — methodology and analyses. Energy Policy 125–139.

Jónsson, T., Pinson, P., Madsen, H., 2010. On the market impact of wind energy forecasts. Energy J. 32 (2), 313–320.

Kalantzis, F.G., Milonas, N.T., 2013. Analyzing the impact of futures trading on spot price volatility: evidence from the spot electricity market in France and Germany. Energy Econ. 36, 454–463.

Ketterer, J.C., 2014. The impact of wind power generation on the electricity price in Germany. Energy Econ. 44, 270–280.

Kunz, F., 2013. Improving congestion management: how to facilitate the integration of renewable generation in Germany. Energy J. 34 (4), 55–78.

Mauritzen, J., 2010. What happens when it's windy in Denmark? An empirical analysis of wind power on price volatility in the Nordic electricity market. Discussion Papers 2010/18 Department of Business and Management Science, Norwegian School of Economics.,

Mauritzen, J., 2013. Dead battery? Wind power, the spot market, and hydropower interaction in the Nordic electricity market. Energy J. 34 (1), 103–123.

Mauritzen, J., 2015. Now or later? Trading wind power closer to real-time: how poorly designed subsidies can lead to higher balancing costs. Energy J. 36 (4), 1–16.

Morales, J., Conejo, A., Perez-Ruiz, J., 2011. Simulating the impact of wind production on locational marginal prices. IEEE Trans. Power Syst. 26 (2), 820–828.

Mulder, M., Scholtens, B., 2013. The impact of renewable energy on electricity prices in the Netherlands. Renew. Energy 57, 94–100.

Spot, Nord Pool, 2014. Hydro Reservoir. http://nordpoolspot.com/Market-data1/Power-system-data/hydro-reservoir1/ALL/Hourly/?view=table.

Spot, Nord Pool, 2016. Historical Market Data. http://nordpoolspot.com/historical-market-data/.

Paraschiv, F., Erni, D., Pietsch, R., 2014. The impact of renewable energies on EEX day-ahead electricity prices. Energy Policy 73, 196–210.

Core Team, R., 2015. R: A Language and Environment for Statistical Computing. R Foundation for Statistical Computing, Vienna, Austria. https://www.R-project.org/.

Shumway, R.H., Stoffer, D.S., 2011. Time Series Analysis and Its Applications: With R Examples. 3rd ed., Springer-Verla, New York.

von Hirschhausen, C., 2014. The German 'Energiewende' — an introduction. Econ. Energy Environ. Policy 3 (2), 1–12.

Weron, R., 2014. Electricity price forecasting: a review of the state-of-the-art with a look into the future. Int. J. Forecast. 30 (4), 1030–1081.

Würzburg, K., Labandeira, X., Linares, P., 2013. Renewable generation and electricity prices: taking stock and new evidence for Germany and Austria. Energy Econ. 40 (S1), S159–S171.

Yip, C.M.A., Gunturu, U.B., Stenchikov, G.L., 2016. Wind resource characterization in the Arabian Peninsula. Appl. Energy 164, 826–836.

Zugno, M., Pinson, P., Madsen, H., 2013. Impact of wind power generation on European cross-border power flows. IEEE Trans. Power Syst. 28, 3566–3575.

Appendix A ADF Tests

Lag	5			10			15		
Variable \ Area	DK1	DK2	DE	DK1	DK2	DE	DK1	DK2	DE
v_d	0.01	0.01	0.01	0.01	0.01	0.01	0.01	0.01	0.07
p_d^{op1}	0.01	0.01	0.01	0.01	0.01	0.01	0.01	0.01	0.01
p_d^{op2}	0.01	0.01	0.01	0.01	0.01	0.01	0.01	0.01	0.01
p_d^p	0.01	0.01	0.01	0.01	0.01	0.01	0.01	0.01	0.01
$wind_d$	0.01	0.01	0.01	0.01	0.01	0.01	0.01	0.01	0.01
$wind_d^{op1}$	0.01	0.01	0.01	0.01	0.01	0.01	0.01	0.01	0.01
$wind_d^{op2}$	0.01	0.01	0.01	0.01	0.01	0.01	0.01	0.01	0.01
$wind_d^p$	0.01	0.01	0.01	0.01	0.01	0.01	0.01	0.01	0.01
$wind\_pen_d$	0.01	0.01	0.01	0.01	0.01	0.01	0.01	0.01	0.01
$wind\_pen_d^{op1}$	0.01	0.01	0.01	0.01	0.01	0.01	0.01	0.01	0.01
$wind\_pen_d^{op2}$	0.01	0.01	0.01	0.01	0.01	0.01	0.01	0.01	0.01
$wind\_pen_d^p$	0.01	0.01	0.01	0.01	0.01	0.01	0.01	0.01	0.01
$solar_d$			0.25			0.56			0.89
$solar_d^p$			0.18			0.66			0.92
$solar\_pen_d$			0.25			0.52			0.87
$solar\_pen_d^p$			0.18			0.63			0.91
vre_d			0.01			0.01			0.01
vre_d^p			0.01			0.01			0.01
vre_pen_d			0.01			0.01			0.01
$vre\_pen_d^p$			0.01			0.01			0.01
$exim_d^{op1}$	0.01	0.01	0.01	0.01	0.01	0.04	0.04	0.03	0.09
$exim_d^{op2}$	0.01	0.01	0.01	0.01	0.01	0.01	0.02	0.01	0.03
$exim_d^p$	0.01	0.01	0.01	0.01	0.01	0.01	0.01	0.01	0.01
gas_d	0.19	0.19	0.15	0.40	0.40	0.37	0.35	0.35	0.36
v_w	0.01	0.01	0.01	0.04	0.01	0.32	0.03	0.03	0.44
$wind_w$	0.02	0.04	0.63	0.03	0.09	0.41	0.01	0.08	0.09
$wind_w^{std}$	0.01	0.01		0.01	0.03		0.03	0.18	
$wind\_pen_w$	0.01	0.02	0.49	0.03	0.16	0.43	0.02	0.26	0.19
$solar_w$			0.36			0.04			0.06
$solar\_pen_w$			0.33			0.02			0.04
vre_w			0.03			0.42			0.22
vre_w^{std}			0.17			0.58			0.11
vre_pen_w			0.02			0.41			0.25
$exim_w$	0.36	0.18	0.08	0.24	0.12	0.09	0.20	0.09	0.08
gas_w	0.48	0.48	0.65	0.09	0.09	0.42	0.08	0.08	0.43

Table 11: Augmented Dickey-Fuller test p-values. All figures have been rounded to two decimal places. Empty cells indicate that the variable is not used for all areas.

Lag	5			10			15		
Variable \ Area	DK1	DK2	DE	DK1	DK2	DE	DK1	DK2	DE
$\Delta solar_d$			0.01			0.01			0.01
$\Delta solar_d^p$			0.01			0.01			0.01
$\Delta solar\_pen_d$			0.01			0.01			0.01
$\Delta solar\_pen_d^p$			0.01			0.01			0.01
Δgas_d	0.01	0.01	0.01	0.01	0.01	0.01	0.01	0.01	0.01
$\Delta wind_w$			0.01			0.04			0.67
$\Delta wind\_pen_w$			0.01			0.01			0.60
$\Delta solar_w$			0.17			0.16			0.22
$\Delta solar\_pen_w$			0.13			0.23			0.19
Δvre_w^{std}			0.01			0.01			0.42
$\Delta exim_w$	0.01	0.01		0.01	0.01		0.05	0.01	
Δgas_w	0.01	0.01	0.01	0.01	0.01	0.11	0.01	0.01	0.20

Table 12: Augmented Dickey-Fuller test p-values for differenced time series. All figures have been rounded to two decimal places. Empty cells indicate that the variable is not used for all areas.

Appendix B Model Selection

	DK1		DK2		DE	
Model \ Test	AIC	L-B	AIC	L-B	AIC	L-B
SARMA(1,0)(1,0)[7]	3115.82	3	3403.95	3	684.30	3
SARMA(1,1)(1,0)[7]	3102.47	3	3388.85	3	676.24	6
SARMA(1,0)(1,1)[7]	3022.43	3	3293.06	3	549.72	3
SARMA(1,1)(1,1)[7]	2963.46	3	3245.79	3	513.45	3
SARMA(1,2)(1,1)[7]	2913.48	26	3196.09	7	503.46	30
SARMA(1,2)(2,1)[7]			3181.10	30	491.84	30
SARMA(1,2)(1,2)[7]	2908.93	30				
SARMA(2,1)(2,1)[7]	2908.53	30	3180.41	30	490.67	30

Table 13: Statistically significant and AIC-improving iteration steps of the daily model for DK1, DK2, and DE.

	DK1		DK2		DE	
Model \ Test	AIC	L-B	AIC	L-B	AIC	L-B
SARMA(1,0)(1,0)[7]	-319.22	4	-467.38	3	142.30	7
SARMA(1,1)(1,0)[7]	-332.18	3	-476.81	3	138.09	7
SARMA(1,0)(1,1)[7]	-541.08	4	-660.86	3	37.90	2
SARMA(1,1)(1,1)[7]	-556.92	3	-675.71	3	24.25	30
SARMA(1,2)(1,1)[7]	-584.98	4	-738.37	6		
SARMA(1,1)(2,1)[7]					20.65	30
SARMA(1,1)(1,2)[7]					19.30	30
SARMA(1,2)(2,1)[7]	-586.73	4	-746.59	6		
SARMA(2,1)(1,1)[7]	-586.38	4				
SARMA(1,2)(1,2)[7]	-586.94	4	-747.18	6		
SARMA(2,1)(2,1)[7]	-588.51	4				

Table 14: Statistically significant and AIC-improving iteration steps of the intraday model for DK1, DK2, and DE. The reported figures are for peak hours.

	DK1		DK2		DE	
Test / Model	AIC	L-B	AIC	L-B	AIC	L-B
AR(1)	441.11	4	502.10	6	172.94	30
MA(1)	447.06	2	504.61	4	173.91	30
SARMA(1,0)(1,0)[4]	432.23	30	498.08	30		
SARMA(1,0)(0,1)[4]	431.86	30	497.32	30		

Table 15: Statistically significant and AIC-improving iteration steps of the weekly model for DK1, DK2, and DE.

Appendix C Alternative Specifications

Variable \ Area	DK1	DK2	DE	DE
$wind_d$	-0.0897[a]	-0.0687	0.0329[a]	
	(0.0158)	(0.0146)	(0.0145)	
$\Delta solar_d$				-0.0360[b]
				(0.0191)
α_0	2.4019	2.2073	1.9365	2.2393
α_1	0.9494	0.9301	0.9861	0.9864
α_7	0.9982	0.9994	0.9996	0.9998
β_1	-0.5889	-0.5371	-0.7538	-0.7409
β_2	-0.1881	-0.1732	-0.1389	-0.1470
β_7	-0.9180	-0.8885	-0.8233	-0.8306
β_{14}	-0.0599[a]	-0.0964	-0.1614	-0.1592
AIC	2879.03	3161.19	489.95	491.03
L-B	30	30	30	30

[a] significant at 5% level
[b] significant at 10% level

Table 16: An alternative specification for the daily volatility model. All coefficients are statistically significant at the 1% level unless otherwise noted.

Area	DK1	DK2	DE	DK1	DK2	DE	DE	DE	DK1	DK2	DE
Variable \ Block	Off-peak 1	Off-peak 1	Off-peak 1	Peak	Peak	Peak	Peak	Peak	Off-peak 2	Off-peak 2	Off-peak 2
$wind_d$	-0.1524	-0.0937	-0.2854	-0.1065	-0.0659	-0.1488			-0.0943	-0.0623	-0.1888
	(0.0076)	(0.0060)	(0.0153)	(0.0045)	(0.0038)	(0.0089)			(0.0043)	(0.0040)	(0.0080)
$\Delta solar_d$							-0.0508				
							(0.0139)				
vre_d								-0.1710			
								(0.0132)			
α_0	4.3733	3.9516	5.7170	4.4112	4.1188	4.9638	3.7154	3.7189	4.2444	3.9636	5.2483
α_1	1.1257	0.9235	0.6688	1.1390	0.9137	0.7256	0.6432	0.6139	1.0447	0.9543	0.7929
α_2	-0.1862			-0.2116					-0.0882		
α_7	0.9870	0.9296	0.9272	0.9968	0.9687	0.9380	0.9376	0.9350	0.9260	0.9616	0.9491
α_{14}	-0.0289[a]			-0.0310[a]					0.0360[a]		
β_1	-0.7736	-0.4865	-0.3413	-0.7504	-0.4264	-0.4346	-0.2939	-0.2061	-0.7118	-0.6085	-0.4830
β_2		-0.1627			-0.1943					-0.0806	
β_7	-0.8863	-0.7768	-0.6929	-0.8144	-0.7371	-0.5425	-0.5462	-0.5111	-0.9122	-0.9226	-0.8095
β_{14}		-0.0450[a]	-0.0459[a]		-0.0744	-0.0464[a]	-0.0892	-0.0967		0.0112[a]	0.0210[a]
AIC	854.01	635.59	605.94	-1065.55	-1021.47	-217.34	-8.81	-145.37	-1239.92	-828.71	-775.89
L-B	30	30	4	4	6	30	30	30	4	5	8

[a] not significant

Table 17: Alternative specifications for the intraday model. All coefficients are statistically significant at the 1% level unless otherwise noted.

Variable \ Area	DK1	DK2	DE	DE	DE
$wind_w$	0.2070	0.1010^c			
	(0.0723)	(0.0734)			
$\Delta wind_w$			0.1370^a		
			(0.0578)		
$\Delta solar_w$				-0.1901^c	
				(0.1163)	
vre_w					0.2013^b
					(0.1159)
α_0	0.2357^c	1.1097	1.9681	1.9698	0.1351^c
α_1	0.5996	0.6309	0.8790	0.8413	0.9035
β_1	-0.3404^c	-0.3295^c	-0.7690	-0.7099^a	-0.8048
AIC	435.11	503.62	168.83	171.76	171.99
L-B	11	5	30	30	30

[a] significant at 5% level
[b] significant at 10% level
[c] not significant

Table 18: An alternative specification for the weekly volatility model. All coefficients are statistically significant at the 1% level unless otherwise noted.

Publication II

T. Rintamäki, A. S. Siddiqui, and A. Salo. How much is enough? Optimal support payments in a renewable-rich power system. *Energy*, 117(1), 300-313, 2016.

Energy 117 (2016) 300–313

Contents lists available at ScienceDirect

Energy

journal homepage: www.elsevier.com/locate/energy

How much is enough? Optimal support payments in a renewable-rich power system

Tuomas Rintamäki [a], Afzal S. Siddiqui [b, c, *], Ahti Salo [a]

[a] Systems Analysis Laboratory, Department of Mathematics and Systems Analysis, School of Science, Aalto University, Finland
[b] Department of Statistical Science, University College London, United Kingdom
[c] Department of Computer and Systems Sciences, Stockholm University, Sweden

ARTICLE INFO

Article history:
Received 7 December 2015
Received in revised form
16 September 2016
Accepted 18 October 2016
Available online 1 November 2016

Keywords:
Renewable energy
Support payments
Day-ahead market
Balancing market
Congestion management
Mathematical programming with equilibrium constraints

ABSTRACT

The large-scale deployment of intermittent renewable energy sources may cause substantial power imbalance. Together with the transmission grid congestion caused by the remoteness of these sources from load centers, this creates a need for fast-adjusting conventional capacity such as gas-fired plants. However, these plants have become unprofitable because of lower power prices due to the zero marginal costs of renewables. Consequently, policymakers are proposing new measures for mitigating balancing costs and securing supply. In this paper, we take the perspective of the regulator to assess the effectiveness of support payments to flexible generators. Using data on the German power system, we implement a bi-level programming model, which shows that such payments for gas-fired plants in southern Germany reduce balancing costs and can be used as part of policy to integrate renewable energy.

1. Introduction

In deregulated electricity industries, the expansion of wind and solar power has decreased power prices and, thus, eroded the viability of coal, lignite, and gas-fired conventional electricity generation units [38]. At the same time, the intermittency of renewables and insufficient transmission capacity has increased the need for grid congestion management and flexible conventional generation capacity [35]. Indeed, the lack of flexibility may risk grid stability under scenarios with high load or sudden changes in renewable energy generation.

As a potential solution to the threat to security of supply in the long term, capacity markets to entice conventional power plants have been proposed. In these schemes, an authority ensures a sufficient level of capacity through payments or obligations [18]. On the other hand, [15] envisages an energy-only "electricity market 2.0" scheme that permits high price peaks, develops intraday markets, and promotes new technologies such as demand response, for instance.

As a response to insufficient flexible generation capacity in southern Germany, a regional transmission system operator (TSO), TenneT, and the Federal Network Agency, Bundesnetzagentur, have agreed to compensate fixed costs of two flexible plants via support payments [33]. Therefore, in this paper, we develop a complementarity model to assess the increased dispatch of fast-adjusting conventional capacity through support payments, which, in effect, reduce the bid prices of these generators. Specifically, we cast the sequential model in Ref. [23] as a bi-level problem in which the day-ahead decisions are taken at the upper level and congestion management decisions at the lower level. The latter are guided by the upper-level support payment decisions that the regulator takes in order to minimize the total generation costs. We develop a novel set of constraints to enforce the merit order and cast the problem as a mixed-

* Corresponding author. Department of Statistical Science, University College London, United Kingdom.
E-mail addresses: tuomas.rintamaki@aalto.fi (T. Rintamäki), afzal.siddiqui@ucl.ac.uk (A.S. Siddiqui), ahti.salo@aalto.fi (A. Salo).

http://dx.doi.org/10.1016/j.energy.2016.10.058
0360-5442/

integer linear program (MILP) by using a linearization technique [13]. Hence, we assess the performance of a recently implemented regulation for a realistic test network via a rigorous mathematical programming approach.

We calibrate the model to the German power system using realistic data and identify the congested parts of the transmission network to provide insights about the geographical distribution of optimal support payments under different demand and renewable energy scenarios. We also test the performance of the optimal decisions by introducing spatially correlated imbalances in the balancing market. Moreover, we contribute to the ongoing debate by comparing the optimal support payments to the nodal pricing mechanism [24] and demonstrate that they lead to similar patterns of generation that reduce re-dispatching. In particular, we find that re-dispatch volumes are halved when support payments are introduced. We also extend the model to multiple time periods to show how support payments mitigate the intermittency of renewables by utilizing the fast-ramping capabilities of the flexible units. Thus, alternative market designs such as support payments and nodal pricing improve the flexibility of the power system and reduce the costs of integrating renewables.

The paper is organized as follows. In Section 2, we discuss complementarity models of electricity markets, the challenges posed by the higher penetration of renewables in the day-ahead and balancing markets, and the relevant policy alternatives. Section 3 presents the structure of our bi-level model, and Section 4 gives numerical results for a model calibrated to the German power system along with sensitivity analysis of the optimal decisions. We provide conclusions on the likely impacts of support payments in Germany and discuss directions for future research in Section 5.

2. Literature review

Complementarity models are often used to analyze electricity markets in which prices are formed endogenously and strategic interactions occur among players. [30] give an overview of these models, and a thorough treatise can be found in Ref. [12]. [25] develop a large-scale perfect competition model of the European electricity market that covers transmission, variable demand, wind power, and pumped storage, for example. In bi-level models, a group of players in the lead role make optimal decisions anticipating the reaction of a group of follower players, e.g., see Ref. [1].

[23] presents a sequential model for Germany with a high level of wind generation in which the production schedules determined by a day-ahead market model ignoring the physical transmission network are fed into a congestion management model, which minimizes the re-dispatch costs, i.e., the costs of relieving congestion. [23] uses data on realistic projections to 2020 of the increase in demand and renewable energy generation in Germany and finds that annual national congestion management costs increase from €40 million to €147 million without transmission grid extensions.

The need for fast-ramping units to balance generation from intermittent renewables is supported by recent empirical data, e.g. [29], show that the variability of wind and solar power increases the volatility of German hourly and daily electricity prices. [19] conclude that there is a dramatic increase in flexibility requirements when the share of renewables of annual electricity consumption exceeds 30%. However, renewable generation has a negative impact on power prices due to its zero marginal costs and prevents the deployment of high-cost flexible plants [39].

Also, [34] show that gas-fired plants are required when short-term variability of renewables is introduced into a long-term German power system model with an 80% emission reduction target. Indeed, gas-fired plants have lower CO_2 emissions and higher fuel efficiency than coal plants [16]. However, major utilities in the UK, France, Germany, and Italy, among others, have recently closed or mothballed gas-fired power plants in response to low profitability [6].

Apart from flexible gas-fired plants, there are several other mechanisms to integrate renewables into power systems. At specific sites, the variability of wind power can be reduced by coupling it with wave power [11]. [37] analyze the economic viability of high-voltage direct current (HVDC) transmission lines from windy northern Germany to load centers in the west and south assuming extensive wind power deployment. They conclude that the welfare gains resulting from full wind power utilization and lower price levels would quickly cover the lines' investment costs. In a similar vein, [20] postulate that the expansion of the cross-border HDVC network allows the hydro-dominant power systems in the Nordic countries to balance the variability of renewable generation in continental Europe by adjusting hydro production. On the demand side, more flexible pricing schemes could also integrate renewables [8]. Likewise, storage and power-to-gas technologies have been explored to increase flexibility [21,31].

Price-based policies, which directly grant the generating capacity a payment, have been implemented in Spain and Italy, for example [3]. In Italy, in particular, the policy aimed to keeping existing capacity in operation and compensates generators when prices are too low [4]. Conversely, quantity-based policies, e.g., as implemented in the UK, determine the capacity payment in an auction to cover a quantity considered to secure supply. Typically, they enforce the availability of the procured capacity by setting a strike price for the spot market price above which the generators need to compensate the regulator [36]. [17] show that capacity payments can reduce the impact of renewable energy generation on the profitability of gas-fired plants and, thus, prevent their mothballing.

By contrast, energy-only policies such as the "electricity market 2.0" concept have the virtue that they minimize interventions in the electricity market. Even under these policies, some kind of back-up reserves are maintained [2]. A BMWi white paper [5] outlines a reserve capacity based mainly on old lignite plants, which are started up when a market price cannot be formed. Moreover, the white paper describes a reserve to relieve congestion in southern Germany.

Conceptually, our model resembles [26] and [22] in using a bi-level approach for integrating renewables by comparing alternative market-clearing schemes. However, we seek to find the optimal trade-off between the least-cost day-ahead market dispatch and the support payments, which have the potential to reduce congestion management and balancing costs by enticing the dispatch of flexible but more expensive power plants.

3. Mathematical formulation

3.1. Notation

Sets and indices	
Φ	auxiliary decision variables
Ω^{DV}	lower-level dual variables
Ω^{UL}	upper-level primal decision variables
Ω^{LL}	lower-level primal decision variables
$n,k \in N$	nodes
$n' \in N$	reference node
$u,o \in U$	generation types
$t \in T$	time periods
$i \in I$	discrete support payment levels
$\ell \in L$	transmission lines
Parameters	
$cons_{n,t}$	consumption at node n during period t
$\bar{s}_{n,u,i}$	support payments levels for unit u at node n
$c^{m}_{n,u}$	bid price of generation of unit u at node n
$c^{up}_{n,u}$	up-reserve bid price of unit u at node n
$c^{down}_{n,u}$	down-reserve bid price of unit u at node n
$g^{max}_{n,u,t}$	maximum generation capacity of unit u at node n during period t
$\varepsilon^{da^{up}}_{n,u}$	day-ahead ramp-up rate of unit u at node n
$\varepsilon^{da^{down}}_{n,u}$	day-ahead ramp-down rate of unit u at node n
$\varepsilon^{reserve^{up}}_{n,u}$	up-reserve deployment rate of unit u at node n
$\varepsilon^{reserve^{down}}_{n,u}$	down-reserve deployment rate of unit u at node n
cap^{max}_{ℓ}	thermal capacity of power line ℓ
$H_{\ell,k}$	branch susceptance matrix $\ell \times k$
$B_{n,k}$	node susceptance matrix $n \times k$
sw_n	reference node switch variable equals 1 for n' and 0 otherwise
Scalars	
eps	a small positive constant
M_1	a large positive constant
$K_1,\ldots,K_8$	constants for disjunctive constraints
$K_{g^{da}}, K_v$	constants for linearization
Variables	
$\lambda^{cm}_{n,t}$	re-dispatch price at node n during period t
$\delta_{n,t}$	phase angle at node n during period t
$\gamma_{n,t}$	dual for the swing bus constraint at node n during period t
Positive variables	
$s_{n,u}$	support payment for unit u at node n
$g^{f}_{n,u,t}$	full generation of unit u at node n during period t in the day-ahead market
$g^{r}_{n,u,t}$	residual generation of unit u at node n during period t in the day-ahead market
$g^{da}_{n,u,t}$	total day-ahead generation of unit u at node n during period t
$g^{up}_{n,u,t}$	up-reserve deployment of unit u at node n during period t
$g^{down}_{n,u,t}$	down-reserve deployment of unit u at node n during period t
$\beta^{da}_{n,u,t}$	dual for maximum generation capacity of unit u at node n during period t in the day-ahead market
$\beta^{up}_{n,u,t}$	dual for absolute maximum up-reserve deployment of unit u at node n during period t
$\beta^{down}_{n,u,t}$	dual for absolute maximum down-reserve deployment of unit u at node n during period t
$\theta^{up}_{n,u,t}$	dual for relative maximum up-reserve deployment of unit u at node n during period t
$\theta^{down}_{n,u,t}$	dual for relative maximum down-reserve deployment of unit u at node n during period t
$\overline{\mu_{\ell,t}}$	dual for positive line capacity constraint on line ℓ during t
$\underline{\mu_{\ell,t}}$	dual for negative line capacity constraint on line ℓ during t
$v_{n,u,i,t}$	discretization of $s_{n,u} \cdot g^{da}_{n,u,t}$ of unit u at node n during t
Binary variables	
$r1,\ldots,r8$	disjunctive variables
$q^{g^{da}}_{n,u,t}$	indicator variables equal to 1 when $g^{da}_{n,u,t} > 0$
$q_{n,u,i}$	indicator variables equal to 1 if i^{th} support payment level is selected
$q^{v}_{n,u,i,t}$	indicator variables equal to 1 when $q^{g^{da}}_{n,u,t}$ and $q_{n,u,i}$ are 1
$f_{n,u,t}$	indicator variables equal to 1 when unit u is fully dispatched
$r_{n,u,t}$	indicator variables equal to 1 when unit u is partially dispatched

3.2. Bi-level formulation

In the upper level of our bi-level model, the objective function of a regulator (1) is to minimize the costs of day-ahead generation, including the possible support payments and the anticipated costs of re-dispatch and real-time balancing power, i.e., increasing (deploying up-reserves) and decreasing (deploying down-reserves) the generation of power plants. In the day-ahead market, supply and demand match at every time period (2) and the generation of plant (n,u) in time period t is the sum of full generation $g^{f}_{n,u,t}$ and residual generation $g^{r}_{n,u,t}$ (3). As per the rules of the German market, physical transmission constraints are neglected at the time of day-ahead dispatch and applied only in the re-dispatching phase. If the decision variable $f_{n,u,t}$ equals to 1, then constraint (4) forces the plant to produce at its maximum capacity. Otherwise, the plant is not fully dispatched. However, if the decision variable $r_{n,u,t}$ in (5) equals to 1, then the plant is operating at a level below its maximum capacity that is set by the decision variable $g^{r}_{n,u,t}$. Constraint (6) ensures that the plant cannot be fully and partially dispatched at the same time. Finally, the inequalities (7) and (8) exclude unrealistic ramping of power plants and avoid discontinuities between time periods.

$$\underset{\Omega^{UL}}{\text{Minimize}} \sum_t \sum_n \sum_u \left(\left(c^{m}_{n,u} + s_{n,u} \right) g^{da}_{n,u,t} + c^{up}_{n,u} g^{up}_{n,u,t} - c^{down}_{n,u} g^{down}_{n,u,t} \right) \tag{1}$$

s.t.

$$\sum_n cons_{n,t} = \sum_n \sum_u g^{da}_{n,u,t} \quad \forall t \tag{2}$$

$$g^{da}_{n,u,t} = g^{f}_{n,u,t} + g^{r}_{n,u,t} \quad \forall n,u,t \tag{3}$$

$$g^{f}_{n,u,t} = f_{n,u,t} g^{max}_{n,u,t} \quad \forall n,u,t \tag{4}$$

$$g^{r}_{n,u,t} \le r_{n,u,t} \left(g^{max}_{n,u,t} - eps \right) \quad \forall n,u,t \tag{5}$$

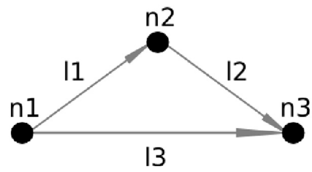

Fig. 1. Three-node network indicating conventional direction of flow.

$$f_{n,u,t} + r_{n,u,t} \le 1 \quad \forall n,u,t \tag{6}$$

$$g^{da}_{n,u,t} - \left(g^{da}_{n,u,t-1} + g^{up}_{n,u,t-1} \right) \le \epsilon^{da^{up}}_{n,u} g^{max}_{n,u,t} \quad \forall n,u, \text{ and } \forall t \ge 2 \tag{7}$$

$$\left(g^{da}_{n,u,t-1} - g^{down}_{n,u,t-1} \right) - g^{da}_{n,u,t} \le \epsilon^{da^{down}}_{n,u} g^{max}_{n,u,t} \quad \forall n,u, \text{ and } \forall t \ge 2 \tag{8}$$

$$c^{m}_{n,u} - s_{n,u} - M_1 \left(1 - f_{n,u,t} \right) \le c^{m}_{k,o} - s_{k,o} + M_1 f_{k,o,t} \quad \forall t, (n,u) \ne (k,o) \tag{9}$$

$$c^{m}_{n,u} - s_{n,u} - M_1 \left(1 - r_{n,u,t} \right) \le c^{m}_{k,o} - s_{k,o} + M_1 f_{k,o,t} \quad \forall t, (n,u) \ne (k,o) \tag{10}$$

$$\left\{ \begin{array}{llll}
\underset{\Omega^{LL}}{\text{Minimize}} \sum_t \sum_n \sum_u \left(c^{up}_{n,u} g^{up}_{n,u,t} - c^{down}_{n,u} g^{down}_{n,u,t} \right) & & & (11) \\
\text{s.t.} & & & \\
cons_{n,t} - \sum_u \left(g^{da}_{n,u,t} + g^{up}_{n,u,t} - g^{down}_{n,u,t} \right) - \sum_k B_{n,k} \delta_{k,t} = 0 & \lambda^{cm}_{n,t} \ (\text{free}) & \forall n,t & (12) \\
g^{da}_{n,u,t} + g^{up}_{n,u,t} \le g^{max}_{n,u,t} & \beta^{up}_{n,u,t} \ge 0 & \forall n,u,t & (13) \\
g^{down}_{n,u,t} \le g^{da}_{n,u,t} & \beta^{down}_{n,u,t} \ge 0 & \forall n,u,t & (14) \\
g^{up}_{n,u,t} \le \varepsilon^{reserve^{up}}_{n,u} g^{max}_{n,u,t} & \theta^{up}_{n,u,t} \ge 0 & \forall n,u,t & (15) \\
g^{down}_{n,u,t} \le \varepsilon^{reserve^{down}}_{n,u} g^{max}_{n,u,t} & \theta^{down}_{n,u,t} \ge 0 & \forall n,u,t & (16) \\
\sum_n H_{\ell,n} \delta_{n,t} \le cap^{max}_{\ell} & \overline{\mu_{\ell,t}} \ge 0 & \forall \ell,t & (17) \\
-\sum_n H_{\ell,n} \delta_{n,t} \le cap^{max}_{\ell} & \underline{\mu_{\ell,t}} \ge 0 & \forall \ell,t & (18) \\
sw_n \delta_{n,t} = 0 & \gamma_{n,t} \ (\text{free}) & \forall n,t & (19)
\end{array} \right.$$

where $\Omega^{UL} = \left\{ \underbrace{s_{n,u}, g^{da}_{n,u,t}, g^{f}_{n,u,t}, g^{r}_{n,u,t}}_{\geq 0}, \underbrace{f_{n,u,t}, r_{n,u,t}}_{\in\{0,1\}} \right\}$ and Ω^{LL}

$$= \left\{ \underbrace{g^{up}_{n,u,t}, g^{down}_{n,u,t}}_{\geq 0}, \delta_{n,t} \right\}.$$

The support payments are determined by constraints (9) and (10). If plant (n,u) is fully dispatched and plant (k,o) is not, then the *final* bid price of plant (n,u), i.e., the *original* bid price of (n,u) minus the possible support payment, is less than or equal to the *final* bid price of plant (k,o); otherwise Eq. (9) is not binding. Moreover, constraint (10) requires that the *final* bid price of (n,u) is less than or equal to the *final* bid price of (k,o) if plant (n,u) is partially dispatched and plant (k,o) is not fully dispatched; otherwise, (10) is not binding. Consequently, Eqs. (3)–(10) make sure that no expensive generator is dispatched before the cheaper ones.

At the lower level, the TSO chooses the cost-minimizing (11) deployment of up- ($g^{up}_{n,u,t}$) and down-reserves ($g^{down}_{n,u,t}$) as well as voltage angles ($\delta_{n,t}$) to match supply to demand at every node (12). These nodes represent subregions, which aggregate demand and generation, and in which transmission constraints can be ignored. Eqs. (13)–(16) define the feasible up- and down-reserve deployment intervals for each plant. Furthermore, Eqs. (17)–(19) implement the linearized DC load flow transmission in keeping with [13] and [23].

The regulator can perfectly anticipate the outcomes of the lower level. Also, generation cost parameters are not affected by support payments, although producers who do not receive them may increase their bid prices because they know that producers who receive them are dispatched in any case. Consequently, the results of our model on given support payments and the associated costs need to be regarded as a lower bound. This interpretation is supported by the simplification that there is one cost-minimizing TSO inside a price area (in Germany, there are four) and imperfect coordination does not cause extra costs.

In general, bi-level problems of this form require re-formulation as mathematical programs with equilibrium constraints (MPECs) and subsequently as MILPs in order to be solved. However, in this case, our problem has a special structure that reduces it to a single-level problem in which there is no lower-level objective function. This is because all of the terms from the lower-level objective function are present in the upper level and there is no interaction between lower-level dual variables and upper-level primal variables. Thus, the two objective functions are not in conflict, and the upper-level objective function may simply be minimized subject to upper- and lower-level constraints (see Ref. [14] and Proposition 1 of [40]). Nevertheless, we will proceed with the re-formulation because a regulator may have other concerns besides simply minimizing generating costs, e.g., minimizing costs of emissions [32] or congestion, which may cause the upper- and lower-level objective functions to be in conflict. Indeed, while we use previously developed resolution techniques, our methodological contribution here is the development of a novel set of constraints in Eqs. (3)–(10) that enforce the day-ahead merit order regardless of the objective function. This technique may now be applied by researchers exploring the impact of policy measures on both day-ahead and balancing markets through customized upper-level objective functions. Otherwise, only social welfare maximization would be possible without violating the merit order. We provide the detailed MPEC and MILP formulations in Appendices A and B, respectively.

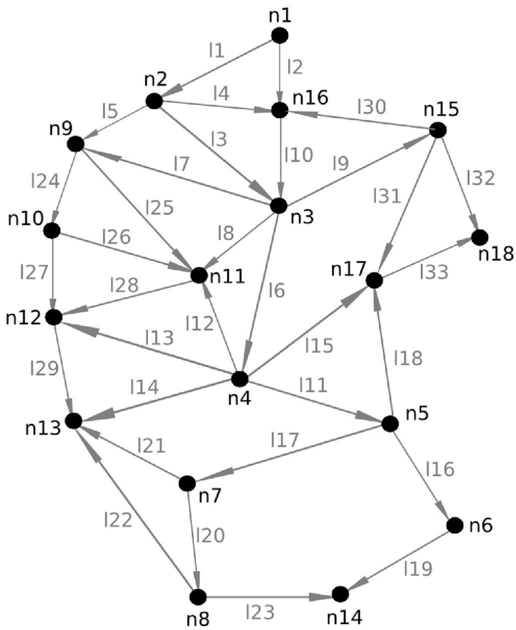

Fig. 2. Germany as an 18-node network with 33 cross-node transmission lines.

Table 1
Summary of the results of the three-node example.

measure	policy		
	no support	support	nodal
day-ahead cost (€)	3000	3600	3300
re-dispatch cost (€)	700	0	0
total cost (€)	3700	3600	3300
re-dispatch volume (MW)	40	0	0
congested lines	2, 3	1, 3	–

4. Numerical examples

4.1. A three-node example

To illustrate the effect of different policies, we run our model with and without support payments as well as a nodal pricing model similar to [23] (see Appendix E for the formulation) by considering a three-node network in which there is one generation unit at each node (see Fig. 1). The nodes represent locations in the network with generation units and load, while transmission lines connect the nodes. The network as well as demand and generation parameters are in Tables 5 and 6 of Appendix C, respectively.

The detailed transmission and generation results of our model are in Tables 7 and 8 of Appendix C, while Table 1 summarizes the key outcomes of the policies. In the absence of support payments, only power plants at nodes 1 and 2 are dispatched because they have the lowest bid prices, thereby leading to the lowest day-ahead cost of € 3000. However, because lines 2 and 3 to node 3 are

Table 2
Summary of the results of the German single-period case.

Scenario	Base			Extreme		
Measure	Policy					
	No support	Support	Nodal	No support	Support	Nodal
Day-ahead cost (M€)	1.379	1.379	1.388	1.289	1.400	1.381
Re-dispatch cost (M€)	0.018	0.018	0	0.175	0.061	0
Total cost (M€)	1.397	1.397	1.388	1.464	1.461	1.381
Re-dispatch volume (GW)	1.2	1.2	0	9.6	3.0	0
Congested lines	14, 18	14, 18	–	14, 18	14, 18	9, 14, 18

congested, the day-ahead solution does not allow demand to be served at node 3. The situation is resolved by deploying down-reserves of the plants at nodes 1 and 2 and up-reserves of the plant at node 3, which causes a re-dispatch cost of € 700.

When support payments are introduced, it is optimal to give the plant at node 3 a support payment of €10/MWh. This reduces the bid price of the plant 3 so that it is dispatched in the day-ahead market, thereby replacing part of the generation of the plant at node 2. The support payments increase the cost of day-ahead dispatch to € 3600, but now, transmission lines can be utilized to serve demand at all nodes without re-dispatching. Consequently, the total generation cost of € 3600 is slightly lower than that of the case without support payments.

Finally, the nodal pricing model achieves an even lower cost of € 3300 by considering the transmission constraints already in the day-ahead dispatch. Consequently, the plant at node 3 is dispatched out of merit order in the day-ahead market without giving any support payments.

4.2. German power system

Next, we model the German power system to assess the impacts of the different policies on the welfare and power system. More specifically, we use demand, generation and transmission network data from Ref. [10] to divide Germany into 18 DENA nodes [7], which correspond to large cities and their surroundings. The nodes and the transmission lines between them are shown in Fig. 2. Demand, generation capacity, generation cost, and transmission network parameters are provided in Tables 9–12 of Appendix D, in which we specify the calibration process.

In the following cases, we limit the set of discrete support payment levels only to zero and the differences in bid prices of different power plant types. Other support payment levels would be sub-optimal because the regulator at the upper level can, in view of lower-level outcomes, select which plants to dispatch from a set of plants with equal *final* bid prices. These restrictions decrease the size of the problem and speed up the computation without having an impact on the results. The model is implemented with GAMS 24.2 and solved with CPLEX 12.6 on an Intel i5 2.40 GHz processor and 4 GB RAM. The results for the following single- and multi-period cases are computed in less than 5 s. Constraints with continuous variables (such as ramping constraints) are not expected to affect the computational efficiency significantly, whereas new binary variables for constraints (such as startups of power plants) are likely to increase the computation time appreciably.

4.3. Single-period case

In the single-period case, we neglect the time index t in the formulation of Section 3. Consequently, constraints (7) and (8) can be disregarded. We examine two scenarios to study the need for support payments. First, in our base scenario, the demand is at the baseline level (Table 9), while wind, solar, and hydro power production are at 40%, 20%, and 20% levels of their maximum generation capacities (Table 10 in Appendix D), respectively. By comparison, since the average wind power generation was 17%, solar 11%, and hydro 13% in 2012 [9], we have taken a day with relatively high renewable generation as our base. In this scenario, support payments do not improve the welfare (see Table 2). Table 13 in Appendix D shows that coal plants are the last plants to be dispatched, and, thus, the day-ahead price is at the level of their bid price of € 40/MWh. Only small re-dispatch volumes are needed for (i) some deployment of gas-fired up-reserves in southern and western Germany and (ii) deployment of down-reserves of coal plants in eastern Germany (Table 14 in Appendix D). Table 15 in Appendix D shows that lines l14 and l18 are congested, which indicates strong flow to western and southern Germany.

Second, we run an extreme scenario in which we increase demand by 15% in southern and western German nodes (specifically, nodes 4–14). Furthermore, we increase wind power production to a very high 80% level of maximum capacity and decrease solar power production to 10%, while keeping hydro power production at the 20% level. Such hours occurred, for example, from 3 January 2012 to 5 January 2012, when hourly prices declined to €-75.04/MWh at minimum and increased to € 57.42/MWh at maximum. Now, gas plants at nodes 5 (Nuremberg area) and 6 (Munich area) are given an optimal support payment of € 15/MWh, which decreases their *final* bid price to the level of coal plants. Consequently, gas plants are dispatched at those nodes, while production from coal plants in northern Germany decreases (Table 16 in Appendix D). Table 17 in Appendix D shows that re-dispatch volumes increase from the base scenario, and up-reserves of gas-fired plants are now deployed in southern and western Germany, whereas the down-reserves of lignite and coal plants are deployed in eastern and northern Germany.

Table 2 shows that support payments increase day-ahead generation costs but decrease re-dispatch costs resulting in equal or lower total costs in both scenarios. In particular, when we disable support payments in the extreme scenario, both re-dispatch volumes and costs triple. The resulting re-dispatch volume of 9.6 GW can be compared with the maximum re-dispatch of 10.8 GW in 2014 [27]. However, we note that the change in total welfare is mainly affected by the costs of support payments relative to those of deploying up-reserves, and it is dependent on the parameters $c^{m}_{n,u}$ and $c^{up}_{n,u}$ in the model. Nevertheless, nodal pricing achieves even lower costs in both

Table 3
Summary of the results of the German multi-period case.

Measure	Policy		
	No support	Support	Nodal
Day-ahead cost (M€)	2.668	2.732	2.774
Re-dispatch cost (M€)	0.193	0.125	0
Total cost (M€)	2.861	2.857	2.774
Re-dispatch volume (GW)	10.8	7.2	0
Congested lines	14, 18	14, 18	9, 14, 18

Table 4
Summary of the results of the sensitivity analysis.

Measure	Policy		
	No support	Support	Nodal
Day-ahead cost (M€)	1.289	1.400	1.381
Expected re-dispatch cost (M€)	0.172	0.061	0.002
Expected total cost (M€)	1.461	1.461	1.383
Expected re-dispatch volume (GW)	9.7	3.4	0.8
Expected congested lines	14, 18	14, 18	9, 14, 18

scenarios. Table 20 in Appendix D shows that nodal pricing finds it optimal to dispatch gas plants in the extreme scenario and that their dispatch at nodes 5 and 6 is close to that of the model with support payments in Table 16 in Appendix D. Consequently, support payments enable policymakers to increase the flexibility and the stability of the power system because they decrease the need for re-dispatch and increase the dispatch of flexible gas-fired plants already in the day-ahead market. Furthermore, the need for north-to-south grid expansion considered by Ref. [23] is alleviated as nodal pricing and the model with support payments cause the flow to drop in this direction compared to the model without support payments (see Tables 18, 19, and 21 in Appendix D).

4.4. Multi-period case

Next, we combine our scenarios in a multi-period model in which the system moves from the base scenario to the extreme scenario. Thus, the main drivers are the increase of wind power from the 40% level to the 80% level, the 15% increase of demand at nodes 4–14, and the decrease of solar power from 20% to 10% level. We note that such a large change is hypothetical, but, given the trend toward increasing penetration of intermittent renewables, greater *absolute* hourly fluctuations (in MW) are likely to be observed in the future.

As in the extreme case, we see that a support payment of € 15/MWh to gas-fired plants at nodes 5 and 6 displaces coal-fired production in north-eastern Germany (Tables 22 and 23 in Appendix D). Unlike in the single-period base scenario, in which support payments are not optimal, there is now gas-fired production at node 5 at time t1, which decreases the need for re-dispatch by 42% (Table 24 in Appendix D). Consequently, support payments can reduce the costs of re-dispatch under normal, non-extreme wind conditions, too. Similar to the single-period extreme scenario, down-reserves of lignite plants are deployed in eastern Germany in period 2, but, additionally, some slow-ramping coal plants dispatched in period 1 need to deploy their down-reserves in north-eastern Germany.

If we disable support payments in the multi-period case, then there is only a 0.1% increase in total costs (see Table 3), while the re-dispatch volumes increase by 50%. More specifically, the deployment of gas-fired up-reserves and down-reserves of coal as well as lignite plants increases, whereas with support payments, the gas-fired plants offset the significant change in demand and renewable generation already in the day-ahead market. Thus, policymakers can utilize support payments to mitigate short-term variability, which allows for higher penetration of renewables. As a comparison, Table 3 shows that nodal pricing saves 3% on total costs vis-à-vis support payments by eliminating the need for re-dispatching.

4.5. Sensitivity analysis with respect to uncertainty in demand and renewable generation

To test the robustness of the support payment decisions, we run a stochastic version of the lower-level problem in Eqs. (11)–(19) with fixed upper-level decisions from the single-period extreme scenario in Section 4. Specifically, we introduce imbalances such as demand as well as wind and solar power forecast errors by adding the term $imb_{n,t}$ to the left-hand-side of the nodal power balance equation (12) and evaluate the expected balancing volume and cost by averaging the total balancing volume and cost of all imbalance scenarios, respectively. These scenarios are generated by sampling N unique four-dimensional vectors from quarter-hourly imbalances for the four German TSOs in 2012 [28] using the MATLAB 2015a function *datasample*. Each TSO-wise imbalance is distributed to its nodes in accordance to their shares of demand and generation capacity. The samples have weak positive correlation, and the marginal distributions are characterized by a spike close to zero and relatively fat tails.

With $N=10000$ and expected imbalances of 1.2 GW, the expected total generation costs with and without support payments are equal at €1.461 million (see Table 4 in which expected congestion is defined as congestion in more than 50% of the scenarios). As the expected balancing volumes are 3.4 GW and 9.7 GW, respectively, both models need to do substantial re-dispatching in order to eliminate the imbalances. By contrast, the nodal pricing model is able to net positive and negative imbalances as the expected re-dispatch volume at 0.8 GW is lower than the expected imbalance. Nevertheless, support payments to gas-fired plants in southern Germany can reduce re-dispatch volumes caused by imbalances substantially, and, thus, respond better to forecast errors of variable renewable generation, for example. Performing the sensitivity analysis with $N=10000$ scenarios takes approximately 7 min.

In addition, we test the multi-period model by increasing consumption in the second time step. Only a 3% increase in consumption causes the model without support payments to become infeasible due to inadequate flexibility to deploy down-reserves in northern and eastern Germany and to deploy up-reserves in southern and western Germany. However, the model with support payments finds a solution even when consumption is 9% higher by dispatching gas-fired plants, thereby indicating that policymakers can proactively increase the reliability of the power system with support payments.

5. Conclusions

In this paper, we have developed a complementarity model to study the impacts of support payments on total generation costs and balancing market volumes in Germany and, thus, their implications for power system flexibility. In our base scenario - which corresponds to normal conditions with modest renewable energy generation - support payments are not needed, but with high wind power production in northern Germany and high demand in southern and western Germany, support payments to gas-fired power plants in southern Germany become optimal. However, the savings in total generation costs are small because the costs of support payments and re-dispatch largely offset each other, but re-dispatch volumes decrease significantly by a factor of 1–2. Moreover, in the multi-period scenario, we find that support payments allow gas-fired plants to be dispatched day-ahead and reduce re-dispatch volumes by offsetting the variability of renewable energy generation by utilizing their fast-ramping capabilities. Even in non-extreme wind conditions, re-dispatch costs are reduced so that the uneven distribution of wind power is mitigated.

Sensitivity analysis of the optimal support payments indicates that they can reduce expected balancing volumes and costs. Also, the power system with support payments is able to withstand quicker changes in consumption and renewable generation. On the other hand, our results show that nodal pricing would be the most effective method to decrease balancing and re-dispatch volumes. However, the regulator has outlined that uniform pricing will be maintained [5]. Therefore, support payments would be an effective medium-term measure to integrate renewables. One drawback is that the regulator cannot predict the market outcomes perfectly, and, thus, excess support payments may be needed, thereby resulting in welfare losses. Also, some capacity mechanisms have failed to enforce timely availability [2].

From the modeling perspective, the lack of cross-border flows and the simplicity of the day-ahead bidding model, in particular, can give overly strong indications about the need for support payments. Extending the model to a stochastic bi-level problem would give more insight into optimal support payments under spatio-temporally correlated imbalances. More extensive vulnerability assessment of short-term supply adequacy could be conducted with a so-called interdiction model, where the upper- and lower-level conflict. On the one hand, future research could seek to develop more detailed short-term models, but on the other hand, long-term security of supply or possible market power issues were not addressed. However, as we maintain the merit order using constraints, we can specify customized objective functions that do not minimize generation costs only, which allows for new types of power market simulations. For example, one such possibility is to replace support payments with CO_2 prices in order to study their impacts on power systems.

Acknowledgements

This research has been supported by funding from the STEEM project of the Aalto Energy Efficiency programme. Siddiqui acknowledges the support of the RISKY-RES project (number 228811) funded by the Research Council of Norway. We are grateful for feedback from attendees of the 2014 GOR, 2015 NESS, and 2015 ISMP conferences. In particular, insights from lead discussant Juan Miguel Morales of DTU at the NESS conference are greatly appreciated. Comments from three anonymous referees and the handling editor have also improved this work. All remaining errors are the authors' own.

Appendix A. MPEC formulation

We cast the bi-level program (1)–(19) as a single-level MPEC, which is then used to formulate the linearized model. In the MPEC, the upper-level Eqs. (1)–(10) remain unchanged, and the decision variables consist of upper- and lower-level decision variables as well as the dual variables of the lower-level problem [12]. Since the lower-level problem is convex, it can be replaced by its Karush-Kuhn-Tucker (KKT) conditions (A-2)–(A-12).

$$\underset{\Omega^{UL}\cup\Omega^{LL}\cup\Omega^{DV}}{\text{Minimize}} \sum_t \sum_n \sum_u \left(\left(c^m_{n,u} + s_{n,u} \right) g^{da}_{n,u,t} + c^{up}_{n,u} g^{up}_{n,u,t} - c^{down}_{n,u} g^{down}_{n,u,t} \right) \tag{A-1}$$

s.t.

Eqs. (2)–(10)

$$\lambda^{cm}_{n,t} \text{ (free)}, \; cons_{n,t} - \sum_u \left(g^{da}_{n,u,t} + g^{up}_{n,u,t} - g^{down}_{n,u,t} \right) - \sum_k B_{n,k}\delta_{k,t} = 0 \quad \forall n,t \tag{A-2}$$

$$\delta_{n,t} \text{ (free)}, \; -\sum_k B_{k,n}\lambda^{cm}_{k,t} + \sum_l H_{l,n}\overline{\mu_{l,t}} - \sum_l H_{l,n}\underline{\mu_{l,t}} + sw_n\gamma_{n,t} = 0 \quad \forall n,t \tag{A-3}$$

$$\gamma_{n,t} \text{ (free)}, \; sw_n\delta_{n,t} = 0 \quad \forall n,t \tag{A-4}$$

$$g^{up}_{n,u,t} \geq 0 \perp c^{up}_{n,u} - \lambda^{cm}_{n,t} + \beta^{up}_{n,u,t} + \theta^{up}_{n,u,t} \geq 0 \quad \forall n,u,t \tag{A-5}$$

$$g^{down}_{n,u,t} \geq 0 \perp -c^{down}_{n,u} + \lambda^{cm}_{n,t} + \beta^{down}_{n,u,t} + \theta^{down}_{n,u,t} \geq 0 \quad \forall n,u,t \tag{A-6}$$

$$\beta^{up}_{n,u,t} \geq 0 \perp g^{max}_{n,u,t} - g^{da}_{n,u,t} - g^{up}_{n,u,t} \geq 0 \quad \forall n,u,t \tag{A-7}$$

$$\beta^{down}_{n,u,t} \geq 0 \perp g^{da}_{n,u,t} - g^{down}_{n,u,t} \geq 0 \quad \forall n,u,t \tag{A-8}$$

$$\theta^{up}_{n,u,t} \geq 0 \perp \varepsilon^{reserve^{up}}_{n,u} g^{max}_{n,u,t} - g^{up}_{n,u,t} \geq 0 \quad \forall n,u,t \tag{A-9}$$

$$\theta^{down}_{n,u,t} \geq 0 \perp \varepsilon^{reserve^{down}}_{n,u} g^{max}_{n,u,t} - g^{down}_{n,u,t} \geq 0 \quad \forall n,u,t \tag{A-10}$$

$$\overline{\mu_{\ell,t}} \geq 0 \perp cap^{max}_{\ell} - \sum_n H_{\ell,n}\delta_{n,t} \geq 0 \quad \forall \ell,t \tag{A-11}$$

$$\underline{\mu_{\ell,t}} \geq 0 \perp cap^{max}_{\ell} + \sum_n H_{\ell,n}\delta_{n,t} \geq 0 \quad \forall \ell,t \tag{A-12}$$

$$\text{where } \Omega^{DV} = \left\{ \lambda^{cm}_{n,t}, \gamma_{n,t}, \underbrace{\beta^{up}_{n,u,t}, \beta^{down}_{n,u,t}, \theta^{up}_{n,u,t}, \theta^{down}_{n,u,t}, \overline{\mu_{\ell,t}}, \underline{\mu_{\ell,t}}}_{\geq 0} \right\}.$$

Appendix B. MILP formulation

Our MPEC is non-linear due to the bi-linear terms $s_{n,u}g_{n,u,t}$ in Eq. (A-1) and complementarity conditions (A-5)–(A-12). We apply the linearization procedure of [13]. First, the complementarity conditions in (A-5)–(A-12) are associated with disjunctive variables $r1,\ldots,r8$ and two corresponding disjunctive constraints in the set of Eqs. (A-20)–(A-35). Second, we introduce valid discrete support payment levels $\bar{s}_{n,u,i}$ and binary indicator variables $q_{n,u,i}$ that equal 1 only when the ith discrete support payment level is selected. Moreover, the binary indicator variables $q^{g^{da}}_{n,u,t}$ equal to 1 when $g^{da}_{n,u,t} > 0$ and 0 otherwise. Thus, the bi-linear terms in the objective function can be replaced with the following variable

$$v_{n,u,i,t} = \begin{cases} \bar{s}_{n,u,i} g^{da}_{n,u,t} \text{ if } q_{n,u,i} = q^{g^{da}}_{n,u,t} = 1 \\ 0 \text{ otherwise} \end{cases} \tag{A-13}$$

The logic is modeled with constraints (A-15)–(A-19) as follows. If plant (n,u) is running at time period t, then $q^{g^{da}}_{n,u,t}$ is equal to one (Eq. (A-15)). Constraint (A-16) ensures that the variable $q_{n,u,i}$ is equal to 1 when the ith discrete support payment level $\bar{s}_{n,u,i}$ is selected and zero otherwise. Constraint (A-17) ensures that only one payment level is selected for each (n,u). Next, constraint (A-18) allows the binary variable $q^{v}_{n,u,i,t}$ to be one only if both $q^{g^{da}}_{n,u,t}$ and $q_{n,u,i}$ are one. Consequently, if $q^{v}_{n,u,i,t}$ is zero, then constraint (A-19) drives the bi-linear term $v_{n,u,i,t}$ to zero. When $q^{v}_{n,u,i,t}$ becomes one, the lower bound of $v_{n,u,i,t}$ becomes $\bar{s}_{n,u,i}g^{da}_{n,u,t}$, which is the optimal value for $v_{n,u,i,t}$ to minimize the objective function.

$$\underset{\Omega^{UL}\cup\Omega^{LL}\cup\Omega^{DV}\cup\Phi}{\text{Minimize}} \sum_t \sum_n \sum_u \left[\left(c^m_{n,u} g^{da}_{n,u,t} + c^{up}_{n,u} g^{up}_{n,u,t} - c^{down}_{n,u} g^{down}_{n,u,t} \right) + \sum_i v_{n,u,i,t} \right] \tag{A-14}$$

s.t.

$$K_{g^{da}} q^{g^{da}}_{n,u,t} - g^{da}_{n,u,t} \geq 0 \quad \forall n,u,t \tag{A-15}$$

$$s_{n,u} = \sum_i q_{n,u,i} \bar{s}_{n,u,i} \quad \forall n,u \tag{A-16}$$

$$\sum_i q_{n,u,i} - 1 = 0 \quad \forall n,u \tag{A-17}$$

$$\begin{cases} q^v_{n,u,i,t} \leq q^{g^{da}}_{n,u,t} & \forall n,u,i,t \\ q^v_{n,u,i,t} \leq q_{n,u,i} & \forall n,u,i,t \\ q_{n,u,i} + q^{g^{da}}_{n,u,t} - 1 \leq q^v_{n,u,i,t} & \forall n,u,i,t \end{cases} \tag{A-18}$$

$$\begin{cases} 0 \leq v_{n,u,i,t} \leq K_v q^v_{n,u,i,t} & \forall n,u,i,t \\ 0 \leq \bar{s}_{n,u,i} g^{da}_{n,u,t} - v_{n,u,i,t} \leq K_v \left(1 - q^v_{n,u,i,t}\right) & \forall n,u,i,t \end{cases} \tag{A-19}$$

Eqs. (2)–(10)
Eqs. (A–2)–(A–4)

$$K_1 r1_{n,u,t} \geq c^{up}_{n,u} - \lambda^{cm}_{n,t} + \beta^{up}_{n,u,t} + \theta^{up}_{n,u,t} \geq 0 \quad \forall n,u,t \tag{A-20}$$

$$K_1 (1 - r1_{n,u,t}) \geq g^{up}_{n,u,t} \geq 0 \quad \forall n,u,t \tag{A-21}$$

$$K_2 r2_{n,u,t} \geq -c^{down}_{n,u} + \lambda^{cm}_{n,t} + \beta^{down}_{n,u,t} + \theta^{down}_{n,u,t} \geq 0 \quad \forall n,u,t \tag{A-22}$$

$$K_2 (1 - r2_{n,u,t}) \geq g^{down}_{n,u,t} \geq 0 \quad \forall n,u,t \tag{A-23}$$

$$K_3 r3_{n,u,t} \geq g^{max}_{n,u,t} - g^{da}_{n,u,t} - g^{up}_{n,u,t} \geq 0 \quad \forall n,u,t \tag{A-24}$$

$$K_3 (1 - r3_{n,u,t}) \geq \beta^{up}_{n,u} \geq 0 \quad \forall n,u,t \tag{A-25}$$

$$K_4 r4_{n,u,t} \geq g^{da}_{n,u,t} - g^{down}_{n,u,t} \geq 0 \quad \forall n,u,t \tag{A-26}$$

$$K_4 (1 - r4_{n,u,t}) \geq \beta^{down}_{n,u,t} \geq 0 \quad \forall n,u,t \tag{A-27}$$

$$K_5 r5_{n,u,t} \geq \varepsilon^{reserve^{up}}_{n,u} g^{max}_{n,u,t} - g^{up}_{n,u,t} \geq 0 \quad \forall n,u,t \tag{A-28}$$

$$K_5 (1 - r5_{n,u,t}) \geq \theta^{up}_{n,u,t} \geq 0 \quad \forall n,u,t \tag{A-29}$$

$$K_6 r6_{n,u,t} \geq \varepsilon^{reserve^{down}}_{n,u} g^{max}_{n,u,t} - g^{down}_{n,u,t} \geq 0 \quad \forall n,u,t \tag{A-30}$$

$$K_6 (1 - r6_{n,u,t}) \geq \theta^{down}_{n,u,t} \geq 0 \quad \forall n,u,t \tag{A-31}$$

$$K_7 r7_{\ell,t} \geq cap^{max}_\ell - \sum_n H_{\ell,n} \delta_{n,t} \geq 0 \quad \forall \ell,t \tag{A-32}$$

$$K_7 (1 - r7_{\ell,t}) \geq \overline{\mu_{\ell,t}} \geq 0 \quad \forall \ell,t \tag{A-33}$$

$$K_8 r8_{\ell,t} \geq cap^{max}_\ell + \sum_n H_{\ell,n} \delta_{n,t} \geq 0 \quad \forall \ell,t \tag{A-34}$$

$$K_8 (1 - r8_{\ell,t}) \geq \underline{\mu_{\ell,t}} \geq 0 \quad \forall \ell,t \tag{A-35}$$

where $\Phi = \{ \underbrace{v_{n,u,i,t}}_{\geq 0}, \underbrace{q^{g^{da}}_{n,u,t}, q^v_{n,u,i,t}, q_{n,u,i}, r1, \ldots, r8}_{\in\{0,1\}} \}$

Appendix C. Calibration and detailed results of the three-node example

Table 5
Network parameters of the three-node example

Parameter	l1	l2	l3
cap^{max}_ℓ (MW)	10	10	10

Table 6
Demand and generation parameters of the three-node example

Parameter	Node 1	Node 2	Node 3
$cons_n$ (MW)	40	40	40
$c^m_{n,u}$ (€/MWh)	20	30	40
$c^{up}_{n,u}$ (€/MWh)	60	60	60
$c^{down}_{n,u}$ (€/MWh)	20	30	40
$g^{max}_{n,u}$ (MW)	60	60	60

Table 7
Network flow results of the three-node example

Support payments	Disabled			Enabled		
	l1	l2	l3	l1	l2	l3
Flow (MW)	0	10	10	10	0	10

Table 8
Generation results of the three-node example

Support payments	Disabled			Enabled		
Variable	node 1	node 2	node 3	node 1	node 2	node 3
$s_{n,u}$ (€/MWh)	0	0	0	0	0	10
$g^{da}_{n,u}$ (MW)	60	60	0	60	30	30
$g^{up}_{n,u}$ (MW)	0	0	20	0	0	0
$g^{down}_{n,u}$ (MW)	10	10	0	0	0	0

Appendix D. Calibration and detailed results of the German power system model

We use data for the 18 DENA nodes from Ref. [10]. The baseline demand for each zone in Table 9 is computed by averaging the off-peak and on-peak demand share of each zone. Furthermore, we scale these figures up by 10% to remove the impact of weekends and holidays.

In compiling the maximum generation capacities in Table 10, we neglect power plants that use biomass, waste, or oil because they have relatively small generation capacities. For simplicity, we combine different types of power plants using the same fuel under one category. Furthermore, the capacities of nuclear, lignite, and coal plants have been reduced by 15% to account for maintenance outages. Table 11 shows the different costs and ramping efficiencies of the power plants based on our rough estimations. We note that wind, solar, and nuclear production cannot be up- or down-reserved and that lignite and coal plants ramp-up relatively slowly, whereas gas-fired plants are characterized by flexibility [16].

The transmission network parameters in Table 12 have been compiled by adding the thermal capacities, resistances, and reactances of all 220 kV and 380 kV circuits for each pair of nodes. In calculating the thermal capacity, we assume that one 220 kV circuit corresponds to thermal capacity of 490 MW and one 380 kV to 1700 MW [10]. We assume bi-directional current flow on every line, and if technical characteristics of the line depend on the flow direction, then we take the maximum of every parameter. To account for network security constraints, we limit the thermal capacity of each line to 80% of the maximum capacity.

Table 9
Baseline demand for each node in GW

	n1	n2	n3	n4	n5	n6	n7	n8	n9	n10	n11	n12	n13	n14	n15	n16	n17	n18
$cons_{n,t}$	1.1	3.0	4.4	3.2	3.1	5.2	3.6	5.4	1.2	9.9	3.7	6.5	5.6	1.5	4.8	1.9	2.4	3.4

Table 10
Maximum generation capacity ($g^{max}_{n,u,t}$) for each node in GW

Node	Type						
	Wind	Solar	Nuclear	Hydro	Lignite	Coal	Gas
n1	3.6	1.1	1.2	0	0	0.4	0
n2	4.4	1.5	0	0	0	1.4	0.7
n3	2.9	1	1.2	0.3	0.3	2	0.6
n4	1	1.4	0	0.7	0	0.9	0.5
n5	0.7	3.3	1.1	0.5	0	0	1.3
n6	0.1	4	1.2	1.4	0	0.7	2.4
n7	0.2	1.3	2.3	0.1	0	1.5	0.6
n8	0.4	3.1	0	2.5	0	0.8	0.4
n9	1.1	1	1.1	0	0	0.7	1.8
n10	0.5	1.4	0	0.2	2.2	6.2	2.6
n11	1.3	1.3	0	0.2	0	1.8	2
n12	1.3	1.1	0	0.2	6.6	0	1.5
n13	1.6	1.8	0	0.2	0	3.1	1.9
n14	0.1	2.1	2.2	0.4	0	0	0.1
n15	7.2	2.7	0	0	0.2	1.1	2.2
n16	0.4	0.2	0	0.1	0	0.4	0.1
n17	2.4	1.7	0	1.6	0.9	0	0.8
n18	2.9	2.5	0	1.2	7.6	0	0.7

Table 12
Transmission network parameters

line	capacity (GW)	resistance (Ω)	reactance (Ω)
l1	2.7	1.7	14.9
l2	4.3	11.4	67.5
l3	2.2	5.2	38.3
l4	2.7	3.2	27.4
l5	2.7	1.4	7.7
l6	3.5	3.5	27.3
l7	1.4	2.4	20.6
l8	3.5	5	31.7
l9	2.7	1.5	12.7
l10	2.7	0.9	7.4
l11	2.7	4.4	38
l12	4.1	2.6	22.8
l13	1.4	1.6	14.2
l14	2.7	1.3	11.5
l15	2.7	5.7	49
l16	5.3	17.9	115.4
l17	2.7	5.8	50.4
l18	2.7	1.7	14.6
l19	2.7	1.5	13
l20	9.4	15	122.9
l21	2.6	15.4	98.2
l22	2.7	13.3	72
l23	6.6	8.9	56.5
l24	3.1	9.1	66.4
l25	3.1	8.1	61.8
l26	4.3	11.8	66.2
l27	13.4	15.6	102.5
l28	0.8	3.1	16.6
l29	7.6	20.7	147.3
l30	2.7	2.6	22.7
l31	2.7	3.6	31
l32	5.8	20.5	165.4
l33	5.3	33.1	212.7

Table 11
Power plant cost and efficiency parameters

type	$c^{m}_{n,u}$ (€/MWh)	$c^{up}_{n,u}$ (€/MWh)	$c^{down}_{n,u}$ (€/MWh)	$\varepsilon^{da^{up}}_{n,u}$	$\varepsilon^{da^{down}}_{n,u}$	$\varepsilon^{reserve^{up}}_{n,u}$	$\varepsilon^{reserve^{down}}_{n,u}$
$u1$ (wind)	0	999	−999	1	1	0	0
$u2$ (solar)	0	999	−999	1	1	0	0
$u3$ (nuclear)	1	100	−100	0	0	0	0
$u4$ (hydro)	5	30	5	0.5	0.7	0.5	0.7
$u5$ (lignite)	30	40	25	0.3	0.7	0.2	0.6
$u6$ (coal)	40	50	35	0.3	0.7	0.2	0.6
$u7$ (gas)	55	65	55	0.9	1	0.8	0.9

Table 13
Day-ahead generation of each power plant type in GW in the base scenario (empty cells are zero)

Node	Type						
	Wind	Solar	Nuclear	Hydro	Lignite	Coal	Gas
n1	1.44	0.22	1.19			0.43	
n2	1.76	0.30				1.36	
n3	1.16	0.20	1.19	0.06	0.34	2.04	
n4	0.40	0.28		0.14		0.94	
n5	0.28	0.66	1.11	0.10			
n6	0.04	0.80	1.19	0.28		0.68	
n7	0.08	0.26	2.30	0.02		1.53	
n8	0.16	0.62		0.50		0.77	
n9	0.44	0.20	1.11			0.68	
n10	0.20	0.28		0.04	2.21	6.21	
n11	0.52	0.26		0.04		1.79	
n12	0.52	0.22		0.04	6.63		
n13	0.64	0.36		0.04		3.06	
n14	0.04	0.42	2.21	0.08			
n15	2.88	0.54			0.17	0.76	
n16	0.16	0.04		0.02		0.43	
n17	0.96	0.34		0.32	0.85		
n18	1.16	0.50		0.24	7.57		

Table 14
Deployment of up- and down-reserves in the base scenario (empty rows and columns have been removed to save space)

Node	Type	
	Coal	Gas
n7		0.43
n13		0.17
n15	−0.59	

Table 17
Deployment of up- and down-reserves in the extreme scenario with and without support payments (empty rows and columns have been removed to save space)

Node	Support payments enabled		Support payments disabled		
	Type				
	Lignite	Gas	Lignite	Coal	Gas
n1				−0.26	
n2				−0.48	
n3				−0.97	
n5		0.22			1.04
n6					1.92
n7		0.48			0.48
n8		0.32			0.32
n13		0.69			0.97
n14					0.08
n17	−0.51		−0.51		
n18	−1.20		−2.60		

Table 15
Transmission flows in the base scenario (congested lines are indicated by *)

l1 1.67	l2 0.51	l3 0.42	l4 0.45	l5 1.24	l6 −1.93	l7 −0.18	l8 1.25	l9 −1.12	l10 −0.87	l11 −0.07
l12 −0.56	l13 −0.72	l14* 2.70	l15 −0.86	l16 1.33	l17 0.36	l18* −2.70	l19 −0.85	l20 1.19	l21 0.15	l22 −1.79
l23 −0.36	l24 0.78	l25 0.71	l26 −0.12	l27 −0.06	l28 0.14	l29 0.28	l30 0.34	l31 0.81	l32 −3.35	l33 −2.70

Table 16
Day-ahead generation of each power plant type in GW in the extreme scenario with and without support payments (empty cells are zero)

Node	Support payments enabled							Support payments disabled					
	Type												
	Wind	Solar	Nuclear	Hydro	Lignite	Coal	Gas	Wind	Solar	Nuclear	Hydro	Lignite	Coal
n1	2.88	0.11	1.19					2.88	0.11	1.19			0.26
n2	3.52	0.15						3.52	0.15				0.48
n3	2.32	0.10	1.19	0.06	0.34			2.32	0.10	1.19	0.06	0.34	2.03
n4	0.80	0.14		0.14		0.94		0.80	0.14		0.14		0.94
n5	0.56	0.33	1.11	0.10			1.05	0.56	0.33	1.11	0.10		
n6	0.08	0.40	1.19	0.28		0.68	2.39	0.08	0.40	1.19	0.28		0.68
n7	0.16	0.13	2.30	0.02		1.53		0.16	0.13	2.30	0.02		1.53
n8	0.32	0.31		0.50		0.77		0.32	0.31		0.50		0.77
n9	0.88	0.10	1.11					0.88	0.10	1.11			0.68
n10	0.40	0.14		0.04	2.21	6.21		0.40	0.14		0.04	2.21	6.21
n11	1.04	0.13		0.04		1.79		1.04	0.13		0.04		1.79
n12	1.04	0.11		0.04	6.63			1.04	0.11		0.04	6.63	
n13	1.28	0.18		0.04		3.06		1.28	0.18		0.04		3.06
n14	0.08	0.21	2.21	0.08				0.08	0.21	2.21	0.08		
n15	5.76	0.27			0.17			5.76	0.27			0.17	
n16	0.32	0.02		0.02				0.32	0.02		0.02		
n17	1.92	0.17		0.32	0.85			1.92	0.17		0.32	0.85	
n18	2.32	0.25		0.24	7.57			2.32	0.25		0.24	7.57	

Table 18
Transmission flows in the extreme scenario with support payments (congested lines are denoted with *)

l1 2.40	l2 0.68	l3 0.58	l4 1.09	l5 1.42	l6 2.22	l7 0.36	l8 1.72	l9 −2.57	l10 −1.53	l11 −0.58
l12 −0.25	l13 −0.05	l14* 2.70	l15 −1.25	l16 1.10	l17 0.84	l18* −2.70	l19 0.18	l20 1.17	l21 0.11	l22 −1.82
l23 −0.98	l24 1.37	l25 0.77	l26 −0.65	l27 −0.37	l28 0.29	l29 0.21	l30 0.94	l31 1.03	l32 −3.17	l33 −2.59

Table 19
Transmission flows in the extreme scenario without support payments (congested lines are denoted with *)

l1 2.38	l2 0.70	l3 0.59	l4 0.90	l5 1.60	l6 2.49	l7 0.10	l8 1.82	l9 −1.80	l10 −1.35	l11 −0.25
l12 −0.42	l13 −0.20	l14* 2.70	l15 −1.00	l16 1.26	l17 0.78	l18* −2.70	l19 −0.13	l20 1.21	l21 0.01	l22 −2.02
l23 −0.76	l24 1.46	l25 0.91	l26 −0.61	l27 −0.33	l28 0.40	l29 0.23	l30 0.56	l31 1.36	l32 −2.36	l33 −2.01

Table 20
Day-ahead generation of each power plant type in GW in the extreme scenario with nodal pricing

Node	Type						
	Wind	Solar	Nuclear	Hydro	Lignite	Coal	Gas
n1	2.88	0.11	1.19				
n2	3.52	0.15					
n3	2.32	0.10	1.19	0.06	0.34		
n4	0.80	0.14		0.14		0.94	
n5	0.56	0.33	1.11	0.10			1.30
n6	0.08	0.40	1.19	0.28		0.68	2.31
n7	0.16	0.13	2.30	0.02		1.53	0.55
n8	0.32	0.31		0.50		0.77	0.26
n9	0.88	0.10	1.11				
n10	0.40	0.14		0.04	2.21	6.00	
n11	1.04	0.13		0.04		1.79	
n12	1.04	0.11		0.04	6.63		
n13	1.28	0.18		0.04		3.06	0.73
n14	0.08	0.21	2.21	0.08			
n15	5.76	0.27			0.17		
n16	0.32	0.02		0.02			
n17	1.92	0.17		0.32			
n18	2.32	0.25		0.24	6.91		

Table 21
Transmission flows in the extreme scenario with nodal pricing

l1 2.40	l2 0.68	l3 0.58	l4 1.13	l5 1.39	l6 2.27	l7 0.41	l8 1.77	l9* −2.70	l10 −1.56	l11 −0.58
l12 −0.23	l13 −0.02	l14* 2.70	l15 −1.25	l16 1.15	l17 0.82	l18* −2.70	l19 0.15	l20 1.21	l21 0.12	l22 −1.87
l23 −0.96	l24 1.45	l25 0.78	l26 −0.72	l27 −0.42	l28 0.29	l29 0.21	l30 1.00	l31 1.13	l32 −3.47	l33 −2.84

Table 22
Day-ahead generation in each power plant type in the multi-period case with support payments (empty cells are zero)

Node	Type													
	Wind		Solar		Nuclear		Hydro		Lignite		Coal		Gas	
	t1	t2	t1	t2	t1	t2	t1	t2	t1	t2	t1	t2	t1	t2
n1	1.44	2.88	0.22	0.11	1.19	1.19					0.43	0.26		
n2	1.76	3.52	0.30	0.15							1.36	0.60		
n3	1.16	2.32	0.20	0.10	1.19	1.19	0.06	0.06	0.34	0.34	2.04	0.61		
n4	0.40	0.80	0.28	0.14			0.14	0.14			0.94	0.94		
n5	0.28	0.56	0.66	0.33	1.11	1.11	0.10	0.10					0.26	1.30
n6	0.04	0.08	0.80	0.40	1.19	1.19	0.28	0.28			0.68	0.68		0.34
n7	0.08	0.16	0.26	0.13	2.30	2.30	0.02	0.02			1.53	1.53		
n8	0.16	0.32	0.62	0.31			0.50	0.50			0.77	0.77		
n9	0.44	0.88	0.20	0.10	1.11	1.11					0.68	0.20		
n10	0.20	0.40	0.28	0.14			0.04	0.04	2.21	2.21	6.21	6.21		
n11	0.52	1.04	0.26	0.13			0.04	0.04			1.79	1.79		
n12	0.52	1.04	0.22	0.11			0.04	0.04	6.63	6.63				
n13	0.64	1.28	0.36	0.18			0.04	0.04			3.06	3.06		
n14	0.04	0.08	0.42	0.21	2.21	2.21	0.08	0.08						
n15	2.88	5.76	0.54	0.27					0.17	0.17	0.50			
n16	0.16	0.32	0.04	0.02			0.02	0.02			0.43	0.13		
n17	0.96	1.92	0.34	0.17			0.32	0.32	0.85	0.85				
n18	1.16	2.32	0.50	0.25			0.24	0.24	7.57	7.57				

Table 23
Day-ahead generation in each power plant type in the multi-period case without support payments (empty cells are zero)

Node	Type											
	Wind		Solar		Nuclear		Hydro		Lignite		Coal	
	t1	t2	t1	t2	t1	t2	t1	t2	t1	t2	t1	t2
n1	1.44	2.88	0.22	0.11	1.19	1.19					0.43	0.26
n2	1.76	3.52	0.30	0.15							1.36	0.82
n3	1.16	2.32	0.20	0.10	1.19	1.19	0.06	0.06	0.34	0.34	2.04	1.06
n4	0.40	0.80	0.28	0.14			0.14	0.14			0.94	0.94
n5	0.28	0.56	0.66	0.33	1.11	1.11	0.10	0.10				
n6	0.04	0.08	0.80	0.40	1.19	1.19	0.28	0.28			0.68	0.68
n7	0.08	0.16	0.26	0.13	2.30	2.30	0.02	0.02			1.53	1.53
n8	0.16	0.32	0.62	0.31			0.50	0.50			0.77	0.77
n9	0.44	0.88	0.20	0.10	1.11	1.11					0.68	0.68
n10	0.20	0.40	0.28	0.14			0.04	0.04	2.21	2.21	6.21	6.21
n11	0.52	1.04	0.26	0.13			0.04	0.04			1.79	1.79
n12	0.52	1.04	0.22	0.11			0.04	0.04	6.63	6.63		
n13	0.64	1.28	0.36	0.18			0.04	0.04			3.06	3.06
n14	0.04	0.08	0.42	0.21	2.21	2.21	0.08	0.08				
n15	2.88	5.76	0.54	0.27					0.17	0.17	0.76	0.38
n16	0.16	0.32	0.04	0.02			0.02	0.02			0.43	0.26
n17	0.96	1.92	0.34	0.17			0.32	0.32	0.85	0.85		
n18	1.16	2.32	0.50	0.25			0.24	0.24	7.57	7.57		

Table 24
Deployment of up- and down-reserves in the multi-period case with and without support payments (empty rows and columns have been removed to save space)

Node	Support payments enabled						Support payments disabled					
	Type											
	Lignite		Coal		Gas		Lignite		Coal		Gas	
	t1	t2	t1	t2	t1	t2	t1	t2	t1	t2	t1	t2
n1				−0.26						−0.26		
n2				−0.60						−0.82		
n3				−0.61								1.04
n5											0.42	1.92
n6						1.92						
n7						0.48						0.48
n8						0.32						0.32
n9				−0.20								
n13					0.34	0.71					0.17	0.97
n14						0.08						0.08
n15			−0.34						−0.59	−0.38		
n16				−0.13						−0.26		
n17		−0.51						−0.51				
n18		−1.20						−2.60				

Appendix E. Nodal pricing model

For the nodal pricing model below, we introduce non-negative dual variables $\beta^{da}_{n,u,t}$, $\beta^{da^{up}}_{n,u,t}$, and $\beta^{da^{down}}_{n,u,t}$ for Eqs. (A-38)–(A-40), respectively.

$$\underset{\substack{g^{da}_{n,u,t},\delta_{n,u,t} \\ \geq 0}}{\text{Minimize}} \sum_t \sum_n \sum_u c^m_{n,u} g^{da}_{n,u,t} \tag{A-36}$$

s.t.

$$cons_{n,t} - \sum_u g^{da}_{n,u,t} - \sum_k B_{n,k}\delta_{k,t} = 0 \quad \lambda^{cm}_{n,t}\ (\text{free}) \quad \forall n,t \tag{A-37}$$

$$g^{da}_{n,u,t} \leq g^{max}_{n,u,t} \quad \beta^{up}_{n,u,t} \geq 0 \quad \forall n,u,t \tag{A-38}$$

$$g^{da}_{n,u,t} - g^{da}_{n,u,t-1} \leq \varepsilon^{da^{up}}_{n,u} g^{max}_{n,u,t} \quad \beta^{da^{up}}_{n,u,t} \geq 0 \quad \forall n,u, \text{ and } \forall t \geq 2 \tag{A-39}$$

$$g^{da}_{n,u,t-1} - g^{da}_{n,u,t} \leq \varepsilon^{da^{down}}_{n,u} g^{max}_{n,u,t} \quad \beta^{da^{down}}_{n,u,t} \geq 0 \quad \forall n,u, \text{ and } \forall t \geq 2 \tag{A-40}$$

$$\sum_n H_{\ell,n}\delta_{n,t} \leq cap^{max}_{\ell} \quad \overline{\mu_{\ell,t}} \geq 0 \quad \forall \ell,t \tag{A-41}$$

$$-\sum_n H_{\ell,n}\delta_{n,t} \leq cap^{max}_{\ell} \quad \underline{\mu_{\ell,t}} \geq 0 \quad \forall \ell,t \tag{A-42}$$

$$sw_n \delta_{n,t} = 0 \quad \gamma_{n,t} \text{ (free)} \quad \forall n, t \tag{A-43}$$

References

[1] Baringo L, Conejo A. Wind power investment within a market environment. Appl Energy 2011;88:3239–47.
[2] Batlle C, Rodilla P. A critical assessment of the different approaches aimed to secure electricity generation supply. Energy Policy 2010;38:7169–79.
[3] Batlle C, Vázquez C, Rivier M, Pérez-Arriaga IJ. Enhancing power supply adequacy in Spain: migrating from capacity payments to reliability options. Energy Policy 2007;35(9):4545–54.
[4] Benini M, Cremonesi F, Gallanti M, Gelmini A, Martini R. Capacity payment schemes in the Italian electricity market. CIGRE General Session. 2006.
[5] Bundesministerium für Wirtschaft und Energie (BMWi). Ein Strommarkt für die Energiewende. Ergebnispapier des Bundesministeriums für Wirtschaft und Energie (Weißbuch). 2015.
[6] Caldecott B, McDaniels J. Stranded generation assets: implications for European capacity mechanisms, energy markets and climate policy. Working paper. Smith School of Enterprise and the Environment, University of Oxford; 2014.
[7] Deutsche Energie-Agentur. dena-Netzstudie II. Integration erneuerbarer Energien in die deutsche Stromversorgung im Zeitraum 2015 – 2020 mit Ausblick 2025. 2010.
[8] Dupont B, Jonghe CD, Olmos L, Belmans R. Demand response with locational dynamic pricing to support the integration of renewables. Energy Policy 2014;67:344–54.
[9] EEX. EEX transparency platform. 2014. http://www.transparency.eex.com/en/.
[10] Egerer J, Gerbaulet C, Ihlenburg R, Kunz F, Reinhard B, von Hirschhausen C, et al. Electricity sector data for policy-relevant modeling: data documentation and applications to the German and European electricity markets. Deutsches Institut für Wirtschaftsforschung; 2014.
[11] Fusco F, Nolan G, Ringwood JV. Variability reduction through optimal combination of wind/wave resources – an Irish case study. Energy 2010;35:314–25.
[12] Gabriel SA, Conejo AJ, Fuller JD, Hobbs BF, Ruiz C. Complementarity Modeling in energy Markets. New York: Springer; 2013.
[13] Gabriel SA, Leuthold FU. Solving discretely-constrained MPEC problems with applications in electric power markets. Energy Econ 2010;32(1):3–14.
[14] Garcés LP, Conejo AJ, García-Bertrand R, Romero R. A bilevel approach to transmission expansion planning within a market environment. IEEE Trans Power Syst 2009;24(3):1513–22.
[15] German Federal Ministry for Economic Affairs and Energy (BMWi). An electricity market for Germany's energy transition. Discussion paper of the Federal Ministry for Economic Affairs and Energy (Green paper). 2014.
[16] Gutiérrez-Martín F, Da Silva-Álvarez RA, Montoro-Pintado P. Effects of wind intermittency on reduction of CO_2 emissions: the case of the Spanish power system. Energy 2013;61:108–17.
[17] Hach D, Spinler S. Capacity payment impact on gas-fired generation investments under rising renewable feed-in – a real options analysis. Energy Econ 2016;53:270–80.
[18] Hary N, Rious V, Saguan M. The electricity generation adequacy problem: assessing dynamic effects of capacity remuneration mechanisms. Energy Policy 2016;91:113–27.
[19] Huber M, Dimkova D, Hamacher T. Integration of wind and solar power in Europe: assessment of flexibility requirements. Energy 2014;69:236–46.
[20] Jaehnert S, Wolfgang O, Farahmand H, Völler S, Huertas-Hernando D. Transmission expansion planning in Northern Europe in 2030 – methodology and analyses. Energy Policy 2013;61:125–39.
[21] Jentsch M, Trost T, Sterner M. Optimal use of power-to-gas energy storage systems in an 85% renewable energy scenario. Energy Procedia 2014;46:254–61.
[22] Khazaei J, Downward A, Zakeri G. Modelling counter-intuitive effects on cost and air pollution from intermittent generation. Ann Operations Res 2014;222(1):389–418.
[23] Kunz F. Improving congestion management: how to facilitate the integration of renewable generation in Germany. Energy J 2013;34(4):55–78.
[24] Leuthold FU, Weigt H, von Hirschhausen C. Efficient pricing for European electricity networks - the theory of nodal pricing applied to feeding-in wind in Germany. Util Policy 2008;16(4):284–91.
[25] Leuthold FU, Weigt H, von Hirschhausen C. A large-scale spatial optimization model of the European electricity market. Netw Spatial Econ 2012;12(1):75–107.
[26] Morales JM, Zugno M, Pineda S, Pinson P. Electricity market clearing with improved scheduling of stochastic production. Eur J Oper. Res 2014;235(3):765–74.
[27] Netztransparenz.de. Redispatch-Massnahmen. 2015. http://www.netztransparenz.de/de/Redispatch.htm.
[28] Regelleistung. Platform for control reserve tendering. 2015. https://www.regelleistung.net/ip/action/index.
[29] Rintamäki T, Siddiqui AS, Salo A. Does renewable energy generation decrease the volatility of electricity prices? A comparative analysis of Denmark and Germany. Working paper. Systems Analysis Laboratory, Aalto University; 2014.
[30] Ruiz C, Conejo AJ, Fuller JD, Gabriel SA, Hobbs BF. A tutorial review of complementarity models for decision-making in energy markets. EURO J Decis Process 2013;2(1–2):91–120.
[31] Schill W-P, Kemfert C. Modeling strategic electricity storage: the case of pumped hydro storage in Germany. Energy J 2011;32(3):59–88.
[32] Siddiqui AS, Tanaka M, Chen Y. Are targets for renewable portfolio standards too low? The impact of market structure on energy policy. Eur J Oper. Res 2016;250(1):328–41.
[33] TenneT TSO GmbH. TenneT reserviert Irsching 4 und 5 für re-dispatch. 2013. http://www.tennet.eu/de/news-presse/article/tennet-reserviert-irsching-4-und-5-fuer-re-dispatch.html.
[34] Ueckerdt F, Brecha R, Luderer G, Sullivan P, Schmid E, Bauer N, et al. Representing power sector variability and the integration of variable renewables in long-term energy-economy models using residual load duration curves. Energy 2015;90:1799–814.
[35] Van den Bergh K, Couckuyt D, Delarue E, D'haeseleer W. Redispatching in an interconnected electricity system with high renewables penetration. Electr Power Syst Res 2015;127:64–72.
[36] Vazquez C, Rivier M, Perez-Arriaga I. A market approach to long-term security of supply. IEEE Trans Power Syst 2002;17(2):349–57.
[37] Weigt H, Jeske T, Leuthold F, von Hirschhausen C. Take the long way down: integration of large-scale North Sea wind using HVDC transmission. Energy Policy 2010;38:3164–73.
[38] Winkler J, Gaio A, Pfluger B, Ragwitz M. Impact of renewables on electricity markets - do support schemes matter? Energy Policy 2016;93:157–67.
[39] Würzburg K, Labandeira X, Linares P. Renewable generation and electricity prices: taking stock and new evidence for Germany and Austria. Energy Econ 2013;40(S1):159–71.
[40] Zeng B, An Y. Solving bilevel mixed integer program by reformulations and decomposition. Working paper. Department of Industrial and Management Systems Engineering, University of South Florida; 2014.

Publication III

T. Rintamäki, A. S. Siddiqui, and A. Salo. Strategic offering of a flexible producer in day-ahead and intraday power markets. *European Journal of Operational Research*, 284(3), 1136-1153, 2020.

European Journal of Operational Research 284 (2020) 1136–1153

Contents lists available at ScienceDirect

European Journal of Operational Research

journal homepage: www.elsevier.com/locate/ejor

Innovative Applications of O.R.

Strategic offering of a flexible producer in day-ahead and intraday power markets

Tuomas Rintamäki[a], Afzal S. Siddiqui[b,c,d,*], Ahti Salo[a]

[a] Systems Analysis Laboratory, Department of Mathematics and Systems Analysis, School of Science, Aalto University, Finland
[b] Department of Statistical Science, University College London, United Kingdom
[c] Department of Computer and Systems Sciences, Stockholm University, Sweden
[d] Department of Decision Sciences, HEC Montréal, Canada

ARTICLE INFO

Article history:
Received 28 March 2018
Accepted 22 January 2020
Available online 27 January 2020

Keywords:
OR in energy
Day-ahead market
Intraday market
Strategic offering
Mathematical programming with equilibrium constraints

ABSTRACT

The increase in intraday electricity market volumes due to intermittent renewable generation may give a strategic producer an opportunity to exert market power. We study offering strategies of a flexible producer in day-ahead and intraday markets using a bi-level model in which the upper level represents the profit-maximization problem of the producer and the lower-level problems clear the day-ahead and intraday markets sequentially. Using a three-node network, we first demonstrate that a flexible producer with perfect forecasts can increase its profit in both markets by coordinating its offer so as to cause transmission grid congestion or lack of competitive generation capacity. Moreover, we show that strategic behavior is possible even when the day-ahead and intraday markets are cleared simultaneously to lower balancing costs. We next assess these market designs in a Nordic test network and offer an explanation for high Nordic intraday prices. Finally, via an annual simulation using the Nordic market data, we verify that strategic offering in day-ahead and intraday markets under imperfect forecasts leads to increased profits vis-à-vis perfect competition but are mitigated through simultaneous market clearing.

1. Introduction

In the continental European and Nordic electricity markets, the initial generation, load, and transmission flow plans are revealed after the clearing of the day-ahead spot market. As a result of asset failures and updated forecasts, these day-ahead plans may be altered in the intraday market until one hour (Nordic countries) or 15 minutes (Germany) before delivery. Ultimately, transmission system operators (TSOs) balance real-time deviations from the final plans by activating balancing power (see Fig. 1 and Mauritzen, 2015; Pape, Hagemann, & Weber, 2016). While such a clearing mechanism may have been adequate for power systems based on conventional generation, it may not be effective in integrating intermittent renewable energy resources in line with EU policy (European Commission, 2014; Morales, Zugno, Pineda, & Pinson, 2014). Indeed, from 2010 to 2016, intraday volumes have surged up to 200% in northwestern Europe due to the increase in the generation of intermittent renewables such as wind power (Nord Pool, 2017; EPEX Spot, 2017). Flexible producers such as hydropower and gas-fired generators can profit from trading in the intraday market because a deficit leads to a higher intraday price than the day-ahead spot price given that less expensive offers have already been settled in the spot market. By contrast, a surplus causes the intraday price to be lower than the day-ahead spot price, which enables the flexible producer to replace its expensive generation with cheaper output from the intraday market (Boomsma, Juul, & Fleten, 2014).

In this paper, we study how a flexible strategic producer can use day-ahead and intraday offers to exploit market designs in the presence of high intraday volumes. Because the day-ahead and intraday markets typically face inflexible demand and share the same generation and transmission constraints, such a strategic producer may affect the market-clearing transmission flows and the generation plans of its rivals in both markets. By correctly anticipating a deficit or surplus in the intraday market via time-series forecasting, for example (Klæboe, Eriksrud, & Fleten, 2015), a flexible producer can increase its profit by decreasing or increasing

* Corresponding author at: Department of Statistical Science, University College London, United Kingdom.

E-mail addresses: tuomas.rintamaki@aalto.fi (T. Rintamäki), afzal.siddiqui@ucl.ac.uk (A.S. Siddiqui), ahti.salo@aalto.fi (A. Salo).

https://doi.org/10.1016/j.ejor.2020.01.044
0377-2217/

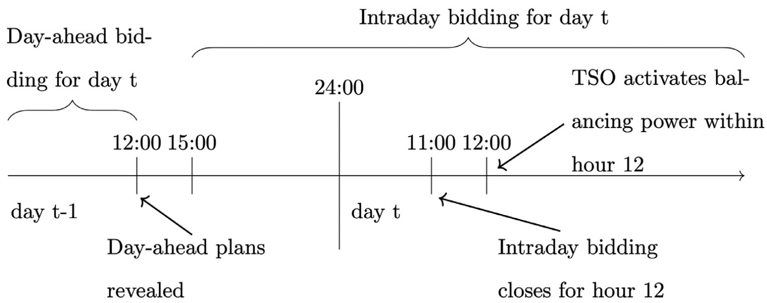

Fig. 1. Timeline of day-ahead and intraday markets in the Nordic countries.

its offering to the day-ahead spot market, respectively. However, if the deviations do not realize as forecasted, then the producer can make a loss as it may not deploy its generation assets optimally.

We build a stochastic bi-level model in which the strategic producer maximizes its profit in the upper level and the day-ahead and intraday markets are cleared in the lower level. Our main contribution is an assessment of coordinated strategic offering in both markets by allowing for endogenous determination of prices in the day-ahead and intraday markets in the presence of ramp restrictions and possible transmission grid congestion. Earlier work assumes exogenous intraday prices (e.g., Baringo & Conejo, 2016; Boomsma et al., 2014; Wozabal & Rameseder, 2020), Cournot competition without a transmission network model (Ito & Reguant, 2016; Knaut & Obermüller, 2016), or a producer with limited opportunities for strategic behavior (Dai & Qiao, 2015; Dai & Qiao, 2017). To this end, we address three objectives:

1) We employ a representative test network to illustrate how a range of coordinated offering strategies in the day-ahead and intraday markets may be formed when the strategic producer has perfect forecasts for all market data.
2) Building on these strategies, we conduct a case study using real market data to provide evidence for the very high intraday prices observed in Nord Pool in early 2016.
3) By employing the real market data in a simulation of day-ahead and intraday markets over a year, we estimate the expected impact of strategic offering on both day-ahead and intraday profits and generation costs when the offer curves are built with imperfect forecasts.

In addition, we show that an alternative market design that simultaneously minimizes day-ahead and expected intraday costs (Morales et al., 2014) can be manipulated by a strategic producer. However, via an annual simulation to assess the mean performance of the market designs, we find that this alternative market design mitigates the impact of strategic behavior vis-à-vis the conventional dispatch model in expectation. Methodologically, we provide computationally tractable model reformulations using duality theory (Ruiz & Conejo, 2009) and by extending binary expansion (Barroso, Carneiro, Granville, Pereira, & Fampa, 2006) for signed quantities.

This paper is organized as follows. In Section 2, we discuss models for day-ahead and intraday electricity markets as well as strategic offering. Section 3 presents our bi-level model, and Section 4 gives numerical results for objectives (1)–(3). Section 5 concludes and provides directions for future work.

2. Literature review

Offering into day-ahead electricity markets is well-studied in the literature. Fleten and Kristoffersen (2007) develop a stochastic programming model for building detailed offer curves of a flexible hydropower producer when market prices are modeled by an exogenous stochastic process. Using a bi-level model, Ruiz and Conejo (2009) build offer curves of a strategic producer for a single transmission-constrained electricity market under uncertainty about demand bids and offer curves of rival firms. To maximize its profits, the strategic producer can withhold generation and utilize transmission grid congestion as well as limited ramping speed of its rivals (Clements, Hurn, & Li, 2016). Moiseeva, Hesamzadeh, and Biggar (2015) consider a market design in which producers bid their ramp rates and show that flexible strategic generators seek to lift prices by bidding ramp rates below their technical capability. By contrast, Kazempour, Conejo, and Ruiz (2015) consider a strategic consumer with elastic demand who seeks to increase its utility by decreasing its bid prices. Kwon and Frances (2012) review such mathematical programming models for a power producer's offers with both strategic and perfectly competitive assumptions.

The day-ahead offering models can readily consider additional markets such as intraday markets by introducing exogenous prices. For example, Baringo and Conejo (2013b) build wind power offer curves while taking exogenous balancing market price scenarios into account. Kardakos, Simoglou, and Bakirtzis (2016) model a virtual power plant with load, generation, and storage that maximizes expected profit resulting from endogenous day-ahead sales revenue and exogenous balancing costs. On the other hand, Rahimiyan and Baringo (2015) use robust optimization to determine offers into uncertain but perfectly competitive day-ahead and regulation markets.

Ito and Reguant (2016) consider a Cournot competition model in which a monopolist decides its commitment into two sequential markets such as the electricity day-ahead and real-time markets. The demand that the monopolist faces in the day-ahead and intraday market is assumed to be linearly dependent on the day-ahead price and the price difference between the two markets, respectively. As a result, their theoretical framework predicts that the monopolist withholds quantity in the day-ahead market and increases its commitment in the intraday market. Meanwhile, price-taking competitive producers have an incentive to arbitrage the price difference between the two markets by selling more in the day-ahead market. The authors analyze market and plant-level data from the Iberian electricity market to confirm the predictions for the monopolist and competitive producers.

Knaut and Obermüller (2016) model Cournot competition between strategic renewable energy and competitive conventional producers in a day-ahead market with uncertainty about renewable generation, which is resolved in a sequentially cleared intraday market. They find that it is optimal for renewable energy producers to sell less than their expected generation in the day-ahead market. However, the sales volume approaches expected production if either the number of symmetric renewable energy producers increases or the flexibility of conventional producers in the intraday market decreases.

Dai and Qiao (2015) consider a strategic wind power producer that builds offer curves for sequentially cleared day-ahead and real-time markets. They find that the producer can increase its profits in both markets with strategic offering. However, the strategic producer has limited offering possibilities into the real-time market as it needs to correct its deviations from the day-ahead dispatch caused by wind power forecast errors. Dai and Qiao (2017) find that day-ahead and real-time profits and prices increase further in the presence of multiple strategic wind power and conventional producers. However, due to computational challenges, they use an approximation algorithm to determine the strategies of wind power producers and a discrete set of strategies for the conventional generators, which are likely to ignore possibilities for strategic behavior. Bjørndal, Bjørndal, and Rud (2013) search iteratively for strategic spot price offers that lead to transmission grid congestion, higher prices in the intraday market, and lower social welfare.

Morales et al. (2014) find that the market design that minimizes the sum of day-ahead and expected intraday costs is more economical than the sequential dispatch. Even though their market design can anticipate the cost-increasing impact of strategic offers in the intraday market, we show that a strategic player can still coordinate its offer to increase prices in the day-ahead market. Our result is in line with that of Lei, Zhang, Dong, and Ye (2016) who show that the strategic behavior of a wind power producer reduces social welfare when the day-ahead and intraday markets are cleared simultaneously.

Indeed, there is recent empirical support for strategic behavior in different power markets: Tangerås and Mauritzen (2018) find evidence for day-ahead market power by flexible producers in certain Swedish price areas in Nord Pool, Just and Weber (2015) for the German balancing market, Amountzias, Dagdeviren, and Patokos (2017) for the U.K. wholesale and retail markets, and California ISO (2018) for the 5-minute market in California. To this end, our objectives are to illustrate coordinated offering strategies into day-ahead and intraday markets, provide evidence for very high observed prices in Nord Pool using these strategies, and estimate the expected impact of strategic offering on both day-ahead and intraday generation costs.

3. Mathematical model for strategic offering in day-ahead and intraday markets

3.1. Overview of day-ahead and intraday bidding

To enter the possibly more profitable intraday market, a flexible producer may choose to alter its day-ahead offer curves based on anticipated intraday deviations. As an example, the producer can offer lower volume in the day-ahead market if it anticipates a deficit and higher prices in the intraday market. Consequently, the two markets need to be considered jointly already when bidding to the day-ahead market. When the day-ahead plans are revealed around noon as shown in Fig. 1, the producer can start submitting offer curves into intraday and balancing markets. The producer can update these initial intraday offer curves as new information, such as updated wind power forecasts or outage schedules, becomes available. This process, which repeats every trading day, is done by all producers and consumers in the market.

We focus on modeling the building of day-ahead and intraday offer curves from the perspective of a flexible and strategic producer. In addition to adjusting the day-ahead and intraday offer curves based on external factors such as anticipated intraday deviations due to wind power forecast errors, the producer can pursue higher profits by manipulating prices in both markets by setting strategic price and volume offers. More specifically, strategic producer (SP) $x \in \mathcal{X}$ coordinates the building of day-ahead and intraday offer curves by selecting price (p^{da}, p^{up}, and p^{down}) and quantity offers (q^{da}) to maximize its expected profit in the day-ahead and intraday markets. To this end, the SP solves a bi-level problem in which the upper level represents the profit maximization of the SP and sets exchange-specific constraints on the permitted price and quantity offers. In turn, the profit of the SP is affected by the day-ahead and intraday prices (λ_s^{da} and λ_s^{intra}) and generation (g_s^{da}, g_s^{up}, and g_s^{down}), which are determined as the solution to a collection of lower-level problems that minimize the costs of generation in each scenario s given the price and quantity offers of the SP. Other producers are assumed to be perfectly competitive in that the price and quantity offers of these competitive producers (CPs) equal their marginal generation costs (C^{da}, C^{up}, and C^{down}) and available generation capacities (G^{max}), respectively. These parameters can be estimated using market data.

Similarly, we assume that all consumers are competitive and the total consumption in the day-ahead and intraday markets is represented using parameters D_s^{da} and D_s^{intra}, respectively. We make this simplification because (i) demand is very inelastic (Cialani & Mortazavi, 2018), (ii) demand-side flexibility is limited in availability (Müller & Möst, 2018), and (iii) a part of D_s^{intra} is not controlled by consumers due to unexpected weather changes, for example. We do not model an explicit linkage between D_s^{da} and D_s^{intra}, but practitioners may use existing market data and predictive models for estimating D_s^{da} and D_s^{intra} so that possible correlations or consumer behavior are implicitly reflected in the parameter values for each scenario s when the SP builds its offer curves.

In this conventional dispatch model (ConvD), the day-ahead and intraday markets clear sequentially so that the intraday market is dependent on the generation and transmission flows in the day-ahead market (g^{da} and f^{da}). An illustration of strategic offer curve building in day-ahead and intraday markets with ConvD is shown in Fig. 2.

We compare the aforementioned ConvD model, which clears the day-ahead and intraday markets sequentially, to a market design that clears the day-ahead and intraday markets simultaneously by representing the two markets with a single lower-level problem for each scenario. This design is similar to the StochD model of Morales et al. (2014) and may cause a generator to be dispatched out of merit order in the day-ahead market if that generator lowers the expected intraday cost. An illustration of building strategic day-ahead and intraday offer curves with StochD is shown in Fig. 3.

Moreover, we compare strategic offering with ConvD and StochD to a perfectly competitive (PC) model in which the price and quantity offers of the SP equal its marginal generation costs and available generation capacities, respectively. Consequently, the SP becomes one of the CPs and can no longer manipulate prices in the day-ahead and intraday markets. An illustration of the PC model is shown in Fig. 4.

In what follows, we present the mathematical formulation for building strategic offer curves with the ConvD model. The formulation for PC and StochD models is presented in Appendix A and Appendix C, respectively.

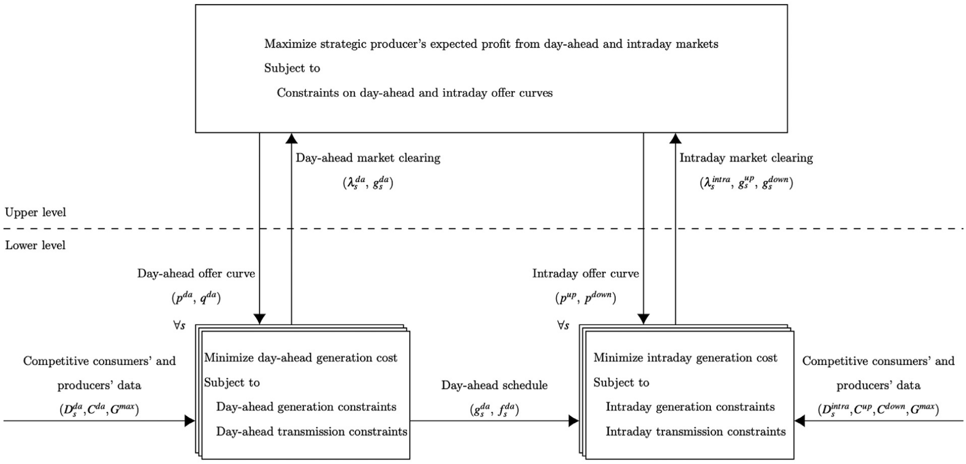

Fig. 2. Illustration of strategic offer curve building in day-ahead and intraday markets with ConvD (all variable indices except scenarios s have been omitted).

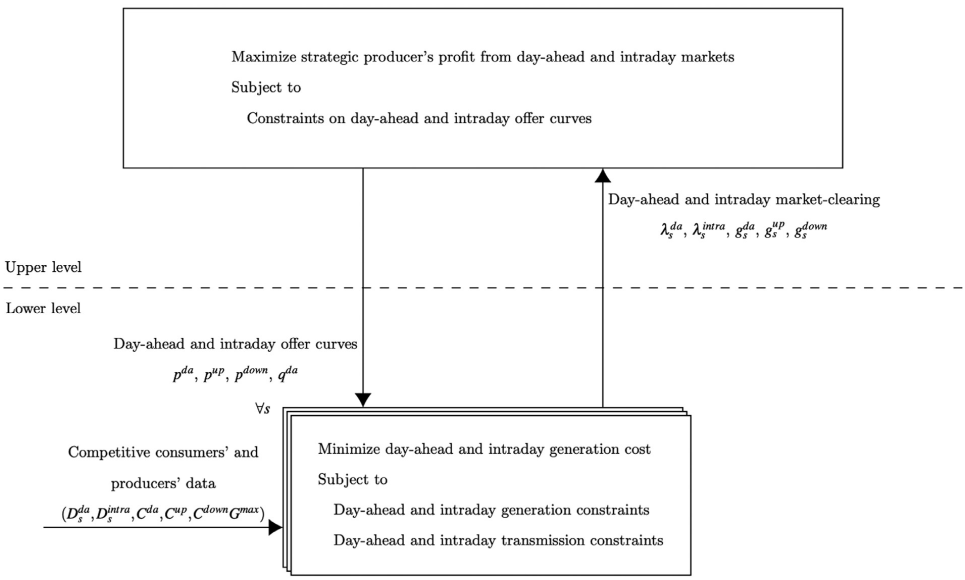

Fig. 3. Illustration of strategic offer curve building in day-ahead and intraday markets with StochD (all variable indices except scenarios s have been omitted).

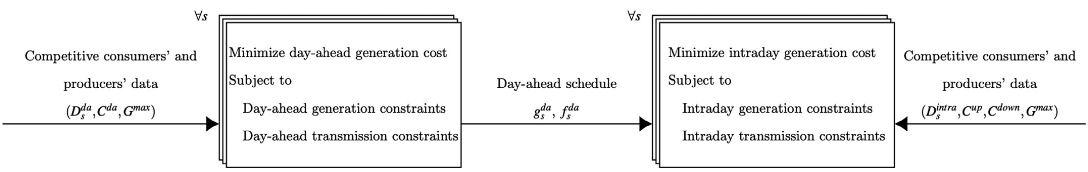

Fig. 4. Illustration of PC in which the SP is no longer strategic but is one of the CPs (all variable indices except scenarios s have been omitted).

3.2. Mathematical formulation

3.2.1. Notation

Sets and indices	
$n \in \mathcal{N}$	Nodes
$u \in \mathcal{U}$	Generation units
$b \in \mathcal{B}$	Generation blocks
$\ell \in \mathcal{L}$	Transmission lines
$s \in \mathcal{S}$	Scenarios
$f \in \mathcal{F}$	Generation firms
$x \in \mathcal{X} \subset \mathcal{F}$	Strategic firms } $\mathcal{X} \cap \mathcal{Y} = \emptyset$ and $\mathcal{X} \cup \mathcal{Y} = \mathcal{F}$
$y \in \mathcal{Y} \subset \mathcal{F}$	Competitive firms
Parameters	
W_s	The probability of scenario s
$D^{da}_{s,n}$	Demand at node n in scenario s in the day-ahead market (megawatt)
$D^{intra}_{s,n}$	Demand at node n in scenario s in the intraday market (megawatt)
$C^{da}_{f,n,u,b}$	Day-ahead marginal cost of generation of the bth block of firm f's unit u at node n (€ per megawatt)
$C^{up/down}_{f,n,u,b}$	Up/down-regulation cost of the bth block of firm f's unit u at node n (€ per megawatt)
$G^{max}_{f,n,u,b}$	Maximum generation capacity of the bth block of firm f's unit u at node n (megawatt)
$G^{up/down,ramp}_{f,n,u,b}$	Maximum up/down-regulation ramp of the bth block of firm f's unit u at node n (megawatt)
$NTC^{max/min}_{\ell}$	Maximum/minimum transmission flow on the line ℓ (megawatt)
$Y_{\ell,n}$	Transmission line and node incidence matrix $\ell \times n$
$\Lambda^{da,max/min}$	Maximum/minimum day-ahead price in the power exchange (€ per megawatt)
$\Lambda^{intra,max/min}$	Maximum/minimum intraday price in the power exchange (€ per megawatt)
Free variables	
$\lambda^{da}_{s,n}$	Day-ahead price in scenario s at node n (€ per megawatt)
$\lambda^{intra}_{s,n}$	Intraday price in scenario s at node n (€ per megawatt)
$p^{da}_{x,n,u,b}$	Price offer of the bth block of strategic firm x's unit u at node n for the day-ahead market (€ per megawatt)
$p^{up/down}_{x,n,u,b}$	Price offer of the b:th block of strategic firm x's unit u at node n for up/down-regulation (€ per megawatt)
$f^{da}_{s,\ell}$	Transmission flow on line ℓ in scenario s in the day-ahead market (megawatt)
$f^{intra}_{s,\ell}$	Transmission flow on line ℓ in scenario s in the intraday market (megawatt)
Positive variables	
$q^{da}_{x,n,u,b}$	Quantity offer of the bth block of strategic firm x's unit u at node n for the day-ahead market (megawatt)
$g^{da}_{s,f,n,u,b}$	Day-ahead generation of the bth block of firm f's unit u at node n in scenario s (megawatt)
$g^{up/down}_{s,f,n,u,b}$	Up/down-regulation of the bth block of firm f's unit u at node n in scenario s (megawatt)
$\beta^{da}_{s,f,n,u,b}$	Dual for maximum day-ahead generation of the bth block of firm f's unit u at node n in scenario s (€ per megawatt)
$\beta^{up/down}_{s,f,n,u,b}$	Dual for maximum up/down-regulation of the bth block of firm f's unit u at node n in scenario s (€ per megawatt)
$\beta^{up/down,ramp}_{s,f,n,u,b}$	Dual for maximum up/down-regulation ramp of the bth block of firm f's unit u at node n in scenario s (€ per megawatt)
$\mu^{da,max/min}_{s,\ell}$	Dual for maximum/minimum flow on line ℓ in scenario s in the day-ahead market (€ per megawatt)
$\mu^{intra,max/min}_{s,\ell}$	Dual for maximum/minimum flow on line ℓ in scenario s in the intraday market (€ per megawatt)
Binary variables	
$up_{s,x,n}$	Indicator variables equal 1 if strategic firm x up-regulates at node n in scenario s

3.2.2. Upper-level problem

The bi-level problem is solved with respect to $\Omega^{UL} = \{q^{da}_{x,n,u,b}, p^{da}_{x,n,u,b}, p^{up}_{x,n,u,b}, p^{down}_{x,n,u,b}, up_{s,x,n}\}$, $\Omega^{LL^{da}} = \{g^{da}_{s,f,n,u,b}, f^{da}_{s,\ell}\}$, and $\Omega^{LL^{intra}} = \{g^{up}_{s,f,n,u,b}, g^{down}_{s,f,n,u,b}, f^{intra}_{s,\ell}\}$. The upper level of the bi-level problem is:

$$\text{Minimize}_{\Omega^{UL}\cup\Omega^{LL^{da}}\cup\Omega^{LL^{intra}}} \sum_s W_s\Bigg[\sum_n\sum_u\sum_b\Big(g^{da}_{s,x,n,u,b}\big(C^{da}_{x,n,u,b}-\lambda^{da}_{s,n}\big) + g^{up}_{s,x,n,u,b}\big(C^{up}_{x,n,u,b}-\lambda^{intra}_{s,n}\big) - g^{down}_{s,x,n,u,b}\big(C^{down}_{x,n,u,b}-\lambda^{intra}_{s,n}\big)\Big)\Bigg] \quad (1)$$

s.t.

$$\Lambda^{da,min} \le p^{da}_{x,n,u,b} \le \Lambda^{da,max} \quad \forall n,u,b \quad (2)$$

$$\Lambda^{intra,min} \le p^{up}_{x,n,u,b} \le \Lambda^{intra,max} \quad \forall n,u,b \quad (3)$$

$$\Lambda^{intra,min} \le p^{down}_{x,n,u,b} \le \Lambda^{intra,max} \quad \forall n,u,b \quad (4)$$

$$p^{da}_{x,n,u,b} \ge p^{da}_{x,n,u,b-1} \quad \forall n,u, \text{ and } \forall b>1 \quad (5)$$

$$p^{up}_{x,n,u,b} \ge p^{up}_{x,n,u,b-1} \quad \forall n,u, \text{ and } \forall b>1 \quad (6)$$

$$p^{down}_{x,n,u,b} \le p^{down}_{x,n,u,b-1} \quad \forall n,u, \text{ and } \forall b>1 \quad (7)$$

$$q^{da}_{x,n,u,b} \le G^{max}_{x,n,u,b} \quad \forall n,u,b \quad (8)$$

$$g^{up}_{s,x,n,u,b} \le M\cdot up_{s,x,n} \quad \forall s,n,u,b \quad (9)$$

$$g^{down}_{s,x,n,u,b} \le M\cdot(1-up_{s,x,n}) \quad \forall s,n,u,b, \quad (10)$$

Day-ahead market dispatch in Eqs. (11)–(15)

Intraday market dispatch in Eqs. (16)–(22)

The objective function (1) represents the maximization of the expected profit of the SP over a set of a scenarios s by adding the expected day-ahead profit to the expected profit from increasing and decreasing generation in the intraday market. We assume that every generation unit is divided into blocks that have a constant cost for day-ahead generation ($C^{da}_{f,n,u,b}$) as well as up- and down-regulation ($C^{up}_{f,n,u,b}$ and $C^{down}_{f,n,u,b}$, respectively), i.e., increasing or decreasing generation in the intraday market, respectively. Note that in case of day-ahead generation and up-regulation, the generators lose $C^{da}_{f,n,u,b}$ or $C^{up}_{f,n,u,b}$ and receive $\lambda^{da}_{s,n}$ or $\lambda^{intra}_{s,n}$ from a buyer, respectively, and in case of down-regulation, the generators save $C^{down}_{f,n,u,b}$ and pay $\lambda^{intra}_{s,n}$ to a seller. The SP can specify a price offer for each of its generation blocks for both the day-ahead and intraday market, while a quantity offer is set only for the day-ahead market. This is because we assume that the volumes that are not dispatched in the day-ahead market are available in the intraday market.

The upper-level problem is constrained by Eqs. (2)–(4), which define maximum and minimum price offers of the SP for the day-ahead and intraday markets. Moreover, Eqs. (5)–(7) ensure that offer curves are increasing. The day-ahead quantity offers are limited by the generation capacity of each block (8). Eqs. (9) and (10) forbid simultaneous up- and down-regulation at each node through the binary variable $up_{s,x,n}$ so that the SP is not able to increase its up-regulation profit by adversely down-regulating while it is also up-regulating.

3.2.3. Day-ahead market dispatch

The day-ahead market is given by a collection of lower-level problems in Eqs. (11)–(15).

$$\forall s \begin{cases} \text{Minimize}_{\Omega^{LL^{da}}} \\ \sum_n \sum_u \sum_b p^{da}_{x,n,u,b} g^{da}_{s,x,n,u,b} + \sum_y \sum_n \sum_u \sum_b C^{da}_{y,n,u,b} g^{da}_{s,y,n,u,b} & & & (11) \\ \text{s.t.} \\ D^{da}_{s,n} = \sum_f \sum_u \sum_b g^{da}_{s,f,n,u,b} + \sum_\ell Y_{\ell,n} f^{da}_{\ell,n} & \lambda^{da}_{s,n} \text{ free} & \forall n & (12) \\ g^{da}_{s,x,n,u,b} \le q^{da}_{x,n,u,b} & \beta^{da}_{s,x,n,u,b} \ge 0 & \forall n,u,b & (13) \\ g^{da}_{s,y,n,u,b} \le G^{max}_{y,n,u,b} & \beta^{da}_{s,y,n,u,b} \ge 0 & \forall y,n,u,b & (14) \\ NTC^{min}_\ell \le f^{da}_{s,\ell} \le NTC^{max}_\ell & \mu^{da,min/max}_{s,\ell} \ge 0 & \forall \ell & (15) \end{cases}$$

The objective function (11) minimizes the day-ahead cost of generation in each scenario s, which consists of the price offers of the SP and the marginal costs of the CPs. Eq. (12) ensures that, in each scenario and node, supply matches demand, which is given by the parameters $D^{da}_{s,n}$. These constraints consider the effect of flows $f^{da}_{s,\ell}$ using an incidence matrix Y whose element (ℓ, n) equals to 1 if node n is the starting point of the line ℓ, -1 if n is the end point, and 0 otherwise. Such a flow model is used in the Nordic market, for example Nord Pool (2009). Also, the dual variables on the right-hand side of Eq. (12) correspond to nodal day-ahead prices. Eqs. (13) and (14) limit the generation of the SP blocks by the quantity offers and the CP blocks by the block capacities, respectively. Eq. (15) bounds day-ahead transmission flows so that congestion occurs in the transmission network in the day-ahead market if any of these constraints becomes binding.

3.2.4. Intraday market dispatch

The intraday market is given by a collection of lower-level problems in Eqs. (16)–(22).

$$\forall s \begin{cases} \text{Minimize}_{\Omega^{LL^{intra}}} \\ \sum_n \sum_u \sum_b \left(p^{up}_{x,n,u,b} g^{up}_{s,x,n,u,b} - p^{down}_{x,n,u,b} g^{down}_{s,x,n,u,b}\right) + \sum_y \sum_n \sum_u \sum_b \left(C^{up}_{y,n,u,b} g^{up}_{s,y,n,u,b} - C^{down}_{y,n,u,b} g^{down}_{s,y,n,u,b}\right) & & & (16) \\ \text{s.t.} \\ D^{intra}_{s,n} = \sum_f \sum_u \sum_b \left(g^{up}_{s,f,n,u,b} - g^{down}_{s,f,n,u,b}\right) + \sum_\ell Y_{\ell,n} f^{intra}_{\ell,n} & \lambda^{intra}_{s,n} \text{ free} & \forall n & (17) \\ g^{down}_{s,f,n,u,b} \le g^{da}_{s,f,n,u,b} & \beta^{down}_{s,f,n,u,b} \ge 0 & \forall f,n,u,b & (18) \\ g^{da}_{s,f,n,u,b} + g^{up}_{s,f,n,u,b} \le G^{max}_{f,n,u,b} & \beta^{up}_{s,f,n,u,b} \ge 0 & \forall f,n,u,b & (19) \\ g^{down}_{s,f,n,u,b} \le G^{down,ramp}_{f,n,u,b} & \beta^{down,ramp}_{s,f,n,u,b} \ge 0 & \forall f,n,u,b & (20) \\ g^{up}_{s,f,n,u,b} \le G^{up,ramp}_{f,n,u,b} & \beta^{up,ramp}_{s,f,n,u,b} \ge 0 & \forall f,n,u,b & (21) \\ NTC^{min}_\ell \le f^{da}_{s,\ell} + f^{intra}_{s,\ell} \le NTC^{max}_\ell & \mu^{intra,min/max}_{s,\ell} \ge 0 & \forall \ell & (22) \end{cases}$$

Similar to the day-ahead market, the objective function (16) minimizes the cost of intraday generation in each scenario s given the intraday price offers of the SP and the marginal costs of the CPs. In intraday balance Eq. (17), scenario- and node-wise intraday demand $D^{intra}_{s,n}$ is a parameter that can take on either positive or negative values because real-time demand can be higher or lower than anticipated in the day-ahead market, respectively. Note that $D^{intra}_{s,n}$ can be estimated by an exogenous model that correlates it with day-ahead demand $D^{da}_{s,n}$. Also, the dual variables on the right-hand side of Eq. (17) correspond to nodal intraday prices. The intraday dispatch takes the day-ahead generation and transmission plans as an input so that Eqs. (18) and (19) ensure that the final generation of each block is between zero and the block capacity if ramping constraints (20) and (21) are not already met. Finally, Eq. (22) constrains the final transmission flows between the minimum and maximum transmission capacity (NTC^{min}_ℓ and NTC^{max}_ℓ, respectively).

We compare the results of the above conventional dispatch (ConvD) model with a perfectly competitive (PC) model in which just the two lower-level problems (11)–(15) and (16)–(22) are run sequentially. Similar to the CPs, the price and quantity offers of the SP are set to its blockwise generation costs ($p^{da/up/down}_{x,n,u,b} = C^{da/up/down}_{x,n,u,b}$) and capacities ($q^{da}_{x,n,u,b} = G^{max}_{x,n,u,b}$), respectively. Moreover, we compare our results to the StochD model of Morales et al. (2014) that combines the two lower-level problems by adding the intraday objective function (16) to that of the day-ahead market clearing (11) and by augmenting the constraints of the day-ahead problem (12)–(15) with the intraday constraints (17)–(22). Morales et al. (2014) consider only perfect competition, and we show that their market design can be manipulated by a strategic producer even if it leads to lower total generation cost than ConvD in expectation.

Following the solution procedure of Gabriel and Leuthold (2010), the bi-level ConvD problem is reformulated as a single-level mathematical program with equilibrium constraints (MPEC) in Appendix A, which is further reformulated and solved as a mixed-integer linear programming (MILP) problem in Appendix B. For ConvD, the bilinear terms $g^{up}_{s,x,n,u,b}\lambda^{intra}_{s,n}$ and $g^{down}_{s,x,n,u,b}\lambda^{intra}_{s,n}$ in Eq. (1) are discretized using a reformulation of binary expansion of Barroso et al. (2006) so that the terms can become negative. The discretization may lead to suboptimal results, but the suboptimality can be reduced by making the related discretization intervals $\bar{G}^{up/down}_{x,n,u,b} > 0$ smaller. For StochD, we are able to provide an exact MILP reformulation without discretization using strong duality (Ruiz & Conejo, 2009) in Appendix C. The PC model can be solved exactly as a series of linear systems as detailed in Appendix A.

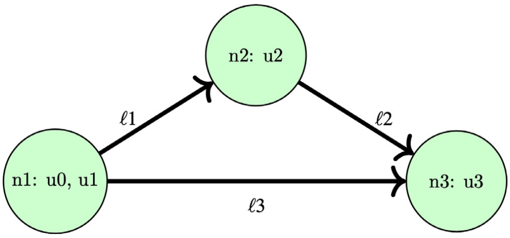

Fig. 5. Three-node network indicating conventional direction of flow and each node's units.

4. Numerical results

In Section 4.1, we address our first objective to demonstrate the logic of coordinated offering strategies in detail using a representative test network. Consequently, we take only the perspective of a strategic producer by building the day-ahead and intraday offer curves and by analyzing what would happen in the day-ahead and intraday markets if both would realize exactly as the SP anticipates. In Section 4.2, we use the strategies and insights from Section 4.1 to address our second objective to explain high prices observed in Nord Pool in 2016. Finally, in Section 4.3, we address our third objective to estimate the expected impact of strategic offering on day-ahead and intraday costs by considering a more realistic setting in which a market operator clears the day-ahead and intraday markets sequentially given real market data and the coordinated day-ahead and intraday offer curves that the SP builds using estimated market data. This process simulates the real timeline of day-ahead and intraday markets as shown in Fig. 1.

4.1. Three-node network

To address our objective (1) to demonstrate coordinated offering strategies in day-ahead and intraday markets, we first consider an illustrative three-node network in which there is demand at each node and each transmission line has a capacity of 10 megawatts in both directions (Fig. 5). The SP operates a flexible generation unit at node 1 (unit 0), while the remaining less flexible, but low marginal cost units at nodes 1, 2, and 3 (units 1, 2, 3, respectively) are owned by a CP (see Table 1 for generation-related parameters). We illustrate three distinct cases in which strategic behavior can lead to higher profits through three scenarios: (1) the scenario "Congestion" demonstrates how the SP can cause and profit from transmission network congestion, (2) the scenario "Ramp limit" demonstrates how the SP can profit from limited flexibility of other producers, (3) the scenario "Surplus" illustrates how the SP can profit from not only deficit but also a large surplus in the intraday market.

Table 1
Blockwise generation parameters in the three-node example.

	SP	CP		
	Unit	Unit		
Parameter	u0	u1	u2	u3
$C^{da}_{f,n,u,b}$ (€ per megawatt)	8	5	6	7
$C^{up}_{f,n,u,b}$ (€ per megawatt)	25	10	15	20
$C^{down}_{f,n,u,b}$ (€ per megawatt)	1	4	3	2
$G^{max}_{f,n,u,b}$ (megawatt)	25	2	25	25
$G^{up,ramp}_{f,n,u,b}$ (megawatt)	5	2	2	2
$G^{down,ramp}_{f,n,u,b}$(megawatt)	5	2	2	2

Table 2
Demand parameters in the three-node example (in the intraday market, positive figures indicate a deficit and negative figures a surplus).

	Parameter					
	$D^{da}_{s,n}$			$D^{intra}_{s,n}$		
	Node			Node		
Scenario	n1	n2	n3	n1	n2	n3
Congestion	22	22	22	10	0	0
Ramp limit	4	2	2	10	0	0
Surplus	14	22	30	−9	0	0

Table 3
Offer curve of the SP in the three-node example with PC.

	Variable			
	$p_{x,n,u,b}$ (€ per megawatt)		$q_{x,n,u,b}$ (megawatt)	
	Block		Block	
Offer	$b1$	$b2$	$b1$	$b2$
Day-ahead	8	8	25	25
Up-regulation	25	25	–	–
Down-regulation	1	1	–	–

The demand in the day-ahead and intraday markets for each equally weighted scenario is in Table 2. Each generation unit is divided into two blocks, and, with ConvD, the discretization interval of the binary expansion for up- and down-regulation of the SP ($\bar{G}^{up}_{x,n,u,b,j}$ and $\bar{G}^{down}_{x,n,u,b,k}$) is 1 megawatt, which causes no error in the results with the selected parameter values.[1] Maximum and minimum day-ahead and intraday prices are set to 3000 and −500 € per megawatt, respectively, to match those of Nord Pool (2019). Note that in this illustrative example, we assume that the SP has perfect knowledge of all model parameters including the intraday demand, the real value of which would be revealed only after the intraday market is cleared. In what follows, we study scenariowise generation and transmission flows in the day-ahead and intraday markets resulting from the offer curves of the SP. These values are obtained by solving Eqs. (1)–(22) (ConvD), or (C.1)-(C.5) (StochD), or (11)–(15) as well as (16)–(22) (PC) with the above input data.

Table 3 shows the offer curve with PC. Table 4 shows that, in each scenario, most of the demand in day-ahead and intraday markets is met by the CP units 1, 2, and 3 as the SP unit 0 has higher marginal costs. Both day-ahead and intraday prices are at the marginal costs of the different units.

Tables 5 and 7 show the offer curves, and Tables 6 and 8 indicate the resulting generation, flows, and prices with ConvD and StochD, respectively. With ConvD, the SP's day-ahead price offer $p^{da}_{x,n,u,b1/b2} = 7$ € per megawatt is not competitive enough for the SP unit to be dispatched in the day-ahead market in the scenario "Congestion." As a result, the CP unit 1 at node 1 is fully dispatched in the day-ahead market and the transmission lines to node 1 are nearly congested to meet the high day-ahead demand at node 1. The SP recognizes that, in the intraday market, there is no more CP capacity available at node 1 and only a part of the intraday demand at node 1 can be met by the CP before the transmission lines to node 1 become fully congested. Thus, the SP is able to cover the remaining intraday demand at a high profit by setting its up-regulation price offer $p^{up}_{x,n,u,b1/b2}$ to maximum price

[1] All parameters are integral and the discretization interval is 1 megawatt. Also, since all cost parameters are distinct, there do not exist multiple solutions in which one producer would produce $0 \leq x \leq D$ and another one $D - x$ for some constant demand D. Thus, the discretization does not lead to errors.

Table 4
Day-ahead and intraday generation, flows, and prices in the three-node example with PC, where positive (negative) intraday generation corresponds to up-regulation (down-regulation).

	Variable																			
	$\sum_b g^{da}_{s,f,n,u,b}$ (megawatt)				$f^{da}_{s,\ell}$ (megawatt)			$\lambda^{da}_{s,n}$ (€ per megawatt)			$\sum_b g^{up/down}_{s,f,n,u,b}$ (megawatt)				$f^{intra}_{s,\ell}$ (megawatt)			$\lambda^{intra}_{s,n}$ (€ per megawatt)		
	Unit				Line			Node			Unit				Line			Node		
Scenario	u0	u1	u2	u3	ℓ_1	ℓ_2	ℓ_3	n1	n2	n3	u0	u1	u2	u3	ℓ_1	ℓ_2	ℓ_3	n1	n2	n3
Congestion		4	42	20	−10	10	−8	7	6	7	8			2			−2	25	3	20
Ramp limit		4	4			2		6	6	6	2		4	4	−4		−4	25	15	20
Surplus		4	42	20	−10	10		7	6	7		−4	−4	−1	4		1	1	3	2

Table 5
Offer curve of the SP with ConvD.

	Variable			
	$p_{x,n,u,b}$ (€ per megawatt)		$q_{x,n,u,b}$ (megawatt)	
	Block		Block	
Offer	$b1$	$b2$	$b1$	$b2$
Day-ahead	7	7	0	25
Up-regulation	3000	3000	–	–
Down-regulation	−500	−500	–	–

Table 7
Offer curve of the SP with StochD.

	Variable			
	$p_{x,n,u,b}$ (€ per megawatt)		$q_{x,n,u,b}$ (megawatt)	
	Block		Block	
Offer	$b1$	$b2$	$b1$	$b2$
Day-ahead	−500	2991	0	6
Up-regulation	3000	3000	–	–
Down-regulation	−500	−500	–	–

of 3000 € per megawatt. In Section 4.2, we show how a similar offering strategy can explain very high intraday prices in Nord Pool.

Likewise, in scenario "Congestion" with StochD, the SP sets the same high up-regulation price offer $p^{up}_{x,n,u,b1/b2} =$ 3000 € per megawatt. With StochD, the market operator is able to anticipate the high intraday cost caused by the combination of the SP's high up-regulation offer, congestion, and the lack of CP capacity at node 1 in the intraday market. To counter this, the market operator can dispatch the SP already in the day-ahead market. However, the SP is able to anticipate this action and sets a strategic day-ahead offer $p^{da}_{x,n,u,b2} = 2991$ € per megawatt with a positive capacity. As a result, the market operator chooses to dispatch the SP unit both in the day-ahead and intraday markets in quantities that minimize its objective function. Indeed, we check numerically that (1) perturbing the SP's price offer $p^{da}_{x,n,u,b2} = 2991$ € per megawatt even by a small constant ϵ leads to a lower profit for the SP, and (2) having higher dispatch for the SP in the day-ahead or intraday market does not lead to an improvement in the market operator's objective. Consequently, this scenario shows that the SP is able to game also the alternative dispatch method StochD.

In scenario "Ramp limit" with ConvD, the low day-ahead demand is covered without any congestion on the transmission lines to node 1 by having the cheapest CP unit 1 fully dispatched and the second cheapest CP unit 2 partially dispatched. Regardless of the abundant transmission capacity left for the intraday market, the high intraday demand at node 1 cannot be met by the CP units 2 and 3 because they are limited by ramping constraints. As a consequence, the SP is able to lift the intraday price to the maximum level even though none of the transmission lines is congested. By contrast, StochD is able to anticipate the limited ramping of the CP units 2 and 3 and decides to deviate from the lowest cost day-ahead dispatch by not dispatching the CP unit 1. Consequently, the CP unit 1 is available in the intraday market and displaces the SP unit with the high up-regulation offer. Thus, this shows how StochD can mitigate the impact of strategic offering in some scenarios.

In scenario "Surplus," there is high demand in the day-ahead market and a large surplus at node 1 in the intraday market. With ConvD, the CP units are not able to down-regulate all of the surplus due to (1) limited capacity of the CP unit 1, (2) limited ramping of the CP unit 2, and (3) transmission network congestion that leaves the CP unit 3 unutilized. Again, the SP anticipates this situation and sets its down-regulation price $p^{down}_{x,n,u,b1/b2}$ to the minimum intraday price of −500 € per megawatt to gain a high profit. Indeed, negative intraday prices are caused by insufficient downward flexibility (Brijs, Vos, Jonghe, & Belmans, 2015). However, with StochD, the market operator is able to anticipate and avoid the SP's expensive down-regulation offer. By increasing the CP unit 3's day-ahead generation, transmission congestion is alleviated in the intraday market and the CP unit 3 is able to replace the SP unit's down-regulation. Therefore, intraday costs are greatly reduced with StochD in this scenario.

If the day-ahead and intraday markets would realize as in these three scenarios, then, with ConvD, the SP would achieve an expected profit of € 9979.53, whereas with StochD, its expected profit would be € 7869.84 (Table 9). Compared to ConvD, StochD leads to 69% lower intraday costs because in scenario "Congestion,"

Table 6
Day-ahead and intraday generation, flows, and prices in the three-node example with ConvD.

	Variable																			
	$\sum_b g^{da}_{s,f,n,u,b}$ (megawatt)				$f^{da}_{s,\ell}$ (megawatt)			$\lambda^{da}_{s,n}$ (€ per megawatt)			$\sum_b g^{up/down}_{s,f,n,u,b}$ (megawatt)				$f^{intra}_{s,\ell}$ (megawatt)			$\lambda^{intra}_{s,n}$ (€ per megawatt)		
	Unit				Line			Node			Unit				Line			Node		
Scenario	u0	u1	u2	u3	ℓ_1	ℓ_2	ℓ_3	n1	n2	n3	u0	u1	u2	u3	ℓ_1	ℓ_2	ℓ_3	n1	n2	n3
Congestion		4	42	20	−10	10	−8	7	6	7	8			2			−2	3000	3	20
Ramp limit		4	4			2		6	6	6	2		4	4	−8	−4		3000	3000	3000
Surplus	10	4	42	10	−10	10	10	7	6	7	−1	−4	−4		4			−500	−500	20

Table 8
Day-ahead and intraday generation, flows, and prices in the three-node example with StochD.

	Variable																			
	$\sum_b g^{da}_{s,f,n,u,b}$ (megawatt)				$f^{da}_{s,\ell}$ (megawatt)			$\lambda^{da}_{s,n}$ (€ per megawatt)			$\sum_b g^{up/down}_{s,f,n,u,b}$ (megawatt)				$f^{intra}_{s,\ell}$ (megawatt)			$\lambda^{intra}_{s,n}$ (€ per megawatt)		
	Unit				Line			Node			Unit				Line			Node		
Scenario	u0	u1	u2	u3	ℓ_1	ℓ_2	ℓ_3	n1	n2	n3	u0	u1	u2	u3	ℓ_1	ℓ_2	ℓ_3	n1	n2	n3
Congestion	6		38	22	−10	6	−6	2991	6	7	2	4	4			4	−4	3000	15	16
Ramp limit			8		−4	2		6	6	6		4	4	2	−4		−2	20	20	20
Surplus		4	42	20	−10	10		7	6	7		−4	−4	−1	4		1	2	2	2

Table 9
Expected profits and costs in the three-node example.

Metric	Design		
	Conventional dispatch	Stochastic dispatch	Perfect competition
SP day-ahead profit (€)	−3.3	5906.34	0.0
SP intraday profit (€)	9982.83	1963.5	0.0
SP total profit (€)	9979.53	7869.84	0.0
CP day-ahead profit (€)	6.6	2.64	6.6
CP intraday profit (€)	9203.04	3970.56	3.96
CP total profit (€)	9209.64	3973.2	10.56
Day-ahead generation cost (€)	293.04	6202.68	293.04
Intraday generation cost (€)	19318.2	6019.86	135.96
Total generation cost (€)	19611.24	12222.54	429.0

StochD reduces the SP's expensive up-regulation and in scenarios "Ramp limit" and "Surplus" the SP's expensive intraday price offers are avoided entirely by dispatching CP units out of merit order in the day-ahead market. As a consequence, the total day-ahead generation costs increase by approximately 20 times. Such a large increase can occur because the objective function of StochD (C.3) does not model the changes to the day-ahead price and, thus, day-ahead generation costs caused by out-of-merit-order dispatch. Nevertheless, the total generation costs are still 38% lower with StochD, and, as we show later in Section 4.3, StochD outperforms ConvD in expectation in real market conditions, too. With PC, the SP has no profit, and the total generation costs are only a fraction of those of ConvD and StochD. All problem instances are solved in one second with Gurobi 8.1.1 with an Intel i7 4.2 gigahertz processor with 8 gigabytes RAM.

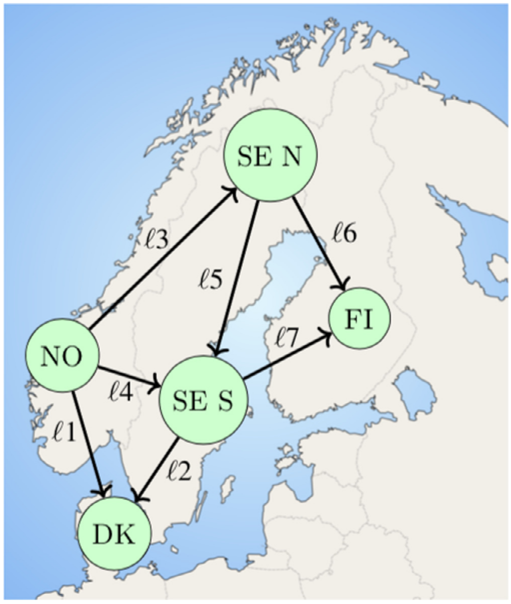

Fig. 6. Nordic network indicating conventional direction of flow (SE N and SE S refer to Sweden north and south, respectively).

4.2. Case study: strategic behavior in Nord Pool in 2016

In 2016, extremely high intraday prices were observed in Nord Pool. For example, on 22 January 2016, the Finnish up-regulation price peaked at € 3000 per megawatt hour. In accordance with our objective (2), we seek to examine reasons for these high prices using the offering strategies from Section 4.1.

We model the electricity markets in the Nordic countries with a simplified five-node network in Fig. 6, which is adequate for capturing congestion and the resulting area price differences. We obtain transmission capacities for the lines shown in Fig. 6 from Nord Pool (2016) and show them in Table 13 of Appendix D. In this network, each node contains demand as well as generators of different types. The day-ahead demand and generation capacities of wind, nuclear, and thermal in Tables 14 and 15, respectively, are set by averaging realized peak-hour data in January 2016 from Nord Pool, ENTSO-E, and the Finnish and Swedish TSOs (ENTSO-E, 2016; Fingrid, 2016; Svenska Kraftnät, 2016; Nord Pool, 2016). Due to the flexibility of hydropower, we take the maximum generation as its capacity. Also, we adjust the day-ahead demand with the average peak-hour exchange with neighboring countries such as Germany and Estonia. The piecewise constant generation cost parameters in Table 16 are fitted to match to the observed day-ahead and regulation price range approximately. We round generation and transmission capacity as well as demand data to the nearest 50 megawatt and, with ConvD, set the discretization interval of the binary expansion for up- and down-regulation of the SP ($\bar{G}^{up}_{x,n,u,b,j}$ and $\bar{G}^{down}_{x,n,u,b,k}$) to match the 50 megawatt precision, which leads to optimal results.[2] Using a higher precision keeps our conclusions unchanged because the 50 megawatt precision introduces only small discrepancies to the computed values as it is small compared to the market-clearing transmission flows and generation.

Corresponding to maximum regulation volumes observed in January 2016, we study two scenarios: one with 400 megawatt up-regulation ("Maximum deficit") and one with 300 megawatt down-regulation in Finland ("Maximum surplus"). We place a hypothetical SP with 500 megawatt capacity in Finland because the extremely high Finnish intraday price was set by a producer in Finland as the transmission lines from Sweden to Finland were congested. The SP with 500 megawatt capacity may correspond

[2] Since cost parameters are not distinct now, there are likely to be solutions with different generation and transmission flows but with the same objective value.

Table 10
Price and quantity offers of the strategic producer in the Nordic example.

	Conventional dispatch				Stochastic dispatch				Perfect competition			
	$p_{x,n,u,b}$ (€ per megawatt)		$q_{x,n,u,b}$ (megawatt)		$p_{x,n,u,b}$ (€ per megawatt)		$q_{x,n,u,b}$ (megawatt)		$p_{x,n,u,b}$ (€ per megawatt)		$q_{x,n,u,b}$ (megawatt)	
	Block		Block		Block		Block		Block		Block	
Offer	$b1$	$b2$	$b1$	$b2$	$b1$	$b2$	$b1$	$b2$	$b1$	$b2$	$b1$	$b2$
Day-ahead	50	50	250	250	2990	2990	250	50	20	30	250	250
Up-regulation	3000	3000	–	–	3000	3000	–	–	30	40	–	–
Down-regulation	20	20	–	–	3000	2960	–	–	20	15	–	–

Table 11
Expected profits and costs in the Nordic example.

	Policy		
Metric	Conventional dispatch	Stochastic dispatch	Perfect competition
SP day-ahead profit (k€)	6.25	152.75	12.5
SP intraday profit (k€)	148.5	−0.125	0.0
SP total profit (k€)	154.75	152.625	12.5
CP day-ahead profit (k€)	732.0	15136.0	732.0
CP intraday profit (k€)	438.0	2.0	0.0
CP total profit (k€)	1170.0	15138.0	732.0
Day-ahead generation cost (k€)	2005.0	16562.0	2005.0
Intraday generation cost (k€)	597.0	5.0	13.0
Total generation cost (k€)	2602.0	16567.0	2018.0

to a single large conventional plant or a few hydropower plants. All other generation capacities in Table 15 are assigned to CPs. The day-ahead generation as well as up- and down-regulation marginal costs of the SP are the same as those of hydropower (Table 16). In the following, the SP builds offer curves with the above input data, and we analyze the resulting generation and transmission flows in the day-ahead and intraday markets in the scenarios "Maximum deficit" and "Maximum surplus."

The optimal price and quantity offers are in Table 10. The generation, transmission flow, and price results in the day-ahead and intraday markets for each scenario are in Tables 17–22 of Appendix D, respectively. In both PC scenarios, the SP is fully dispatched in the day-ahead market as its marginal cost equals that of hydropower. All up- and down-regulation is done by the CPs.

By contrast, with ConvD, the SP sets its day-ahead price offer at the same level as the most expensive thermal generation so that in scenario "Maximum deficit," the SP does not produce in the day-ahead market but, rather, lets the transmission lines between Sweden and Finland become congested. Also, the SP's withdrawal from the day-ahead market results in high CP day-ahead generation and, thus, lack of CP capacity in the intraday market. Consequently, the SP can increase its up-regulation price to the maximum and gain a high profit as in the scenario "Congestion" of the three-node example. This leads to the very high intraday price of 3000 € per megawatt with ConvD in Finland as observed in the market data.

As in scenario "Congestion" in the three-node example with StochD, the strategic offer $p^{da}_{x,n,u,b} = 2990$ € per megawatt $<$ $p^{up}_{x,n,u,b} = 3000$ € per megawatt causes the market operator in scenario "Maximum deficit" to (i) dispatch the SP in the day-ahead market and (ii) reserve CP capacity from the day-ahead market to the intraday market to avoid a high intraday cost. Thus, StochD effectively introduces an opportunity for the SP to affect the day-ahead market with intraday offers unlike with ConvD. However, this offering strategy leads to very high total day-ahead generation costs as the day-ahead price of Finland becomes high. This was not considered by Morales et al. (2014) as they assume perfect competition. Indeed, if we disable strategic offering in the intraday market, then the SP does not withhold generation in the day-ahead market but seeks to increase it both with ConvD and StochD because the SP anticipates that the intraday price remains at its marginal cost. This supports the interpretation that the high prices in Nord Pool were caused by strategic offering and shows that the possibility for high intraday profits impacts the SP's day-ahead generation decisions.

In scenario "Maximum surplus" with ConvD, the SP competes against the thermal generators and becomes fully dispatched in the day-ahead market. As a consequence, it can participate in balancing the down-regulation need. However, the SP observes that there is abundant down-regulation capacity in Finland and in the adjacent nodes, and, thus, it sets its down-regulation price offer at the same level as the cost of down-regulation for hydropower. Indeed, in 2016, the lowest down-regulation price in Finland was 0 € per megawatt, which is close to the marginal cost of hydropower and other renewables. With StochD, the SP is dispatched out of merit order in the day-ahead market as it offers down-regulation at a price higher than any of the CPs. This leads to higher total profits because the day-ahead profit of the SP is higher than its intraday loss as the SP buys back the capacity it offered in the day-ahead market.

If the day-ahead and intraday markets would realize as in these two scenarios, then the SP would make an expected profit of 154.75 k€ with ConvD and 152.625 k€ with StochD Table 11. Thus, StochD is not able to reduce the profit of the SP significantly. Moreover, the total generation costs of StochD are significantly higher because of the extremely high day-ahead prices in Finland in scenario "Maximum deficit." However, as we show in Section 4.3, possibilities for adverse offering similar to scenario "Maximum deficit" are rare, and, therefore, StochD can outperform ConvD in expectation. In the perfectly competitive case, the SP makes a profit of 12.5 k€ as the SP is dispatched together with hydropower. In summary, the extremely high peak prices observed in Finland can be attributed to the combination of low up-regulation capacity, transmission congestion, and strategic behavior. All problem instances are solved to optimality in approximately one second.

4.3. Mean performance of the market designs in Nord Pool

Finally, in order to address our objective (3) to estimate the expected impact of the offering strategies on day-ahead and intraday costs, we conduct a simulation that resembles the real timeline of day-ahead and intraday markets as shown in Fig. 1 and the procedure in Baringo and Conejo (2016). The decision sequence is as follows:

1) The SP generates a set of initial day-ahead and intraday demand scenarios ($D^{da}_{s,n}, D^{intra}_{s,n}$) by applying k-means clustering to historical data.
2) The SP builds coordinated offer curves ($p^{da/up/down}_{x,n,u,b}$ and $q^{da}_{x,n,u,b}$) for the day-ahead and intraday markets by solving Eqs. (B.2)–(B.42) (ConvD) or (C.12)–(C.15) (StochD) given the initial

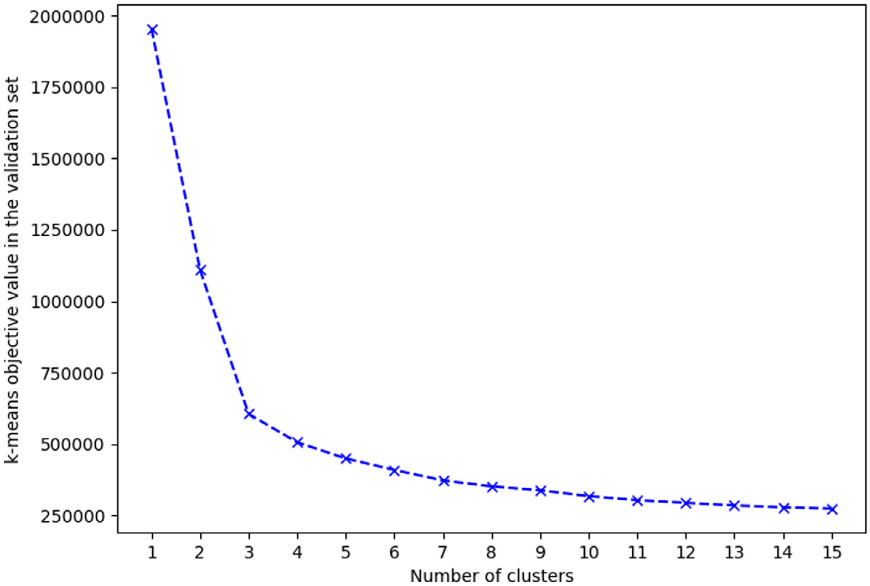

Fig. 7. Impact of the number of clusters on the k-means objective function value in the validation set.

day-ahead and intraday scenarios from 1). With PC, the SP sets $p^{da/up/down}_{x,n,u,b} = C^{da/up/down}_{x,n,u,b}$ and $q^{da}_{x,n,u,b} = G^{max}_{x,n,u,b}$.

3) The market operator receives the offer curves of the participants. It clears the day-ahead market by solving Eqs. (11)–(15) (ConvD and PC) or (C.3)–(C.5) (StochD) using real market data and communicates the resulting generation, transmission flows, and prices to the participants.
4) The SP generates an updated set of intraday scenarios by applying k-means clustering to historical data selected based on the day-ahead realization.
5) The SP updates its intraday offer curves ($p^{up/down}_{x,n,u,b}$) by solving Eqs. (E.6)–(E.9) (ConvD and StochD) using the updated intraday scenarios and the day-ahead results. With PC, no update is required.
6) The market operator receives the intraday offer curves of the participants and clears the intraday market by solving Eqs. (16)–(22) using real market data.

The steps 2)–6) are repeated for 1000 randomly sampled time steps t to obtain good estimates of expected profits and costs. We use the Nord Pool network from Section 4.2, and each time step $t \in [1, 8760]$ is defined by realized hourly day-ahead demand, generation, flows to neighboring countries, and regulation volumes in 2016. Similar to Section 4.2, input data are rounded to 50 megawatt precision to match the discretization intervals $\bar{G}^{up}_{x,n,u,b,j}$ and $\bar{G}^{down}_{x,n,u,b,k}$ of ConvD. The mean rounding error for the input data is less than 1 megawatt, which may cause small discrepancies in the estimated values but does not affect our conclusions. The transmission and generation capacity data used in the market clearings are assumed to be known exactly when building the offer curves.

The day-ahead and intraday scenarios at step 1) are given by

$$(D^{da}_{s,n}, D^{intra}_{s,n}) = (\hat{D}^{da}_{t,n} + \tilde{e}^{da}_{s,n}, \tilde{e}^{intra}_{s,n}), \tag{23}$$

where $\hat{D}^{da}_{t,n}$ is the predicted day-ahead demand in node n at time step t and $(\tilde{e}^{da}_{s,n}, \tilde{e}^{intra}_{s,n})$ are estimated day-ahead forecast error and regulation volume in scenario s at node n, respectively. Following Baringo and Conejo (2013a), we compute $(\tilde{e}^{da}_{s,n}, \tilde{e}^{intra}_{s,n})$ by applying k-means clustering from scikit-learn (Pedregosa et al., 2011) to nodewise, hourly total of forecast errors for demand and wind power in 2015 and to the nodewise, hourly regulation volumes in 2015 obtained from Nord Pool data, respectively. Consequently, each data point $(\tilde{e}^{da}_{n1}, \ldots, \tilde{e}^{da}_{n5}, \tilde{e}^{intra}_{n1}, \ldots, \tilde{e}^{intra}_{n5})$ is a vector of length 10. This representation of the data allows us to capture spatial correlations between the nodes as well as possible correlations between the day-ahead and intraday markets. We randomize the order of the data points and use 80% of the data for fitting the clusters and the remaining 20% as a validation set. We select seven clusters ($k = 7$), because additional clusters increase solution times while not improving the k-means objective function value in the validation set significantly as shown by Fig. 7. By assigning each of the seven cluster centers to one scenario, we obtain seven 10-vectors $[(\tilde{e}^{da}_{s1,n1}, \ldots, \tilde{e}^{da}_{s1,n5}, \tilde{e}^{intra}_{s1,n1}, \ldots, \tilde{e}^{intra}_{s1,n5}), \ldots, (\tilde{e}^{da}_{s7,n1}, \ldots, \tilde{e}^{da}_{s7,n5}, \tilde{e}^{intra}_{s7,n1}, \ldots, \tilde{e}^{intra}_{s7,n5})]$, which, using Eq. (23), allow us to compute seven day-ahead and intraday scenarios $(D^{da}_{s,n}, D^{intra}_{s,n}), \forall s \in (s1, \ldots, s7), \forall n \in (n1, \ldots, n5)$. The weight of a scenario is the weight of the corresponding cluster defined as the ratio of the number of data points belonging to the cluster to the total number of data points. Fig. 8 indicates that there is a positive correlation between the day-ahead and intraday deviations. Finally, near-zero and negative deviations have the highest probability, which is consistent with the fact that down-regulation is more frequent than up-regulation in the Nord Pool market as shown by Nord Pool regulation data.

Using these seven day-ahead and intraday scenarios including negative, near-zero, and positive deviations as an input to Eqs. (B.2)–(B.42) (ConvD) or (C.12)–(C.15) (StochD), the SP builds coordinated day-ahead and intraday offer curves ($p^{da/up/down}_{x,n,u,b}$ and $q^{da}_{x,n,u,b}$) at step 2). As an additional uncertainty, we sample uni-

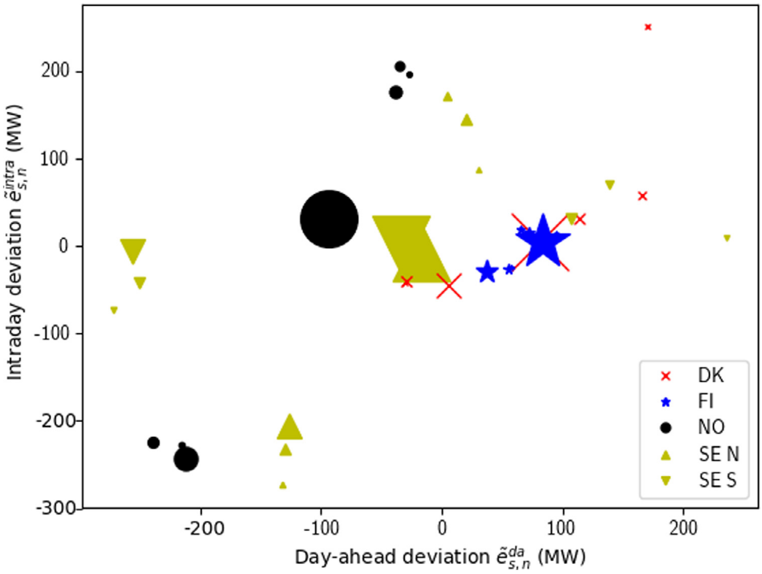

Fig. 8. Nodewise day-ahead and intraday clusters, where the diameter of the marker indicates the weight of a cluster.

form noise from U(−5 € per megawatt, 5 € per megawatt) to the day-ahead and intraday generation cost parameters of the CP ($C^{da}_{y,n,u,b}$, $C^{up}_{y,n,u,b}$, $C^{down}_{y,n,u,b}$). Note that, as shown in Sections 4.1 and 4.2, coordinated offering requires considering the intraday market when building the day-ahead offer curve. However, with PC, the offer curve building reduces to setting $p^{da}_{x,n,u,b} = C^{da}_{x,n,u,b}$, $p^{up}_{x,n,u,b} = C^{up}_{x,n,u,b}$, $p^{down}_{x,n,u,b} = C^{down}_{x,n,u,b}$, and $q^{da}_{x,n,u,b} = G^{max}_{x,n,u,b}$. Given the offer curves and realized hourly day-ahead demand ($D^{da}_{t,n}$), the market operator clears the day-ahead market at step 3) by solving Eqs. (11)–(15) (ConvD and PC) or (C.3)–(C.5) (StochD). The market operator communicates the day-ahead market-clearing generation, transmission flows, and prices to the participants.

Then, given the day-ahead results from step 3), the SP updates its intraday scenarios at step 4). We update the values of $D^{intra}_{s,n}$ by running k-means clustering on the set of regulation volumes corresponding to the 1000 closest (in terms of mean L^2 distance) day-ahead demand and wind power realizations in historical data. The weights of the scenarios are defined as above. At step 5), the SP updates its intraday offer curves by solving Eqs. (E.6)–(E.9) (ConvD and StochD) by using the updated intraday scenarios and the realized day-ahead generation and transmission flows. With PC, the intraday offer curves from step 2) remain unchanged. Finally, the market operator clears the intraday market at step 6) by solving Eqs. (16)–(22) given the updated intraday offer curves, realized day-ahead generation, transmissions flows, and intraday demand ($D^{intra}_{t,n}$).

Table 12 shows the results of this simulation. The total generation costs and the profits of the SP are approximately 123% and 466% higher with ConvD than with PC, respectively. StochD leads to lower costs and SP profits at approximately 100% and 404% higher than PC, respectively. Consequently, the StochD model is able to mitigate strategic behavior to some extent, but cannot eliminate it in all cases as our examples illustrate. The PC, ConvD, and StochD simulations are executed in approximately 20 seconds, 18 hours and 15 minutes, and 7 hours and 5 minutes, respectively.

Table 12
Expected profits and costs in the mean performance analysis.

Metric	Policy		
	Conventional dispatch	Stochastic dispatch	Perfect competition
SP day-ahead profit (k€)	42.61	37.61	8.15
SP intraday profit (k€)	3.53	3.43	0.0
SP total profit (k€)	46.14	41.04	8.15
CP day-ahead profit (k€)	2305.23	1992.36	619.96
CP intraday profit (k€)	0.20	1.11	0.23
CP total profit (k€)	2305.43	1993.47	620.18
Day-ahead generation cost (k€)	3123.95	2807.10	1420.11
Intraday generation cost (k€)	6.04	5.02	2.81
Total generation cost (k€)	3129.99	2812.12	1404.92
Regulation volume (megawatt)	450	446	450

5. Conclusion

Due to high barriers to entry, many day-ahead electricity markets have major players that can exert market power. Often, intraday markets have even less competition because flexible capacity is required. In fact, Knaut and Paschmann (2017) find restricted participation to be one reason for the high price volatility of the 15-minute German intraday products. Moreover, there may be less competition in areas that have low transmission capacity to neighboring areas. Consequently, as day-ahead prices decrease due to the increasing penetration of renewable energy with zero marginal costs, it is plausible to expect that higher profits are being pursued in the intraday market. Motivated by this possibility, we have developed a model that captures strategic offering not only in the day-ahead but also in the intraday market. Indeed, in Section 4.1 (objective 1), we show using a three-node network that transmission grid congestion and the lack of flexible capacity allow an SP to increase its profit in the day-ahead and intraday markets. On the one hand, withholding generation from the day-ahead market forces the CPs to generate more, which can lead to higher prices in the intraday market as the non-dispatched competitive capacity decreases. On the other hand, the SP can put forward generation in the day-ahead market and buy it back at a lower price from the intraday market if there is a surplus. Also, in Section 4.2 (objective 2), we have provided evidence that such strategic offering can explain high intraday prices observed in Nord Pool in 2016. Finally, Section 4.3 (objective 3) shows that strategic offering based on forecasts leads to higher expected profits and total generation costs vis-à-vis perfect competition (PC). However, the stochastic dispatch model of Morales et al. (2014) (StochD) can reduce the expected impact of strategic offering on total generation costs compared to the conventional dispatch model (ConvD).

Our model simplifies the building of day-ahead and intraday offer curves by ignoring more complex bid types spanning multiple time periods, for example. In addition, our model has only one intraday market, whereas, in reality, one-hour and 15-minute intraday trades can be made several hours before delivery and closer to real-time at different response times. Due to these structures and a low degree of competition, there are likely additional strategies for exerting market power. However, the impact of strategic offering will be mitigated if other players change their behavior in response to the strategic offers. Exploring the impact of multiple supply- and demand-side strategic players is left as a future research direction as it would result in an equilibrium problem with equilibrium constraints (EPEC) problem that generally requires custom heuristics to obtain a Nash equilibrium possibly out of many.

Additionally, the model could be made more realistic by introducing multiple time steps, elastic demand, and piecewise linear offer curves for hydropower, in particular. Regardless of the simplifications, the ConvD model is still computationally intensive due to the discretization procedure applied to non-convexities. Consequently, alternative solution methods –, such as reformulating the discretization procedure through Benders decomposition of the products of binary and continuous variables –, could be explored to tackle larger problem instances. Also, it is often possible to build smaller problem instances by reducing the size of the network by aggregating nearby areas into larger areas like in our Nordic network in Section 4.2 and by using clustering methods such as k-means (Section 4.3) for scenario reduction. Moreover, the endogenously computed day-ahead ($\lambda^{da}_{s,n}$) and intraday prices ($\lambda^{intra}_{s,n}$) can be replaced with exogenous values before solving only the upper-level problem in Eqs. (1)–(10) to quickly construct competitive coordinated offering into day-ahead and intraday markets.

Our results indicate that more transmission and flexible-generation capacity as well as development of more robust dispatch mechanisms may mitigate the impact of market power in intraday markets with a high penetration of variable renewable generation. As strategic behavior could be detected from plant-level data (Clements et al., 2016), data-transparency policies are also warranted.

Acknowledgement

This research has been partly supported by funding from the Aalto Science Institute and the STEEM project of the Aalto Energy Efficiency Research Programme. We are grateful to the handling editor and three anonymous referees for their constructive feedback. Any remaining errors are our own.

Appendix A. MPEC formulation

The lower-level problems (11)–(15) and (16)–(22) are linear, and, therefore, convex. To solve the bi-level program as if it were a single optimization problem, we reformulate it as a single-level mathematical program with equilibrium constraints (MPEC) by replacing the lower-level problems by their Karush–Kuhn–Tucker (KKT) conditions (A.2)–(A.9) and (A.10)–(A.21), respectively (Gabriel & Leuthold, 2010). Correspondingly, the set of dual variables is denoted by $\Omega^{DV} = \{\lambda^{da}_{s,n}, \lambda^{intra}_{s,n}, \beta^{da}_{s,f,n,u,b}, \beta^{up}_{s,f,n,u,b}, \beta^{down}_{s,f,n,u,b}, \beta^{up,ramp}_{s,f,n,u,b}, \beta^{down,ramp}_{s,f,n,u,b}, \mu^{da,max}_{s,\ell}, \mu^{da,min}_{s,\ell}, \mu^{intra,max}_{s,\ell}, \mu^{intra,min}_{s,\ell}\}$. The MPEC is non-convex due to the bilinear terms $g^{da}_{s,x,n,u,b}\lambda^{da}_{s,n}$, $g^{up}_{s,x,n,u,b}\lambda^{intra}_{s,n}$, and $g^{down}_{s,x,n,u,b}\lambda^{intra}_{s,n}$ in Eq. (A.1) and the complementarity conditions (A.4)–(A.9) and (A.12)–(A.21). These non-convexities are resolved in Appendix B.

Minimize$_{\Omega^{UL} \cup \Omega^{LL^{da}} \cup \Omega^{LL^{intra}} \cup \Omega^{DV}}$

$$\sum_s W_s \Bigg[\sum_n \sum_u \sum_b \Big(g^{da}_{s,x,n,u,b}\big(C^{da}_{x,n,u,b} - \lambda^{da}_{s,n}\big) + g^{up}_{s,x,n,u,b}\big(C^{up}_{x,n,u,b} - \lambda^{intra}_{s,n}\big) - g^{down}_{s,x,n,u,b}\big(C^{down}_{x,n,u,b} - \lambda^{intra}_{s,n}\big)\Big)\Bigg] \quad (A.1)$$

s.t.

Eqs. (2)–(10) (upper-level conditions)

$$f^{da}_{s,\ell} \text{ free}, \; -\sum_n Y_{l,n}\lambda^{da}_{s,n} + \mu^{da,max}_{s,\ell} - \mu^{da,min}_{s,\ell} = 0 \qquad \forall s, \ell \quad (A.2)$$

$$\lambda^{da}_{s,n} \text{ free}, \; D^{da}_{s,n} - \sum_f \sum_u \sum_b g^{da}_{s,f,n,u,b} - \sum_\ell Y_{\ell,n} f^{da}_{\ell,n} = 0 \quad \forall s, n \quad (A.3)$$

$$g^{da}_{s,x,n,u,b} \geq 0 \perp p^{da}_{x,n,u,b} - \lambda^{da}_{s,n} + \beta^{da}_{s,x,n,u,b} \geq 0 \qquad \forall s, x, n, u, b \quad (A.4)$$

$$g^{da}_{s,y,n,u,b} \geq 0 \perp C^{da}_{y,n,u,b} - \lambda^{da}_{s,n} + \beta^{da}_{s,y,n,u,b} \geq 0 \qquad \forall s, y, n, u, b \quad (A.5)$$

$$\beta^{da}_{s,x,n,u,b} \geq 0 \perp q^{da}_{x,n,u,b} - g^{da}_{s,x,n,u,b} \geq 0 \qquad \forall s, x, n, u, b \quad (A.6)$$

$$\beta^{da}_{s,y,n,u,b} \geq 0 \perp G^{max}_{y,n,u,b} - g^{da}_{s,y,n,u,b} \geq 0 \qquad \forall s, y, n, u, b \quad (A.7)$$

$$\mu^{da,max}_{s,\ell} \geq 0 \perp NTC^{max}_\ell - f^{da}_{s,\ell} \geq 0 \qquad \forall s, \ell \quad (A.8)$$

$$\mu^{da,min}_{s,\ell} \geq 0 \perp f^{da}_{s,\ell} - NTC^{min}_\ell \geq 0 \qquad \forall s, \ell \quad (A.9)$$

$$f^{intra}_{s,\ell} \text{ free}, \; -\sum_n Y_{l,n}\lambda^{intra}_{s,n} + \mu^{intra,max}_{s,\ell} - \mu^{intra,min}_{s,\ell} = 0 \qquad \forall s, \ell \quad (A.10)$$

$$\lambda^{intra}_{s,n} \text{ free}, \; D^{intra}_{s,n} - \sum_f \sum_u \sum_b \big(g^{up}_{s,f,n,u,b} - g^{down}_{s,f,n,u,b}\big) - \sum_\ell Y_{\ell,n} f^{intra}_{\ell,n} = 0 \quad \forall s, n \quad (A.11)$$

$$g^{up}_{s,x,n,u,b} \geq 0 \perp p^{up}_{x,n,u,b} - \lambda^{intra}_{s,n} + \beta^{up}_{s,x,n,u,b} + \beta^{up,ramp}_{s,x,n,u,b} \geq 0 \quad \forall s, x, n, u, b \quad (A.12)$$

$$g^{up}_{s,y,n,u,b} \geq 0 \perp C^{up}_{y,n,u,b} - \lambda^{intra}_{s,n} + \beta^{up}_{s,y,n,u,b} + \beta^{up,ramp}_{s,y,n,u,b} \geq 0 \quad \forall s, y, n, u, b \quad (A.13)$$

$$g^{down}_{s,x,n,u,b} \geq 0 \perp -p^{down}_{x,n,u,b} + \lambda^{intra}_{s,n} + \beta^{down}_{s,x,n,u,b} + \beta^{down,ramp}_{s,x,n,u,b} \geq 0 \quad \forall s, x, n, u, b \quad (A.14)$$

$$g^{down}_{s,y,n,u,b} \geq 0 \perp -C^{down}_{y,n,u,b} + \lambda^{intra}_{s,n} + \beta^{down}_{s,y,n,u,b} + \beta^{down,ramp}_{s,y,n,u,b} \geq 0 \quad \forall s, y, n, u, b \quad (A.15)$$

$$\beta^{up}_{s,f,n,u,b} \geq 0 \perp G^{max}_{f,n,u,b} - g^{da}_{s,f,n,u,b} - g^{up}_{s,f,n,u,b} \geq 0 \qquad \forall s, f, n, u, b \quad (A.16)$$

$$\beta^{down}_{s,f,n,u,b} \geq 0 \perp g^{da}_{s,f,n,u,b} - g^{down}_{s,f,n,u,b} \geq 0 \qquad \forall s, f, n, u, b \quad (A.17)$$

$$\beta^{up,ramp}_{s,f,n,u,b} \geq 0 \perp G^{up,ramp}_{f,n,u,b} - g^{up}_{s,f,n,u,b} \geq 0 \qquad \forall s, f, n, u, b \quad (A.18)$$

$$\beta^{down,ramp}_{s,f,n,u,b} \geq 0 \perp G^{down,ramp}_{f,n,u,b} - g^{down}_{s,f,n,u,b} \geq 0 \qquad \forall s, f, n, u, b \quad (A.19)$$

$$\mu^{intra,max}_{s,\ell} \geq 0 \perp NTC^{max}_\ell - f^{da}_{s,\ell} - f^{intra}_{s,\ell} \geq 0 \qquad \forall s, \ell \quad (A.20)$$

$$\mu^{intra,min}_{s,\ell} \geq 0 \perp f^{da}_{s,\ell} + f^{intra}_{s,\ell} - NTC^{min}_\ell \geq 0 \qquad \forall s, \ell \quad (A.21)$$

In the PC model, the systems (A.2)–(A.9) and (A.10)–(A.21) are solved to optimality sequentially by setting $p^{da}_{x,n,u,b} = C^{da}_{x,n,u,b}$, $p^{up}_{x,n,u,b} = C^{up}_{x,n,u,b}$, $p^{down}_{x,n,u,b} = C^{down}_{x,n,u,b}$, and $q^{da}_{x,n,u,b} = G^{max}_{x,n,u,b}$.

Appendix B. MILP formulation

First, the day-ahead lower-level problem in Eqs. (11)–(15) is linear, and, thus, strong duality holds. Consequently, we can follow the procedure in Ruiz and Conejo (2009) and linearize the non-convex term $g^{da}_{s,x,n,u,b}\lambda^{da}_{s,n}$ exactly by using Eqs. (A.2)–(A.9):

$$\begin{aligned} v^{da}_{s,x} &= \sum_n \sum_u \sum_b g^{da}_{s,x,n,u,b}\lambda^{da}_{s,n} \\ &= \sum_y \sum_n \sum_u \sum_b \left(-C^{da}_{y,n,u,b} g^{da}_{s,y,n,u,b} - \beta^{da}_{s,y,n,u,b} G^{max}_{y,n,u,b}\right) \\ &\quad + \sum_\ell \left(-\mu^{da,max}_{s,\ell} NTC^{max}_\ell + \mu^{da,min}_{s,\ell} NTC^{min}_\ell\right) + \sum_n D^{da}_{s,n}\lambda^{da}_{s,n} \end{aligned} \tag{B.1}$$

Second, the bilinear term $g^{up}_{s,x,n,u,b}\lambda^{intra}_{s,n}$ is replaced by the term $v^{up}_{s,x,n,u,b}$ using our reformulation of binary expansion (Barroso et al., 2006) that allows the term to become negative, which can happen if $\lambda^{intra}_{s,n}$ is negative. We do this because applying the procedure of Ruiz and Conejo (2009) to $g^{up}_{s,x,n,u,b}\lambda^{intra}_{s,n}$ would require a more expensive reformulation of a larger number of bilinear terms $g^{up}_{s,y,n,u,b}\beta^{up}_{s,y,n,u,b}$. To this end, Eq. (B.3) represents $g^{up}_{s,x,n,u,b}$ as a binary number scaled by the discretization interval $\bar{G}^{up}_{x,n,u,b} > 0$ by selecting binary variables $h^{up}_{s,x,n,u,b,j}$. If $h^{up}_{s,x,n,u,b,j}$ equals to one, then (B.4) enforces $\hat{h}^{up}_{s,x,n,u,b,j}$ to equal $\lambda^{intra}_{s,n}$ but (B.5) limits its value between $\Lambda^{intra,min}$ and $\Lambda^{intra,max}$. However, if $h^{up}_{s,x,n,u,b,j}$ equals to zero, then (B.4) is not binding but (B.5) sets $\hat{h}^{up}_{s,x,n,u,b,j}$ to zero. As a result, (B.6) sets $v^{up}_{s,x,n,u,b}$ to the sum of selected generation levels multiplied by the intraday price. The term $g^{down}_{s,x,n,u,b}\lambda^{intra}_{s,n}$ is linearized similarly in Eqs. (B.7)–(B.10) using the binary variable $h^{down}_{s,x,n,u,b,k}$ and free variable $\hat{h}^{down}_{s,x,n,u,b,k}$. This reformulation may lead to suboptimal results, but the suboptimality can be reduced by making the discretization intervals $\bar{G}^{up/down}_{x,n,u,b} > 0$ smaller.

Third, the complementarity conditions (A.4)–(A.9) and (A.12)–(A.21) are modeled by disjunctive constraints in Eqs. (B.11)–(B.42) as in Gabriel and Leuthold (2010). In the following formulation, we have set $\Omega^{MILP} = \{v^{da}_{s,x}, v^{up}_{s,x,n,u,b,j}, v^{down}_{s,x,n,u,b,k}, h^{up}_{s,x,n,u,b,j}, h^{down}_{s,x,n,u,b,k}, \hat{h}^{up}_{s,x,n,u,b,j}, \hat{h}^{down}_{s,x,n,u,b,k}, r1, \ldots, r16\}$ and we use $M = 2\Lambda^{da,max}$ in all numerical results in Section 4.

$$\text{Minimize}_{\Omega^{UL}\cup\Omega^{LL^{da}}\cup\Omega^{LL^{intra}}\cup\Omega^{DV}\cup\Omega^{MILP}}$$

$$\sum_s W_s\left[\sum_{n,u,b}\left(C^{da}_{x,n,u,b}g^{da}_{s,x,n,u,b} + C^{up}_{x,n,u,b}g^{up}_{s,x,n,u,b} - C^{down}_{x,n,u,b}g^{down}_{s,x,n,u,b} - v^{up}_{s,x,n,u,b} + v^{down}_{s,x,n,u,b}\right) - v^{da}_{s,x}\right] \tag{B.2}$$

s.t.

$$g^{up}_{s,x,n,u,b} = \bar{G}^{up}_{x,n,u,b}\sum_j 2^{j-1}h^{up}_{s,x,n,u,b,j} \qquad \forall s,x,n,u,b \tag{B.3}$$

$$-M(1-h^{up}_{s,x,n,u,b,j}) \le \lambda^{intra}_{s,n} - \hat{h}^{up}_{s,x,n,u,b,j} \le M(1-h^{up}_{s,x,n,u,b,j}) \quad \forall s,x,n,u,b,j \tag{B.4}$$

$$\Lambda^{intra,min}h^{up}_{s,x,n,u,b,j} \le \hat{h}^{up}_{s,x,n,u,b,j} \le \Lambda^{intra,max}h^{up}_{s,x,n,u,b,j} \qquad \forall s,x,n,u,b,j \tag{B.5}$$

$$v^{up}_{s,x,n,u,b} = \bar{G}^{up}_{x,n,u,b}\sum_j 2^{j-1}\hat{h}^{up}_{s,x,n,u,b,j} \qquad \forall s,x,n,u,b \tag{B.6}$$

$$g^{down}_{s,x,n,u,b} = \bar{G}^{down}_{x,n,u,b}\sum_k 2^{k-1}h^{down}_{s,x,n,u,b,k} \qquad \forall s,x,n,u,b \tag{B.7}$$

$$-M(1-h^{down}_{s,x,n,u,b,k}) \le \lambda^{intra}_{s,n} - \hat{h}^{down}_{s,x,n,u,b,k} \le M(1-h^{down}_{s,x,n,u,b,k}) \quad \forall s,x,n,u,b,k \tag{B.8}$$

$$\Lambda^{intra,min}h^{down}_{s,x,n,u,b,k} \le \hat{h}^{down}_{s,x,n,u,b,k} \le \Lambda^{intra,max}h^{down}_{s,x,n,u,b,k} \qquad \forall s,x,n,u,b,k \tag{B.9}$$

$$v^{down}_{s,x,n,u,b} = \bar{G}^{down}_{x,n,u,b}\sum_k 2^{k-1}\hat{h}^{down}_{s,x,n,u,b,k} \qquad \forall s,x,n,u,b \tag{B.10}$$

Eqs. (2)–(10) (upper-level conditions)

Eqs. (A.2), (A.3), (A.10), (A.11) (lower-level equality conditions)

$$Mr1_{s,x,n,u,b} \ge p^{da}_{x,n,u,b} - \lambda^{da}_{s,n} + \beta^{da}_{s,x,n,u,b} \ge 0 \qquad \forall s,x,n,u,b \tag{B.11}$$

$$M(1-r1_{s,x,n,u,b}) \ge g^{da}_{s,x,n,u,b} \ge 0 \qquad \forall s,x,n,u,b \tag{B.12}$$

$$Mr2_{s,y,n,u,b} \ge C^{da}_{y,n,u,b} - \lambda^{da}_{s,n} + \beta^{da}_{s,y,n,u,b} \ge 0 \qquad \forall s,y,n,u,b \tag{B.13}$$

$$M(1-r2_{s,y,n,u,b}) \ge g^{da}_{s,y,n,u,b} \ge 0 \qquad \forall s,y,n,u,b \tag{B.14}$$

$$Mr3_{s,x,n,u,b} \ge q^{da}_{x,n,u,b} - g^{da}_{s,x,n,u,b} \ge 0 \qquad \forall s,x,n,u,b \tag{B.15}$$

$$M(1-r3_{s,x,n,u,b}) \ge \beta^{da}_{s,x,n,u,b} \ge 0 \qquad \forall s,x,n,u,b \tag{B.16}$$

$$Mr4_{s,y,n,u,b} \ge G^{max}_{y,n,u,b} - g^{da}_{s,y,n,u,b} \ge 0 \qquad \forall s,y,n,u,b \tag{B.17}$$

$$M(1-r4_{s,y,n,u,b}) \ge \beta^{da}_{s,y,n,u,b} \ge 0 \qquad \forall s,y,n,u,b \tag{B.18}$$

$$Mr5_{s,\ell} \ge NTC^{max}_\ell - f^{da}_{s,\ell} \ge 0 \qquad \forall s,\ell \tag{B.19}$$

$$M(1-r5_{s,\ell}) \ge \mu^{da,max}_{s,\ell} \ge 0 \qquad \forall s,\ell \tag{B.20}$$

$$Mr6_{s,\ell} \ge f^{da}_{s,\ell} - NTC^{min}_\ell \ge 0 \qquad \forall s,\ell \tag{B.21}$$

$$M(1-r6_{s,\ell}) \ge \mu^{da,min}_{s,\ell} \ge 0 \qquad \forall s,\ell \tag{B.22}$$

$$Mr7_{s,x,n,u,b} \ge p^{up}_{x,n,u,b} - \lambda^{intra}_{s,n} + \beta^{up}_{s,x,n,u,b} + \beta^{up,ramp}_{s,x,n,u,b} \ge 0 \quad \forall s,x,n,u,b \tag{B.23}$$

$$M(1-r7_{s,x,n,u,b}) \ge g^{up}_{s,x,n,u,b} \ge 0 \qquad \forall s,x,n,u,b \tag{B.24}$$

$$Mr8_{s,y,n,u,b} \ge C^{up}_{y,n,u,b} - \lambda^{intra}_{s,n} + \beta^{up}_{s,y,n,u,b} + \beta^{up,ramp}_{s,y,n,u,b} \ge 0 \quad \forall s,y,n,u,b \tag{B.25}$$

$$M(1-r8_{s,y,n,u,b}) \ge g^{up}_{s,y,n,u,b} \ge 0 \qquad \forall s,y,n,u,b \tag{B.26}$$

$$Mr9_{s,x,n,u,b} \ge -p^{down}_{x,n,u,b} + \lambda^{intra}_{s,n} + \beta^{down}_{s,x,n,u,b} + \beta^{down,ramp}_{s,x,n,u,b} \ge 0 \quad \forall s,x,n,u,b \tag{B.27}$$

$$M(1-r9_{s,x,n,u,b}) \ge g^{down}_{s,x,n,u,b} \ge 0 \qquad \forall s,x,n,u,b \tag{B.28}$$

$$Mr10_{s,y,n,u,b} \ge -C^{down}_{y,n,u,b} + \lambda^{intra}_{s,n} + \beta^{down}_{s,y,n,u,b} + \beta^{down,ramp}_{s,y,n,u,b} \ge 0 \quad \forall s,y,n,u,b \tag{B.29}$$

$$M(1-r10_{s,y,n,u,b}) \ge g^{down}_{s,y,n,u,b} \ge 0 \qquad \forall s,y,n,u,b \tag{B.30}$$

$$Mr11_{s,f,n,u,b} \ge G^{max}_{f,n,u,b} - g^{da}_{s,f,n,u,b} - g^{up}_{s,f,n,u,b} \ge 0 \qquad \forall s,f,n,u,b \tag{B.31}$$

$$M(1-r11_{s,f,n,u,b}) \ge \beta^{up}_{s,f,n,u,b} \ge 0 \qquad \forall s,f,n,u,b \tag{B.32}$$

$$Mr12_{s,f,n,u,b} \ge g^{da}_{s,f,n,u,b} - g^{down}_{s,f,n,u,b} \ge 0 \qquad \forall s,f,n,u,b \tag{B.33}$$

$$M(1-r12_{s,f,n,u,b}) \ge \beta^{down}_{s,f,n,u,b} \ge 0 \qquad \forall s,f,n,u,b \tag{B.34}$$

$$Mr13_{s,f,n,u,b} \geq G^{up,ramp}_{f,n,u,b} - g^{up}_{s,f,n,u,b} \geq 0 \qquad \forall s, f, n, u, b \tag{B.35}$$

$$M(1 - r13_{s,f,n,u,b}) \geq \beta^{up,ramp}_{s,f,n,u,b} \geq 0 \qquad \forall s, f, n, u, b \tag{B.36}$$

$$Mr14_{s,f,n,u,b} \geq G^{down,ramp}_{f,n,u,b} - g^{down}_{s,f,n,u,b} \geq 0 \qquad \forall s, f, n, u, b \tag{B.37}$$

$$M(1 - r14_{s,f,n,u,b}) \geq \beta^{down,ramp}_{s,f,n,u,b} \geq 0 \qquad \forall s, f, n, u, b \tag{B.38}$$

$$Mr15_{s,\ell} \geq NTC^{max}_{\ell} - f^{da}_{s,\ell} - f^{intra}_{s,\ell} \geq 0 \qquad \forall s, \ell \tag{B.39}$$

$$M(1 - r15_{s,\ell}) \geq \mu^{intra,max}_{s,\ell} \geq 0 \qquad \forall s, \ell \tag{B.40}$$

$$Mr16_{s,\ell} \geq f^{da}_{s,\ell} + f^{intra}_{s,\ell} - NTC^{min}_{\ell} \geq 0 \qquad \forall s, \ell \tag{B.41}$$

$$M(1 - r16_{s,\ell}) \geq \mu^{intra,min}_{s,\ell} \geq 0 \qquad \forall s, \ell \tag{B.42}$$

Appendix C. Stochastic dispatch (StochD) formulation

In the following StochD bi-level formulation, Eqs. (C.1) and (C.2) are the upper-level objective function and constraints, respectively, which are constrained by the lower-level objective functions and constraints in Eqs. (C.3) and (C.4)–(C.5), respectively:

$$\text{Minimize}_{\Omega^{UL} \cup \Omega^{LL^{da}} \cup \Omega^{LL^{intra}}}$$

$$\sum_s W_s \Bigg[\sum_n \sum_u \sum_b \left(g^{da}_{s,x,n,u,b} \left(C^{da}_{x,n,u,b} - \lambda^{da}_{s,n} \right) + g^{up}_{s,x,n,u,b} \left(C^{up}_{x,n,u,b} - \lambda^{intra}_{s,n} \right) - g^{down}_{s,x,n,u,b} \left(C^{down}_{x,n,u,b} - \lambda^{intra}_{s,n} \right) \right) \Bigg] \tag{C.1}$$

s.t.

Eqs. (2)–(10) (upper-level conditions) (C.2)

$$\forall s \begin{cases} \text{Minimize}_{\Omega^{LL^{da}} \cup \Omega^{LL^{intra}}} \\ \sum_n \sum_u \sum_b p^{da}_{x,n,u,b} g^{da}_{s,x,n,u,b} + \sum_y \sum_n \sum_u \sum_b C^{da}_{y,n,u,b} g^{da}_{s,y,n,u,b} \\ \quad + \sum_n \sum_u \sum_b \left(p^{up}_{x,n,u,b} g^{up}_{s,x,n,u,b} - p^{down}_{x,n,u,b} g^{down}_{s,x,n,u,b} \right) \\ \quad + \sum_y \sum_n \sum_u \sum_b \left(C^{up}_{y,n,u,b} g^{up}_{s,y,n,u,b} - C^{down}_{y,n,u,b} g^{down}_{s,y,n,u,b} \right) & \text{(C.3)} \\ \text{s.t.} \\ \quad \text{Eqs. (12)–(15) (day-ahead constraints)} & \text{(C.4)} \\ \quad \text{Eqs. (17)–(22) (intraday constraints)} & \text{(C.5)} \end{cases}$$

Compared to ConvD, there is only one lower-level problem with the objective functions (C.3). Consequently, the KKT conditions (A.2) and (A.4)–(A.5) are replaced by:

$$f^{da}_{s,\ell} \text{ free}, \; -\sum_n Y_{l,n} \lambda^{da}_{s,n} + \mu^{da,max}_{s,\ell} - \mu^{da,min}_{s,\ell} + \mu^{intra,max}_{s,\ell} - \mu^{intra,min}_{s,\ell} = 0 \quad \forall s, \ell \tag{C.6}$$

$$g^{da}_{s,x,n,u,b} \geq 0 \perp p^{da}_{x,n,u,b} - \lambda^{da}_{s,n} + \beta^{da}_{s,x,n,u,b} - \beta^{down}_{s,x,n,u,b} + \beta^{up}_{s,x,n,u,b} \geq 0 \quad \forall s, x, n, u, b \tag{C.7}$$

$$g^{da}_{s,y,n,u,b} \geq 0 \perp C^{da}_{y,n,u,b} - \lambda^{da}_{s,n} + \beta^{da}_{s,y,n,u,b} - \beta^{down}_{s,y,n,u,b} + \beta^{up}_{s,y,n,u,b} \geq 0 \quad \forall s, y, n, u, b \tag{C.8}$$

As a result, the disjunctive constraints (B.11) and (B.13) become:

$$Mr1_{s,x,n,u,b} \geq p^{da}_{x,n,u,b} - \lambda^{da}_{s,n} + \beta^{da}_{s,x,n,u,b} - \beta^{down}_{s,x,n,u,b} + \beta^{up}_{s,x,n,u,b} \geq 0 \quad \forall s, x, n, u, b \tag{C.9}$$

$$Mr2_{s,y,n,u,b} \geq C^{da}_{y,n,u,b} - \lambda^{da}_{s,n} + \beta^{da}_{s,y,n,u,b} - \beta^{down}_{s,y,n,u,b} + \beta^{up}_{s,y,n,u,b} \geq 0 \quad \forall s, y, n, u, b \tag{C.10}$$

Using strong duality and Eqs. (C.7)–(C.8) and (A.12)–(A.19), we can linearize the bilinear terms in the upper level objective function in Eq. (C.1) exactly:

$$\begin{aligned} &\sum_n \sum_u \sum_b \left(g^{da}_{s,x,n,u,b} \lambda^{da}_{s,n} + g^{up}_{s,x,n,u,b} \lambda^{intra}_{s,n} - g^{down}_{s,x,n,u,b} \lambda^{intra}_{s,n} \right) \\ &= \nu^{da}_{s,x} + \sum_y \sum_n \sum_u \sum_b \Big(-C^{up}_{y,n,u,b} g^{up}_{s,y,n,u,b} + C^{down}_{y,n,u,b} g^{down}_{s,y,n,u,b} \\ &\quad - \beta^{up}_{s,y,n,u,b} G^{max}_{y,n,u,b} - \beta^{up,ramp}_{s,y,n,u,b} G^{up,ramp}_{y,n,u,b} - \beta^{down,ramp}_{s,y,n,u,b} G^{down,ramp}_{y,n,u,b} \Big) \\ &\quad - \sum_l \left(\mu^{intra,max}_{s,\ell} NTC^{max}_{\ell} - \mu^{intra,min}_{s,\ell} NTC^{min}_{\ell} \right) \\ &\quad + \sum_n D^{intra}_{s,n} \lambda^{intra}_{s,n} = \nu^{da}_{s,x} + \nu^{StochD}_{s,x} \end{aligned} \tag{C.11}$$

Therefore, the discretization scheme in Eqs. (B.3)–(B.10) can be omitted from the following StochD MILP formulation in which we have set $\Omega^{MILP,StochD} = \{\nu^{da}_{s,x}, \nu^{StochD}_{s,x}, r1, \ldots, r16\}$:

$$\text{Minimize}_{\Omega^{UL} \cup \Omega^{LL^{da}} \cup \Omega^{LL^{intra}} \cup \Omega^{DV} \cup \Omega^{MILP,StochD}}$$

$$\sum_s W_s \Bigg[\sum_{n,u,b} \left(C^{da}_{x,n,u,b} g^{da}_{s,x,n,u,b} + C^{up}_{x,n,u,b} g^{up}_{s,x,n,u,b} - C^{down}_{x,n,u,b} g^{down}_{s,x,n,u,b} \right) - \nu^{da}_{s,x} - \nu^{StochD}_{s,x} \Bigg] \tag{C.12}$$

s.t.

Eqs. (2)–(10) (upper-level conditions) (C.13)

Eqs. (C.6), (A.3), (A.10), (A.11)
(lower-level equality conditions) (C.14)

Eqs. (C.9), (B.12), (C.10), (B.14), (B.15)–(B.42)
(disjunctive constraints) (C.15)

Appendix D. Calibration and results for the Nordic example

Table 13
Network parameters of the Nordic example.

	Line						
Parameter	$\ell1$	$\ell2$	$\ell3$	$\ell4$	$\ell5$	$\ell6$	$\ell7$
NTC^{max}_{ℓ} (megawatt)	1600	2000	1600	2100	7300	1500	1200
NTC^{min}_{ℓ} (megawatt)	−1600	−2400	−1900	−2100	−7300	−1100	−1200

Table 14
Demand parameters in the Nordic example.

	Node				
Parameter	DK	FI	NO	SE N	SE S
$D^{da}_{s,n}$ (megawatt)	4900	12,900	21,600	3700	17,600

Table 15
Total generation capacities (in megawatt) in the Nordic example.

Node	Type Wind	Nuclear	Hydro	Thermal	SP
DK	1800			2900	
FI	200	2800	2400	4400	500
NO	300		26,100	400	
SE N	600		11,200	200	
SE S	1100	8100	2200	1500	

Table 16
Generation parameters in the Nordic example.

Parameter	Type, block: Wind $b1$	Wind $b2$	Nuclear $b1$	Nuclear $b2$	Hydro $b1$	Hydro $b2$	Thermal $b1$	Thermal $b2$	SP $b1$	SP $b2$
$C^{da}_{f,n,u,b}$ (€ per megawatt)	0	0	5	5	20	30	40	50	20	30
$C^{up}_{f,n,u,b}$ (€ per megawatt)					30	40	60	80	30	40
$C^{down}_{f,n,u,b}$ (€ per megawatt)					20	15	10	5	20	15
$G^{up,ramp}_{f,n,u,b}$ (megawatt)					1000	1000	1000	1000	250	250
$G^{down,ramp}_{f,n,u,b}$ (megawatt)					1000	1000	1000	1000	250	250

Table 17
Total day-ahead generation of marginal units in FI in the Nordic example.

	$\sum_b g^{da}_{s,f,n,u,b}$ (megawatt)								
	ConvD			StochD			PC		
	Type			Type			Type		
Scenario	Hydro	Thermal	SP	Hydro	Thermal	SP	Hydro	Thermal	SP
Maximum deficit	2400	4100		2400	4400	100	2400	3600	500
Maximum surplus	2400	3600	500	2400	3800	300	2400	3600	500

Table 18
Day-ahead exchange between FI and SE in the Nordic example.

	$f^{da}_{s,\ell}$ (megawatt)					
	ConvD		StochD		PC	
	Line		Line		Line	
Scenario	$\ell6$	$\ell7$	$\ell6$	$\ell7$	$\ell6$	$\ell7$
Maximum deficit	1500	1200	1500	800	1500	1200
Maximum surplus	1500	1200	1500	1200	1500	1200

Table 19
Total intraday generation of marginal units in the Nordic example, where positive (negative) figures correspond to up-regulation (down-regulation).

	$\sum_b g^{up/down}_{s,f,n,u,b}$ (megawatt)						
	ConvD			StochD		PC	
	Type			Type		Type	
Scenario	Hydro (NO)	Thermal	SP	Hydro (NO)	SP	Thermal	hydro
Maximum deficit		300	100	400		400	
Maximum surplus	−300				−300		−300

Table 20
Intraday exchange between FI and SE in the Nordic example.

	$f^{da}_{s,\ell}$ (megawatt)					
	ConvD		StochD		PC	
	Line		Line		Line	
Scenario	$\ell6$	$\ell7$	$\ell6$	$\ell7$	$\ell6$	$\ell7$
Maximum deficit				400		
Maximum surplus	−300					

Table 21
Day-ahead price results in the Nordic example.

	$\lambda^{da}_{s,n}$ (€ per megawatt)														
	ConvD					StochD					PC				
	Node					Node					Node				
Scenario	DK	FI	NO	SE N	SE S	DK	FI	NO	SE N	SE S	DK	FI	NO	SE N	SE S
Maximum deficit	30	50	30	30	30	30	2990	30	30	30	30	50	30	30	30
Maximum surplus	30	50	30	30	30	30	50	30	30	30	30	50	30	30	30

Table 22
Intraday price results in the Nordic example.

	$\lambda^{intra}_{s,n}$ (€ per megawatt)		
	ConvD	StochD	PC
	Node	Node	Node
Scenario	FI	FI	FI
Maximum deficit	3000	3000	80
Maximum surplus	20	20	20

Appendix E. Model for updating intraday offer curves

The intraday offer curves ($\Omega^{UL,intra} = \{p^{up}_{x,n,u,b}, p^{down}_{x,n,u,b}, up_{s,x,n}\}$) can be updated by solving the following problem with $g^{da}_{s,f,n,u,b}$ and $f^{da}_{s,\ell}$ fixed to the values $G^{da}_{f,n,u,b}$ and F^{da}_{ℓ} from the day-ahead market clearing, respectively:

$$\text{Minimize}_{\Omega^{UL,intra}\cup\Omega^{LL^{intra}}}$$
$$\sum_s W_s\Big[\sum_n\sum_u\sum_b\Big(g^{up}_{s,x,n,u,b}(C^{up}_{x,n,u,b}-\lambda^{intra}_{s,n}) - g^{down}_{s,x,n,u,b}(C^{down}_{x,n,u,b}-\lambda^{intra}_{s,n})\Big)\Big] \quad (E.1)$$

s.t.

Eqs. (3), (4), (6), (7), (9), (10) (intraday upper-level conditions) (E.2)

$$\forall s \begin{cases} \text{Minimize}_{\Omega^{LL^{intra}}} \\ \sum_n\sum_u\sum_b\left(p^{up}_{x,n,u,b}g^{up}_{s,x,n,u,b} - p^{down}_{x,n,u,b}g^{down}_{s,x,n,u,b}\right) \\ +\sum_y\sum_n\sum_u\sum_b\left(C^{up}_{y,n,u,b}g^{up}_{s,y,n,u,b} - C^{down}_{y,n,u,b}g^{down}_{s,y,n,u,b}\right) \quad (E.3) \\ \text{s.t.} \\ \quad \text{Eqs. (17)–(22) (intraday constraints) (E.4)} \end{cases}$$

Using strong duality, the bilinear terms in the objective function (E.1) can be linearized exactly:

$$\sum_n\sum_u\sum_b\left(g^{up}_{s,x,n,u,b}\lambda^{intra}_{s,n} - g^{down}_{s,x,n,u,b}\lambda^{intra}_{s,n}\right)$$
$$= \sum_y\sum_n\sum_u\sum_b\Big(-C^{up}_{y,n,u,b}g^{up}_{s,y,n,u,b} + C^{down}_{y,n,u,b}g^{down}_{s,y,n,u,b} - \beta^{up}_{s,y,n,u,b}(G^{max}_{y,n,u,b}-G^{da}_{y,n,u,b}) - \beta^{down}_{s,y,n,u,b}G^{da}_{y,n,u,b} - \beta^{up,ramp}_{s,y,n,u,b}G^{up,ramp}_{y,n,u,b} - \beta^{down,ramp}_{s,y,n,u,b}G^{down,ramp}_{y,n,u,b}\Big) - \sum_l(\mu^{intra,max}_{s,\ell}(NTC^{max}_{\ell}-F^{da}_{\ell}) - \mu^{intra,min}_{s,\ell}(NTC^{min}_{\ell}-F^{da}_{\ell})) + \sum_n D^{intra}_{s,n}\lambda^{intra}_{s,n} = v^{intra}_{s,x} \quad (E.5)$$

Therefore, discretization is not required for the following MILP formulation for updating the intraday offer curves in which we have set $\Omega^{MILP,intra} = \{v^{intra}_{s,x}, r7, \ldots, r16\}$ and $\Omega^{DV,intra} = \{\lambda^{intra}_{s,n}, \beta^{up}_{s,f,n,u,b}, \beta^{down}_{s,f,n,u,b}, \beta^{up,ramp}_{s,f,n,u,b}, \beta^{down,ramp}_{s,f,n,u,b}, \mu^{intra,max}_{s,\ell}, \mu^{intra,min}_{s,\ell}\}$:

$$\text{Minimize}_{\Omega^{UL,intra}\cup\Omega^{LL^{intra}}\cup\Omega^{DV,intra}\cup\Omega^{MILP,intra}}$$
$$\sum_s W_s\Big[\sum_{n,u,b}\left(C^{up}_{x,n,u,b}g^{up}_{s,x,n,u,b} - C^{down}_{x,n,u,b}g^{down}_{s,x,n,u,b}\right) - v^{intra}_{s,x}\Big] \quad (E.6)$$

s.t.

Eqs. (3), (4), (6), (7), (9), (10) (intraday upper-level conditions) (E.7)

Eqs. (A.10), (A.11) (intraday lower-level equality conditions) (E.8)

Eqs. (B.23)–(B.42) (intraday disjunctive constraints) (E.9)

References

Amountzias, C., Dagdeviren, H., & Patokos, T. (2017). Pricing decisions and market power in the UK electricity market: A VECM approach. *Energy Policy, 108*, 467–473.
Baringo, L., & Conejo, A. (2013a). Correlated wind-power production and electric load scenarios for investment decisions. *Applied Energy, 101*(C), 475–482.
Baringo, L., & Conejo, A. (2013b). Strategic offering for a wind power producer. *IEEE Transactions on Power Systems, 28*(4), 4645–4654.
Baringo, L., & Conejo, A. J. (2016). Offering strategy of wind-power producer: A multi-stage risk-constrained approach. *IEEE Transactions on Power Systems, 31*(2), 1420–1429.
Barroso, L. A., Carneiro, R. D., Granville, S., Pereira, M. V., & Fampa, M. H. C. (2006). Nash equilibrium in strategic bidding: A binary expansion approach. *IEEE Transactions on Power Systems, 21*(2), 629–638.
Bjørndal, E., Bjørndal, M., & Rud, L. (2013). Congestion management by dispatch or re-dispatch: Flexibility costs and market power effects. In *Proceedings of 10th international conference on the european energy market (EEM)* (pp. 1–8).
Boomsma, T. K., Juul, N., & Fleten, S. E. (2014). Bidding in sequential electricity markets: The Nordic case. *European Journal of Operational Research, 238*(3), 797–809.
Brijs, T., Vos, K. D., Jonghe, C. D., & Belmans, R. (2015). Statistical analysis of negative prices in European balancing markets. *Renewable Energy, 80*, 53–60.
Cialani, C., & Mortazavi, R. (2018). Household and industrial electricity demand in europe. *Energy Policy, 122*, 592–600.
Clements, A., Hurn, A., & Li, Z. (2016). Strategic bidding and rebidding in electricity markets. *Energy Economics, 59*, 24–36.
Dai, T., & Qiao, W. (2015). Optimal bidding strategy of a strategic wind power producer in the short-term market. *IEEE Transactions on Sustainable Energy, 6*(3), 707–719.
Dai, T., & Qiao, W. (2017). Finding equilibria in the pool-based electricity market with strategic wind power producers and network constraints. *IEEE Transactions on Power Systems, 32*(1), 389–399.
European Commission (2014). A policy framework for climate and energy in the period from 2020 to 2030. http://eur-lex.europa.eu/legal-content/EN/TXT/?uri=CELEX:52014DC0015.
ENTSO-E (2016). Transparency platform. https://transparency.entsoe.eu/.
Fingrid (2016). Load and generation. http://www.fingrid.fi/en/electricity-market/load-and-generation/Pages/default.aspx.
Fleten, S. -E., & Kristoffersen, T. K. (2007). Stochastic programming for optimizing bidding strategies of a Nordic hydropower producer. *European Journal of Operational Research, 181*(2), 916–928.

Gabriel, S. A., & Leuthold, F. U. (2010). Solving discretely-constrained MPEC problems with applications in electric power markets. *Energy Economics, 32*(1), 3–14.
California ISO (2018). Annual report on market issues and performance – 2017. http://www.caiso.com/Documents/2017AnnualReportonMarketIssuesandPerformance.pdf, Folsom, CA.
Ito, K., & Reguant, M. (2016). Sequential markets, market power, and arbitrage. *American Economic Review, 106*(7), 1921–1957.
Just, S., & Weber, C. (2015). Strategic behavior in the German balancing energy mechanism: Incentives, evidence, costs and solutions. *Journal of Regulatory Economics, 48*(2), 218–243.
Kardakos, E. G., Simoglou, C. K., & Bakirtzis, A. G. (2016). Optimal offering strategy of a virtual power plant: A stochastic bi-level approach. *IEEE Transactions on Smart Grid, 7*(2), 794–806.
Kazempour, S. J., Conejo, A. J., & Ruiz, C. (2015). Strategic bidding for a large consumer. *IEEE Transactions on Power Systems, 30*(2), 848–856.
Klæboe, G., Eriksrud, A. L., & Fleten, S. E. (2015). Benchmarking time series based forecasting models for electricity balancing market prices. *Energy Systems, 6*(1), 43–61.
Knaut, A., & Obermüller, F. (2016). How to sell renewable electricity – Interactions of the intraday and day-ahead market under uncertainty. EWI Working Papers, 2016(4).
Knaut, A., & Paschmann, M. (2019). Price volatility in commodity markets with restricted participation. Energy Economics, 81, 37–51.
Svenska Kraftnät, S. (2016). Statistik. http://www.svk.se/aktorsportalen/elmarknad/statistik/.
Kwon, R. H., & Frances, D. (2012). Optimization-based bidding in day-ahead electricity auction markets: A review of models for power producers. In A. Sorokin, S. Rebennack, P. Pardalos, N. Iliadis, & M. Pereira (Eds.), *Handbook of networks in power systems i. energy systems.*. Berlin, Heidelberg: Springer.
Lei, M., Zhang, J., Dong, X., & Ye, J. J. (2016). Modeling the bids of wind power producers in the day-ahead market with stochastic market clearing. *Sustainable Energy Technologies and Assessments, 16*, 151–161.
Mauritzen, J. (2015). Now or later? Trading wind power closer to real-time: How poorly designed subsidies can lead to higher balancing costs. *The Energy Journal, 36*(4), 149–164.
Moiseeva, E., Hesamzadeh, M. R., & Biggar, D. R. (2015). Exercise of market power on ramp rate in wind-integrated power systems. *IEEE Transactions on Power Systems, 30*(3), 1614–1623.
Morales, J. M., Zugno, M., Pineda, S., & Pinson, P. (2014). Electricity market clearing with improved scheduling of stochastic production. *European Journal of Operational Research, 235*(3), 765–774.
Müller, T., & Möst, D. (2018). Demand response potential: Available when needed? *Energy Policy, 115*, 181–198.
Pape, C., Hagemann, S., & Weber, C. (2016). Are fundamentals enough? Explaining price variations in the german day-ahead and intraday power market. *Energy Economics, 54*, 376–387.
Pedregosa, F., Varoquaux, G., Gramfort, A., Michel, V., Thirion, B., Grisel, O., … Duchesnay, E. (2011). Scikit-learn: Machine learning in Python. *Journal of Machine Learning Research, 12*, 2825–2830.
Nord Pool (2009). The Nordic electricity exchange and the Nordic model for a liberalized electricity market. https://www.nordpoolgroup.com/globalassets/download-center/rules-and-regulations/the-nordic-electricity-exchange-and-the-nordic-model-for-a-liberalized-electricity-market.pdf.
Nord Pool (2016). Historical market data. http://nordpoolspot.com/historical-market-data/.
Nord Pool (2017). Strong volumes foundation for expansion – Nord Pool 2016. http://www.nordpoolspot.com/message-center-container/newsroom/exchange-message-list/2017/q1/strong-volumes-foundation-for-expansion--nord-pool-2016/.
Nord Pool (2019). Curtailment, price thresholds and decoupling. https://www.nordpoolgroup.com/trading/Day-ahead-trading/Curtailment-price-thresholds-and-decoupling/.
Rahimiyan, M., & Baringo, L. (2015). Strategic bidding for a virtual power plant in the day-ahead and real-time markets: A price-taker robust optimization approach. *IEEE Transactions on Power Systems, 31*(4), 2676–2687.
Ruiz, C., & Conejo, A. (2009). Pool strategy of a producer with endogenous formation of locational marginal prices. *IEEE Transactions on Power Systems, 24*(4), 1855–1866.
EPEX Spot (2017). EPEX Spot intraday markets reach all-time high in 2016. https://www.epexspot.com/en/press-media/press/details/press/EPEX_SPOT_Intraday_markets_reach_all-time_high_in_2016.
Tangerås, T. P., & Mauritzen, J. (2018). Real-time versus day-ahead market power in a hydro-based electricity market. *The Journal of Industrial Economics, 66*(4), 904–941.
Wozabal, D., & Rameseder, G. (2020). Optimal bidding of a virtual power plant on the Spanish day-ahead and intraday market for electricity. *European Journal of Operational Research, 280*(2), 639–655. forthcoming

Publication IV

T. Rintamäki, F. Oliveira, A. S. Siddiqui, and A. Salo. Achieving emission-reduction goals: Multi-period power-system expansion under short-term operational uncertainty. *IEEE Transactions on Power Systems*, 39(1), 119-131, 2024.

Achieving Emission-Reduction Goals: Multi-Period Power-System Expansion Under Short-Term Operational Uncertainty

Tuomas Rintamäki, Fabricio Oliveira, Afzal S. Siddiqui, and Ahti Salo

***Abstract*—Stochastic adaptive robust optimization is capable of handling short-term uncertainties in demand and variable renewable-energy sources that affect investment in generation and transmission capacity. We build on this setting by considering a multi-year investment horizon for finding the optimal plan for generation and transmission capacity expansion while reducing greenhouse gas emissions. In addition, we incorporate multiple hours in power-system operations to capture hydropower operations and flexibility requirements for utilizing variable renewable-energy sources such as wind and solar power. To improve the computational performance of existing exact methods for this problem, we employ Benders decomposition and solve a mixed-integer quadratic programming problem to avoid computationally expensive big-M linearizations. The results for a realistic case study for the Nordic and Baltic region indicate which investments in transmission, wind power, and flexible generation capacity are required for reducing greenhouse gas emissions. Through out-of-sample experiments, we show that the stochastic adaptive robust model leads to lower expected costs than a stochastic programming model under increasingly stringent environmental considerations.**

***Index Terms*—Emission reduction, generation and transmission expansion, robust optimization, stochastic programming, Benders decomposition.**

Nomenclature

Indices

$n/u/\ell$	node/generation unit/transmission line.
o	operating condition.
t/τ	time step in the master problem/subproblem.
ν/k	iteration in the column-and-constraint algorithm/Benders decomposition.

Sets

$\Psi^{G/L}$	existing generation units/transmission lines.
$\Psi^{G,H/L,AC}$	existing hydropower units/alternating current (AC) transmission lines.
$\Psi^{G+/L+}$	candidate generation units/transmission lines.
$\Phi^{L1/L2/L3}$	1st/2nd/3rd level decision variables.
$\Omega^{M/S}$	master problem/subproblem decision variables.
Ω/Ξ	uncertainty/feasibility set.
$r(\ell)/s(\ell)$	receiving/sending node of line ℓ
$\mathrm{T}^{0/-1}$	first/last subproblem time step within each master problem time step.
T^{r}	subproblem time steps in which the ramp constraints are considered.

Parameters

P	scaling factor to make investment and operation costs comparable.
W_o	weight of operating condition o
D	demand growth factor.
$\tilde{D}/\hat{D}_{o,\tau,n}$	nominal demand/demand increase at node n in condition o in period τ (MWh)
E_t	CO_2 emission target in period t (tonne)
R	discount factor.
$C^{x}_{t,u}$	investment cost of candidate unit u in period t (€ /MW)
$C^{y}_{t,\ell}$	investment cost of building candidate transmission line ℓ in period t (€)
$C^{g}_{o,\tau,u}$	generation cost of unit u in condition o in period τ (€ /MWh)
$A_{o,\tau,u}$	availability of unit u in condition o in period τ (%)
X_u	maximum invested capacity in candidate unit u(MW)
$\bar{G}_{o,\tau,u}$	maximum generation of unit u in condition o in period τ (MWh)
$\bar{G}/\underline{G}^{r}_{o,\tau,u}$	maximum ramp up/ramp down of unit u in condition o in period τ (MWh)
G^{e}_{u}	CO_2 emission rate of unit u (tonne/MWh)
$S^{0}_{o,\tau,u}$	initial storage level of hydropower unit u in condition o in period τ (MWh)

Manuscript received 11 March 2022; revised 11 July 2022, 21 October 2022, and 5 January 2023; accepted 31 January 2023. Date of publication 13 February 2023; date of current version 26 December 2023. This work was supported in part by the Swedish Energy Agency under Project 49259-1, in part by Academy of Finland under Project 326346, and in part by the Academy of Finland under Project 348094. Paper no. TPWRS-00342-2022. *(Corresponding author: Afzal S. Siddiqui.)*

Tuomas Rintamäki, Fabricio Oliveira, and Ahti Salo are with the Department of Mathematics and Systems Analysis, Aalto University, 00076 Aalto, Finland (e-mail: tuomas.rintamaki@aalto.fi; fabricio.oliveira@aalto.fi; ahti.salo@aalto.fi).

Afzal S. Siddiqui is with the Department of Computer and Systems Sciences, Stockholm University, Kista, Sweden, and also with the Department of Mathematics and Systems Analysis, Aalto University, 00076 Aalto, Finland (e-mail: Siddiqui,asiddiq@dsv.su.se).

Color versions of one or more figures in this article are available at https://doi.org/10.1109/TPWRS.2023.3244668.

Digital Object Identifier 10.1109/TPWRS.2023.3244668

$\bar{S}/\underline{S}_{o,\tau,u}$ maximum/minimum final storage level of hydropower unit u in condition o in period τ (MWh)
$I_{o,\tau,u}$ inflow to hydropower unit u in condition o in period τ (MWh)
$\bar{F}/\underline{F}_{o,\tau,\ell}$ maximum/minimum flow on line ℓ in condition o in period τ (MWh)
B_ℓ susceptance of line ℓ (S)
Λ^w demand uncertainty budget.
$\bar{\Lambda}/\underline{\Lambda}$ minimum/maximum price in the exchange (€ /MWh)

Binary variables

$y/\hat{y}_{t,\ell}$ equals 1 if the candidate transmission line ℓ is available/built in period t
w_n equals 1 if demand is increased from the nominal level at node n

Continuous variables

$x/\hat{x}_{t,u}$ total/new capacity of candidate generation unit u in period t (MW)
$d_{o,\tau,n}$ demand at node n in condition o in period τ (MWh)
$z_{o,\tau,n}$ auxiliary variables for linearizing $\lambda_{o,\tau,n}d_{\tau,n}$ (€)
$\lambda_{o,\tau,n}$ price in condition o at node n in period τ (€ /MWh)
$\tilde{\lambda}_{o,\tau,n}$ auxiliary variables for linearizing $\lambda_{o,\tau,n}d_{\tau,n}$ (€)
$f_{o,\tau,\ell}$ transmission flow in line ℓ in condition o in period τ (MWh)
$\delta_{o,\tau,n}$ voltage angle at node n in condition o in period τ (rad)
$g_{o,\tau,u}$ generation at unit u in condition o in period τ (MWh)
$s_{o,\tau,u}$ storage level at hydropower unit u in condition o in period τ (MWh)
$\bar{\beta}/\underline{\beta}_{o,\tau,u}$ dual variable for maximum/minimum generation of unit u in condition o in period τ (€ /MWh)
$\bar{\beta}/\underline{\beta}^r_{o,\tau,u}$ dual variable for maximum/minimum ramp of unit u in condition o in period τ (€ /MWh)
β^e_t dual variable for maximum CO_2 emissions in period t (€ /tonne)
$\phi^0_{o,\tau,u}$ dual variable for initial storage level of hydropower unit u in condition o in period τ (€ /MWh)
$\underline{\phi}_{o,\tau,u}$ dual variable for minimum storage of hydropower unit u in condition o in period τ (€ /MWh)
$\phi_{o,\tau,u}$ dual variable for storage level of hydropower unit u in condition o in period τ (€ /MWh)
$\bar{\phi}/\underline{\phi}^{-1}_{o,\tau,u}$ dual variable for maximum/minimum final storage level of hydropower unit u in condition o in period τ (€ /MWh)
$\mu_{o,\tau,\ell}$ dual variable for flow in AC line ℓ in condition o in period τ (€ /MWh)
$\bar{\mu}/\underline{\mu}_{o,\tau,\ell}$ dual variable for maximum/minimum flow in line ℓ in condition o in period τ (€ /MWh)
$\bar{\mu}/\underline{\mu}^{va}_{o,\tau,n}$ dual variable for maximum/minimum voltage angle at node n in condition o in period τ (€ /rad)
$\mu^{ref}_{o,\tau}$ dual variable for reference node voltage angle in condition o in period τ (€ /rad)
θ auxiliary variable for the CC master problem objective function (€)
$\sigma_{o,\tau,n}$ dual variable for Benders decomposition (€ /MWh)
η auxiliary variable for Benders decomposition (€)

I. Introduction

Most nations have ratified the Paris Agreement that aims at capping the increase in the global average temperature by lowering greenhouse gas (GHG) emissions [1]. To this end, there are national policies that set specific goals for GHG emission reductions through measures such as increasing energy efficiency and the share of renewable energy of total energy consumption [2]. Due to the limited availability of dispatchable renewable-energy sources (RES) such as hydropower and biomass, investments in non-dispatchable variable RES (VRES), such as wind and solar power, are required. However, integrating substantial VRES capacities in existing power systems is likely to require significant investments in transmission capacity as well as flexible generation technologies (e.g., combined cycle gas turbines, CCGT) and storage to guarantee power-system adequacy and security [3].

Given this background, we consider the generation and transmission expansion planning (G&TEP) problem, i.e., the required infrastructural expansions, e.g., transmission line, VRES, and other generation, for meeting long-term GHG emission-reduction goals. We require meeting short-term operational constraints on demand, transmission, generator ramping, and availability taking into account related uncertainties and the decision maker's robustness requirements. Thus, we employ a two-stage robust optimization model that can be formulated as a tri-level model, in which the first stage and level consider a multi-year investment horizon for generation and transmission expansion. At the second stage, the second level uses robust optimization (RO) to choose a worst-case demand for the third level that uses stochastic programming (SP) to minimize the cost of detailed, multi-hour power-system operation under a set of operating conditions (scenarios) for uncertain parameters such as VRES output and generation costs. We choose demand as the uncertain variable at the second level as it is a key driver for the long-term uncertainty of investment decisions and generation adequacy, which are the foremost interests of our analysis. Meanwhile, at the third level, we capture short-term, hourly operational uncertainties. This combination of RO and SP in two stages is called stochastic adaptive robust optimization (SARO) [4]. We apply the framework to a realistic case study covering Denmark, Estonia, Finland, Latvia, Lithuania, Norway, and Sweden.

The two-stage robust optimization problems, also known as SARO problems, for G&TEP are computationally challenging. [5] combine the best features of earlier exact solution algorithms to develop a more effective solution method based on the column-and-constraint (CC) algorithm in which solving the first-level and the second- as well as third-level problems alternate until their costs match. These alternating problems are called the master problem and subproblem, respectively. In the context of G&TEP, the master problem is a mixed-integer linear program (MILP) and the subproblem is a mixed-integer non-linear problem (MINLP), which can be reformulated as a computationally expensive MILP using a big-M-based linearization. To this end, [6] develop an approximate block coordinate descent method to avoid the expensive linearization of the subproblem. Other inexact solution methods involve metaheuristics such as genetic algorithms [7]. However, in this paper, we note that the subproblem is a mixed-integer quadratic program (MIQP), which can be solved faster than the linearized MILP using modern solvers such as Gurobi [8]. The MIQP solution method removes the need for additional constraints and parameters, which facilitates its application to other bi-level model instances, too. Moreover, we profile the CC algorithm and note that the master problem is a computational bottleneck as its size increases at every CC iteration. Consequently, we employ Benders decomposition [9] to break up the large MILP master problem into a small MILP and a large linear program (LP), which are faster to solve for large problem instances and lend themselves to parallelization. Accelerating the CC master problem allows us to solve larger problem instances faster and with less computational resources. To the best of our knowledge, our paper is the first one to accelerate the CC master problem in the SARO setting.

The two-stage robust optimization framework is employed for the G&TEP problem in [4], [5], and [10] but without the multi-year and multi-hour time dimensions and a goal for GHG emission reduction. [11] and [12] consider multiple years, but they do not focus on GHG emission reduction, do not model storage or hydropower, and do not provide an accelerated solution method for the master problem. [13] and [14] consider multiple years, but they do not use either a GHG emission-reduction goal or an accelerated solution method for the master problem. Also, the G&TEP problem has been studied extensively in single- ([15], [16], [17]) and bi-level settings ([18], [19], [20]), but these do not employ RO as an uncertainty modeling framework. Consequently, our SARO model for the G&TEP problem extends the state of the art to enable us to make policy contributions on the large-scale integration of VRES.

Likewise, approaches for GHG emission reduction in the power system have been studied extensively. [21], [22], [23], [24], [25] explore the long-term plan toward a fully renewable power system in the Baltic region, Germany, Australia, California, and Japan, respectively. They all find that significant amounts of VRES generation need to be complemented with dispatchable RES generation as well as storage technologies. However, their methodologies are limited in that they consider fixed cases for generation and transmission expansion and omit details such as the transmission network or ramping in short-term power-system operations. In fact, [26] solve a deterministic mixed-integer linear program (MILP) to optimize an expansion plan with constraints on GHG emissions and the share of RES generation and show that ignoring operational constraints leads to large errors in estimating GHG emissions.

Typically, the G&TEP problem is solved from the perspective of a central planner such as the transmission system operator (TSO). Although transmission investments are often made by such a central planner, the generation investments are usually made by independent market participants [4]. However, the central planner may use policies to incentivize investment in certain generation units [27], [28]. Also, alternative market designs could be considered to ensure cost recovery [29]. Nevertheless, [30], [31], [32] consider multiple companies investing in generation, but this leads to problems with multiple equilibria, which require custom solution algorithms, possibly with computationally expensive linearization schemes and no optimality guarantees. These approaches are outside the scope of our work.

Given this context, the contributions of this paper are:

C1) To consider multi-year and multi-hour time scales as well as detailed power-system operations, e.g., hydropower and a constraint for GHG emissions, in a SARO problem for G&TEP.

C2) To improve the solution time of earlier exact methods by applying Benders decomposition to the master problem and by solving the subproblem as an MIQP. Using MIQP removes the need for the expensive big-M linearization used in earlier work.

C3) To show which investments in transmission, wind power, and flexible generation capacity are required for reducing GHG emissions in a centrally planned system using a realistic case study for Nordic and Baltic countries. We show that these investments are robust to changes in uncertainty parameters with a preference for wind power at higher uncertainty levels.

C4) Through out-of-sample comparisons, to lay bare how investment plans obtained using an SP model or a model with less detailed power-system operations would not be able to cope with random load changes under increasingly stringent environmental considerations. By contrast, a SARO-based investment plan would mitigate the severest economic consequences by adopting more VRES generation.

The remainder of this paper is organized as follows. Section II presents the mathematical formulation of our SARO problem, and Section III details our solution methods. Section IV presents the results from a realistic case study. Finally, Section V summarizes and provides future research directions.

II. Problem Description

At the 1st stage and level of the SARO G&TEP problem, we consider a central planner that makes an expansion plan in a long-term horizon consisting of time steps t that we interpret as years. While doing this, the central planner considers the 2nd stage, where the 2nd level chooses the worst-case demand so as to maximize power-system operation costs. Also, at the 2nd stage, the central planner considers the 3rd level in which a market operator minimizes the operational costs in multiple operating conditions o and time steps τ for each 1st level time step t given the worst-case demand determined by the 2nd level. In order to capture the intraday demand and VRES generation profile, we model power-system operations within each 1st level time step t using a number of 3rd level time steps τ that we interpret as hours. To model several different intraday demand and VRES generation profiles, we consider multiple operating conditions o at the 3rd level. In addition to minimizing operational costs, the driver for the expansion plan is an upper bound for emissions in each 1st level time step.

A combination of RO and SP is used for modeling uncertainty when making the expansion plan. Following [4], we use RO at the 2nd level to identify the worst-case realization for the demand level. The demand level is seen as a long-term uncertainty that is affected by economic development and electrification of different sectors, for example. The demand level and its uncertainty are key drivers for investment decisions and generation adequacy. The demand-level uncertainty is controlled using an uncertainty budget. On the other hand, following [4] (and other references, e.g., [15], [16], [31])), we use an SP-based formulation that simultaneously considers multiple operating conditions and their respective weights (which are analogous to scenarios and probabilities, respectively) at the 3rd level to model uncertain parameters such as the short-term variability of VRES generation, demand, conventional generation capacities and costs, transmission capacities, and hydro inflows. To capture the short-term variability of demand and VRES generation, i.e., their intraday profiles, we define multiple operating conditions o and 3rd level time steps τ within each 1st level time step t. These intraday profiles are sampled from real power-system data using the hierarchical clustering method of [33]. In addition, we represent short-term uncertainty in conventional generation capacities and costs, transmission capacities, and hydro inflows by sampling from a probability distribution in each operating condition o and 3rd level time step τ.

A. Model Formulation

In the following, Ω denotes the uncertainty set from which the worst-case demand is selected and Ξ denotes the feasibility set for the operational decisions once the 1st and 2nd level decisions have been made. The mathematical formulation for our SARO G&TEP problem is:

$$\min_{\Phi^{L1}} P \sum_t R^{-t} \left[\sum_{u \in \Psi^{G+}} C^x_{t,u} \hat{x}_{t,u} + \sum_{\ell \in \Psi^{L+}} C^y_{t,\ell} \hat{y}_{t,\ell} \right] + \max_{\Phi^{L2} \in \Omega} \min_{\Phi^{L3} \in \Xi} \sum_o W_o \sum_\tau R^{-t(\tau)} \sum_u C^g_{o,\tau,u} g_{o,\tau,u} \quad (1)$$

s.t.

$$x_{t,u} = \sum_{t'=1}^{t} \hat{x}_{t',u} \quad \forall t, u \in \Psi^{G+} \quad (2)$$

$$y_{t,\ell} = \sum_{t'=1}^{t} \hat{y}_{t',\ell} \quad \forall t, \ell \in \Psi^{L+} \quad (3)$$

$$x_{t,u} \le X_u \quad \forall t, u \in \Psi^{G+}, \quad (4)$$

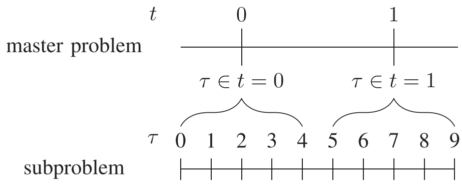

$$T^0 = \{0, 5\}, \quad T^{-1} = \{4, 9\}$$
$$T^r = \{0, 1, 2, 3, 5, 6, 7, 8\}, t(\tau) = \left\lfloor \frac{\tau}{5} \right\rfloor$$

Fig. 1. T^0, T^r, T^{-1}, $t(\tau)$, and $\tau \in t$ in an example problem with five subproblem time steps within each of the two master problem time steps.

where

$$\Phi^{L1} = \{\hat{x}_{t,u}, x_{t,u}, \forall u \in \Psi^{G+}; \hat{y}_{t,\ell}, y_{t,\ell}, \forall \ell \in \Psi^{L+}\}, \forall t,$$

$$\Phi^{L2} = \{d_{o,\tau,n}, \forall o, \tau; w_n\}, \forall n, \text{and } \Phi^{L3} = \{g_{o,\tau,u}, \forall u;$$

$$s_{o,\tau,u}, \forall u \in \Psi^{G,H}; f_{o,\tau,\ell}, \forall \ell; \delta_{o,\tau,n}, \forall n\}, \forall o, \tau.$$

In the objective function (1), the first minimization problem represents the generation and transmission expansion costs (1st level), and the maximization problem represents the selection of the worst-case demand (2nd level) for the second minimization problem of attaining the least-cost power-system operations (3rd level). The parameter P is used to annualize the expansion costs to make them comparable with operational costs. Constraints (2) and (3) define the capacities of candidate units and transmission lines that are available at each 1st level time step t, respectively. Constraints (4) define maximum investments in the new generation units.

Following [5] and [4], the uncertainty set Ω is given by:

$$\{d_{o,\tau,n} = D^{t(\tau)}(\tilde{D}_{o,\tau,n} + w_n \hat{D}_{o,\tau,n}) \quad \forall o, \tau, n \quad (5)$$

$$\sum_n w_n \le \Lambda^w\}. \quad (6)$$

Equation (5) defines that the demand is equal to the sum of nominal demand ($\tilde{D}_{o,\tau,n}$) and a possible demand increase ($\hat{D}_{o,\tau,n}$) multiplied by demand growth factor (D) that compounds at each 1st level time step t. The demand increase is selected using binary variables w_n in an attempt to maximize the operation costs. (6) sets an uncertainty budget on the number of demand increases the 2nd level model can activate.

For formulating power-system operations in (7)–(20), we define $n(u)$ as the node at which unit u is located. Also, the notation $\tau \in t$ indicates the 3rd level time steps τ within a 1st level time step t, and an inverse mapping $t(\tau)$ gives the 1st level time step t that the 3rd level time step τ belongs to. The definition of the two different time scales and the related sets are shown in Fig. 1. Consequently, given the optimal values $x^*_{t,u}, \forall t, u \in \Psi^{G+}$, $y^*_{t,\ell}, \forall t, \ell \in \Psi^{L+}$, and $d^*_{o,\tau,n}, \forall o, \tau, n$, the feasibility set $\Xi(g_{o,\tau,u}, s_{o,\tau,u}, f_{o,\tau,\ell}, \delta_{o,\tau,n})$ is:

$$\Bigg\{ \sum_{u|n(u)=n} g_{o,\tau,u} - \sum_{\ell|s(\ell)=n} f_{o,\tau,\ell} + \sum_{\ell|r(\ell)=n} f_{o,\tau,\ell} = d^*_{o,\tau,n} \quad \forall o,\tau,n \tag{7}$$

$$0 \le g_{o,\tau,u} \le A_{o,\tau,u}\bar{G}_{o,\tau,u} \quad \forall o,\tau,u \in \Psi^G_n \tag{8}$$

$$0 \le g_{o,\tau,u} \le A_{o,\tau,u}x^*_{t(\tau),u} \quad \forall o,\tau,u \in \Psi^{G+}_n \tag{9}$$

$$\underline{G}^r_{o,\tau,u} \le g_{o,\tau+1,u} - g_{o,\tau,u} \quad \forall o,\tau \in \mathrm{T}^r, u \tag{10}$$

$$g_{o,\tau+1,u} - g_{o,\tau,u} \le \bar{G}^r_{o,\tau,u} \quad \forall o,\tau \in \mathrm{T}^r, u \tag{11}$$

$$s_{o,\tau,u} \ge 0 \quad \forall o,\tau,u \in \Psi^{G,H} \tag{12}$$

$$s_{o,\tau,u} = S^0_{o,\tau,u} \quad \forall o,\tau \in \mathrm{T}^0, u \in \Psi^{G,H} \tag{13}$$

$$s_{o,\tau+1,u} = s_{o,\tau,u} - g_{o,\tau,u} + I_{o,\tau,u} \; \forall o,\tau \in \mathrm{T}^r, u \in \Psi^{G,H} \tag{14}$$

$$\underline{S}_{o,\tau,u} \le s_{o,\tau,u} \le \bar{S}_{o,\tau,u} \quad \forall o,\tau \in \mathrm{T}^{-1}, u \in \Psi^{G,H} \tag{15}$$

$$f_{o,\tau,\ell} = B_\ell(\delta_{o,\tau,s(\ell)} - \delta_{o,\tau,r(\ell)}) \quad \forall o,\tau,\ell \in \Psi^{L,AC} \tag{16}$$

$$\underline{F}_{o,\tau,\ell} \le f_{o,\tau,\ell} \le \bar{F}_{o,\tau,\ell} \quad \forall o,\tau,\ell \in \Psi^L \tag{17}$$

$$\underline{F}_{o,\tau,\ell}y^*_{t(\tau),\ell} \le f_{o,\tau,\ell} \le \bar{F}_{o,\tau,\ell}y^*_{t(\tau),\ell} \quad \forall o,\tau,\ell \in \Psi^{L+} \tag{18}$$

$$-\pi \le \delta_{o,\tau,n} \le \pi \quad \forall o,\tau,n \tag{19}$$

$$\delta_{o,\tau,0} = 0 \quad \forall o,\tau \tag{20}$$

$$\sum_o \sum_{\tau\in t} \sum_u W_o G^e_{o,\tau,u} g_{o,\tau,u} \le E_t \quad \forall t \Bigg\} \tag{21}$$

Equation (7) requires that the (possibly worst-case) demand is equal to the generation and exchange at each node. (8) and (9) impose that the generation of each unit is non-negative but less than or equal to the product of the unit's availability ($A_{o,\tau,u}$) and the maximum capacity of an existing unit ($\bar{G}_{o,\tau,u}$) or the built capacity of a candidate unit $x^*_{t(\tau),u}$, respectively. Moreover, the generation is limited by ramping constraints (10) and (11).

Following [34], we assume that each hydropower unit has one reservoir that can act as storage. (12) imposes that storage levels are non-negative. (13) sets the initial storage level at the first 3rd level time step τ within each 1st level time step t. (14) defines the storage level at the following time step $\tau+1$ as the current storage plus the difference of hydropower generation ($g_{o,\tau,u}, u \in \Psi^{G,H}$) and inflows ($I_{o,\tau,u}$) at τ. To avoid possible storage depletion, (15) requires that the storage level at the last 3rd level time step τ within each 1st level time step t is within desired levels $\underline{S}_{o,\tau,u}$ and $\bar{S}_{o,\tau,u}$. We do not model the link between the final and initial storage levels as these time steps may correspond to representative days many weeks or months apart. Using exogenous values for the initial storage levels reduces the risk of making hydropower too flexible where it could carry too much water between the representative days. As we show in Section IV-E, this hydropower model is more realistic than assuming that hydropower is fully flexible [35], [36]. However, this model does not consider the time value of water or additional constraints imposed by river systems, for example.

The transmission network is represented by alternating current (AC) and direct current (DC) circuits in (16)–(20). For AC lines, the transmission flow is determined by (16). However, flows in existing and candidate transmission lines must be within the capacities of the lines as given by (17) and (18), respectively. Related to the AC circuit, the voltage angles at each node and a reference voltage angle are given by (19) and (20), respectively.

Finally, (21) determines the upper bound for CO_2 emissions, which we use as a proxy for GHG emissions, at each 1st level time step t. This constraint applies to the entire region considered, which allows the model to optimize investments based on renewable generation conditions across the region, for example. The framework allows for other criteria such as a country-wise emissions caps or a lower bound on renewable power generation.

In the above formulation, we have assumed that all candidate transmission lines are DC lines for which flow is determined in the power exchange. This is because we focus on emission reduction and VRES integration using cross-border transmission, which is typically implemented via high-voltage DC (HVDC) lines to minimize heat and other relevant losses. However, the above formulation can readily be extended to cover candidate AC lines, too.

III. Solution Method

Following [5], the problem (1)–(4) is solved using a column-and-constraint (CC) algorithm in which solving the first minimization problem of (1) and solving the max-min problem of (1) alternates. These two problems are called CC master problem and CC subproblem, respectively. The alternation terminates when the total costs computed from the two problems match indicating the convergence of the method. The formulations for CC master problem and subproblem are given in the following subsections (22)–(39) and (40)–(45), respectively) and the solution algorithm is described in detail in Algorithm 1.

A. CC Master Problem

At iteration ν, we have $\Omega^M = \{g_{o,\tau,u,\nu'}, \forall u; s_{o,\tau,u,\nu'}, \forall u \in \Psi^{G,H}; f_{o,\tau,\ell,\nu'}, \forall \ell; \delta_{o,\tau,n,\nu'}, \forall n\}, \forall o,\tau,\nu' \le \nu$. Given $d^*_{o,\tau,n,\nu'}$, $\forall o,\tau,n,\nu' \le \nu$ as input data obtained from all the previous solutions of the subproblem, the master problem at iteration ν is:

$$\min_{\Phi^{L1},\Omega^M,\theta} P \sum_t R^{-t} \left[\sum_{u\in\Psi^{G+}} C^x_{t,u}\hat{x}_{t,u} + \sum_{\ell\in\Psi^{L+}} C^y_{t,\ell}\hat{y}_{t,\ell} \right] + \theta \tag{22}$$

s.t.

$$(2)-(4) \tag{23}$$

$$\theta \ge \sum_o W_o \sum_\tau R^{-t(\tau)} \sum_u C^g_u g_{o,\tau,u,\nu'} \quad \forall \nu' \le \nu \tag{24}$$

Algorithm 1: Algorithm for Solving the Problem (1)–(4).

Input: Problem parameters
Output: Transmission and generation expansion plan
$\epsilon \leftarrow 10^{-6}, LB \leftarrow -\infty, UB \leftarrow \infty, \nu \leftarrow 0$
$d_{o,\tau,n,\nu} \leftarrow \tilde{D}_{o,\tau,n} \quad \forall o,\tau,n$
while $(UB - LB)/UB \leq \epsilon$ **do**
  `// Solve the CC master problem`
  Obtain $x^*_{t,u}, \hat{x}^*_{t,u}, \forall t, u \in \Psi^{G+}; y^*_{t,\ell}, \hat{y}^*_{t,\ell}, \forall t, \ell \in \Psi^{L+}$ by solving CC master problem in Eqs. (22)-(39) using $d_{o,\tau,n,\nu'}, \forall o,\tau,n,\nu' \leq \nu$. LB is updated to the objective value of the master problem.
  `// Solve the CC subproblem`
  Obtain $w_n \, \forall n$ by solving CC subproblem in Eqs. (40)-(45) using the current $x^*_{t,u}, \forall t, u \in \Psi^{G+}; y^*_{t,\ell}, \forall t, \ell \in \Psi^{L+}$. UB is updated to the objective value of the subproblem $+ P \sum_t R^{-t} (\sum_{u \in \Psi^{G+}} C^x_{t,u} \hat{x}^*_{t,u} + \sum_{\ell \in \Psi^{L+}} C^y_{t,\ell} \hat{y}^*_{t,\ell})$
  $\nu \leftarrow \nu + 1$
  $d_{o,\tau,n,\nu} \leftarrow \tilde{D}_{o,\tau,n} + w_n \hat{D}_{o,\tau,n} \quad \forall o,\tau,n$
end

$$\sum_{u|n(u)=n} g_{o,\tau,u,\nu'} - \sum_{\ell|s(\ell)=n} f_{o,\tau,\ell,\nu'} + \sum_{\ell|r(\ell)=n} f_{o,\tau,\ell,\nu'} = d^*_{o,\tau,n,\nu'} \quad \forall o,\tau,n,\nu' \leq \nu \tag{25}$$

$$0 \leq g_{o,\tau,u,\nu'} \leq A_{o,\tau,u}\bar{G}_{o,\tau,u} \quad \forall o,\tau,u \in \Psi^G_n, \nu' \leq \nu \tag{26}$$

$$0 \leq g_{o,\tau,u,\nu'} \leq A_{o,\tau,u}x_{t(\tau),u} \quad \forall o,\tau,u \in \Psi^{G+}_n, \nu' \leq \nu \tag{27}$$

$$\underline{G}^r_{o,\tau,u} \leq g_{o,\tau+1,u,\nu'} - g_{o,\tau,u,\nu'} \quad \forall o,\tau \in \mathrm{T}^r, u, \nu' \leq \nu \tag{28}$$

$$g_{o,\tau+1,u,\nu'} - g_{o,\tau,u,\nu'} \leq \bar{G}^r_{o,\tau,u} \quad \forall o,\tau \in \mathrm{T}^r, u, \nu' \leq \nu \tag{29}$$

$$\sum_o \sum_{\tau \in t} \sum_u W_o G^e_{o,\tau,u} g_{o,\tau,u,\nu'} \leq E_t \quad \forall t, \nu' \leq \nu \tag{30}$$

$$s_{o,\tau,u,\nu'} \geq 0 \quad \forall o,\tau,u \in \Psi^{G,H}, \nu' \leq \nu \tag{31}$$

$$s_{o,\tau,u,\nu'} = S^0_{o,\tau,u} \quad \forall o,\tau \in \mathrm{T}^0, u \in \Psi^{G,H}, \nu' \leq \nu \tag{32}$$

$$s_{o,\tau+1,u,\nu'} = s_{o,\tau,u,\nu'} - g_{o,\tau,u,\nu'} + I_{o,\tau,u} \; \forall o,\tau \in \mathrm{T}^r, u \in \Psi^{G,H}, \nu' \leq \nu \tag{33}$$

$$\underline{S}_{o,\tau,u} \leq s_{o,\tau,u,\nu'} \leq \bar{S}_{o,\tau,u} \quad \forall o,\tau \in \mathrm{T}^{-1}, u \in \Psi^{G,H}, \nu' \leq \nu \tag{34}$$

$$f_{o,\tau,\ell,\nu'} = B_\ell(\delta_{o,\tau,s(\ell),\nu'} - \delta_{o,\tau,r(\ell),\nu'}) \quad \forall o,\tau,\ell \in \Psi^{L,AC}, \nu' \leq \nu \tag{35}$$

$$\underline{F}_{o,\tau,\ell} \leq f_{o,\tau,\ell,\nu'} \leq \bar{F}_{o,\tau,\ell} \quad \forall o,\tau,\ell \in \Psi^L, \nu' \leq \nu \tag{36}$$

$$\underline{F}_{o,\tau,\ell} y_{t(\tau),\ell} \leq f_{o,\tau,\ell,\nu'} \leq \bar{F}_{o,\tau,\ell} y_{t(\tau),\ell} \, \forall o,\tau,\ell \in \Psi^{L+}, \nu' \leq \nu \tag{37}$$

$$-\pi \leq \delta_{o,\tau,n,\nu'} \leq \pi \quad \forall o,\tau,n,\nu' \leq \nu \tag{38}$$

$$\delta_{o,\tau,0,\nu'} = 0 \quad \forall o,\tau,\nu' \leq \nu \tag{39}$$

B. CC Subproblem

For the subproblem, we define the following:

$$\Omega^S = \{\bar{\beta}_{o,\tau,u}, \underline{\beta}_{o,\tau,u}, \bar{\beta}^r_{o,\tau,u}, \underline{\beta}^r_{o,\tau,u}\}, \forall o,\tau,u \cup \beta^e_t, \forall t \cup \{\phi^0_{o,\tau,u}, \forall \tau \in \mathrm{T}^0; \phi_{o,\tau,u}, \forall \tau \in \mathrm{T}^r; \bar{\phi}^{-1}_{o,\tau,u}, \underline{\phi}^{-1}_{o,\tau,u} \forall \tau \in \mathrm{T}^{-1}; \underline{\phi}_{o,\tau,u} \forall \tau\}, \forall o, u \in \Psi^{G,H} \cup \{\mu_{o,\tau,\ell}, \bar{\mu}_{o,\tau,\ell}, \underline{\mu}_{o,\tau,\ell}\}, \forall o,\tau,\ell \cup \{\lambda_{o,\tau,n}, \bar{\mu}^{va}_{o,\tau,n}, \underline{\mu}^{va}_{o,\tau,n}\}, \forall o,\tau,n \cup \mu^{ref}_{o,\tau}, \forall o,\tau.$$

With $x^*_{t,u}, \forall t, u \in \Psi^{G+}$ and $y^*_{t,\ell}, \forall t, \ell \in \Psi^{L+}$ as input data obtained from the previous solution to the master problem, the subproblem is:

$$\begin{aligned}
\max_{\Phi^{L2}, \Omega^S} \sum_o \Bigg(\sum_\tau \Bigg[& \sum_n \lambda_{o,\tau,n} d_{o,\tau,n} \\
& - \sum_{u \in \Psi^G} \bar{\beta}_{o,\tau,u} A_{o,\tau,u} \bar{G}_{o,\tau,u} - \sum_{u \in \Psi^{G+}} \bar{\beta}_{o,\tau,u} A_{o,\tau,u} x^*_{t(\tau),u} \\
& - \sum_{\ell \in \Psi^L} \left(\bar{\mu}_{o,\tau,\ell} \bar{F}_{o,\tau,\ell} - \underline{\mu}_{o,\tau,\ell} \underline{F}_{o,\tau,\ell} \right) \\
& - \sum_{\ell \in \Psi^{L+}} \left(\bar{\mu}_{o,\tau,\ell} \bar{F}_{o,\tau,\ell} - \underline{\mu}_{o,\tau,\ell} \underline{F}_{o,\tau,\ell} \right) y^*_{t(\tau),\ell} \\
& - \sum_n \pi (\bar{\mu}^{va}_{o,\tau,n} + \underline{\mu}^{va}_{o,\tau,n}) \Bigg] \\
& + \sum_{u \in \Psi^{G,H}} \Bigg[\sum_{\tau \in \mathrm{T}^0} \phi^0_{o,\tau,u} S^0_{o,\tau,u} + \sum_{\tau \in \mathrm{T}^r} \phi_{o,\tau,u} I_{o,\tau,u} \\
& + \sum_{\tau \in \mathrm{T}^{-1}} \left(\underline{\phi}^{-1}_{o,\tau,u} \underline{S}_{o,\tau,u} - \bar{\phi}^{-1}_{o,\tau,u} \bar{S}_{o,\tau,u} \right) \Bigg] \\
& + \sum_{\tau \in \mathrm{T}^r} \sum_u \left(\underline{\beta}^r_{o,\tau,u} \underline{G}^r_{o,\tau,u} - \bar{\beta}^r_{o,\tau,u} \bar{G}^r_{o,\tau,u} \right) \Bigg) - \sum_t \beta^e_t E_t
\end{aligned} \tag{40}$$

s.t.

$$\begin{aligned}
& \lambda_{o,\tau,n(u)} - \bar{\beta}_{o,\tau,u} + \underline{\beta}_{o,\tau,u} + \mathbb{1}_{\tau \in \mathrm{T}^r \wedge u \in \Psi^{G,H}} \phi_{o,t,u} \\
& - \mathbb{1}_{\tau \notin \mathrm{T}^0} \bar{\beta}^r_{o,\tau-1,u} + \mathbb{1}_{\tau \notin \mathrm{T}^{-1}} \bar{\beta}^r_{o,\tau,u} + \mathbb{1}_{\tau \notin \mathrm{T}^0} \underline{\beta}^r_{o,\tau-1,u} \\
& - \mathbb{1}_{\tau \notin \mathrm{T}^{-1}} \underline{\beta}^r_{o,\tau,u} - W_o G^e_u \beta^e_{t(\tau)} = R^{-t(\tau)} C^g_{o,\tau,u} W_o \; \forall o,\tau,u
\end{aligned} \tag{41}$$

$$\begin{aligned}
& \mathbb{1}_{\tau \in \mathrm{T}^0} \phi^0_{o,\tau,u} + \underline{\beta}^s_{o,\tau,u} - \mathbb{1}_{\tau \notin \mathrm{T}^{-1}} \phi_{o,\tau,u} + \mathbb{1}_{\tau \notin \mathrm{T}^0} \phi_{o,\tau-1,u} \\
& + \mathbb{1}_{\tau \in \mathrm{T}^{-1}} (\underline{\phi}_{o,\tau,u} - \bar{\phi}_{o,\tau,u}) = 0 \quad \forall o,\tau,u \in \Psi^{G,H}
\end{aligned} \tag{42}$$

$$-\lambda_{o,\tau,s(\ell)} + \lambda_{o,\tau,r(\ell)} + \mathbb{1}_{\ell \in \Psi^{L,AC}} \mu_{o,\tau,\ell}$$

$$-\bar{\mu}_{o,\tau,\ell}+\underline{\mu}_{o,\tau,\ell}=0\quad\forall o,\tau,\ell \tag{43}$$

$$-\sum_{\ell\in\Psi^{L,AC}|s(\ell)=n}B_\ell\mu_{o,\tau,\ell}+\sum_{\ell\in\Psi^{L,AC}|r(\ell)=n}B_\ell\mu_{o,\tau,\ell}$$
$$-\bar{\mu}^{va}_{o,\tau,n}+\underline{\mu}^{va}_{o,\tau,n}+\mathbb{1}_{n=0}\mu^{ref}_{o,\tau}=0\quad\forall o,\tau,n \tag{44}$$

$$(5)-(6), \tag{45}$$

where $\mathbb{1}_{cond}$ equals 1 if *cond* is true and 0 otherwise.

The subproblem can be solved directly as an MIQP using solvers such as Gurobi. Alternatively, the subproblem can be reformulated as an MILP by linearizing the product of the continuous and binary variables in $\lambda_{o,\tau,n}d_{o,\tau,n}=\lambda_{o,\tau,n}D^{-t(\tau)}(\tilde{D}_{o,\tau,n}+w_n\hat{D}_{o,\tau,n})$ in the objective function (40) exactly with $\lambda_{o,\tau,n}d_{o,\tau,n}=D^{-t(\tau)}(z_{o,\tau,n}\hat{D}_{o,\tau,n}+\lambda_{o,\tau,n}\tilde{D}_{o,\tau,n})$ and by adding the following constraints to the subproblem:

$$z_{o,\tau,n}=\lambda_{o,\tau,n}-\tilde{\lambda}_{o,\tau,n}\quad\forall o,\tau,n \tag{46}$$

$$\underline{\Lambda}w_n\le z_{o,\tau,n}\le\bar{\Lambda}w_n\quad\forall o,\tau,n \tag{47}$$

$$\underline{\Lambda}(1-w_n)\le\tilde{\lambda}_{o,\tau,n}\le\bar{\Lambda}(1-w_n)\quad\forall o,\tau,n, \tag{48}$$

where parameters $\underline{\Lambda}$ and $\bar{\Lambda}$ can be set to exchange-specific values such as -500 € /MWh and 3000 € /MWh, respectively.

C. Benders Decomposition of the CC Master Problem

The CC master problem in (22)–(39) is an MILP that grows in the number of constraints at every CC iteration ν, whereas the CC subproblem remains fixed in size. If multiple iterations are required for solving a medium to large problem instance (i.e., several nodes, generation units, transmission lines and time steps), then the CC master problem can become prohibitively large. To tackle this issue, we apply Benders decomposition to the CC master problem to convert it to a small MILP and a large LP that are solved alternatively. Even though these two problems grow also at every CC iteration, they are typically faster to solve than the original MILP, as illustrated in the computational experiments presented in Section IV.

Specifically, the complicating variables in the original CC master problem are the binary variables $y_{t,\ell}$ and $\hat{y}_{t,\ell}$ that, once fixed, render an LP problem. Thus, the Benders master problem at iteration k of the Benders decomposition chooses $\Phi^{L1,BM}=\{y_{t,\ell},\hat{y}_{t,\ell},\forall t,\ell\in\Psi^{L+}\}$ by solving the following problem given $d^*_{o,\tau,n,\nu}$ from the CC subproblem:

$$\min_{\Phi^{L1,BM},\eta} P\sum_t R^{-t}\sum_{\ell\in\Psi^{L+}}C^y_{t,\ell}\hat{y}_{t,\ell}+\eta \tag{49}$$

s.t.

$$\eta-\sum_o\sum_\tau\sum_\nu\Bigg[\sum_{u\in\Psi^G}\Big(A_{o,\tau,u}\bar{G}_{o,\tau,u}\bar{\beta}_{o,\tau,u,\nu}$$
$$+\mathbb{1}_{\tau\in\mathrm{T}^r}(\bar{G}^r_{o,\tau,u}\bar{\beta}^r_{o,\tau,u,\nu}-\underline{G}^r_{o,\tau,u}\underline{\beta}^r_{o,\tau,u,\nu})\Big)$$
$$+\sum_{\ell\in\Psi^{L+}}y_{t(\tau),\ell}(\bar{F}_{o,\tau,\ell}\bar{\mu}_{o,\tau,\ell,\nu}-\underline{F}_{o,\tau,\ell}\underline{\mu}_{o,\tau,\ell,\nu})$$
$$+\sum_n d^*_{o,\tau,n,\nu}\sigma_{o,\tau,n,\nu}+\sum_n\pi(\bar{\mu}^{va}_{o,\tau,n,\nu}+\underline{\mu}^{va}_{o,\tau,n,\nu})$$
$$+\sum_{u\in\Psi^{G,H}}\Big(\mathbb{1}_{\tau\in\mathrm{T}^0}S^0_{o,\tau,u}\phi^0_{o,\tau,u,\nu}+\mathbb{1}_{\tau\in\mathrm{T}^r}I_{o,\tau,u}\phi_{o,\tau,u,\nu}$$
$$+\mathbb{1}_{\tau\in\mathrm{T}^{-1}}(\bar{S}_{o,\tau,u}\bar{\phi}_{o,\tau,u,\nu}-\underline{S}_{o,\tau,u}\underline{\phi}_{o,\tau,u,\nu})\Big)\Bigg]$$
$$-\sum_t\sum_\nu E_t\beta^e_t\ge 0. \tag{50}$$

With $y^*_{t,\ell,k}$ and $\hat{y}^*_{t,\ell,k}$ as input data, the Benders subproblem at the iteration k of the Benders decomposition is then given by $\Phi^{L1,BS}=\{x_{t,u},\hat{x}_{t,u},\forall t,\ell\in\Psi^{G+}\}$

$$\min_{\Phi^{L1,BS},\Omega^M,\theta} P\sum_t R^{-t}\Bigg[\sum_{u\in\Psi^{G+}}C^x_{t,u}\hat{x}_{t,u}+\sum_{\ell\in\Psi^{L+}}C^y_{t,\ell}\hat{y}^*_{t,\ell}\Bigg]+\theta \tag{51}$$

s.t.

1st level constraints (2) and (4)

3rd level constraints (24)-(36), (38), and (39)

$$\underline{F}_{o,\tau,\ell}y^*_{t(\tau),\ell,k}\le f_{o,\tau,\ell,\nu'}\le\bar{F}_{o,\tau,\ell}y^*_{t(\tau),\ell,k}\ \forall o,\tau,\ell\in\Psi^{L+},\nu'\le\nu. \tag{52}$$

The Benders master problem and subproblem are solved in an alternating fashion until their objective values are within a tolerance $\epsilon=10^{-6}$ from each other.

IV. Case Study: Ten-Year Investment Plan for Modified Nordic and Baltic Network

We have made the data and code for our case studies available at https://github.com/tuomasr/robust-dev.

A. Data

In order to examine a robust G&TEP plan with a target for CO_2 emissions, we use the Nordic and Baltic network in Fig. 2 and its generation, load, and transmission-line data from [35] as a base system for developing our case study. The system has a total of 14 nodes, of which six (without country codes) are dummy nodes used to represent the transmission network and have no load. The dashed and solid lines in Fig. 2 are DC and AC links, respectively. We augment this base system by having ten time steps in the CC master problem (t) for making investments. For each master problem time step, we consider 24 time steps in the CC subproblem (τ) to capture the intraday variability of load and renewables. Consequently, the subproblem has 240 time steps in total. To consider increasing electricity demand, we assume that load values increase by a factor of $D=1.01$ at each master problem time step [37].

In addition, we define 15 operational conditions o for each subproblem time step. We apply the hierarchical clustering method of [33] on hourly load and wind power data for 2014 to obtain 15 representative days. In short, we concatenate the hourly load and wind power data for each non-dummy node to

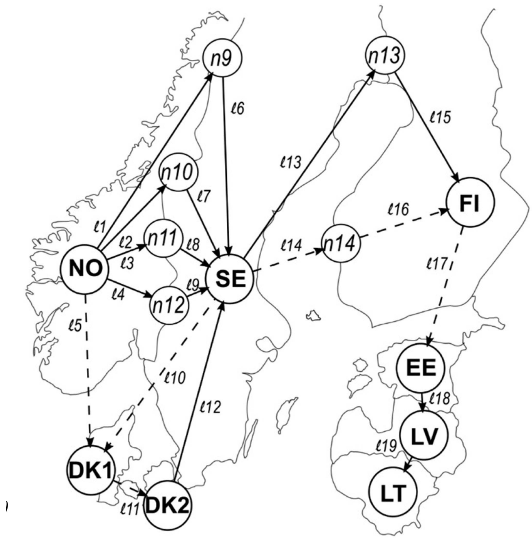

Fig. 2. Nordic and Baltic power system [35].

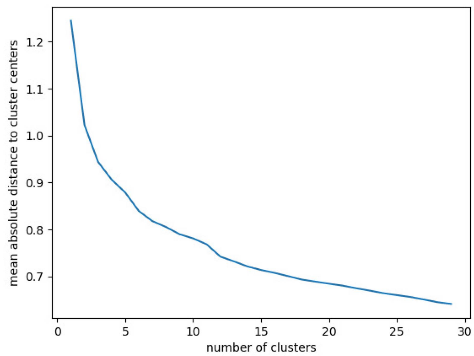

Fig. 3. Mean absolute distance between data points and cluster centers by the number of clusters (representative days).

obtain 365 vectors of length 192 (24 hours $\times$ 8 non-dummy nodes). These vectors are clustered using agglomerative clustering with Ward's linkage into the desired number of representative days (15 in our case). We then find the center of each cluster by taking the mean of the vectors in the cluster. Next, we obtain the representative days by finding the nearest vector to the cluster center using mean absolute distance. The hourly load, wind, and solar power data in these 15 representative days are used as the operational conditions for each set of 24 subproblem time steps. This allows us to capture the short-term variability of load and renewables over 15 representative days for each CC master problem time step (t). We select 15 representative days because we observed that the accuracy of the clustering as measured by mean squared distance from cluster centers does not improve significantly with additional representative days (see Fig. 3), while the solution time of the SARO problem steadily increases. For comparison, reference [33] finds 6 representative days appropriate. In fact, [38] show that if a sufficient number of the constraints corresponding to all scenarios are sampled, then the resulting solution fails to satisfy only a small portion of them.

Since hydropower data such as initial storage levels ($S^0_{o,\tau,u}$) and inflows ($I_{o,\tau,u}$) have weekly granularity, for each operating condition, we take the weekly value corresponding to each representative day. However, for generation ($\bar{G}_{o,\tau,u}$) and transmission capacities ($\bar{F}_{o,\tau,\ell}$ and $\underline{F}_{o,\tau,\ell}$), the operating conditions are defined by sampling uniform noise from $\mathrm{U}(-50\text{ MW}, 50\text{ MW})$ and adding the noise to historical values of these variables from [35]. Likewise, we sample perturbations to conventional generation costs ($C^g_{o,\tau,u}$) from $\mathrm{U}(-1$€/MWh$, 1$€/MWh$)$. These perturbations represent the short-term variability in generation costs as well as generator and transmission capacities due to maintenance and market conditions, for example. The perturbations are small compared to the historical values of these variables. The weights of the operating conditions (W_o) are equal to the weights of the representative days as defined in [33].

Open-cycle gas turbine (OCGT), combined-cycle gas turbine (CCGT), oil, biomass, wind, and solar power can be built at each (non-dummy) node. Each candidate unit has a maximum capacity ($G^{inv,\max}_u$) of 10 GW except for biomass units, which we limit to 1 GW due to limited fuel supply. In addition, neighboring (non-dummy) node pairs can be connected with a candidate DC transmission line with 1 GW of capacity in either direction. The investment costs for OCGT, CCGT, oil, biomass, wind, and solar power are 0.8, 1.0, 0.8, 3.9, 1.6, and 1.8 million € /MW, respectively, and 1000 million € for each transmission line [39]. The discount factor is 1.03, which is typical for this region [40]. We use the factor $P = \frac{1}{365}$ to annualize the expansion costs to the same level as the operational costs.

The initial CO_2 emission limit $E_0 = 90000$ tonnes is obtained from the CO_2 emissions corresponding to the first master problem time step when solving the problem with no investments. This initial emission bound is realistic given that the average daily CO_2 emissions of both power and heat production were approximately $E_0 = 140000$ tonnes in this area in 2014 [41]. We assume that the CO_2 emissions are required to decrease by approximately 6000 tonnes at every master problem time step to a final emission limit of $E_9 = 35000$ tonnes.

The 2nd level of the problem (1)–(4) chooses the worst-case load for power-system operations at the 3rd level. The budget (Δ^w) for choosing the worst-case load in (6) is 4 meaning that the model can increase load at a maximum of four nodes. Each increase that the model makes increases load in a node for all operating conditions and subproblem time steps ($\hat{D}_{o,\tau,n}$) by 5% of average hourly load in that node.

B. Summary of Results

We solve the case study using Algorithm 1 such that, for the CC master problem, we consider MILP and Benders decomposition formulations and, for the CC subproblem, we consider

TABLE I
RESULTS FOR THE DIFFERENT MASTER AND SUBPROBLEM ALGORITHMS USING THE NORDIC AND BALTIC NETWORK

Master problem	Benders		MILP	
Subproblem	MIQP	MILP	MIQP	MILP
Obj. func. value (M€)	124.2963	124.2963	124.2963	124.2963
Solution time (h)	7.08	7.17	15.62	16.19
Subprob. soln. time (h)	0.45	0.66	0.45	0.69
Iterations	3	3	3	3

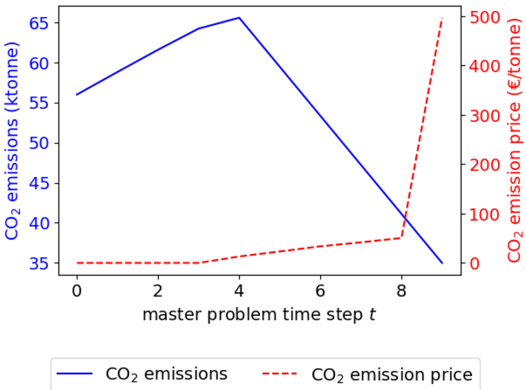

Fig. 4. CO_2 emissions and prices during the planning horizon.

MILP and MIQP formulations. The results in Table I show that all formulations attain the same objective value using the same number of iterations. The majority of the time is spent solving the CC master problems, which Benders decomposition solves nearly 2.5x faster than MILP. For the CC subproblems, MIQP outperforms MILP with a 1.5x speed-up. Consequently, Benders decomposition significantly reduces computational resource usage and, consequently, solution times, at the cost of a more technically complex implementation. The employment of MIQP to solve the subproblems yields smaller improvements in solution times but removes the need for the big-M linearization used in [4], [5], and in many bi-level model instances.[1] This demonstrates contributions C1 and C2.

Fig. 4 shows the evolution of CO_2 emissions to the final desired level during the planning horizon and the corresponding CO_2 emission prices (β_t^e). Already at $t = 0$, 1000 MW transmission lines are built from Finland to Norway and Sweden (see Table II) and a total of 1650 MW of wind power in Finland as well as 1200 MW of CCGT units in Latvia and Lithuania as shown by Fig. 5. As a consequence, CO_2 emissions from $t = 0$ to $t = 4$ are below the limits. To reduce CO_2 emissions to meet the final level under increasing load, an additional 100 MW of CCGT and 2000 MW of biomass units in Finland and in the Baltic countries are built during steps $t = 5$ to $t = 9$. The generation investments are similar to those in [21] except that they have

[1]We acknowledge the computational resources provided by the Aalto Scientific Computing initiative. All cases were solved using Gurobi 9.1 [8] running on a server with two 20-core Intel Xeon Gold 6248 processors at 2.50 GHz base frequency and with 128 GB of RAM.

TABLE II
RESULTS FOR THE IMPACT OF UNCERTAINTY BUDGET ON THE EXPANSION PLAN IN THE SARO MODEL

Uncertainty		Transmission (GW)		Generation (GW)		
Λ^w	$\hat{D}_{o,\tau,n}$ (%)	FI-NO	FI-SE	CCGT	Biomass	Wind
2	3	1.0	1.0	1.22	1.73	0.41
2	5	1.0	1.0	1.21	1.92	1.06
2	7	1.0	1.0	1.23	2.13	1.64
4	3	1.0	1.0	1.21	1.88	0.63
4	5	1.0	1.0	1.30	2.12	1.65
4	7	1.0	1.0	1.81	2.32	2.53
6	3	1.0	1.0	1.22	1.91	0.79
6	5	1.0	1.0	1.43	2.17	1.79
6	7	1.0	1.0	1.96	2.44	2.64

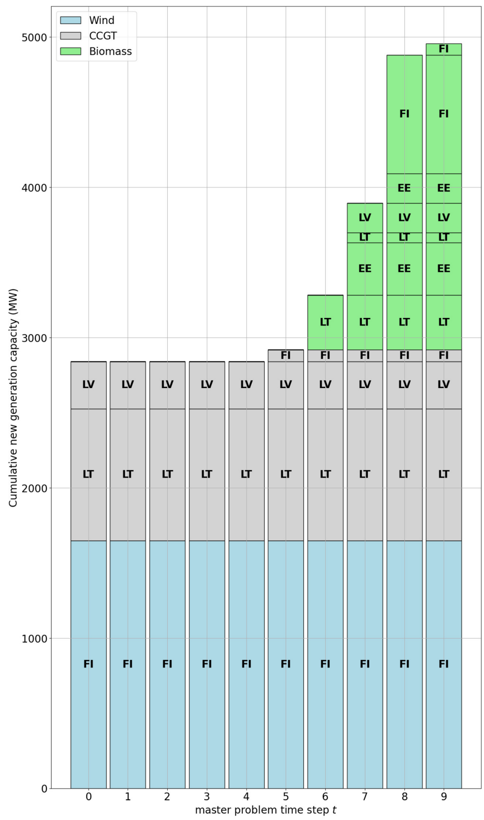

Fig. 5. Generation investments during the planning horizon with country codes indicating the node where each generation unit is built (EE = Estonia, FI = Finland, LV = Latvia, LT = Lithuania).

less CCGT and more solar power. Additionally, we find that our generation-expansion plan remains similar if we decrease the generation-investment costs by 40%-50%. If wind-power investment costs are decreased further, then the model prefers to build more wind-power capacity due to its low operational costs. In all cases, transmission-line expansion remains unchanged. Hence, we have tested the validity of our results with respect to

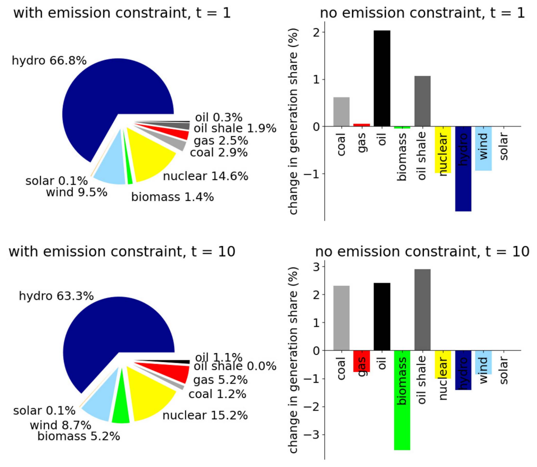

Fig. 6. Generation mix by fuel type in a SARO model with an emission constraint and changes in generation shares without the emission constraint.

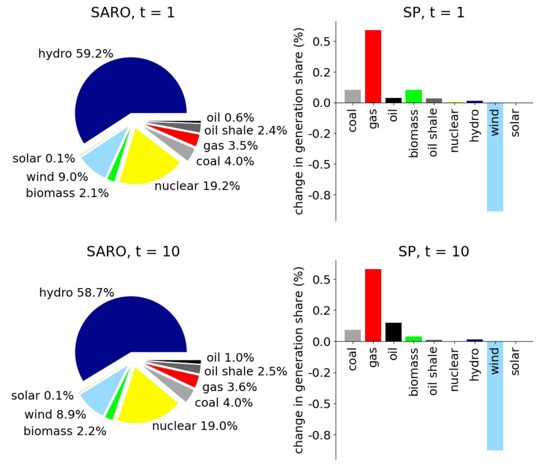

Fig. 7. Generation mix by fuel type in an SARO model and changes in generation shares with an SP or randomly sampled model.

the assumed cost estimates and found that the main insights are unaffected.

The generation mixes in Fig. 6 show that, compared to a solution with minimal investments and no emission constraint, the transmission and generation investments of the SARO model allow for replacing coal-, oil- and oil-shale-fired generation with less-polluting gas- and biomass-fired generation as well as wind power. In addition, new transmission lines between Finland, Norway, and Sweden enable increasing hydropower and nuclear generation close to their maximum capacity.

For the sake of comparison, we consider the investment decisions from an SP or randomly sampled model, in which the 2[nd] level uncertainty is modeled by representing the load increase ($\hat{D}_{o,\tau,n}$) of non-dummy nodes by a set of randomly sampled values. More precisely, we sample a vector of random values $\hat{w}_n$ from a uniform distribution and scale the magnitude of the vector to 1 to obtain the load for the SP or randomly sampled model:

$$\sum_n \hat{w}_n = 1 \tag{53}$$

$$d^*_{o,\tau,n} = D^{t(\tau)}(\tilde{D}_{o,\tau,n} + \hat{w}_n \hat{D}_{o,\tau,n}) \quad \forall o, \tau, n \tag{54}$$

The scaling in (53) is selected to represent an average load increase across all nodes. Consequently, the SP or randomly sampled model is given by

$$\min_{\Phi^{L1}} P \sum_t R^{-t} \left[\sum_{u \in \Psi^{G+}} C^x_{t,u} \hat{x}_{t,u} + \sum_{\ell \in \Psi^{L+}} C^y_{t,\ell} \hat{y}_{t,\ell} \right] + \min_{\Phi^{L3} \in \Xi} \sum_o W_o \sum_\tau R^{-t(\tau)} \sum_u C^g_{o,\tau,u} g_{o,\tau,u} \tag{55}$$

s.t.

(2)–(4) (56)

(53)–(54) (57)

The objective function in (55) is the same as in the SARO model in (1)–(4) except that the 2[nd] level objective function ($\max_{\Phi^{L2} \in \Omega}$) is removed. This is because the 2[nd] level constraints (5)–(6) are replaced by (53)–(54), which allocate the load increase ($\hat{D}_{o,\tau,n}$) to non-dummy nodes randomly instead of finding the worst-case load increase. This makes $d^*_{o,t,n}$ a parameter in the SP or randomly sampled model, whereas in the SARO model $d^*_{o,t,n}$ is a variable. The SP or randomly sampled model has the same constraints (7)–(21) as the SARO model 3[rd] -level constraints (represented by the feasibility set Ξ). Furthermore, the operating conditions (scenarios) remain the same.

The SP or randomly sampled model can, in principle, be solved as an MILP by substituting $x^*_{t,u} = x_{t,u}$ and $y^*_{t,\ell} = y_{t,\ell}$ in the SP or randomly sampled model formulation. However, we solve this SP or randomly sampled model using the same CC algorithm as we use for solving our base SARO model except that in Algorithm 1, we set $d_{o,t,n} = d_{o,t,n,\nu} = d^*_{o,t,n}\ \forall o, t, n, \nu$ using (53)–(54). The CC algorithm can potentially speed-up the computational performance of large problem instances.

Fig. 7 shows the generation mixes of the SARO and SP (or randomly sampled) models using their investment decisions and the same load. Compared to the SP or randomly sampled model, the SARO model allows for replacing coal-, oil-, gas-, and oil-shale-fired generation with wind power. Compared to the worst-case demand increases selected by the SARO model, the randomly allocated demand increases of the SP or randomly sampled model lead to lower transmission network congestion that leads the SP or randomly sampled model to invest less in wind power and utilize more existing hydro, biomass, and less-polluting gas plants.

C. Impact of Uncertainty Budget

The optimal generation and expansion decisions for different uncertainty budgets lead to Finland-Norway and Finland-Sweden transmission lines and gas-fired, biomass, and wind

TABLE III
RESULTS FOR THE IMPACT OF LOAD UNCERTAINTY ON THE EXPANSION PLAN IN THE SP OR RANDOMLY SAMPLED MODEL

Uncertainty	Transmission (GW)		Generation (GW)	
$\hat{D}_{o,\tau,n}$ (%)	FI-NO	FI-SE	CCGT	Biomass
3	1.0	1.0	1.32	1.40
5	1.0	1.0	1.30	1.47
7	1.0	1.0	1.28	1.54

power in all cases, which indicates the robustness of the investment decisions (Table II). Investments in wind power grow in relative terms at higher uncertainty levels. All models are solved using Benders decomposition and MIQP. This demonstrates contribution C3.

Table III shows the investment plan made by an SP or randomly sampled model in which the load increases ($\hat{D}_{o,\tau,n}$) are randomly allocated to the nodes. The transmission line investments are the same as those in the SARO model, but generation investments in biomass are lower without investment in wind power.

D. Cost of Robustness

Next, we demonstrate contribution C4 by evaluating the out-of-sample performance of the investment plan made by the SARO model by computing its expected total costs under different load levels sampled from $d_{o,\tau,n} \sim \tilde{D}_{o,\tau,n}[1 + \mathrm{U}(\min(0, L), \max(0, L))], \forall o, \tau, n$, where $L \in [-0.05, 0.10]$ is a load change. As we have 15 operating conditions, 240 time steps, and 8 non-dummy nodes, we sample a total of $15 \times 240 \times 8 = 28800$ load change values. Otherwise, we use the same parameter values as in our base model in Section IV-B. As a comparison, we use the investment plan made by an SP or randomly sampled model of Section IV-B in which the load increases of 5% ($\hat{D}_{o,\tau,n}$) are randomly allocated to the nodes.

Since the models can become infeasible at higher load levels, we relax the emission constraints and assign different penalty levels for violating them. This penalty corresponds to the marginal emissions cost β_t^e, which reaches the range 50 € /tonne to 500 € /tonne in our base model as shown by Fig. 4. We expect the emission cost to increase as the emission policy is anticipated to get more stringent over time and, hence, consider penalty levels of 100, 1000, and 10000 € /tonne. Fig. 8 indicates that the SARO model is more conservative in that it has higher total costs when load changes are zero or negative. However, for positive load changes, the SARO model can have lower total costs than the SP or randomly sampled model when the penalty for violating the emission constraint is 1000 €/tonne or higher. Moreover, for load changes close to the upper limit, the SP or randomly sampled model becomes infeasible.

E. Impact of Detailed Hydro-Reservoir Modeling

To further demonstrate our contributions C3 and C4, we remove the hydropower storage variable $s_{o,\tau,u}$ and constraints (12)–(15) from the problem (1)–(4) to explore the impact of detailed power-system modeling. In effect, we treat hydro-reservoir generation as if it were a fully flexible resource. We

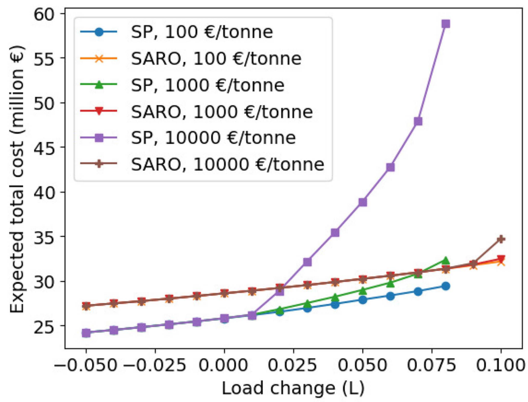

Fig. 8. Out-of-sample performance of the investment plans made by the SARO and SP (or randomly sampled) models under different load levels and penalties for violating the emission constraints.

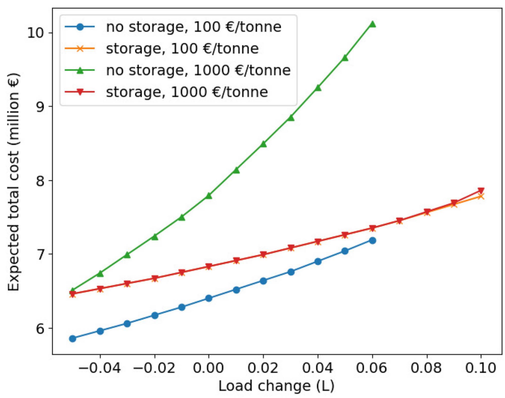

Fig. 9. Out-of-sample performance of the investment plans made by the SARO model with and without hydropower storage variable $s_{o,t,u}$ and constraints (12)–(15) under different load levels and penalties for violating the emission constraints.

find that without the hydropower constraints, there is no new generation investment while 1000 MW transmission lines are built from Finland to Norway and Sweden at $t = 0$ similar to our base model in Section IV-B. Following Section IV-D, we evaluate the investment plan made by the SARO model without the hydropower storage constraints by inserting the storage constraints back and computing the total expected cost under different load changes L and penalties for violating the emission constraints. Fig. 9 shows that the investment plan made by the SARO model with hydropower storage constraints has slightly higher total costs when the penalty for violating the emission constraints is 100 €/tonne. However, when either the penalty is 1000 €/tonne or the load change L is higher than 6%, the investment plan made by the SARO model without storage constraints either leads to significantly higher total costs or results in infeasibility as indicated by the truncated blue series in Fig. 9. Consequently, it is important to model hydropower at a detailed level to obtain realistic investment decisions that can avoid severe economic consequences and issues with power-system adequacy.

V. Conclusion

Many nations have set specific goals for GHG emission reductions through measures such as increasing the share of renewable energy. Integrating substantial VRES capacities in existing power systems is likely to require significant investments in transmission capacity and flexible generation technologies to guarantee power-system adequacy and security in the short and long terms. Therefore, the first contribution (C1) of this paper is to propose a SARO model for the G&TEP problem with multiple long- and short-term time periods along with detailed power-system operations and an emission-reduction goal. Earlier work has either omitted detailed short-term power-system operations, considered fixed investment scenarios, or not focused on emission reduction. Our second contribution (C2) is to deploy Benders decomposition and MIQP reformulations for improving the solution time of the problem. Earlier work has either used expensive big-M linearizations to obtain an expensive MILP or developed methods to accelerate the CC subproblem that may not be the computational bottleneck in all cases. We apply the model to a Nordic and Baltic power system and make the following conclusions on energy policy to contribute to the state-of-the-art policy analysis of large-scale integration of renewable energy in power systems (C3 and C4):

1) New transmission lines are built to make flexible and environmentally friendly hydropower production available in the entire system. The investment decisions are robust to load uncertainty and changes in generation-investment costs.
2) New wind power units are built to reduce emissions. In addition, CCGT and biomass generation units are built to displace more polluting coal, oil, and oil-shale units and to provide flexibility for offsetting the variability of wind and solar power. Building more wind power is preferred at higher uncertainty levels.
3) The SARO model invests more in biomass and wind power than the SP or randomly sampled model does.
4) The investment plan found by the SARO model outperforms that of an SP or randomly sampled model at higher load levels but is more expensive at lower load levels.
5) Omitting hydro-reservoir constraints in modeling leads to significantly lower generation investment, which results in higher expected costs and infeasibility at higher load levels.

Building on our improved computational methods, future work could explore longer-term investment plans with various scenarios on the electrification of transportation as well as deployment of emerging technologies such as storage other than hydropower. Moreover, the model could be extended to cover larger power systems such as all of Europe to find a more globally optimal investment plan that takes into account the pool of resources and spatio-temporal correlations of VRES generation in a larger geographical area. Our model assumes a central planner, while future work could take game-theoretic approaches with multiple independent market participants. The hydropower model could be further improved to consider the time value of water and constraints related to river systems. Also, future research can develop more realistic models for additional sources of uncertainty such as long-term uncertainties in fuel costs, transmission and generation outages, and climate conditions affecting renewable-energy availability that could lead to more robust investment plans for renewable-rich systems. In fact, our framework can be readily extended with additional long- and short-term uncertainties at the 2nd and 3rd levels of the model, respectively. Finally, the large-scale LP in the Benders subproblem remains a bottleneck, which means that further decomposition could lead to significant improvements in solution times.

Acknowledgment

This paper has benefited from presentation at the 2022 Trans-Atlantic Infraday Conference. Comments from three anonymous referees and the handling editor have greatly improved this work. All remaining errors are the authors' own.

References

[1] United Nations, "Paris agreement," 2015. [Online]. Available: https://unfccc.int/sites/default/files/english_paris_agreement.pdf

[2] European Commission, "EU climate action," 2019. [Online]. Available: https://ec.europa.eu/clima/citizens/eu_en

[3] W. Zappa, M. Junginger, and M. van den Broek, "Is a 100% renewable European power system feasible by 2050?," *Appl. Energy*, vol. 233-234, pp. 1027–1050, 2019.

[4] L. Baringo and A. Baringo, "A stochastic adaptive robust optimization approach for the generation and transmission expansion planning," *IEEE Trans. Power Syst.*, vol. 33, no. 1, pp. 792–802, Jan. 2018.

[5] R. Mínguez and R. García-Bertrand, "Robust transmission network expansion planning in energy systems: Improving computational performance," *Eur. J. Oper. Res.*, vol. 248, no. 1, pp. 21–32, 2016.

[6] R. Mínguez, R. García-Bertrand, J. M. Arroyo, and N. Alguacil, "On the solution of large-scale robust transmission network expansion planning under uncertain demand and generation capacity," *IEEE Trans. Power Syst.*, vol. 33, no. 2, pp. 1242–1251, Mar. 2018.

[7] F. Barati, H. Seifi, M. S. Sepasian, A. Nateghi, M. Shafie-khah, and J. P. S. Catalão, "Multi-period integrated framework of generation, transmission, and natural gas grid expansion planning for large-scale systems," *IEEE Trans. Power Syst.*, vol. 30, no. 5, pp. 2527–2537, Sep. 2015.

[8] Gurobi Optimization LLC, "Gurobi 9.1 released," 2020. [Online]. Available: https://support.gurobi.com/hc/en-us/articles/360051963871-Gurobi-9-1-released

[9] A. J. Conejo, E. Castillo, R. Minguez, and R. Garcia-Bertrand, *Decomposition Techniques in Mathematical Programming. Engineering and Science Applications*. Berlin, Germany: Springer, 2006.

[10] A. Moreira, D. Pozo, A. Street, and E. Sauma, "Reliable renewable generation and transmission expansion planning: Co-optimizing system's resources for meeting renewable targets," *IEEE Trans. Power Syst.*, vol. 32, no. 4, pp. 3246–3257, Jul. 2017.

[11] J. Li et al., "Robust coordinated transmission and generation expansion planning considering ramping requirements and construction periods," *IEEE Trans. Power Syst.*, vol. 33, no. 1, pp. 268–280, Jan. 2018.

[12] C. Roldán, A. S. de la Nieta, R. García-Bertrand, and R. Mínguez, "Robust dynamic transmission and renewable generation expansion planning: Walking towards sustainable systems," *Int. J. Electr. Power Energy Syst.*, vol. 96, pp. 52–63, 2018.

[13] F. Verástegui, A. Lorca, D. E. Olivares, M. Negrete-Pincetic, and P. Gazmuri, "An adaptive robust optimization model for power systems planning with operational uncertainty," *IEEE Trans. Power Syst.*, vol. 34, no. 6, pp. 4606–4616, Nov. 2019.
[14] S. Yin and J. Wang, "Generation and transmission expansion planning towards a 100% renewable future," *IEEE Trans. Power Syst*., vol. 37, no. 4, pp. 3274–3285, Jul. 2022.
[15] J. Alvarez Lopez, K. Ponnambalam, and V. H. Quintana, "Generation and transmission expansion under risk using stochastic programming," *IEEE Trans. Power Syst.*, vol. 22, no. 3, pp. 1369–1378, Aug. 2007.
[16] R. Domínguez, A. J. Conejo, and M. Carrión, "Toward fully renewable electric energy systems," *IEEE Trans. Power Syst.*, vol. 30, no. 1, pp. 316–326, Jan. 2015.
[17] X. Chen, J. Lv, M. B. McElroy, X. Han, C. P. Nielsen, and J. Wen, "Power system capacity expansion under higher penetration of renewables considering flexibility constraints and low carbon policies," *IEEE Trans. Power Syst.*, vol. 33, no. 6, pp. 6240–6253, Nov. 2018.
[18] N. Zhang, Z. Hu, C. Springer, Y. Li, and B. Shen, "A bi-level integrated generation-transmission planning model incorporating the impacts of demand response by operation simulation," *Energy Convers. Manage.*, vol. 123, pp. 84–94, 2016.
[19] P. Pisciella, M. Bertocchi, and M. T. Vespucci, "A leader-followers model of power transmission capacity expansion in a market driven environment," *Comput. Manage. Sci.*, vol. 13, no. 1, pp. 87–118, 2016.
[20] L. Maurovich-Horvat, T. K. Boomsma, and A. S. Siddiqui, "Transmission and wind investment in a deregulated electricity industry," *IEEE Trans. Power Syst.*, vol. 30, no. 3, pp. 1633–1643, Mar. 2015.
[21] M. Child, D. Bogdanov, and C. Breyer, "The Baltic sea region: Storage, grid exchange and flexible electricity generation for the transition to a 100% renewable energy system," *Energy Procedia*, vol. 155, pp. 390–402, 2018.
[22] K. Hansen, B. V. Mathiesen, and I. R. Skov, "Full energy system transition towards 100% renewable energy in Germany in 2050," *Renewable Sustain. Energy Rev.*, vol. 102, pp. 1–13, 2019.
[23] A. Blakers, B. Lu, and M. Stocks, "100% renewable electricity in Australia," *Energy*, vol. 133, pp. 471–482, 2017.
[24] P. Colbertaldo, S. B. Agustin, S. Campanari, and J. Brouwer, "Impact of hydrogen energy storage on california electric power system: Towards 100% renewable electricity," *Int. J. Hydrogen Energy*, vol. 44, no. 19, pp. 9558–9576, 2019.
[25] M. Esteban et al., "100% renewable energy system in Japan: Smoothening and ancillary services," *Appl. Energy*, vol. 224, pp. 698–707, 2018.
[26] B. S. Palmintier and M. D. Webster, "Impact of operational flexibility on electricity generation planning with renewable and carbon targets," *IEEE Trans. Sustain. Energy*, vol. 7, no. 2, pp. 672–684, Apr. 2016.
[27] Y. Zhou, L. Wang, and J. D. McCalley, "Designing effective and efficient incentive policies for renewable energy in generation expansion planning," *Appl. Energy*, vol. 88, no. 6, pp. 2201–2209, 2011.
[28] I. Das, K. Bhattacharya, and C. Cañizares, "Optimal incentive design for targeted penetration of renewable energy sources," *IEEE Trans. Sustain. Energy*, vol. 5, no. 4, pp. 1213–1225, Oct. 2014.
[29] J. Kazempour, P. Pinson, and B. F. Hobbs, "A stochastic market design with revenue adequacy and cost recovery by scenario: Benefits and costs," *IEEE Trans. Power Syst.*, vol. 33, no. 4, pp. 3531–3545, Jul. 2018.
[30] S. Jin and S. M. Ryan, "A tri-level model of centralized transmission and decentralized generation expansion planning for an electricity market–Part I," *IEEE Trans. Power Syst.*, vol. 29, no. 1, pp. 132–141, Jan. 2014.
[31] J. H. Roh, M. Shahidehpour, and L. Wu, "Market-based generation and transmission planning with uncertainties," *IEEE Trans. Power Syst.*, vol. 24, no. 3, pp. 1587–1598, Aug. 2009.
[32] D. Pozo, E. E. Sauma, and J. Contreras, "A three-level static MILP model for generation and transmission expansion planning," *IEEE Trans. Power Syst.*, vol. 28, no. 1, pp. 202–210, Feb. 2013.
[33] P. Nahmmacher, E. Schmid, L. Hirth, and B. Knopf, "Carpe diem: A novel approach to select representative days for long-term power system modeling," *Energy*, vol. 112, pp. 430–442, 2016.
[34] S. Debia, D. Benatia, and P.-O. Pineau, "Evaluating an interconnection project: Do strategic interactions matter?," *Energy J.*, vol. 39, no. 6, pp. 99–120, 2018.
[35] V. Virasjoki, A. S. Siddiqui, B. Zakeri, and A. Salo, "Market power with combined heat and power production in the nordic energy system," *IEEE Trans. Power Syst.*, vol. 33, no. 5, pp. 5263–5275, Sep. 2018.
[36] T. Rintamäki, A. S. Siddiqui, and A. Salo, "Strategic offering of a flexible producer in day-ahead and intraday power markets," *Eur. J. Oper. Res.*, vol. 284, no. 3, pp. 1136–1153, 2020.
[37] European Environment Agency, "Overview of electricity production and use in Europe," 2015. [Online]. Available: https://www.eea.europa.eu/data-and-maps/indicators/overview-of-the-electricity-production-1/assessment
[38] G. Calafiore and M. Campi, "Uncertain convex programs: Randomized solutions and confidence levels," *Math. Program.*, vol. 102, no. 1, pp. 25–46, 2005.
[39] U. S. Energy Information Administration, "Cost and performance characteristics of new generating technologies, annual energy outlook 2019," 2019. [Online]. Available: https://web.archive.org/web/20190623232449/https://www.eia.gov/outlooks/aeo/assumptions/pdf/table_8.2.pdf
[40] ENTSO-E, "European electricity transmission grids and the energy transition," 2021. [Online]. Available: https://eepublicdownloads.entsoe.eu/clean-documents/mc-documents/210414_Financeability.pdf
[41] European Environment Agency, "EEA greenhouse gas - Data viewer," 2019. [Online]. Available: https://www.eea.europa.eu/data-and-maps/data/data-viewers/greenhouse-gases-viewer

Tuomas Rintamäki received the M.Sc. degree in engineering physics and mathematics from Aalto University, Espoo, Finland. He is currently working toward the D.Sc. degree with Systems Analysis Laboratory, Department of Mathematics and Systems Analysis, Aalto University. His research interests include optimization and predictive models with applications in energy systems.

Fabricio Oliveira received the B.Sc. and D.Sc. degrees in industrial engineering from the Pontifical Catholic University of Rio de Janeiro, Rio de Janeiro, Brazil. He was a Postdoctoral Researcher with the Department of Mathematical Sciences, RMIT University, Melbourne, VIC, Australia. He is currently an Associate Professor of Operations Research with the Department of Mathematics and Systems Analysis, School of Science, Aalto University, Espoo, Finland. He is also the Leader of the Group of Applied Mathematical Modelling and Optimisation (Gamma-opt). His research interests include mathematical programming, with an emphasis on stochastic programming and robust optimization, and applications related to production systems design and planning.

Afzal S. Siddiqui received the B.S. degree in industrial engineering from Columbia University, New York, NY, USA, and the M.S. and Ph.D. degrees in industrial engineering and operations research from the University of California, Berkeley, CA, USA. He is currently a Professor with the Department of Computer and Systems Sciences, Stockholm University, Kista, Sweden, and an Adjunct Professor with the Department of Mathematics and Systems Analysis, School of Science, Aalto University, Espoo, Finland. His research interests include energy economics, specifically the application of game-theoretic models for analyzing investment incentives and environmental policy in the power sector.

Ahti Salo received the M.Sc. and D.Sc. degrees in systems and operations research from the Helsinki University of Technology, Helsinki, Finland. He is currently a Professor of Systems Analysis with Aalto University, Espoo, Finland. He was a Visiting Professor with the London Business School, Universitã Paris-Dauphine, Paris, France and the University of Vienna, Vienna, Austria. His research interests include topics in decision analysis, risk management and foresight methodologies, with applications in energy and safety-critical systems. He has received the 2019 MCDM Edgeworth-Pareto Award from the International Society on Multiple Criteria Decision Making and the 2022 Frank P. Ramsey Medal from the Decision Analysis Society of the Institute for Operations Research and Management Sciences.